

University of Alberta

DYNAMIC MODELING OF SOLID OXIDE FUEL CELL

by

Yutong Qi



A thesis submitted to the Faculty of Graduate Studies and Research in partial fulfillment
of the requirements for the degree of **Doctor of Philosophy**

in

Process Control

Department of Chemical and Materials Engineering

Edmonton, Alberta
Fall 2007



Library and
Archives Canada

Bibliothèque et
Archives Canada

Published Heritage
Branch

Direction du
Patrimoine de l'édition

395 Wellington Street
Ottawa ON K1A 0N4
Canada

395, rue Wellington
Ottawa ON K1A 0N4
Canada

Your file *Votre référence*
ISBN: 978-0-494-33047-0
Our file *Notre référence*
ISBN: 978-0-494-33047-0

NOTICE:

The author has granted a non-exclusive license allowing Library and Archives Canada to reproduce, publish, archive, preserve, conserve, communicate to the public by telecommunication or on the Internet, loan, distribute and sell theses worldwide, for commercial or non-commercial purposes, in microform, paper, electronic and/or any other formats.

The author retains copyright ownership and moral rights in this thesis. Neither the thesis nor substantial extracts from it may be printed or otherwise reproduced without the author's permission.

AVIS:

L'auteur a accordé une licence non exclusive permettant à la Bibliothèque et Archives Canada de reproduire, publier, archiver, sauvegarder, conserver, transmettre au public par télécommunication ou par l'Internet, prêter, distribuer et vendre des thèses partout dans le monde, à des fins commerciales ou autres, sur support microforme, papier, électronique et/ou autres formats.

L'auteur conserve la propriété du droit d'auteur et des droits moraux qui protègent cette thèse. Ni la thèse ni des extraits substantiels de celle-ci ne doivent être imprimés ou autrement reproduits sans son autorisation.

In compliance with the Canadian Privacy Act some supporting forms may have been removed from this thesis.

Conformément à la loi canadienne sur la protection de la vie privée, quelques formulaires secondaires ont été enlevés de cette thèse.

While these forms may be included in the document page count, their removal does not represent any loss of content from the thesis.

Bien que ces formulaires aient inclus dans la pagination, il n'y aura aucun contenu manquant.


Canada

子曰——

正心修身

齐家治国

平天下

TO MY DAUGHTER AND WIFE, EMMA AND YU

Abstract

In order to operate solid oxide fuel cell (SOFC) systems, it is necessary to investigate dynamic characteristics of SOFC through modeling and simulations. In this thesis, SOFC dynamics is presented in the form of non-linear state-space model (SSM). Performance and responses of SOFC are investigated through simulations. This thesis consists of four stages in solving the problems of interest.

First we investigate how fuel enters the cell surface and produces electricity. Dynamics led by diffusion process and inherent impedance is investigated and modeled. Dynamic correlations between parameters in the primary flow and in the immediate vicinity of the triple phase boundary (*tpb*) are considered in the form of transfer function as well as ordinary differential equation (ODE). A new equivalent circuit that can emulate both internal and external dynamic characteristics of SOFC is proposed to represent the effect of inherent resistance and double layer capacitance. Through simulations, a phenomenon of slow response of voltage in current interrupt experiment is explained.

In the second stage, we consider transport processes from the cell surroundings to a finite volume of tubular SOFC composite, such as internal reforming/shifting reaction, fluid transport, and heat transfer. Combined with dynamics developed from the first stage, a detailed SSM with 28 states is developed. Mole fractions, temperatures, flow velocities etc. are investigated and dynamically modeled through mass/energy/momentum balance. Dynamic responses of each physical variable to step

changes of inlet variables as well as load changes are investigated through simulations.

In the third stage, the dynamic model for the finite volume of tubular SOFC is expanded to a one-dimensional (1-D) dynamic model, in the form of non-linear SSM. With known total current demand, the dynamic current density distribution is developed by solving the equivalent circuit. Non-flowing solid phase variables are dynamically modeled. Dynamics of the flowing phase variables and their distributions are developed in the form of partial differential equations (PDEs).

Aiming to solve the distributed parameter problem approximately, an innovative analytical solution for a 1-D reacting gas flow problem is developed. The solution is applied to the 1-D dynamic model of SOFC. The developed model can reduce computations while maintain reasonable precision. The explicit solution makes the 1-D dynamic model more applicable for further control studies. Dynamic performance and parameter distributions of SOFC are investigated through simulations.

Finally, with the aim for simpler control application, an 2nd order nonlinear lumped parameter SSM is built. Input-output parameters of the SOFC stack are analyzed. Faster processes are approximated by their steady state solutions. Solid phase temperatures are modeled by dynamic equations owing to their slow response and dominant role played in SOFC dynamic responses. Simulations show that the lumped model can reasonably approximate dynamics of the SOFC shown by the detailed model.

Acknowledgements

At the moment when the thesis is going to be finished, recalling the efforts and the gain that I have experienced in the journey to obtain a PhD degree, I would like to express my deep and sincere gratitude to all those who gave me supervision, assistance and support.

Foremost, I would like to acknowledge Prof. Biao Huang, my supervisor, for his outstanding supervision, constant support and enthusiastic encouragement. When exploring the fuel cell first principle dynamic modeling problem, a new field for both of us, I gratefully acknowledge for the confidence and the freedom he gave to me. I am also grateful to him for his patience and tolerance.

I sincerely acknowledge Prof. Karl T. Chuang and Prof. Jingli Luo, for their co-supervision. Prof. Chuang gave me clear and exact guidance and helped me overcome the chaos in the initial phase of the research when I first faced the gap between two different disciplines. With the progress of my research, Prof. Luo led me go further in experimental research.

I wish to express my deep thanks to Dr. Guolin Wei, Dr. Man Liu and Mr. Chin Kui Cheng for their kind and valuable help. I acknowledge their warm and patient introductions to many aspects of fuel cell technologies.

I warmly thank Mr. Zengrong Xu, Dr. Zhijun Mo, Mr. Nemanja Danilovic, and Mr. Rambabu Kandepu. Their help, collaboration and suggestion in the SOFC experiment are priceless.

I own my sincere gratitude to Prof. Krishnaswamy Nandakumar, Prof. Jacob H. Masliyah and Prof. Fraser Forbes for their enthusiastic teaching. They opened the door of numerical solution, fluid dynamics and optimization to me.

Special thanks are due to colleagues in the Computer Process Control for many stimulating discussions and friendly time I had with Dr. Fangwei Xu, Dr. Salim Ahamed, Dr. AKM Monjur Meshed, Dr. Xin Huang, Dr. Zhengang Han, Dr. Xiaorui Wang, Dr. Jiandon Wang, Dr. Liqian Zhang, Dr. Ruoyu Chen, Dr. Ian Alleney, Dr. Rumana Sharmin, Hailei Jiang, Adrian Fuxman, Natalia I. Marcos, Mohammad H. Iqbal, Xinguang Shao, Fei Qi, Barath and many others.

I would also like to thank the department system administrators Bob Barton and Jack Gibeau, the instrument supervisor Walter Boddez, and the secretaries in the department AnnMarie Brereten, Leanne Swekla, Shona Williams, and Lily Laser.

Financial supports from the National Science and Engineering Research Council (NSERC) and the Western Canada Fuel Cell Initiative (WCFCI) program and the financial support in the form of Captain Thomas Farrel Greenhalgh Memorial Scholarship are gratefully acknowledged.

Last but not the least, I would like to thank my dearest daughter, my wife, my parents and my sister. With their unconditional love, support and encouragement, I am able to overcome any challenge.

Contents

1	Introduction	1
1.1	Motivation	1
1.2	Fuel cells	2
1.3	Literature review	5
1.3.1	Steady-state modeling	5
1.3.2	Inherent impedance	5
1.3.3	Dynamic modeling	6
1.4	Objective	8
1.5	Approach	9
1.5.1	Methodology	9
1.5.2	Tools	10
1.6	Outline	11
2	The Effect of Diffusion and Inherent Impedance	12
2.1	Introduction	13
2.2	Fuel cell principles	14
2.2.1	Voltage output	14
2.2.2	Current output	15
2.2.3	Dynamic process of fuel cell	16
2.3	Modeling approach	18
2.3.1	Assumptions	18
2.3.2	I/O variables	18
2.3.3	Diffusion	19
2.3.4	Voltage	22
2.3.5	Inherent impedance	23
2.3.6	Equivalent circuit	24
2.3.7	Model in the state space form	25

2.4	Parameters	28
2.5	Simulation results	28
2.5.1	Steady state output and model validation	28
2.5.2	Step responses due to R_{load} step changes	31
2.5.3	Reactant partial pressure disturbances	33
2.5.4	Effect of concentration loss	36
2.5.5	Effect of diffusion layers	37
2.5.6	Effect of temperature	37
2.6	Conclusion	38
3	The effect of transport dynamics	40
3.1	Introduction	41
3.2	Modeling of SOFC	42
3.2.1	Introduction to tubular SOFC	42
3.2.2	Modeling assumptions	43
3.2.3	Modeling for CV1	44
3.2.4	Modeling for CV2	50
3.2.5	Modeling for other control volumes	56
3.3	State-space model	59
3.3.1	Input/Output variables	60
3.3.2	Non-linear state-space model	61
3.4	Simulations	65
3.4.1	Model validation	66
3.4.2	Step responses due to R_{load} step changes	66
3.4.3	Effect of fuel input	68
3.4.4	Effect of air input	70
3.5	Conclusions	72
4	1-D Dynamic Model and Approximated Analytical Solution	73
4.1	Introduction	74
4.2	1-D dynamic modeling of SOFC	76
4.2.1	Brief introduction to tubular SOFC	76
4.2.2	Electricity	77
4.2.3	Diffusion	80
4.2.4	Solid Phase Temperature	82

4.2.5	Fuel Flow	84
4.2.6	Air Flow	87
4.3	Approximate analytical solution	89
4.3.1	Problem description	90
4.3.2	Assumptions	91
4.3.3	Approximated analytical solution	92
4.3.4	Validation	95
4.3.5	Application to SOFC	95
4.4	State-space model	102
4.5	Simulations	106
4.5.1	Step responses due to current demand changes	107
4.5.2	Effect of fuel inlet	109
4.5.3	Effect of air inlet	114
4.6	Conclusions	118
5	Low-Order State Space Model	121
5.1	Introduction	122
5.2	Introduction to SOFC	123
5.2.1	Fuel cell principles revisit	123
5.2.2	Logic correlations of physical effects	124
5.2.3	Limitations to power output	125
5.2.4	Planar and tubular design	126
5.3	Lumped model of SOFC stack	128
5.3.1	Physical processes	128
5.3.2	Model assumptions	130
5.3.3	I/O variables	130
5.3.4	Voltage	132
5.3.5	Partial pressures	133
5.3.6	Flow rates	135
5.3.7	Temperatures	137
5.4	Nonlinear state-space model	139
5.5	Simulation	141
5.5.1	Validation	141
5.5.2	Step response to inputs	142
5.5.3	Step responses to disturbance	142

5.6 Conclusion	146
6 Conclusions and recommendations	147
6.1 Concluding remarks	147
6.2 Recommendations for future work	150
Bibliography	152
Appendix	158
A-I. Parameters	158
A-II. Gas properties	161

List of Tables

2.1	Input and output variables	19
2.2	Parameters used in simulation	29
3.1	Input and output variables	60
5.1	I/O variables of the model	132
5.2	Variation of species in the SOFC stack from the inlet to the outlet	134
A-1	Simulation input conditions	158
A-2	Model parameters	159
A-3	Inherent property parameters of gas ingredients	161
A-4	Approximation of specific heat of gas ingredients between 700-1500K .	162
A-5	Approximation of viscosity of gas ingredients between 700-1500K . . .	163
A-6	Approximation of Thermal conductivity of gases between 700-1500K .	164
A-7	Approximation of enthalpy of formation between 700-1500K	164

List of Figures

1.1	Principle of solid oxide fuel cell	3
1.2	Tubular SOFC stack developed by Simens-Westinghouse [Fuel Cell Hand Book]	4
1.3	Mass transport to reaction sites and control volumes for a SOFC tube . . .	9
1.4	Flow chart of the modeling	10
1.5	Schematic input/output of each phase modeling	10
2.1	Principle of solid oxide fuel cell	14
2.2	Schematic block diagram of fuel cell	17
2.3	Definition of finite volume in different SOFC cells	18
2.4	Equivalent circuit of inherent impedance	24
2.5	Equivalent circuit of a single fuel cell	25
2.6	Comparison of simulated and experiment V-I plot	30
2.7	Step Responses of SOFC, when load resistance changes	32
2.8	Step Responses of SOFC, when hydrogen pressure changes	33
2.9	Step Responses of SOFC, when air pressure changes	34
2.10	Step Responses of SOFC, when steam pressure in anode gas changes . . .	35
2.11	Step Responses of SOFC, when it enters concentration loss range	36
2.12	Effect of diffusion layer thickness on step responses of SOFC	37
2.13	Effect of temperature on step responses of SOFC	38
3.1	Tubular SOFC design of Siemens-Westinghouse	42
3.2	Definition of control volumes	43
3.3	Mass and energy balance on CV1	44
3.4	Definition of view factor	50
3.5	Mass and energy balance on CV2	51
3.6	Mass and energy balance on CV3	57

3.7	Energy balance on CV4	58
3.8	Energy balance on CV5	59
3.9	Comparison of voltage response trends to load step changes	65
3.10	Step responses of SOFC slice, when R_{load} changes	67
3.11	Step responses of species mole fractions, when R_{load} changes	67
3.12	SOFC step responses, when fuel input P, T, u stepped respectively . . .	69
3.13	Mole fraction responses, when fuel input P, T, u stepped respectively .	69
3.14	SOFC step responses, when air input P, T, u stepped respectively	71
3.15	Mole fraction responses, when air input P, T, u stepped respectively . .	71
4.1	Tubular SOFC stack design of Siemens-Westinghouse	77
4.2	Secondary flows of reactant and electrochemical reactions	78
4.3	Equivalent circuit of local intrinsic impedance	79
4.4	Equivalent circuit of SOFC tube	80
4.5	Comparison of the approximated analytical solutions of velocity and physical variable distributions and the exact analytical solutions.	96
4.6	Comparison of numerically simulated and the approximate analytical solution of steady state reforming reaction rate and fuel velocity profiles.	100
4.7	Comparison of numerically simulated and the approximate analytical solution of isothermal steady state species mole fraction profiles. Parameters: $I = 200A, P_{fuel} = 1atm, T_{fuel} = 923K, u_{fuel}^{in} = 0.927m/s$. .	101
4.8	V_{ct} profile and step response, when I step changes from 100 to 150 Amp at 100 second.	107
4.9	Profiles and step responses of temperatures, when I step changes from 100 to 150 Amp at 100 second.	108
4.10	Profiles and step responses of species fractions, when I step changes from 100 to 150 Amp at 100 second.	108
4.11	V_{ct} profile and step response, when P_{fuel}^{in} step changes from 1 to 2 atm at 100 second.	109
4.12	Profiles and step responses of temperatures, when P_{fuel}^{in} step changes from 1 to 2 atm at 100 second.	110
4.13	Profiles and step responses of species fractions, when P_{fuel}^{in} step changes from 1 to 2 atm at 100 second.	110

4.14	V_{ct} profile and step response, when T_{fuel}^{in} step changes from 823 to 923 K at 100 second.	111
4.15	Profiles and step responses of temperatures, when T_{fuel}^{in} step changes from 823 to 923 K at 100 second.	112
4.16	Profiles and step responses of species fractions, when T_{fuel}^{in} step changes from 823 to 923 K at 100 second.	112
4.17	V_{ct} profile and step response, when u_{fuel}^{in} step changes from 0.927 to 1.927 m/s at 100 second.	113
4.18	Profiles and step responses of temperatures, when u_{fuel}^{in} step changes from 0.927 to 1.927 m/s at 100 second.	113
4.19	Profiles and step responses of species fractions, when u_{fuel}^{in} step changes from 0.927 to 1.927 m/s at 100 second.	114
4.20	V_{ct} profile and step response, when P_{air}^{in} step changes from 1 to 2 atm at 100 second.	115
4.21	Profiles and step responses of temperatures, when P_{air}^{in} step changes from 1 to 2 atm at 100 second.	115
4.22	Profiles and step responses of species fractions, when P_{air}^{in} step changes from 1 to 2 atm at 100 second.	116
4.23	V_{ct} profile and step response, when T_{air}^{in} step changes from 1104 to 1184 K at 100 second.	116
4.24	Profiles and step responses of temperatures, when T_{air}^{in} step changes from 1104 to 1184 K at 100 second.	117
4.25	Profiles and step responses of species fractions, when T_{air}^{in} step changes from 1104 to 1184 K at 100 second.	117
4.26	V_{ct} profile and step response, when u_{air}^{in} step changes from 7.79 to 23.37 m/s at 100 second.	118
4.27	Profiles and step responses of temperatures, when u_{air}^{in} step changes from 7.79 to 23.37 m/s at 100 second.	119
4.28	Profiles and step responses of species fractions, when u_{air}^{in} step changes from 7.79 to 23.37 m/s at 100 second.	119
5.1	Principle of Solid Oxide Fuel Cell	123
5.2	Schematic logic correlations of fuel cell process	125
5.3	Tubular design of SOFC stack and cell	127
5.4	Planar design of SOFC stack and cell	127

5.5	Block diagram of fuel cell process	129
5.6	Fuel and air flow channels in the tubular SOFC stack	135
5.7	Compare of stack voltage response trends to current demand step change	141
5.8	Step response of outputs due to u_1 , the fuel inlet pressure $P_{\text{fuel}}^{\text{in}}$, stepped from 1.0008 to 1.0016 atm	143
5.9	Step response of outputs due to u_2 , the air inlet pressure $P_{\text{air}}^{\text{in}}$, stepped from 1.01 to 1.02 atm	143
5.10	Step response of outputs due to d_1 , the external current demand I , stepped from 300 to 500 amp	144
5.11	Step response of outputs due to d_2 , the fuel inlet temperature $T_{\text{fuel}}^{\text{in}}$, stepped from 823 to 873 K	145
5.12	Step response of outputs due to d_3 , the air inlet temperature $T_{\text{air}}^{\text{in}}$, stepped from 1104 to 1154 K	145

Nomenclature

Nomenclature

A	area (m^2)
A_a	anode side flow channel cross section area (m^2)
A_c	cathode side flow channel cross section area (m^2)
$a_{\text{H}_2\text{O}}$	activity of water vapor
a_{H_2}	activity of hydrogen
a_{O_2}	activity of oxygen
C	concentration (mol m^{-3})
C_{ct}	charge transfer capacity (F)
C_p	specific heat at constant pressure ($\text{J mol}^{-1} \text{K}^{-1}$)
C_v	specific heat at constant volume ($\text{J mol}^{-1} \text{K}^{-1}$)
D	diffusion coefficient ($\text{m}^2 \text{s}^{-1}$)
D	hydraulic diameter (m)
dV	volume of an element control volume (m^3)
E	voltage (V)
$E_{\text{act},a}$	anode reaction activation energy (J mol^{-1})
$E_{\text{act},c}$	cathode reaction activation energy (J mol^{-1})
E_b	radiation energy emitted by black body(J)
E_e	electrical energy (J)
E_r	activation energy of reforming reaction (J mol^{-1})
F	Faraday's constant ($= 96487 \text{ C mol}^{-1}$)
f	friction factor

F_a	force acting on anode side fluid body (N)
F_{c-t}	view factor from cell tube to injection tube
F_c	force acting on cathode side fluid body (N)
$\Delta\bar{g}_f$	Gibbs free energy released (J mol^{-1})
ΔH	reaction heat (J mol^{-1})
H	enthalpy of formation (J mol^{-1})
h	convection heat transfer coefficient ($\text{W m}^{-2} \text{K}^{-1}$)
I	current (A)
i	current density (A m^{-2})
i_0	exchange current density (A m^{-2})
i_l	limit current density (A m^{-2})
j	diffusion flux ($\mu\text{mol s}^{-1} \text{m}^{-2}$)
J^r	reaction rate at reaction sites ($\mu\text{mol s}^{-1}$)
J^s	consumption rate flowing into the outer surface of diffusion layer ($\mu\text{mol s}^{-1}$)
K	reaction rate coefficient
k	conductivity ($\text{W m}^2 \text{K}^{-1}$)
l_a	thickness of anode diffusion layer (m)
l_c	thickness of cathode diffusion layer (m)
$l_{R_{ct}}$	length of charge transfer resistance (m)
l_{R_o}	length of pure ohmic resistance (m)
M	mole mass (g mol^{-1})
m	mass (g)
\dot{n}	mole flow rate (mol s^{-1})
N	mole number (mol)
ΔP	pressure gradient (atm)
P	pressure (atm)
P^0	standard pressure (atm)

$P_{\text{H}_2\text{O}}^0$	vapor pressure of the steam at the temperature considered (atm)
p^b	partial pressure in gas bulk (atm)
p^{tpb}	partial pressure in the immediate vicinity of $tpbs$ (atm)
q	heat flux ($\text{J s}^{-1} \text{m}^{-2}$)
R	gas constant ($= 82.05 \times 10^{-6} \text{ J mol}^{-1} \text{ K}^{-1}$)
R_{ct}	charge transfer resistance (Ω)
R_{load}	load resistance (Ω)
R_o	ohmic resistance (Ω)
R_{rad}	radiation heat transfer resistance
r_r	reforming reaction rate ($\text{mol s}^{-1} \text{m}^{-2}$)
r_s	shifting reaction rate ($\text{mol s}^{-1} \text{m}^{-2}$)
s	Laplace operator
T	temperature (K)
\bar{V}_{ct}	average fuel cell potential (V)
V	voltage (V)
V_{out}	fuel cell voltage out (V)

Greek Letters

ε	porosity
η_{act}	activation loss (V)
μ	viscosity (Pa s)
(ΣV_i)	diffusional volumes
χ	mole fraction
ρ	density (kg m^{-3})
$\rho_{C_{\text{ct}}}$	specific capacitance of charge transfer capacitance (F m^{-2})
$\rho_{R_{\text{ct}}}$	specific resistance of charge transfer resistance ($\Omega \text{ m}^{-1}$)
ρ_{R_o}	specific resistance of pure Ohmic resistance ($\Omega \text{ m}^{-1}$)
σ	Stefan-Boltzmann constant ($= 5.6697 \times 10^{-8} \text{ W m}^{-2} \text{ K}^{-4}$)

τ	shear stress (Pa)
τ	tortuosity
ξ	space constant

Superscripts

0	at standard pressure
b	gas flow bulk
gen	generation
in	inlet
out	outlet
r	flow at the reaction site
s	flow at the upper surface of diffusion layer
<i>tpb</i>	triple phase boundary

Subscripts

0	inner surface of injection tube
1	outer surface of injection tube
12	binary diffusion
2	inner surface of cell tube
3	outer surface of cell tube
a	anode
act	activation
c	cathode
cell	cell tube
cond	conduction
conv	convection
ct	charge transfer
eff	effective
eq	equilibrium
f	fluid

H ₂ O	water vapor
H ₂	hydrogen
i	fuel ingredients
j	air ingredients
k	Knudsen
load	load
N ₂	nitrogen
O ₂	oxygen
o	ohmic
out	output
r	reforming reaction
rad	radiation
ref	reforming reaction
s	shifting reaction
t	inside injection tube
w	wall

1

Introduction

An overview of this work is provided in this chapter. The motivation of first principle dynamic modeling of Solid Oxide Fuel Cell (SOFC) is introduced. The principle of fuel cell technologies is briefly explained. The development of the SOFC modeling is reviewed through published literatures. The objective and the methodology are highlighted, followed by the outline of the thesis.

1.1 Motivation

Fuel cell is a highly efficient power generation technology. It directly converts chemical energy into electrical energy without the traditional combustion \rightarrow heat \rightarrow kinetic \rightarrow electrical process. Solid oxide fuel cell (SOFC) is identified as one of the most likely fuel cell technology that will capture the most significant market in the future. Considerable amount of research and development work has been devoted to investigating SOFC system, making the SOFC system closer to the commercial application. However, before SOFC system can be marketed as a distributed power source, the dynamic operation problem, namely control problem must be resolved.

Thus, dynamic modeling of SOFC is a necessary first step towards this direction.

Although numerous modeling work has been done, study on dynamic characteristics of SOFC is relatively sparse and incomprehensive. So the goal of this study is:

1. Investigate physical processes that affect the dynamic properties of SOFC;
2. Describe these processes through some appropriate mathematical models;
3. Investigate dynamic characteristics of SOFC through simulations.

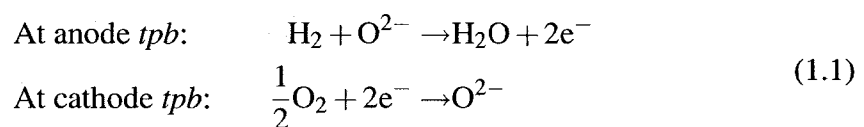
1.2 Fuel cells

Electrochemical fuel cells convert fuel directly to electricity. Their modular nature, coupled with their ability to generate electricity cleanly and efficiently, makes them attractive for a wide variety of applications. There are six different types of fuel cells that have received varying degrees of development:

- Alkaline fuel cell (AFC)
- Proton exchange membrane fuel cell (PEMFC)
- Direct methanol fuel cell (DMFC)
- Phosphoric acid fuel cell (PAFC)
- Molten carbonate fuel cell (MCFC)
- Solid oxide fuel cell (SOFC)

Recently, the low temperature proton exchange membrane fuel cell (PEMFC) and the high temperature solid oxide fuel cell (SOFC) have been identified as the likely fuel cell technologies that will capture the most significant market in the future.

The basic principle of a typical hydrogen SOFC is shown in Fig.1.1. The chemical reactions inside the cell that are directly involved in the production of electricity are:



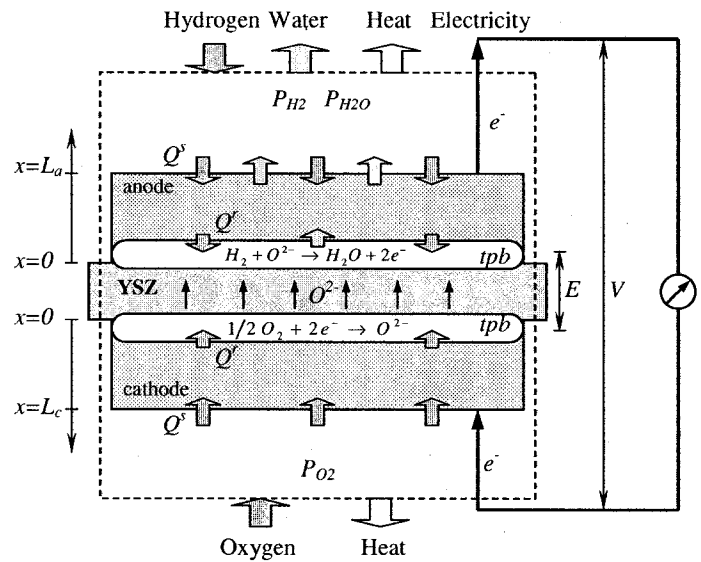


Figure 1.1: Principle of solid oxide fuel cell

At the anode of the SOFC, the hydrogen gas reacts with oxygen ions migrated from the electrolyte, to form water and release electrons. At the cathode, oxygen ionizes with electrons and creates O^{2-} ions. O^{2-} ions are transported to anode through the electrolyte. Electrons produced at the anode flow through an external electrical circuit and reach the cathode. These reactions therefore both proceed continuously, and supply electricity to the external circuit. Usually, SOFC works at a high temperature, in the range of $800 - 1000^\circ\text{C}$, to reach the electrolyte's ionic conductivity requirement.

SOFC stacks have different geometric configurations, but can be generally classified into two categories: planar and tubular. The tubular SOFC appears to be more promising. The most advanced configurations are integrated planar-tubular SOFC (IP-SOFC) design of Rolls-Royce and the integrated tubular-planar SOFC of Siemens-Westhouse. The recent tubular design of Siemens-Westhouse is shown in Fig.1.2. The arrangement of the air-electrode-support (AES) tube can be found in Fig.1.3.

A large amount of literature about SOFC has been published. Most of the work has focused on investigating electrochemical characteristics, such as reaction mechanisms, state-of-the-art cell components, new materials, etc. Modeling of SOFC performance is also an important step in investigating the properties of SOFC.

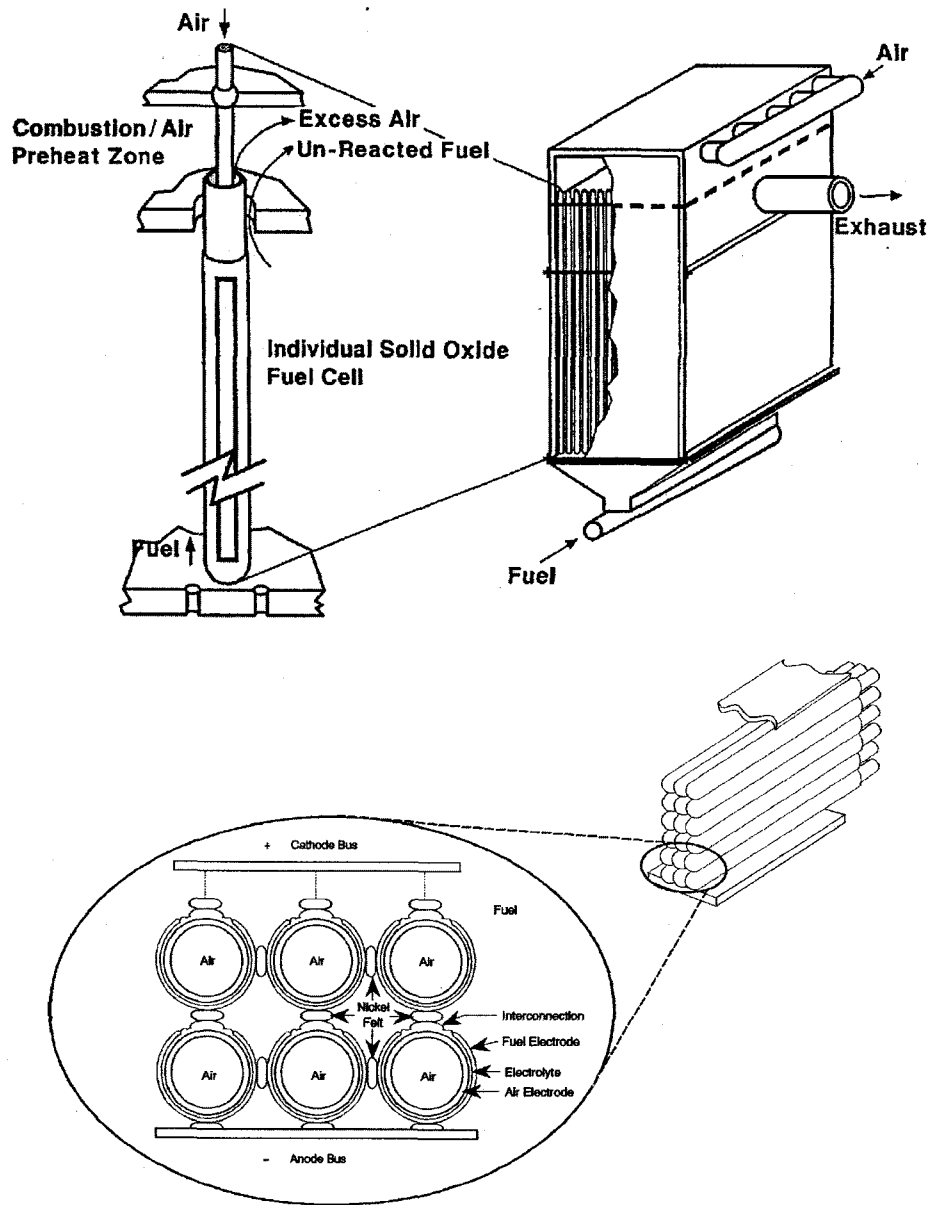


Figure 1.2: Tubular SOFC stack developed by Simens-Westinghouse [Fuel Cell Hand Book]

1.3 Literature review

1.3.1 Steady-state modeling

Modeling of SOFC may be classified according to specific SOFC geometry since the geometry of SOFC affects its performance greatly. Early mathematical modeling of tubular SOFC was performed by Dunbar (1983) and Wepfer and Woolsey (1985). Debendetti and Vayenas (1983) were among the first researchers who modeled planar SOFC. These authors developed 2-D models, which approximate the cell stack as a set of unit cells operating as continuously stirred tank reactors (CSTR). Heat and mass balances are made on the unit cells. For the monolithic cell, a 2-D model was developed by Ahmed *et al.* (1991) following a similar approach as the unit cell approximation described previously.

Limited by manufacturing technologies for monolithic planar SOFCs, the tubular SOFC becomes one of the few practicable designs (Larminie and Dicks, 2003), and most of research interests were turned to tubular SOFC.

Campanari (2001) presented a thermodynamic model of a tubular SOFC stack, with natural gas feed, plus internal reforming of hydrocarbons and internal air preheating. Li and Chyu (2003) modeled and analyzed the heat and species transport processes including reforming process in a tubular SOFC that works in a cell stack, using the 2-D finite element method. In their modeling work, they considered the heat generated by the SOFC cell in a great detail. While Campanari and Iora's (2004) work emphasized more on activation loss in an 1-D finite element model and analyzed the parameter sensitivity.

Varying from simple to detail, these modeling approaches gradually combined mass transport, heat transfer, cell polarizations, and internal reforming etc. The steady-state performance of SOFC becomes clearer with increased details of the models. However, the dynamic properties of SOFC can not be revealed from these studies.

1.3.2 Inherent impedance

One important source that affects the dynamic behavior of fuel cell is the inherent impedance. The inherent impedance of fuel cell is well studied via electrochemical impedance spectroscopy (EIS) method. Now the EIS test has already become one of

the standard methods in investigating the electrochemical properties of fuel cells.

The inherent impedance includes the ohmic resistance, grain boundary resistance, reaction resistance, and the double layer charge transfer capacitance. It is usually modeled as an equivalent circuit. Macdonald (1987) introduced the EIS method in a great detail including some methods of identification of the inherent impedance parameters. A more accurate method to determine the double layer capacitance was proposed by Berthier *et al.* (1995).

By testing EIS at different operating points, Wagner *et al.* (1998) experimentally studied the inherent impedance of SOFC and PEMFC in detail. From the Bode plot of EIS, the behavior of diffusion and the effect of the double layer capacitance were observed and approximated by an equivalent circuit.

The inherent impedance is also related to the electrochemical reactions, and the investigation of the reaction characteristics is therefore an important subject. Holtappels *et al.* (2001) analyzed the electrochemical characterization of SOFC anode, including the Ohmic resistance, and the polarization resistance. While Jørgensen and Mogensen (2001) studied the electrochemical properties of SOFC cathode, Mitterdorfer and Gauckler (1999a) investigated the dynamic reaction kinetics of SOFC as well as the dynamic charge transfer properties. They also developed methods for identification of the reaction mechanism of SOFC (Mitterdorfer and Gauckler, 1999b; Mitterdorfer and Gauckler, 1999c).

By means of the equivalent approximation of inherent impedance, the electrical characteristics of fuel cell may be simplified as equivalent RC circuits. So the effect of inherent impedance on voltage and current dynamic behavior is similar to an RC filter.

1.3.3 Dynamic modeling

In order to investigate dynamic characteristics of SOFC, some dynamic modeling work and simulations have been performed in the molecular scale (Yamamura *et al.*, 1999; Perumal *et al.*, 2002). However such micro dynamic models are not suitable for macro applications.

Early macro dynamic modeling of SOFC was performed by Achenbach (1994; 1995). He examined the transient cell voltage performance of a cross flow planar SOFC

cell due to the temperature changes and the perturbations in current density. In his study, the SOFC is an electrode-supported, direct internal reforming planar SOFC.

Other modeling efforts reveal some discrepancies between zero-, one-, and two-dimensional modeling. Domergue *et al.* (1998) and Lukas *et al.* (1999) have likewise proceeded to model dynamic MCFC performance using lumped models. Models proposed in (Liese, 1999) and (Gemmen, 2000) have demonstrated some success with a one-dimensional methodology on MCFC and SOFC. Because the reforming/shifting reaction in MCFC is similar to that of SOFC, their research is applicable to SOFC development.

The dynamic model given by Padullés *et al.* (2000) included the species dynamics in stack-level the first time. Zhu and Tomsovic (2001) adopted the model of Padullés *et al.* (2000) for analyzing the load-following performance of micro-turbines and fuel cells. Based on their efforts, Sedghisigarchi and Feliachi (2004) combined Achenbach's (1994) heat transfer dynamics and Padullés *et al.*'s (2000) species dynamics together and simulated the dynamic responses. Only the lumped dynamic behavior of species along the fuel/air channel was considered in these models. Besides heat transfer dynamics, Xue *et al.* (2005) and Gemmen and Johnson (2005) considered mass transfer dynamics induced by flowing process in their models. Furthermore, Iora *et al.* (2005) included species dynamics caused by internal reforming/shifting reaction in their model. However, none of these models incorporate the dynamics of diffusion processes, inherent impedance, and the dynamic relations between flow and heat transfer.

Although several dynamic models of SOFC were proposed with different complexity, they are not sufficient to capture the dynamic characteristics of SOFC. The dynamic models proposed in (Achenbach, 1994; Achenbach, 1995; Padullés *et al.*, 2000; Zhu and Tomsovic, 2001; Sedghisigarchi and Feliachi, 2004) aimed to solve control problems but the models are too coarse to capture the essential dynamic properties. The models developed by Xue *et al.* (2005), Gemmen and Johnson (2005), and Iora *et al.* (2005) considered more details but their emphasis are more on mechanism investigation not on dynamics. By considering parameter distributions, these distributed dynamic models are computationally expensive and not suitable for control applications.

Aiming to fill these gaps, this investigation started from the study of the dynamic effects led by diffusion and inherent impedance (Qi *et al.*, 2005). The dynamic effects ranged from fluid dynamics, mass and heat transfer, to the diffusion and the

electrochemical conversion were investigated next (Qi *et al.*, 2006). The distributed 1-D dynamic model was solved by developing an approximated analytical solution for the 1-D reacting gas flow (Qi *et al.*, 2007a); the resulting distributed dynamic model is computationally more efficient and more suitable for control applications. Based on the understanding of the dynamic characteristics of SOFC, a lower order state space model of SOFC that can capture the key dynamic characteristics of SOFC was specially developed for simpler control applications (Qi *et al.*, 2007b).

In the system level, with the understanding of dynamic properties of SOFC through modeling, recent investigations of SOFC system level dynamics have focused on modeling subsystems of SOFC by accounting the lumped parametric mass and energy balance (Stiller *et al.*, 2006; Wächter *et al.*, 2006; Murshed *et al.*, 2007; Kandepu *et al.*, 2007). Considering mass and energy balances, dynamic models developed in these literatures can basically capture the main dynamic characteristics. Therefore, the control strategy and controller development based on these models are meaningful. But the internal reforming/shifting reaction is usually not considered; thus these models have significant deviations from actual SOFC operations.

1.4 Objective

Fuel cell is an energy conversion device. It converts chemical energy of H_2 , O_2 etc. to electricity. The problem we will consider is how fuel and air inputs dynamically affect the electricity energy outputs and temperature distributions in the cell.

In order to control the stack operations, one needs to know not only the static relations between inputs and outputs, but also the dynamic relations. The objectives of this research are to investigate the dynamic relations between fuel and air input flow rates, temperatures, pressures, electricity energy outputs and cell temperatures etc.

In addition, as a tradeoff between the lumped model that has larger error and detailed distributed model that has larger computation demand, an approximate analytical solution for the distributed dynamic model is developed. The objectives can be summarized below:

- Modeling the dynamics of SOFC;
- Simulations and investigations of dynamic properties;

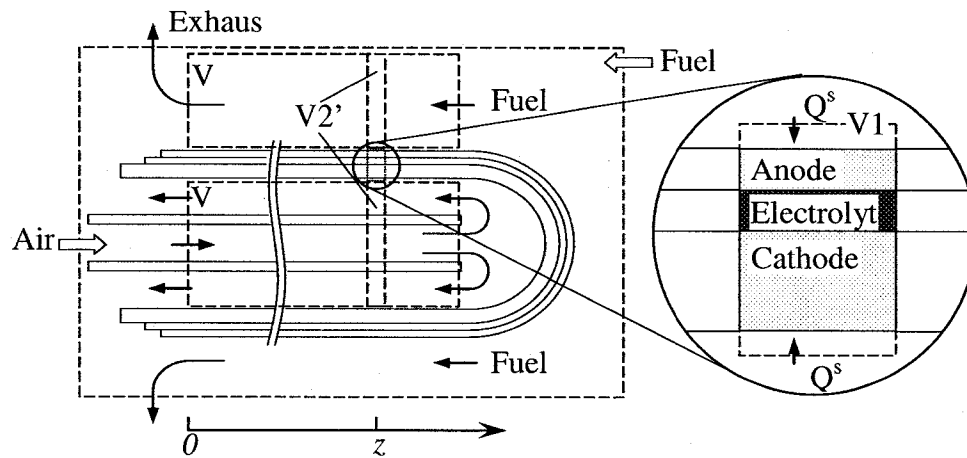


Figure 1.3: Mass transport to reaction sites and control volumes for a SOFC tube

- Approximate analytical solution for 1-D dynamic model;
- Development of control relevant state space models.

1.5 Approach

1.5.1 Methodology

From the entrance, fuel and air must pass through three stages to reach the reaction sites in each cell tube: 1) flow from entrance to flow bulk upon tubes; 2) pass through tubes; 3) diffuse from flow bulk to reaction sites; as shown in Fig.1.3.

Input flow rates are controllable and diffusions determine the electricity output directly. The flow bulk upon the tube connects the input flows and diffusions. These three stages affect each other. The modeling of SOFC is divided into four main phases at different levels of complexity:

1. Modeling the behavior of diffusion and the behavior of electrochemical reaction in the control volume V1, as shown in Fig.1.3.
2. Modeling the heat transfer dynamics in the same control volume V1.
3. Modeling the dynamic mass transport and heat transfer in gas flow in control volume V2'.

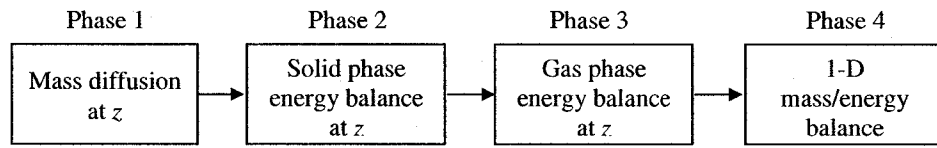


Figure 1.4: Flow chart of the modeling

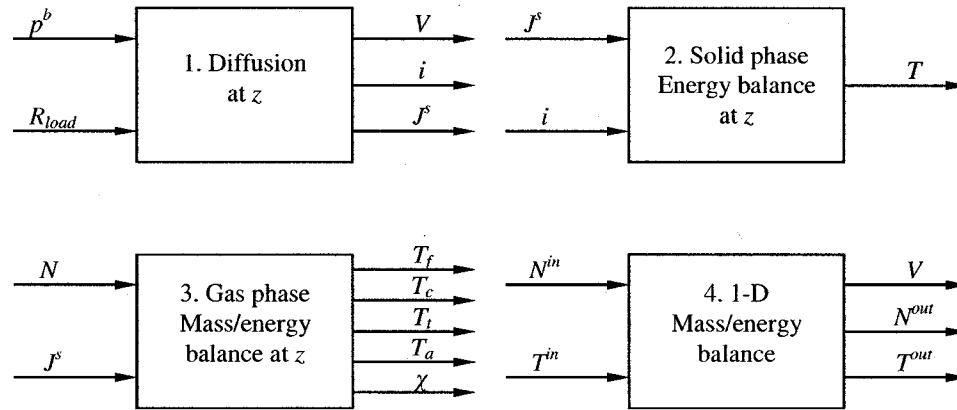


Figure 1.5: Schematic input/output of each phase modeling

- Combining and then expanding the models for the control volume V1 and V2 into the 1-D mass/energy balance dynamic model along the z-axis.

The flow chart of the different phases of modeling is shown in Fig.1.4. The schematic input/output of each model is shown in Fig.1.5.

1.5.2 Tools

To handle the transient behaviors, one of the most important mathematical tools is the Laplace transform. It can convert models from time domain to frequency domain, and convert the partial differential equations (PDE) to ordinary differential equations (ODE).

To develop and solve equations, a useful software is **Maple**, which can perform symbolic calculations and is particularly useful for computations related to Laplace operator. The main simulation platform for the dynamic models is **Matlab**.

1.6 Outline

The thesis is divided into 6 chapters including this chapter according to different research phases. Chapter 2 to 5 provide details in each of the four phases of model developments. This thesis has been written in the format in accordance with the rules and regulations of the Faculty of Graduate Studies and Research, University of Alberta. Some chapters have been published in journals and conference proceedings. In order to link the different chapters, there is some overlap and redundancy of material. This has been done to ensure completeness and cohesiveness of the thesis material and help the reader understand the material easily. A summary of each chapter follows:

1. Dynamic effects led by diffusion and inherent impedance are modeled and investigated through simulations in Chapter 2.
2. Chapter 3 models the dynamics induced by mass/heat/momentum transport processes. Dynamic properties are investigated through simulations.
3. The dynamic model is expanded to a 1-D dynamic model in chapter 4. An approximate analytical solution to 1-D reacting gas flow problem is developed and applied to the dynamic 1-D SOFC model.
4. A low order dynamic model developed for control application is discussed in Chapter 5.
5. Chapter 6 concludes the thesis with a summary of main contributions and future work.

Due to proprietary reasons, SOFC manufacturers do not provide experiment data or the provided data are incomplete, especially the dynamic data. Thus experiment data rarely appear in the literature. In fact, the experiment studies have indicated that the repeatability of SOFC data is low at this stage of SOFC development. This thesis has thus employed validation for the developed models whenever it is feasible and as the best as we can. All validations are performed in accordance with common practice in SOFC literature.

This research aims to exploring and understanding the complex dynamic behavior of SOFC, by considering underlying first-principle mechanisms. Thus calibrating a model to fit experiment data is not within the scope of this thesis.

2

The Effect of Diffusion and Inherent Impedance

With the aim of dynamic simulation and control, a cell-level nonlinear state-space dynamic model of SOFC based on physical principles is built. It demonstrates that reactant diffusion processes from gas flow bulks to triple phase boundaries (*tpb*) play an important role in the dynamic behaviors of SOFC. The simulation shows that under certain condition, the effect of the double layer capacitance may be neglected. The phenomenon of slow rise of voltage in current interrupt experiment may be explained by the dynamic behaviors of partial pressures in the vicinity immediately above *tpbs*. A new equivalent circuit is proposed. Based on the new equivalence circuit, the phenomenon of current overshoot is predicted.¹

keywords:

SOFC, dynamic modeling, simulation, diffusion, impedance

¹A version of this chapter was published in the Journal of Power Sources, 150(2005), 32-47

2.1 Introduction

SOFC is a type of fuel cells identified as the likely fuel cell technologies that will capture the most significant market in the future. SOFC uses a special solid oxide cermet (mostly yttria-stabilized zirconia YSZ) as the electrolyte and usually works at a high temperature, in the range of 800 – 1000°C to reach the electrolyte's ionic conductivity requirement. A large amount of literature has been published about SOFCs as well as other fuel cells. Most of the work has focused on investigating static electrochemical characteristics, such as reaction mechanisms, state-of-the-art cell components, new materials, etc. For the purpose of dynamic simulation and control, the dynamic characteristics of fuel cell must be understood. In this chapter, a dynamic model of SOFC at cell-level is proposed to investigate the dynamic properties of fuel cells.

Early macro dynamic modeling of SOFC was performed by Achenbach (1994; 1995). He examined the transient cell voltage performance of a cross flow planar SOFC cell due to the temperature changes and the perturbations in current density.

The dynamic model given by Padullés *et al.* (2000) included the species dynamics on stack-level the first time. Zhu and Tomsovic (2001) adopted Padullés *et al.*'s (2000) model for analyzing the load-following performance of micro turbines and fuel cells. Sedghisigarchi and Feliachi (2004) combined Achenbach's (1994) heat transfer dynamics and Padullés *et al.*'s (2000) species dynamics, and simulated dynamic responses of SOFC. However, in these models, only lumped dynamic behavior of species along the fuel/air channel is considered. The processes of species transport from flow bulk to triple-phase-boundary (*tpb*) have not been considered.

The model proposed in this chapter is a cell-level species dynamic model. It lies between micro and macro scale. Because behavior of stack is determined by that of cells, the cell-level model is a building block for a stack-level model. Dynamic behaviors of voltage, current, gas consumption rates controlled by different load and partial pressures are demonstrated through simulations.

The remainder of this chapter is organized as follows: the principle of SOFC is discussed in section 2. The dynamic modeling is discussed in Section 3. Relational parameters are shown in Section 4. Simulation results and analysis are given in Section 5, followed by conclusions in Section 6.

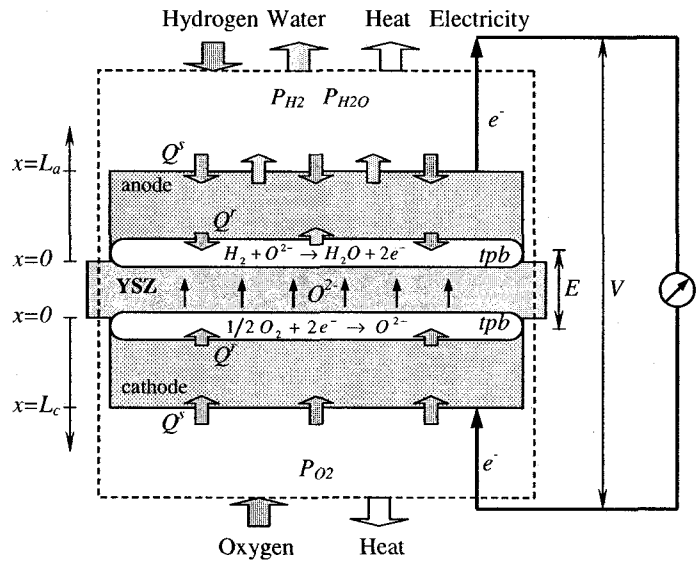
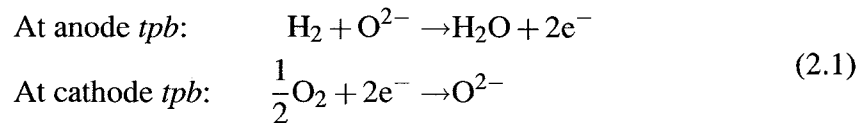


Figure 2.1: Principle of solid oxide fuel cell

2.2 Fuel cell principles

A typical $\text{H}_2 - \text{H}_2\text{O}, \text{Ni}|\text{YSZ}|\text{Pt}, \text{O}_2$ fuel cell is shown in Fig.2.1. The chemical reactions inside the cell that are directly involved in the production of electricity are:



2.2.1 Voltage output

In the ideal situation (reversible), electrical work is equal to the Gibbs free energy released $\Delta\bar{g}_f$, i.e.

$$\Delta\bar{g}_f = -2FE \tag{2.2}$$

The electromotive force (EMF) or reversible open circuit voltage E of the hydrogen fuel cell is given as:

$$E = \frac{-\Delta\bar{g}_f}{2F} \tag{2.3}$$

where F is Faraday constant.

Partial pressures or gas concentrations affect EMF through the Nernst equation

(Larminie and Dicks, 2003):

$$E = E^0 + \frac{RT}{2F} \ln \left(\frac{a_{\text{H}_2} \cdot a_{\text{O}_2}^{0.5}}{a_{\text{H}_2\text{O}}} \right) \quad (2.4)$$

where a_{H_2} , a_{O_2} and $a_{\text{H}_2\text{O}}$ are activities. If gases behave as ideal gases, the activities are:

$$a_{\text{H}_2} = \frac{p_{\text{H}_2}}{P^0}, \quad a_{\text{O}_2} = \frac{p_{\text{O}_2}}{P^0}, \quad a_{\text{H}_2\text{O}} = \frac{p_{\text{H}_2\text{O}}}{P_{\text{H}_2\text{O}}^0}$$

where p_{H_2} , p_{O_2} , and $p_{\text{H}_2\text{O}}$ are reactant partial pressures, P^0 is the standard pressure, $P_{\text{H}_2\text{O}}^0$ is the vapour pressure of the steam at the temperature concerned. E is also called Nernst voltage. If $P^0 = P_{\text{H}_2\text{O}}^0 = 1$, the equation can be simplified to:

$$E = E^0 + \frac{RT}{2F} \ln \left(\frac{p_{\text{H}_2} p_{\text{O}_2}^{\frac{1}{2}}}{p_{\text{H}_2\text{O}}} \right) \quad (2.5)$$

Irreversibilities reduce the cell's voltage. They are mainly activation loss, ohmic loss and concentration loss. The voltage is usually modeled in the steady state form (Larminie and Dicks, 2003):

$$V = E - iR_{\text{in}} - A \ln \left(\frac{i}{i_0} \right) - B \ln \left(1 - \frac{i}{i_l} \right) \quad (2.6)$$

where i is the current produced by the cell. R_{in} is the inherent resistance of the fuel cell. i_0 is the exchange current, an important parameter of weighting the activity of catalyst reaction. i_l is the limiting current, at which the fuel is used up at a rate equal to its maximum supply rate. A and B are coefficients. The second term in the equation represents the ohmic loss; the third term is activation loss and the fourth term represents the concentration loss.

2.2.2 Current output

Neglecting the transit dynamics of the reactions, the relation between current and reactions can be expressed as (Larminie and Dicks, 2003):

$$i = 2FJ_{\text{H}_2}^r = 2FJ_{\text{H}_2\text{O}}^r = 4FJ_{\text{O}_2}^r \quad (2.7)$$

where superscript r represents the fuel consumption or water vapor production rate at $tpbs$.

The maximum current that a cell can output is limited by several factors.

First, current output is limited by reaction rates and the area where reactions take place. In most cases, reactions are fast in anode. However, because cathode reaction is slow (Mitterdorfer and Gauckler, 1999c), current output is limited by the maximum ion production rate.

Second, current output is controlled by voltage and load impedance.

Third, maximum current is limited by ionic conductivity of electrolyte. It follows Ohm's law. The limitation resistance usually merged into the inherent impedance. In normal operating ranges, the reactions usually do not reach the limits mentioned before. Thus the current is determined mainly by Ohm's law.

The fourth one is reactant supply rates. In cell-level, they are controlled by concentration gradients between *tpbs* and gas flow bulks. When the current output increases, the hydrogen and oxygen concentrations at *tpbs* decrease to create larger concentration gradients. Once one of them decreases to zero, the supply rate reaches its maximum. Current can not be increased anymore, and it is the maximum current fuel cell can provide.

2.2.3 Dynamic process of fuel cell

When fuel gases are fed to cell, they must flow through the gas boundary layers, porous support layers and porous electrodes to *tpbs*, where reactions take place. Neglecting the reaction dynamics, these mass transport processes are the main dynamic sources of the fuel cells operated under the isothermal condition. The dynamics of fuel cell including rate determination steps etc. may be expressed by transfer function block diagram, shown in Fig.2.2.

Another important source that affects fuel cell's dynamic behavior is its inherent impedance. Fuel cell including SOFC's inherent impedance is well studied via electrochemical impedance spectroscopy (EIS) method (Macdonald, 1987; Mogensen and Skaarup, 1996; Wagner *et al.*, 1998; Jørgensen *et al.*, 1999; Barbucci *et al.*, 2002; Holtappels *et al.*, 2001; Jørgensen and Mogensen, 2001). They can be simplified as equivalent *RC* circuits. So the effect of inherent impedance to voltage and current dynamic behavior is similar to a *RC* filter.

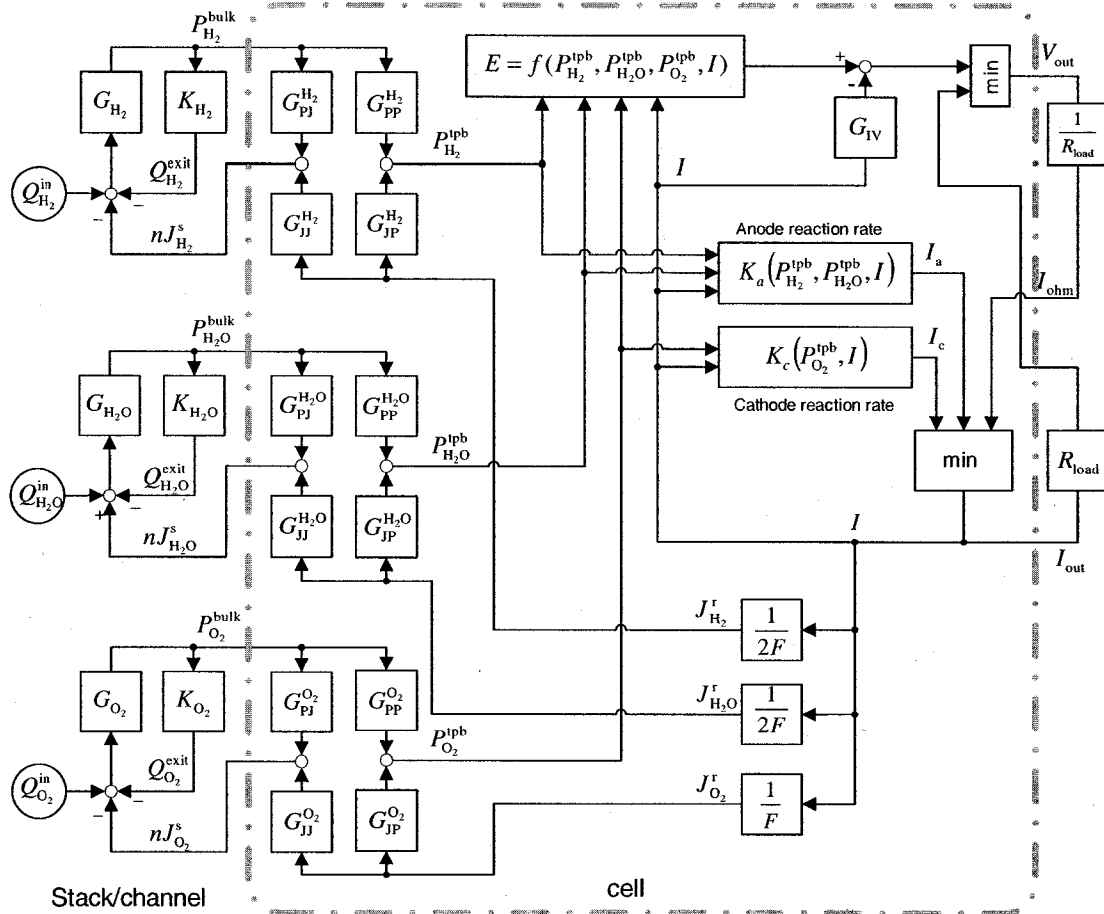


Figure 2.2: Schematic block diagram of fuel cell

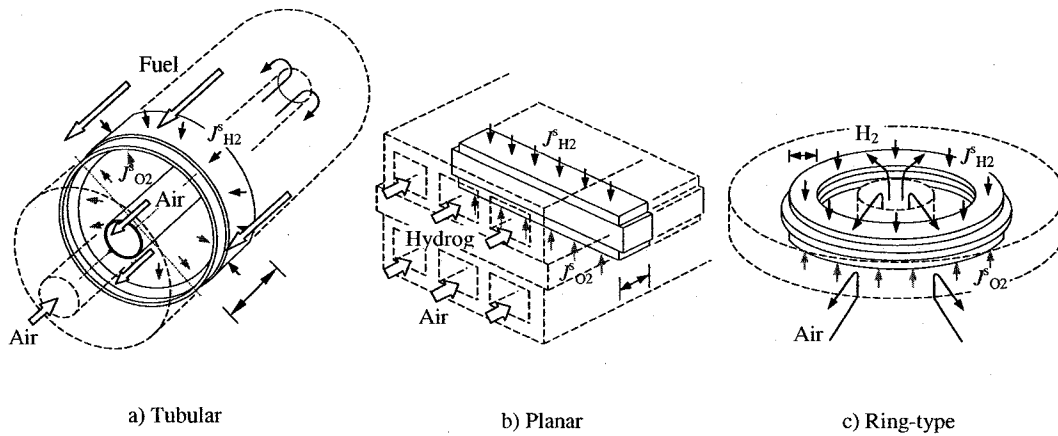


Figure 2.3: Definition of finite volume in different SOFC cells

2.3 Modeling approach

2.3.1 Assumptions

1. An elemental volume of $H_2 - H_2O, Ni|YSZ|LSM, air$ cell (Wagner *et al.*, 1998). The definition of the elemental volume in different SOFC cells is shown in Fig.2.3.
2. Cell's external load is a pure resistance.
3. Temperature is constant and uniform throughout the elemental volume.
4. Gas partial pressures in flow bulks surrounding the elemental volume are uniform.

2.3.2 I/O variables

The aim of the model to be developed is to describe the external characteristics. So input variables are related to inputs of SOFC. Output variables are cell's power outputs, such as voltage, current etc.

The first input variable is the external load. Under the normal operating conditions, it is external load that determines the current output i and so affects the reaction. Different load impedance affects the output properties in different way. In order to investigate the

Table 2.1: Input and output variables

Inputs	R_{load}	Load Resistance
	$p_{\text{H}_2}^{\text{b}}$	Partial pressure of hydrogen in anode gas bulk
	$p_{\text{O}_2}^{\text{b}}$	Partial pressure of oxygen in cathode gas bulk
	$p_{\text{H}_2\text{O}}^{\text{b}}$	Partial pressure of water vapor in anode gas bulk
Outputs	V_{out}	Voltage output of SOFC cell
	i	Current output of SOFC cell
	$J_{\text{H}_2}^{\text{s}}$	Hydrogen consumption rate of SOFC cell
	$J_{\text{O}_2}^{\text{s}}$	Oxygen consumption rate of SOFC cell
	$J_{\text{H}_2\text{O}}^{\text{s}}$	Hydrogen consumption rate of SOFC cell

basic dynamic behavior of the current output, load impedance is assumed to be a pure resistance R_{load} in the model.

Other input variables are partial pressures of reactants in gas bulks. They affect the reactant supplies and reaction rates directly. For a single cell under normal operating condition, reactant concentrations or partial pressures affect the diffusion processes and the Gibbs free energy, and thus the voltage. Therefore, other input variables are $p_{\text{H}_2}^{\text{b}}$, $p_{\text{H}_2\text{O}}^{\text{b}}$, and $p_{\text{O}_2}^{\text{b}}$.

Output variables of the model include potential difference exerted on the load resistance, V_{out} , current flow through the load resistance, i , H_2 and O_2 consumption rates, $J_{\text{H}_2}^{\text{s}}$, $J_{\text{O}_2}^{\text{s}}$, and water production rate $J_{\text{H}_2\text{O}}^{\text{s}}$.

2.3.3 Diffusion

The path of mass transport from the flow bulk to the reaction site involves two stages: First, from the flow bulk to the cell surface layer. Second, through the porous electrode to reaction sites (Campanari and Iora, 2004). In the first stage, mass flux diffuses through the boundary layer to the cell surface. In the second stage, mass flux diffuses inside the porous electrode. In all these two stages, diffusion is the main means of mass transport.

One of the most widely used diffusion models is Fick's law:

$$j = -D \frac{dC}{dx} \quad (2.8)$$

The mass transport equation can be written as:

$$\frac{\partial C}{\partial t} = -D \frac{\partial^2 C}{\partial x^2} \quad (2.9)$$

where C is mass concentration, D diffusion coefficient, A diffusion cross-sectional area, and x diffusion depth as defined in Fig.2.1.

Fick's law shows that concentration is dependent on diffusion thickness. In order to get the concentrations at $tpbs$, one usually applies the finite element method (Mitterdorfer and Gauckler, 1999a; Bieberle and Gauckler, 2000; Chan *et al.*, 2001; Chan and Xia, 2001; Chan *et al.*, 2004). However, by means of Laplace transform, the analytical dynamic relations can be expressed in the form of transfer functions without involving spatial variables.

Developing mass transport transfer function

Perform Laplace's transform on Eqn.2.9 to convert the partial differential equation to the ordinary differential equation (Wayland, 1957):

$$\frac{d^2 C(s)}{dx^2} + \frac{s}{D} C(s) = 0 \quad (2.10)$$

Boundary conditions are:

$$\begin{aligned} j^r(s) &= -D \frac{dC(s)}{dx} \Big|_{x=0} \\ C^b(s) &= C(s) \Big|_{x=l} \end{aligned} \quad (2.11)$$

Solving Eqn.2.10 yields:

$$\begin{aligned} C(s)(x) &= \frac{C^b(s) + \frac{j^r(s)}{\sqrt{Ds}} \exp(-\sqrt{\frac{s}{D}}l)}{\exp(\sqrt{\frac{s}{D}}l) + \exp(-\sqrt{\frac{s}{D}}l)} \exp(\sqrt{\frac{s}{D}}x) \\ &+ \frac{C^b(s) - \frac{j^r(s)}{\sqrt{Ds}} \exp(\sqrt{\frac{s}{D}}l)}{\exp(\sqrt{\frac{s}{D}}l) + \exp(-\sqrt{\frac{s}{D}}l)} \exp(-\sqrt{\frac{s}{D}}x) \end{aligned} \quad (2.12)$$

Assume that the gases are ideal gases and the flow area is A . At $tpbs$ where $x = 0$, the partial pressure in the vicinity of tpb is:

$$\begin{aligned} p^{tpb}(s) &= -\frac{\exp(\sqrt{\frac{s}{D}}l) - \exp(-\sqrt{\frac{s}{D}}l)}{\exp(\sqrt{\frac{s}{D}}l) + \exp(-\sqrt{\frac{s}{D}}l)} \frac{1}{\sqrt{Ds}} \frac{RT}{A} j^r(s) \\ &+ \frac{2}{\exp(\sqrt{\frac{s}{D}}l) + \exp(-\sqrt{\frac{s}{D}}l)} p^b(s) \end{aligned} \quad (2.13)$$

On the surface of the diffusion layer, mass flow rate is $J^s = AD \frac{dC}{dx} \big|_{x=l}$. The dynamic relation is:

$$J^s(s) = \frac{2}{\exp(\sqrt{\frac{s}{D}}l) + \exp(-\sqrt{\frac{s}{D}}l)} J^r(s) + \frac{\exp(\sqrt{\frac{s}{D}}l) - \exp(-\sqrt{\frac{s}{D}}l)}{\exp(\sqrt{\frac{s}{D}}l) + \exp(-\sqrt{\frac{s}{D}}l)} \sqrt{Ds} \frac{A}{RT} p^b(s) \quad (2.14)$$

Approximating mass transport transfer function

Taylor's expansions of $\exp(\sqrt{\frac{s}{D}}l)$ and $\exp(-\sqrt{\frac{s}{D}}l)$ at zero with respect to $\sqrt{\frac{s}{D}}l$ and $-\sqrt{\frac{s}{D}}l$ respectively are:

$$\begin{aligned} \exp(\sqrt{\frac{s}{D}}l) &= 1 + \sqrt{\frac{s}{D}}l + \frac{1}{2} \frac{s}{D} l^2 + \frac{1}{6} \frac{s^{\frac{3}{2}}}{D^{\frac{3}{2}}} l^3 + \frac{1}{24} \frac{s^2}{D^2} l^4 + O\left(\sqrt{\frac{s}{D}}l\right) \\ \exp(-\sqrt{\frac{s}{D}}l) &= 1 - \sqrt{\frac{s}{D}}l + \frac{1}{2} \frac{s}{D} l^2 - \frac{1}{6} \frac{s^{\frac{3}{2}}}{D^{\frac{3}{2}}} l^3 + \frac{1}{24} \frac{s^2}{D^2} l^4 + O\left(\sqrt{\frac{s}{D}}l\right) \end{aligned}$$

Substituting them into Eqn.2.13 and 2.14, and neglecting higher order term yield:

$$\begin{aligned} p^{tpb}(s) &= G_{Jp} J^r(s) + G_{pp} p^b(s) \\ J^s(s) &= G_{JJ} J^r(s) + G_{pJ} p^b(s) \end{aligned} \quad (2.15)$$

where:

$$\begin{aligned} G_{Jp} &= \frac{-\frac{l}{D} - \frac{l^3}{6D^2}s}{1 + \frac{l^2}{2D}s + \frac{l^4}{24D^2}s^2} \frac{RT}{A}, & G_{pp} &= \frac{1}{1 + \frac{l^2}{2D}s + \frac{l^4}{24D^2}s^2}, \\ G_{JJ} &= \frac{1}{1 + \frac{l^2}{2D}s + \frac{l^4}{24D^2}s^2}, & G_{pJ} &= \frac{ls}{1 + \frac{l^2}{2D}s + \frac{l^4}{24D^2}s^2} \frac{A}{RT}, \end{aligned}$$

p^{tpb} is partial pressure in the vicinity of $tpbs$, p^b partial pressure in gas bulks, J^s gas flow into the outer surface of porous material, J^r gas consumption or water production rate at $tpbs$, l layer thickness, A cell area, D effective diffusion coefficient, R gas constant, and T temperature. So dynamic behavior of partial pressures in the vicinity of $tpbs$ and gas flows at electrode surface can be determined uniquely by the behaviors of gas consumption rate and bulk pressure without relying on concentration distribution along the diffusion path.

In this dynamics description, only two parameters are involved. The first one is the thickness of the diffusion layer l . It depends on flow velocity, and can be calculated according to fluid mechanics. The second parameter is diffusion coefficient D . It can be calculated from correlation equations (Welty *et al.*, 1984).

Diffusion coefficient

In porous materials, the effective diffusion coefficient is adjusted by (Welty *et al.*, 1984):

$$D_{\text{eff}} = \frac{\varepsilon}{\tau} D \quad (2.16)$$

where ε is porosity, τ tortuosity of porous materials, and D total diffusion coefficient.

Considering the Knudsen diffusion, the total diffusion coefficient is (Welty *et al.*, 1984):

$$\frac{1}{D} = \frac{1}{D_{12}} + \frac{1}{D_k} \quad (2.17)$$

where D_{12} is binary diffusion coefficient, and D_k is Knudsen diffusion coefficient. If pores are large enough, Knudsen diffusion can be neglected (Welty *et al.*, 1984).

The binary diffusion coefficient D_{12} is modeled by the Fuller's correlation (Welty *et al.*, 1984):

$$D_{12} = \frac{1.013 \times 10^{-2} T^{1.75} \left(\frac{1}{M_1} + \frac{1}{M_2} \right)^{0.5}}{P \left[(\Sigma v_i)_1^{\frac{1}{3}} + (\Sigma v_i)_2^{\frac{1}{3}} \right]^2} \quad (2.18)$$

where T is the temperature, M_1 and M_2 are the mole mass of gas 1 and gas 2, $(\Sigma v_i)_1$ and $(\Sigma v_i)_2$ are the diffusional volumes of gas 1 and gas 2 respectively, and P is the total pressure. Good agreement between the Fuller's correlation and measurements has been reported in (Solheim, 1992).

2.3.4 Voltage

As described before, fuel cell's voltage output is affected by gas partial pressures and is reduced by concentration loss, activation loss and ohmic loss. The dynamic behavior of the voltage is also affected by these factors.

In fact, because reactions take place at *tpbs*, it is partial pressures in the vicinity of *tpbs* that affect the EMF. The more appropriate expression of Nernst equation should be:

$$E = E^0 + \frac{RT}{2F} \ln \left(\frac{p_{\text{H}_2}^{\text{tpb}} p_{\text{O}_2}^{\text{tpb} \frac{1}{2}}}{p_{\text{H}_2\text{O}}^{\text{tpb}}} \right) \quad (2.19)$$

where $p_{\text{H}_2}^{\text{tpb}}$, $p_{\text{O}_2}^{\text{tpb}}$, and $p_{\text{H}_2\text{O}}^{\text{tpb}}$ are partial pressures in the vicinity of *tpbs*.

The H_2/O_2 consumptions lead to their concentration reductions in the vicinity of $tpbs$. The voltage drop caused by this kind of concentration reductions is named as concentration loss in the literature and is usually corrected by a static concentration loss term.

The activation loss is the potential consumed to overcome the activation energy barrier. It is normally described by the Butler-Volmer correlation (Chan *et al.*, 2001):

$$i = i_0 \left\{ \exp \left(\beta \frac{nF\eta_{act}}{RT} \right) - \exp \left[-(1-\beta) \frac{nF\eta_{act}}{RT} \right] \right\} \quad (2.20)$$

where β is the transfer coefficient and i_0 the exchange current. The transfer coefficient is usually taken as 0.5 for the fuel cell application (Chan *et al.*, 2001).

When $\beta = 0.5$, the activation loss can be solved from Eqn.2.20:

$$\begin{aligned} \eta_{act,a} &= \frac{2RT}{nF} \sinh^{-1} \left(\frac{i}{2i_{0,a}} \right) \\ \eta_{act,c} &= \frac{2RT}{nF} \sinh^{-1} \left(\frac{i}{2i_{0,c}} \right) \end{aligned} \quad (2.21)$$

The exchange currents depend on the activation energy, temperature, and partial pressures. They can be calculated as (Campanari and Iora, 2004):

$$\begin{aligned} i_{0,a} &= 7 \times 10^9 A \left(p_{H_2}^{tpb} p_{H_2O}^{tpb} \right) \exp \left(-\frac{E_{act,a}}{RT} \right) \\ i_{0,c} &= 7 \times 10^9 A \left(p_{O_2}^{tpb} \right)^{0.25} \exp \left(-\frac{E_{act,c}}{RT} \right) \end{aligned} \quad (2.22)$$

where $E_{act,a}$, $E_{act,c}$ are anode and cathode activation energy respectively.

Compensating the activation loss, the irreversible voltage is:

$$E = E^0 + \frac{RT}{2F} \ln \left(\frac{p_{H_2}^{tpb} p_{O_2}^{tpb \frac{1}{2}}}{p_{H_2O}^{tpb}} \right) - \eta_{act,a} - \eta_{act,c} \quad (2.23)$$

with $E^0 = 1.273 - 2.7645 \times 10^{-4}T$ (Campanari and Iora, 2004).

2.3.5 Inherent impedance

When current flows through the inherent impedance, voltage is reduced. The voltage drop is called Ohmic loss. The dynamic characteristics of the inherent impedance also affect the dynamic voltage behavior of the fuel cell.

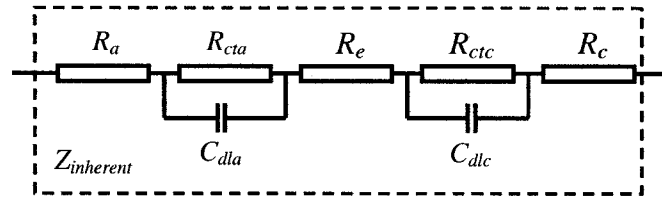


Figure 2.4: Equivalent circuit of inherent impedance

Inherent impedance of SOFC is complex. Basically, it consists of two charge capacitance processes and three resistance processes: anode charge double layer capacitance, cathode charge double layer capacitance, ohmic resistance, grain boundary resistances and electrode reaction resistances. Because their dynamic behaviors are similar to RC circuits, the inherent impedance is usually modeled as equivalent RC circuits. A typical equivalent circuit to inherent impedance is shown in Fig.2.4. Here R_e is the resistance of electrolyte, R_a and R_c represent the ohmic and grain boundary resistances of anode and cathode, R_{cta} and R_{ctc} represent the charge transfer resistances respectively, and C_{dla} and C_{dlc} represent the charge double layer capacitors between anode, cathode and electrolyte.

2.3.6 Equivalent circuit

Theoretically, impedance spectra plane plot indicates two semicircles for the impedance shown in Fig.2.4 (Macdonald, 1987). In SOFC, neglecting diffusion impedance, these two semicircles are merged to one distorted semicircle (Wagner *et al.*, 1998). This means that the whole inherent impedance can be approximated by one RC unit. In another aspect, potential difference is produced between *tpbs*, inside the two metal electrode layers, as shown in Fig.2.1. That means voltage fluctuation due to potential change is smoothed by the double layer capacitance. So a reasonable equivalent circuit of a SOFC cell is shown in Fig.2.5, where R_o is the total ohmic resistance in the inherent impedance, R_{ct} is the total charge transfer resistance, and C_{ct} is the approximated charge transfer capacitance. These three parameters can be identified from impedance spectral plan plot (Macdonald, 1987) or Bode plot (Wagner *et al.*, 1998).

This equivalent circuit is different from the one shown in (Larminie and Dicks, 2003), where the ideal battery is connected in serial with a RC pair. That equivalent circuit shows derivative effect on battery potential change. The derivative phenomenon on fuel cell has not been observed and reported in literature. The model shown in

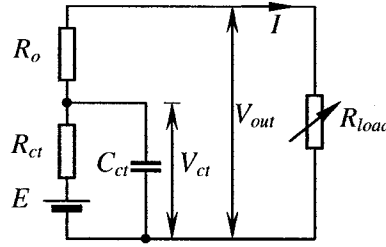


Figure 2.5: Equivalent circuit of a single fuel cell

Fig.2.5 is an integral circuit. It smooths the voltage output, and appears to be more reasonable.

The dynamic behavior of the voltage output based on the equivalent circuit is therefore determined by:

$$\begin{aligned} \dot{V}_{ct} &= \frac{1}{R_{ct}C_{ct}}E - \frac{1}{R_{ct}C_{ct}}V_{ct} - \frac{1}{C_{ct}}i \\ V_{out} &= V_{ct} - iR_o \\ i &= \frac{V_{ct}}{R_o + R_{load}} \end{aligned} \quad (2.24)$$

2.3.7 Model in the state space form

Converting the transfer function form of dynamic relations shown in Eqn.2.15 to differential equation form, the dynamic behaviors can be shown as:

Hydrogen consumption rate:

$$\dot{J}_{H_2}^s = -h_1 J_{H_2}^s - h_2 \dot{J}_{H_2}^s + h_1 J_{H_2}^r + h_3 \frac{A}{RT} \dot{p}_{H_2}^b, \quad (2.25)$$

and partial pressure in the vicinity of anode tpb :

$$\ddot{p}_{H_2}^{tpb} = -h_1 p_{H_2}^{tpb} - h_2 \dot{p}_{H_2}^{tpb} - h_4 \frac{RT}{A} J_{H_2}^r - \frac{4}{l_a} \frac{RT}{A} J_{H_2}^r + h_1 p_{H_2}^b \quad (2.26)$$

where $h_1 = \frac{24D_{H_2}^2}{l_a^4}$, $h_2 = \frac{12D_{H_2}}{l_a^2}$, $h_3 = \frac{24D_{H_2}^2}{l_a^3}$, $h_4 = \frac{24D_{H_2}}{l_a^3}$.

Oxygen consumption rate:

$$\dot{J}_{O_2}^s = -o_1 J_{O_2}^s - o_2 \dot{J}_{O_2}^s + o_1 J_{O_2}^r + o_3 \frac{A}{RT} \dot{p}_{O_2}^b, \quad (2.27)$$

and partial pressure in the vicinity of cathode tpb :

$$\ddot{p}_{O_2}^{tpb} = -o_1 p_{O_2}^{tpb} - o_2 \dot{p}_{O_2}^{tpb} - o_4 \frac{RT}{A} J_{O_2}^r - \frac{4}{l_c} \frac{RT}{A} J_{O_2}^r + o_1 p_{O_2}^b \quad (2.28)$$

where $o_1 = \frac{24D_{O_2}^2}{l_c^4}$, $o_2 = \frac{12D_{O_2}}{l_c^2}$, $o_3 = \frac{24D_{O_2}^2}{l_c^3}$, $o_4 = \frac{24D_{O_2}}{l_c^3}$.

Water vapor production rate:

$$\dot{J}_{H_2O}^s = -w_1 J_{H_2O}^s - w_2 \dot{J}_{H_2O}^s + w_1 J_{H_2O}^r + w_3 \frac{A}{RT} \dot{p}_{H_2O}^b, \quad (2.29)$$

and partial pressure in the vicinity of anode *tpb*:

$$\ddot{p}_{H_2O}^{tpb} = -w_1 p_{H_2O}^{tpb} - w_2 \dot{p}_{H_2O}^{tpb} - w_4 \frac{RT}{A} J_{H_2O}^r - \frac{4}{l_a} \frac{RT}{A} \dot{J}_{H_2O}^r + w_1 p_{H_2O}^b \quad (2.30)$$

where $w_1 = \frac{24D_{H_2O}^2}{l_a^4}$, $w_2 = \frac{12D_{H_2O}}{l_a^2}$, $w_3 = \frac{24D_{H_2O}^2}{l_a^3}$, $w_4 = \frac{24D_{H_2O}}{l_a^3}$.

First order derivative of an input variable can be approximated by (Seborg *et al.*, 1989):

$$sU(s) \approx K \left(1 - \frac{1}{\frac{1}{K}s + 1} \right) U(s) \quad (2.31)$$

in the differential equation form:

$$\begin{aligned} \dot{u} &= Ku - v \\ \dot{v} &= K^2 u - Kv \end{aligned} \quad (2.32)$$

where v is a intermediate variable. K is the approximation factor, usually greater than 10.

Define the input vector as:

$$\mathbf{u} = \left[R_{load} \quad p_{H_2}^b \quad p_{O_2}^b \quad p_{H_2O}^b \right]^T \quad (2.33)$$

output vector as:

$$\mathbf{y} = \left[V_{out} \quad i \quad J_{H_2}^s \quad J_{O_2}^s \quad J_{H_2O}^s \right]^T \quad (2.34)$$

Introduce intermediate variables v_{H_2} , v_{O_2} , v_{H_2O} , v_R and define states as:

$$\mathbf{x} = \left[V_{ct} \quad J_{H_2}^s \quad J_{H_2}^s \quad v_{H_2} \quad J_{O_2}^s \quad J_{O_2}^s \quad v_{O_2} \quad J_{H_2O}^s \quad J_{H_2O}^s \quad v_{H_2O} \quad p_{H_2}^{tpb} \quad \dot{p}_{H_2}^{tpb} \quad p_{O_2}^{tpb} \quad \dot{p}_{O_2}^{tpb} \quad p_{H_2O}^{tpb} \quad \dot{p}_{H_2O}^{tpb} \quad v_R \right]^T \quad (2.35)$$

Combine Eqs.23-32, the state-space model is given by:

Status:

$$\dot{x}_1 = \frac{1}{R_{ct}C_{ct}} E - \frac{1}{R_{ct}C_{ct}} x_1 - \frac{1}{C_{ct}} \frac{x_1}{u_1 + R_o}$$

$$\dot{x}_2 = x_3$$

$$\dot{x}_3 = -h_1 x_2 - h_2 x_3 + h_1 \frac{1}{2F} \frac{x_1}{u_1 + R_0} + h_3 \frac{A}{RT} (Ku_2 - x_4)$$

$$\dot{x}_4 = K^2 u_2 - K x_4$$

$$\dot{x}_5 = x_6$$

$$\dot{x}_6 = -o_1 x_5 - o_2 x_6 + o_1 \frac{1}{4F} \frac{x_1}{u_1 + R_0} + o_3 \frac{A}{RT} (Ku_3 - x_7)$$

$$\dot{x}_7 = K^2 u_3 - K x_7$$

$$\dot{x}_8 = x_9$$

$$\dot{x}_9 = -w_1 x_8 - w_2 x_9 + w_1 \frac{1}{2F} \left(\frac{-x_1}{u_1 + R_0} \right) + w_3 \frac{A}{RT} (Ku_4 - x_{10})$$

$$\dot{x}_{10} = K^2 u_4 - K x_{10}$$

$$\dot{x}_{11} = x_{12}$$

$$\dot{x}_{12} = -h_1 x_{11} - h_2 x_{12} - h_4 \frac{RT}{A} \frac{1}{2F} \frac{x_1}{u_1 + R_0} - \frac{RT}{A} \frac{4}{la} \frac{1}{2F} \left[\frac{\dot{x}_1}{u_1 + R_0} - \frac{x_1}{(u_1 + R_0)^2} (Ku_1 - x_{17}) \right] + h_1 u_2$$

$$\dot{x}_{13} = x_{14}$$

$$\dot{x}_{14} = -o_1 x_{13} - o_2 x_{14} - o_4 \frac{RT}{A} \frac{1}{4F} \frac{x_1}{u_1 + R_0} - \frac{RT}{A} \frac{4}{lc} \frac{1}{4F} \left[\frac{\dot{x}_1}{u_1 + R_0} - \frac{x_1}{(u_1 + R_0)^2} (Ku_1 - x_{17}) \right] + o_1 u_3$$

$$\dot{x}_{15} = x_{16}$$

$$\dot{x}_{16} = -w_1 x_{15} - w_2 x_{16} - w_4 \frac{RT}{A} \frac{1}{2F} \left(\frac{-x_1}{u_1 + R_0} \right) - \frac{RT}{A} \frac{4}{la} \frac{1}{2F} \left[-\frac{\dot{x}_1}{u_1} + \frac{x_1}{(u_1 + R_0)^2} (Ku_1 - x_{17}) \right] + w_1 u_4$$

$$\dot{x}_{17} = K^2 u_1 - K x_{17}$$

Outputs:

$$y_1 = x_1 - \frac{R_o}{u_1 + R_o} x_1$$

$$y_2 = \frac{x_1}{u_1 + R_o}$$

$$y_3 = x_2$$

$$y_4 = x_5$$

$$y_5 = x_8$$

or in a compact form:

$$\begin{aligned} \dot{\mathbf{x}} &= f(\mathbf{x}, \mathbf{u}) \\ \mathbf{y} &= g(\mathbf{x}, \mathbf{u}) \end{aligned} \tag{2.36}$$

2.4 Parameters

This state space model involves several parameters. Numerical values and their sources are listed in Table 2.2. These are default parameters for the simulation. In the validation of the model, using the available data in the literature we will compare with in the following simulations.

2.5 Simulation results

Simulation is done according to the developed state-space model. Steady state and transient behaviors of SOFC at different inputs and disturbances are investigated through the simulation.

2.5.1 Steady state output and model validation

Direct dynamic data that is useful for the validation of the developed model are not available in the literature. We will therefore validate the model according to the static experiment results shown in (Wagner *et al.*, 1998) and (Tsai and Barnett, 1997) respectively.

Table 2.2: Parameters used in simulation

Symbol	Unit	Description	Source
$l_a = 1$	[mm]	Thickness of anode diffusion layer	V-I plot (Tsai and Barnett, 1997)
$l_c = 1$	[mm]	Thickness of cathode diffusion layer	V-I plot (Tsai and Barnett, 1997)
$A = 1$	[cm ²]	Fuel cell effective area	V-I plot (Tsai and Barnett, 1997)
$R_{ct} = 0.9$	[Ohm]	Charge transfer resistance	EIS test (Wagner <i>et al.</i> , 1998)
$R_o = 0.1$	[Ohm]	Ohmic resistance	EIS test (Wagner <i>et al.</i> , 1998)
$C = 300$	[μ F]	Charge transfer capacitance	EIS test (Wagner <i>et al.</i> , 1998)
$E_{act,a} = 110$	[kJ/mol]	Anode activation energy	(Campanari and Iora, 2004)
$E_{act,c} = 120$	[kJ/mol]	Cathode activation energy	(Campanari and Iora, 2004)
$\varepsilon = 0.4$		Porosity	(Welty <i>et al.</i> , 1984)
$\tau = 4$		Tortuosity	(Welty <i>et al.</i> , 1984)
$(\Sigma v_i)_{H_2} = 7.07$		Diffusional volume	(Welty <i>et al.</i> , 1984)
$(\Sigma v_i)_{H_2O} = 12.7$		Diffusional volume	(Welty <i>et al.</i> , 1984)
$(\Sigma v_i)_{O_2} = 16.6$		Diffusional volume	(Welty <i>et al.</i> , 1984)
$(\Sigma v_i)_{N_2} = 17.9$		Diffusional volume	(Welty <i>et al.</i> , 1984)
$T = 1223$	[K]	Work temperature	(Wagner <i>et al.</i> , 1998)
$p_{H_2}^b = 0.97$	[atm]	Input partial pressure	(Wagner <i>et al.</i> , 1998)
$p_{air}^b = 1$	[atm]	Cathode pressure	(Wagner <i>et al.</i> , 1998)
$p_{H_2O}^b = 0.03$	[atm]	Input partial pressure	(Wagner <i>et al.</i> , 1998)

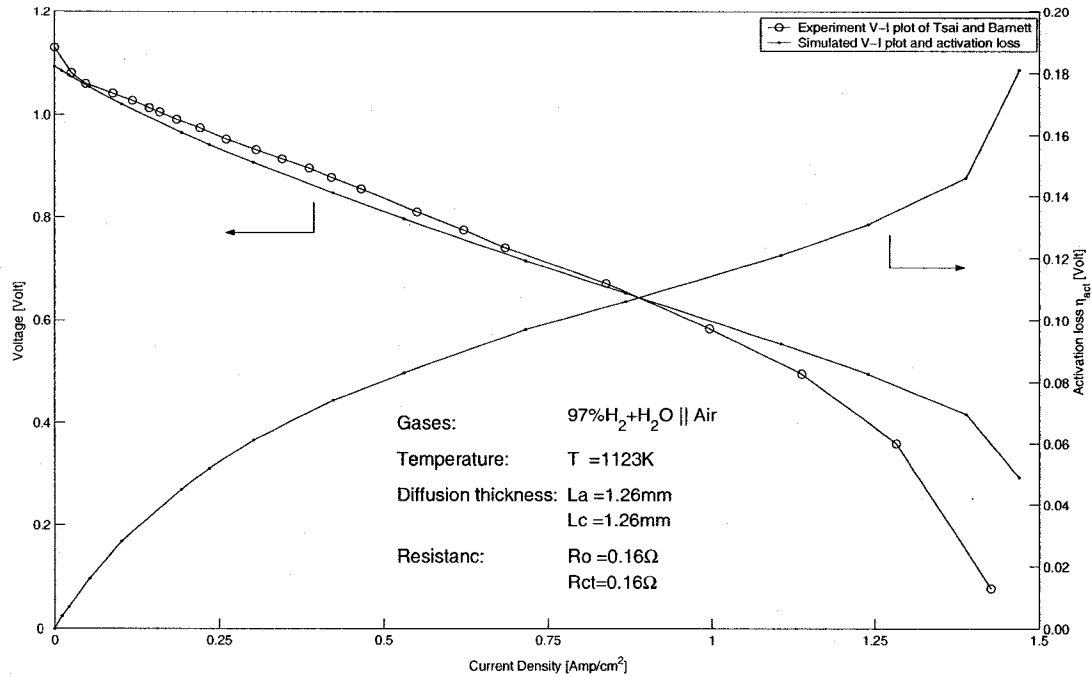


Figure 2.6: Comparison of simulated and experiment V-I plot

Wagner *et al.* (1998) investigated the effect of diffusion of SOFC, and the dynamic properties are shown by EIS Bode plot. Given 3% humidified H_2 , pure O_2 and infinite large load resistance R_{load} , at 1223K, the simulated steady state OCV is 1117mV. This is in a good agreement with measured OCV of 1114mV shown in (Wagner *et al.*, 1998) under the same condition. Because Wagner *et al.* did not present the thickness of diffusion layers, the experiment V-I plot can not be used to verify the dynamic model.

The comparison of the simulated steady state V-I outputs and the experiment result of Tsai and Barnett (1997) is shown in Fig.2.6.

Tsai and Barnett (1997) did not give the thickness of the diffusion layer directly. When i reaches the limiting current density i_l , at which the gas supply rate is maximum, thickness of the diffusion layer can be calculated by the relation:

$$i_l = 4FJ_{O_2}^r = 4FAD_{O_2} \frac{C^b - 0}{l_c} \quad (2.37)$$

Using Eqn.2.37, the thickness is calculated as $l_c = 1.26 \times 10^{-3}$ [m]. Because anode diffusion does not contribute to the limitation, the thickness in anode can not be calculated. l_a is assumed same as l_c in the simulation. The inherent resistance read from the EIS test of (Tsai and Barnett, 1997) is $R_o = 0.16[\Omega]$ and $R_{ct} = 0.16[\Omega]$ at

1123K

The V-I plot shows that the simulated result is overall in agreement with the experiment data with some error. A main reason for the error is the unavoidable model parameter error used in the simulation. They are collected from different sources and are dispersed in a wide range in different literatures.

2.5.2 Step responses due to R_{load} step changes

When load resistance has step changes, current will change immediately according to Ohm's law. Voltage drop on the pure ohmic inherent resistance R_o also changes at once. The result is an immediate rise of V_{out} . For the reason of charge transfer capacity, voltage drop on the charge transfer resistance R_{ct} changes slowly. V_{out} then rises slowly to the final value (Larminie and Dicks, 2003). But the fast initial response and slower response following the fast initial response as shown in Fig.2.7a can not be explained by the above discussion.

For the specific SOFC investigated by Wagner et al., the charge transfer capacity is around several hundred micro Farads (Wagner *et al.*, 1998). The charge transfer resistance is around 1 Ohm. So the time constant is less than 1 millisecond. The effect of charge transfer capacity can not be distinguished from the immediate rise of voltage. The fast initial response in Fig.2.7a is actually the summation of the changes of voltage drop on R_o and R_{ct} .

The slower response following the fast initial response is caused by the slow changes of concentration at the vicinity of *tpbs*. When J^r changes simultaneously with current change, p^{tpb} changes at a slow rate. The behaviors are determined by Eqn.2.26, Eqn.2.28 and Eqn.2.30. Thus, according to Nernst relation, E responses slowly to the new value. Assume the diffusion thickness $l_a = l_c = 1\text{mm}$, simulated time constant of the slower voltage response is around 0.02 second. It is in good agreement with the experiment results shown in (Wagner *et al.*, 1998). In which, a concentration impedance from 10Hz is observed in the EIS test Bode plot. The time constant is identified as 0.018 second.

The voltage output step response is similar to the current interrupt test result shown in (Larminie and Dicks, 2003), where the dynamic behavior of V_{out} is explained only by the charge transfer resistance and capacitance. Contributions from concentration changes in the vicinity of *tpbs* are not noticed. The simulation results show that it

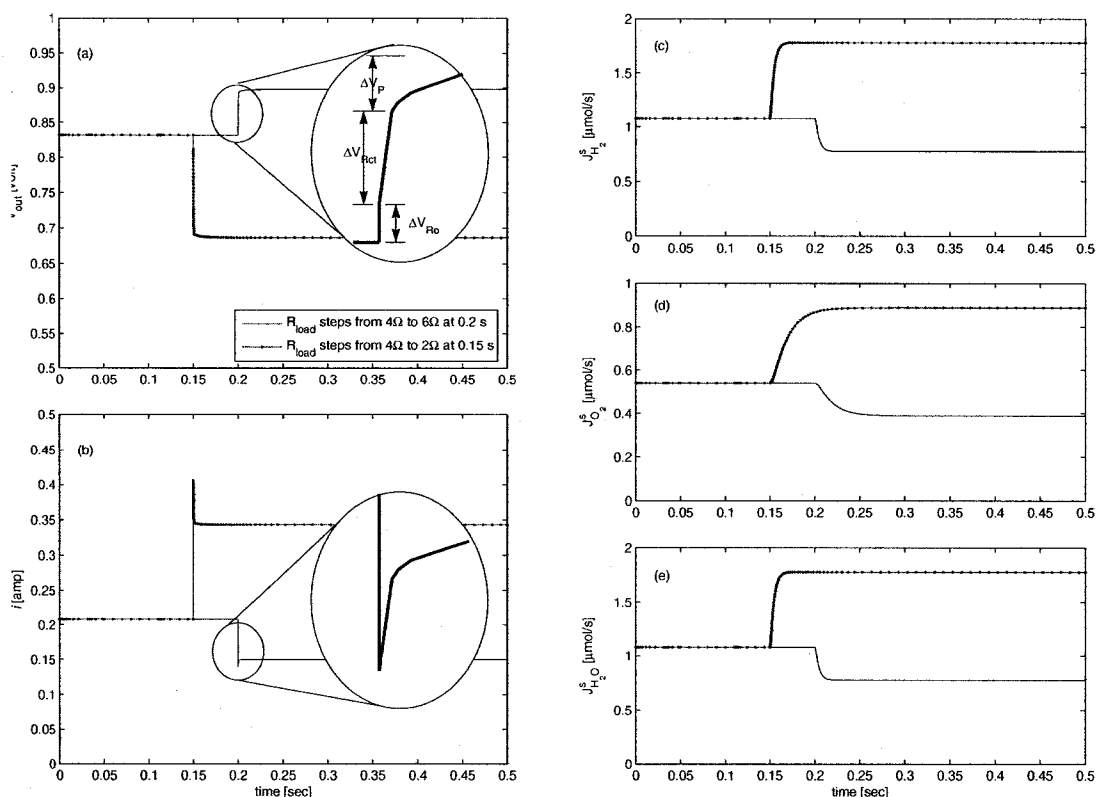


Figure 2.7: Step Responses of SOFC, when load resistance changes

is concentration changes in the vicinity of *tpbs* that are the main reason for the slow voltage rise behavior.

A noticeable phenomenon from the simulation is the step response of the current output, as shown in Fig.2.7b. It shows a significant overshoot when load resistance steps. The reason for such phenomenon is the charge transfer capacity. Some energy stored in the capacitance released suddenly when the balance is broken. The phenomenon is not reported in other literatures. It needs to be confirmed by experiments. The slow response of the current is mainly caused by the slow response of the voltage output. The result shows that the dynamic behavior of the current output is dependent on the properties of the load impedance.

Reactant consumption rates at diffusion layer surface respond at a slow rate, as shown in Fig.2.7c,d,e. Time constant of oxygen is different from that of hydrogen and water. This different response processes lead to different behaviors of reactant partial pressures in a fuel cell stack and in turn affect the electrical power output. The different

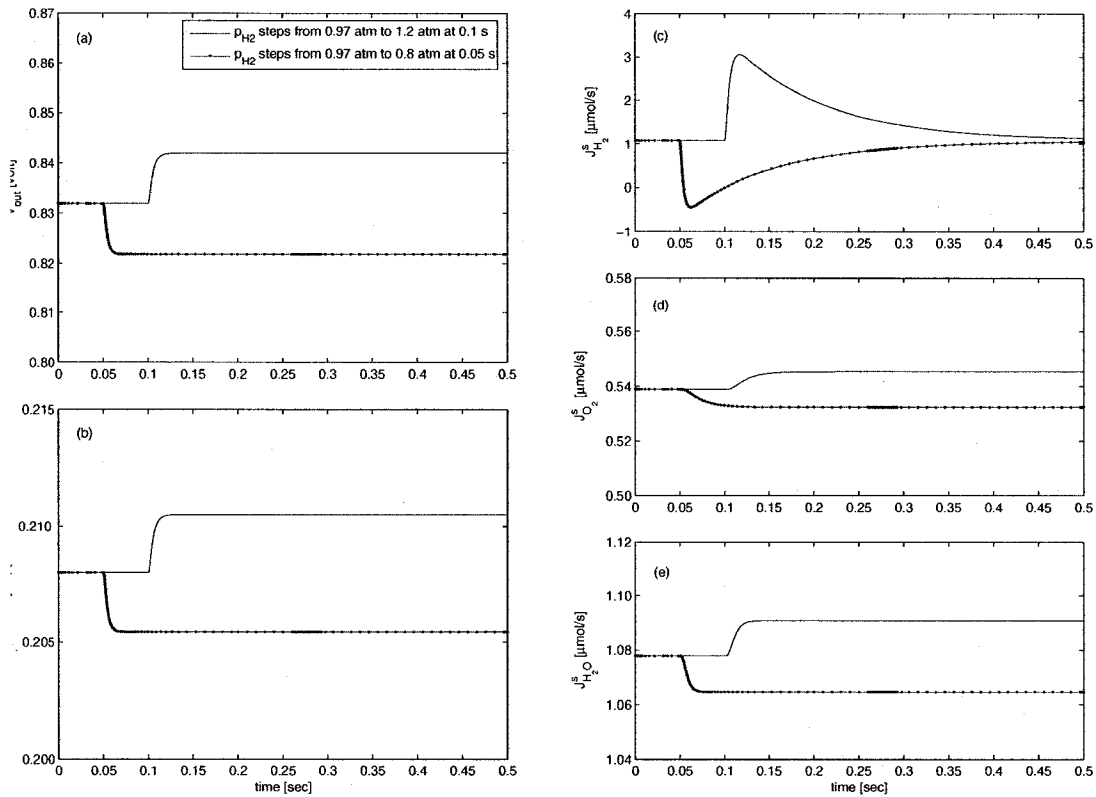


Figure 2.8: Step Responses of SOFC, when hydrogen pressure changes

transient responses will also lead to the change of pressure difference between anode side and cathode side. The reason for these slow dynamic responses is the existence of the diffusion layers. The diffusion layer plays a role like a buffer, which damps the response of fuel transportation to *tpbs*.

2.5.3 Reactant partial pressure disturbances

Partial pressure disturbances in gas bulk lead to electrical power output fluctuation and change the reaction rate. Step responses due to hydrogen, air, and water vapor pressures are shown in Fig.2.8, Fig.2.9, and Fig.2.10 respectively. Simulation results show that influences from pressure disturbances in gas bulks on voltage and current are relatively small. That is because the electrical power output is controlled mainly by reaction and load resistance, and the existence of the buffer effect of the diffusion layer.

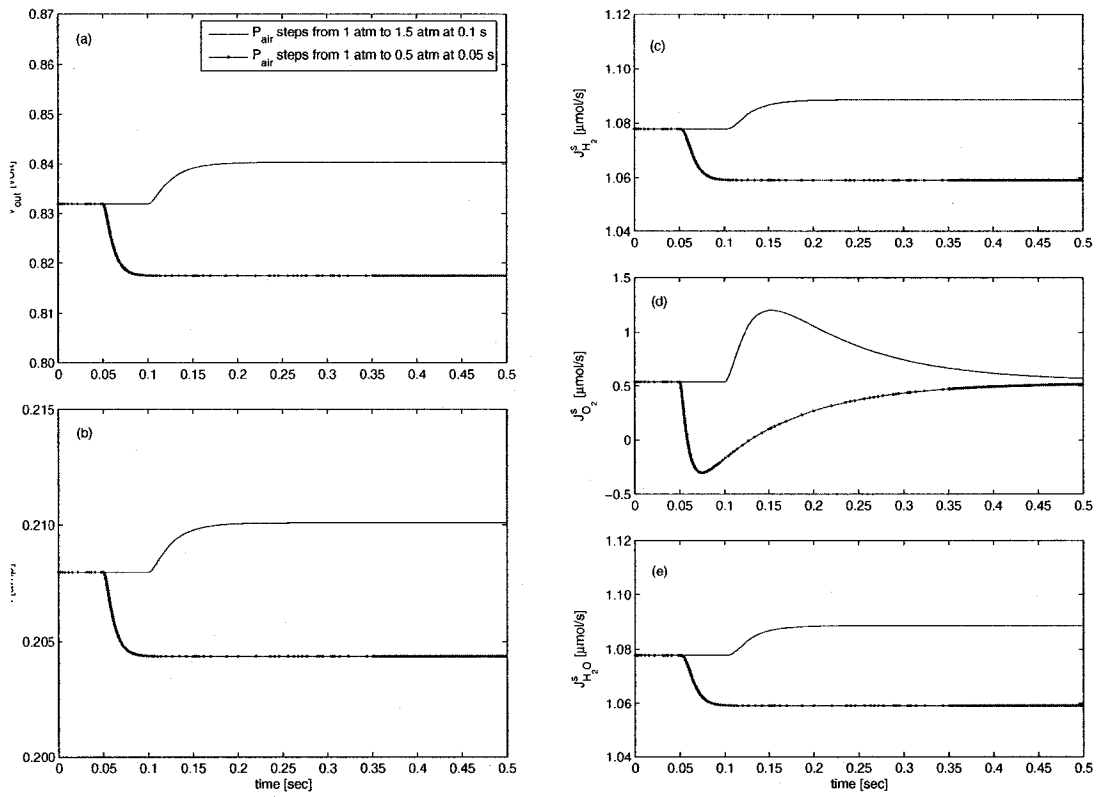


Figure 2.9: Step Responses of SOFC, when air pressure changes

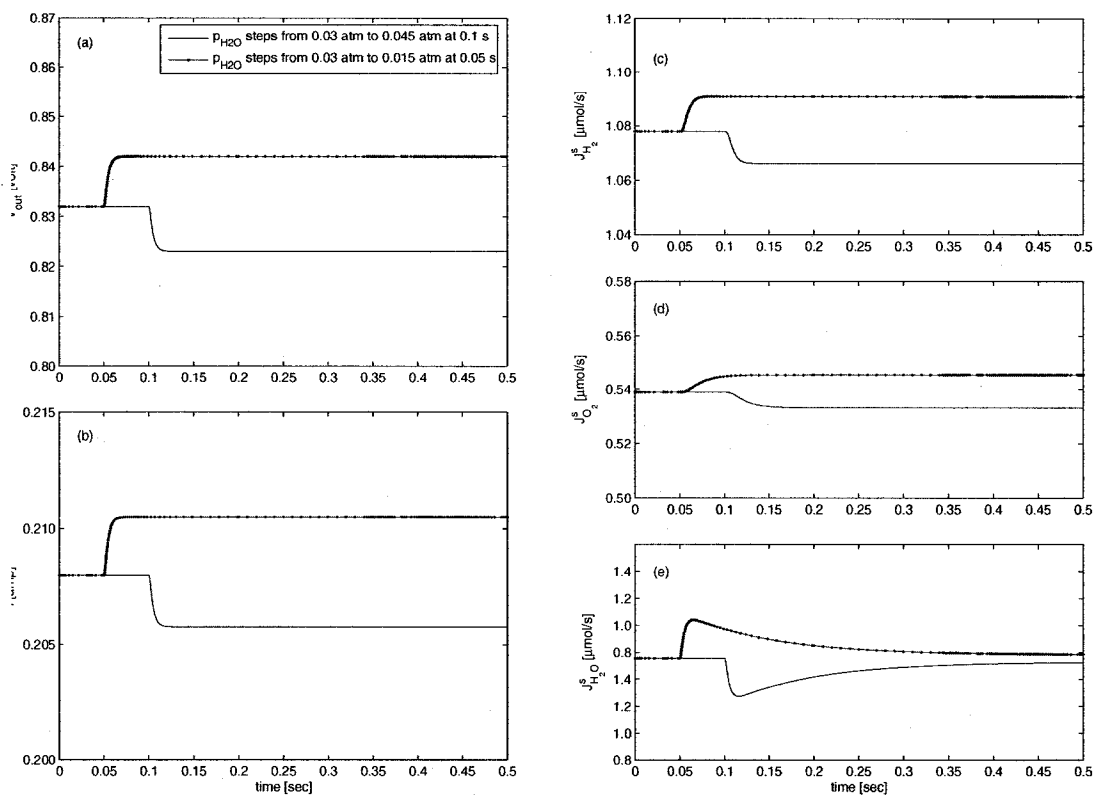


Figure 2.10: Step Responses of SOFC, when steam pressure in anode gas changes

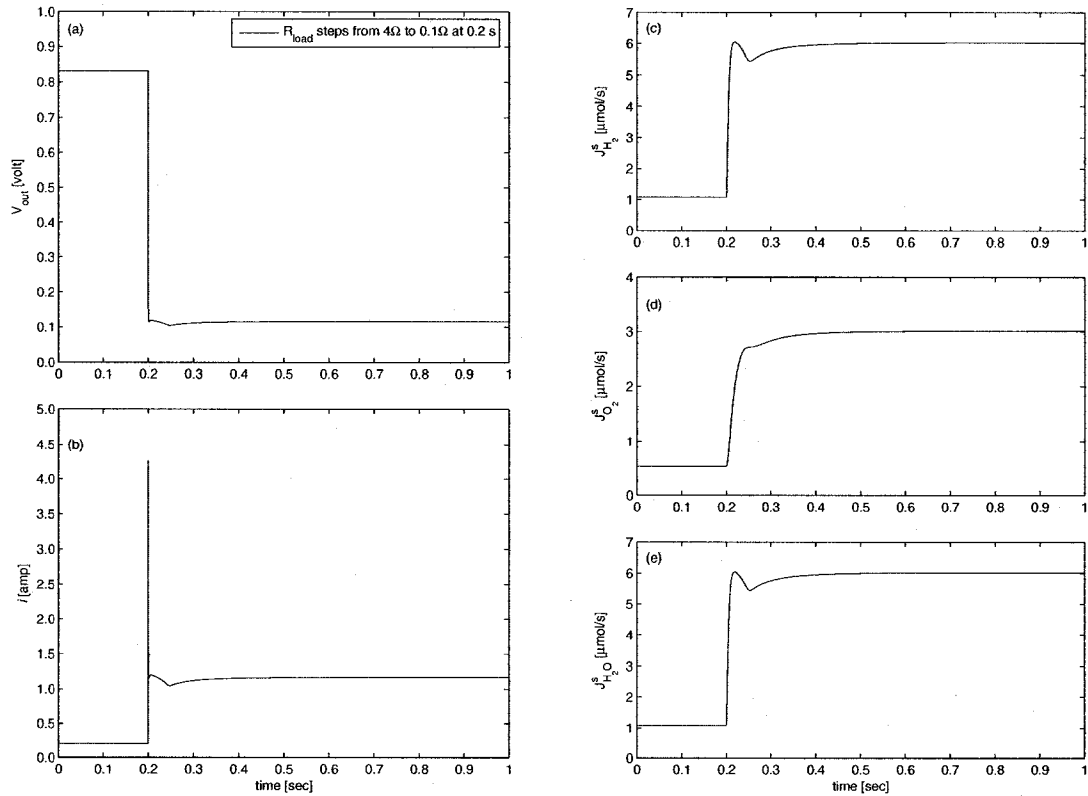


Figure 2.11: Step Responses of SOFC, when it enters concentration loss range

2.5.4 Effect of concentration loss

When load resistance moves to a small value, it leads SOFC to enter the concentration loss dominant region, the dynamic behaviors of SOFC is considerably different from that in ohmic loss range, as shown in Fig.2.11. The transient response processes behave a high order dynamics.

Simulation result shows that in the air fuelled SOFC, it is the oxygen supply that is the main resource of the concentration loss. Because oxygen fraction in air is only around 21%. Oxygen supply also plays the main role in the dynamic behavior of SOFC, since its diffusion coefficient is smaller than that of hydrogen and water.

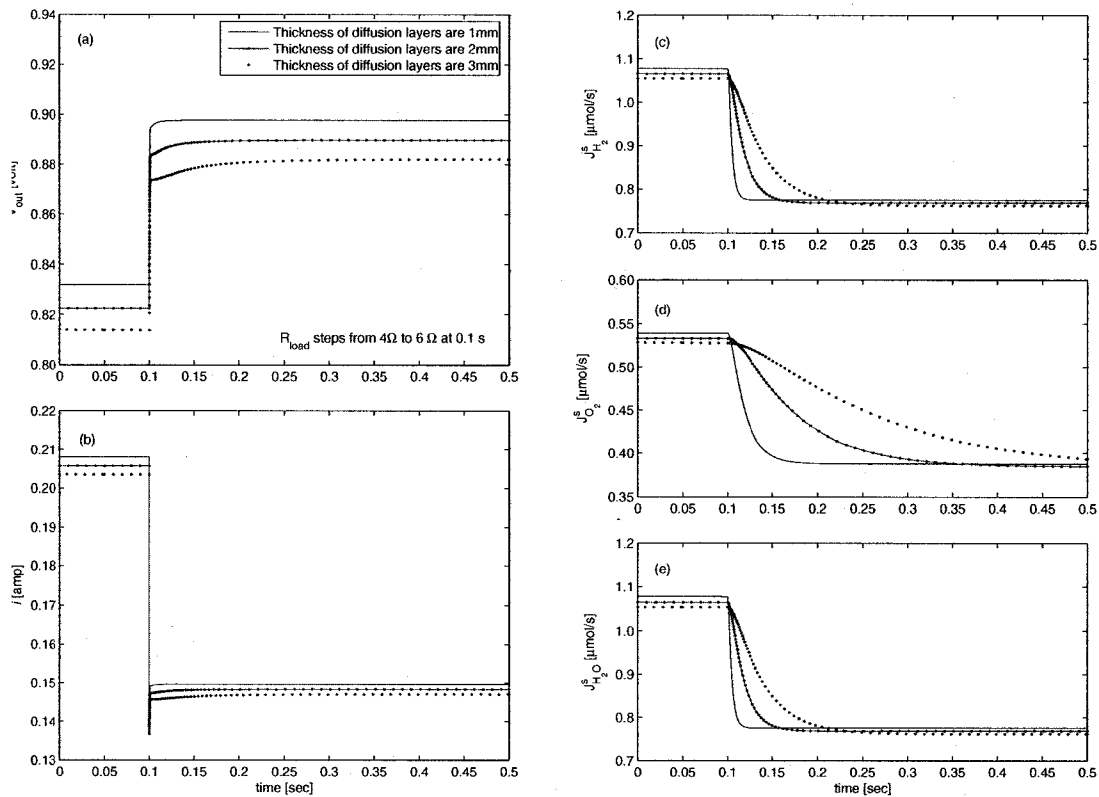


Figure 2.12: Effect of diffusion layer thickness on step responses of SOFC

2.5.5 Effect of diffusion layers

Simulation result shows that the thickness of the diffusion layer has strong effect on properties of SOFC. With the increasing of the thickness, time constants of the dynamics increase. The resistance from diffusion also increases. The effect is shown in Fig.2.12

Diffusion layers in fuel cell consist of not only electrode layer, but also boundary layer. The thicknesses are affected by the status of flow bulks, especially the flow velocity. So the thicknesses of diffusion layers may vary within a large range.

2.5.6 Effect of temperature

Given different temperatures, the simulation shows that compared to its effect on SOFC's dynamics, temperature has larger effect on the voltage output, as shown in

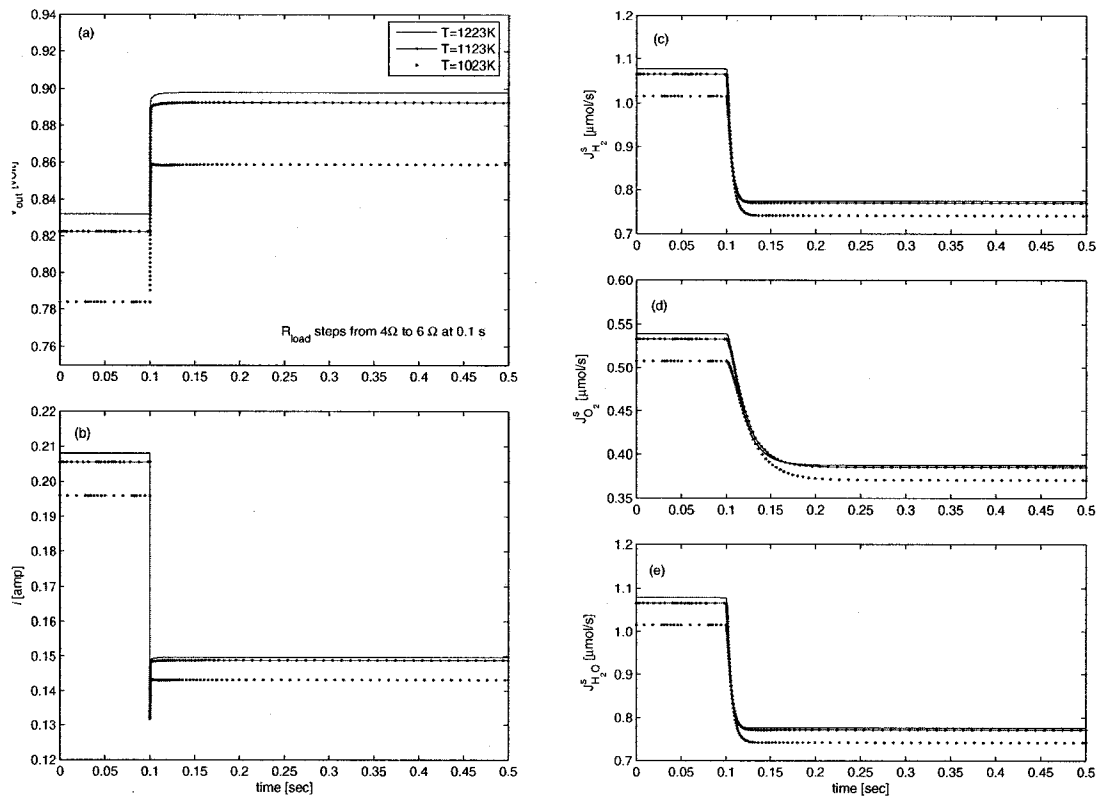


Figure 2.13: Effect of temperature on step responses of SOFC

Fig.2.13.

Temperature affects the Gibb's free energy $\Delta\bar{g}_f$, and thus Nernst voltage. It also affects the conductivity of electrolyte, electrodes and connectors. Simulation shows that the effect of temperature on Gibb's free energy and the Nernst voltage is much larger than on other factors.

As shown in Fig.2.13, the effect of temperature on the transient property of the diffusion response is negligible.

2.6 Conclusion

A dynamic model of solid oxide fuel cell (SOFC) with a focus on the diffusion process at cell-level is derived in the chapter. The species dynamics is built in the form of state-space model. Dynamic properties of SOFC are shown through simulations. It

demonstrates that diffusion processes in porous layers play an important role in the dynamic behavior of SOFC. They affect concentrations in the vicinity of triple phase boundary (*tpb*), and thus the electrical properties.

Simulation shows that it is the dynamic behavior of partial pressures in the vicinity of *tpbs* contribute more to the slow rise of voltage in the step response test and current interrupt experiment, not the charge transfer capacitance. Based on the equivalent circuit of SOFC, the phenomenon of current overshoot is observed through the simulation. Given different diffusion thicknesses, it is found that the voltage output and dynamic behavior of gas consumption rates are affected greatly by the thicknesses of the diffusion layers. Simulations also indicates that temperature has large effect on the voltage output.

3

The effect of transport dynamics

A first principles dynamic model for a finite volume of cell is built in the form of a nonlinear state-space model to investigate dynamic behaviors of tubular SOFC. Dynamic effects induced by diffusions, inherent impedance, fluid dynamics, heat exchange and direct internal reforming/shifting (DIR) reactions are all considered. Cell temperature, ingredient mole fractions etc. are the state variables and their dynamics are investigated. Dynamic responses of each variable when the external load changes are simulated. Simulation results show that fuel flow, inlet pressure and temperature have significant effects on the dynamic performance of SOFC. Further it is shown that, compared to other inlet flow properties, cathode side air inlet temperature has the most significant effect on SOFC solid phase temperature and performance. Compared with inlet pressures and temperatures, the effect of flow velocity is not significant. Simulation also indicates that the transient response of SOFC is controlled mainly by the dynamics of cell temperature owing to its large heat capacity.¹

keywords:

SOFC, dynamic modeling, simulation, heat transfer, mass transfer, reforming/shifting

¹A version of this chapter was published in the Chemical Engineering Science, 61(2006), 6057-6076

3.1 Introduction

SOFC works at high temperature, in the range of 800 – 1000°C to reach the required high electrolyte ionic conductivity. The high temperature means that feed gases such as natural gas can be used directly, or “internally reformed” within the fuel cell, without the need for a separate unit. It also means that SOFC’s exhaust gases and heat can be recycled, leading to a higher energy conversion efficiency. Considerable amounts of research and development work have been devoted to SOFC, making the SOFC close to wide commercial applications. For the purpose of dynamic control and simulation, the dynamic characteristics of SOFC must be understood and modeled.

Besides lumped parameter approaches (Achenbach, 1994; Achenbach, 1995; Padullés *et al.*, 2000; Zhu and Tomsovic, 2001; Sedghisigarchi and Feliachi, 2004), Xue *et al.* (2005) and Gemmen and Johnson (2005) considered more detailed mass transfer dynamics induced by flow processes. Iora *et al.* (2005) included species dynamics caused by internal reforming/shifting reactions. However, none of these models considered the dynamics led by fluid dynamics and consequent energy and mass transfer, as well as the dynamics of diffusion and inherent impedance.

In this chapter, we will develop a model to simulate the mass /energy /momentum transport dynamics including the internal reforming/shifting reactions for tubular SOFC. When combined with the dynamic models developed in Chapter 2, the model developed in this chapter forms a nonlinear state-space model with 28 states. Dynamic behaviors of SOFC will then be investigated and demonstrated through simulations.

Fuel cell processes are complex and involve almost all transport phenomena such as mass, energy and momentum. How these transport processes interact, especially how they dynamically affect each other and which process plays the dominant role, have not yet been fully elucidated. The main objective of this work is to investigate these interactions, with the objective of enhancing understanding of the macroscopic dynamic performance of the fuel cell. To this end, the approach we have taken is to focus on a finite volume of SOFC. This volume can be chosen to be sufficiently small so that the properties within this volume can be considered uniform. By doing so, we can neglect the effect of geometry and focus on chemical process. Modeling a finite slice of SOFC must be achieved first to enable development of a model for comprehensive fuel cell dynamics. The work described here thus provides a foundation for further development of the complete dynamic model in which we will consider the effect of geometry.

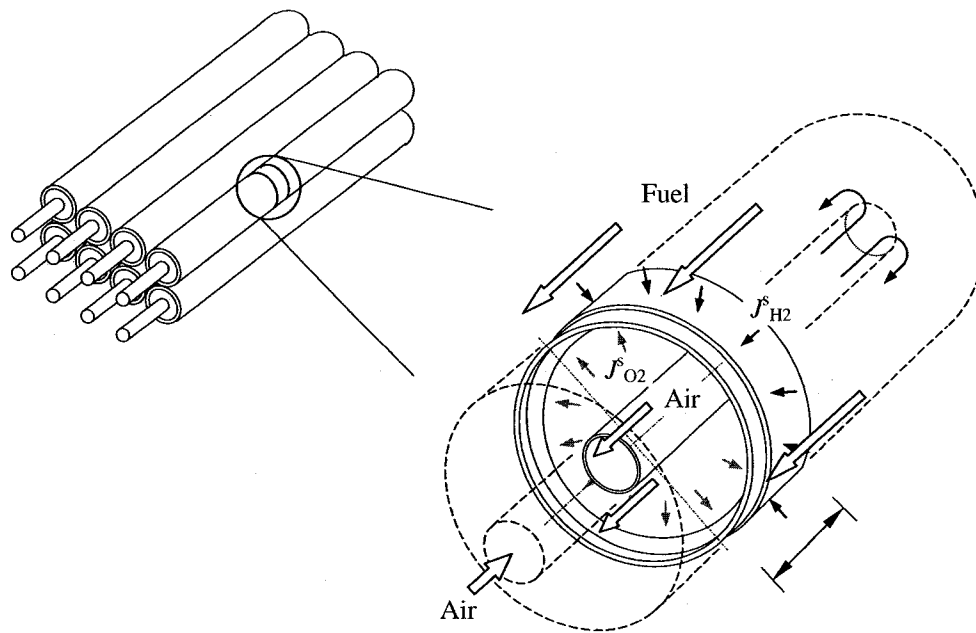


Figure 3.1: Tubular SOFC design of Siemens-Westingshouse

The remainder of this chapter is organized as follows: Analysis and modeling of dynamics are discussed in section 2. The nonlinear state-space model is derived in section 3. Dynamic behaviors through simulation are studied in section 4, and conclusions are presented in section 5.

3.2 Modeling of SOFC

3.2.1 Introduction to tubular SOFC

The strength and durability of materials limit the mechanical properties of SOFC component materials. Consequently, the practical and successful SOFC developed by Siemens-Westingshouse is tubular in design. Their SOFC stack consists of hundreds of similar cell tube composites. Each composite consists of two tubes, cell tube and injection tube, as shown in Fig.3.1.

The outer tube is the SOFC cell. It is an air-electrode-support (AES) tube, onto which the electrolyte is deposited, followed by the anode. The inner tube is the air injection and guidance tube, made of alumina, from which, pre-heated air injected

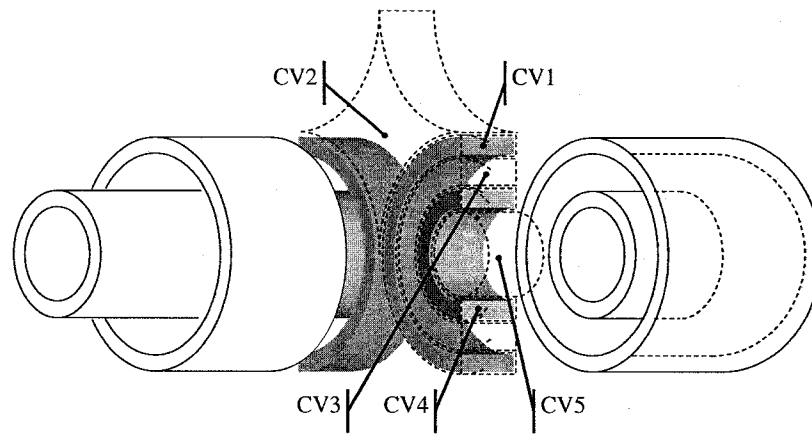


Figure 3.2: Definition of control volumes

into the bottom of the cell tube flows over the cathode surface of cell through the gap between the injection tube and cell tube. Fuel gas flows over the anode surface through the gaps among cell composites.

3.2.2 Modeling assumptions

In this chapter we will investigate dynamic effect of mass transfer and energy transfer on cell voltage and focus on a finite volume of the cell. The dimensions of the fuel cell slice are selected to be small enough so that properties such as temperature, pressure can be assumed uniform.

The slice is divided into five control volumes as shown in Fig.3.2. Control volume 1 (CV1) encloses the cell tube slice, CV2 the fuel flow in the anode side flow channel, CV3 the air flow in the cathode side air flow channel, CV4 the injection tube, and CV5 the air flow inside the injection tube.

Li and Chyu's (2003) numerical simulation shows that inside each control volume the property gradients such as pressure, temperature are not significant, and so the following assumptions can be made:

1. Flow velocities are the average velocity along radius direction.
2. Partial pressures, temperatures and flow velocities in each control volumes are uniform, whether in the axial direction or in the radial direction.

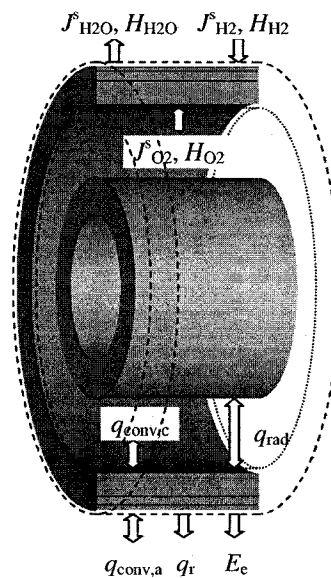


Figure 3.3: Mass and energy balance on CV1

3. Outlet partial pressures, temperatures, and velocities are equal to the pressures, temperatures and velocities inside the control volume.
4. Specific properties such as conductivities, heat capacities, viscosities, and densities etc. are uniform in each control volumes.
5. The external load is pure resistance.

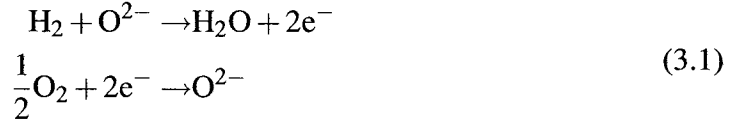
3.2.3 Modeling for CV1

CV1 encloses the SOFC cell tube slice, anode, cathode, electrolyte and inter-connector. Fuel and oxygen diffuse across control surfaces and enter the control volume. Through electrochemical reactions, part of the chemical energy converts to electrical energy and supplies the external demand, while the other part is converted to heat energy and released to the surroundings of the control volume, as shown in Fig.3.3, according to the laws of mass and energy conservation.

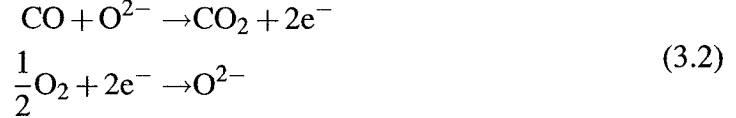
Electricity conversion dynamics

Chemical energy is converted to electrical energy through electrochemical reactions.

Conversion of hydrogen:



Conversion of CO:



Continuous electrons flow is necessary to maintain continuous electricity output. That is, reactants are consumed continuously and have to be replenished continuously from surroundings. Therefore, fuel cell's porous electrode layers, inherent impedance and the double layer capacity all affect the behaviors of the voltage V_{out} , the current i , and the reactant flows, J_i^s , diffusing into electrodes.

Diffusion

Given boundary conditions and the thickness of the diffusion layer l , the dynamic correlations among the partial pressures in the immediate vicinity of the triple phase boundary (*tpb*) p^{tpb} , in the main flow body p^b , mass consumption rate measured at the control surface J^s , and at the reaction site J^r can be described and modeled in the form of transfer functions developed in Chapter 2:

$$\begin{aligned} p^{tpb}(s) &= G_{Jp}J^r(s) + G_{pp}p^b(s) \\ J^s(s) &= G_{JJ}J^r(s) + G_{pJ}p^b(s) \end{aligned} \quad (3.3)$$

where:

$$\begin{aligned} G_{Jp} &= \frac{-\frac{l}{D} - \frac{l^3}{6D^2}s}{1 + \frac{l^2}{2D}s + \frac{l^4}{24D^2}s^2} \frac{RT}{A}, & G_{pp} &= \frac{1}{1 + \frac{l^2}{2D}s + \frac{l^4}{24D^2}s^2}, \\ G_{JJ} &= \frac{1}{1 + \frac{l^2}{2D}s + \frac{l^4}{24D^2}s^2}, & G_{pJ} &= \frac{ls}{1 + \frac{l^2}{2D}s + \frac{l^4}{24D^2}s^2} \frac{A}{RT}, \end{aligned}$$

and s is the Laplace operator. The correlations can then be converted to time dependent ordinary differential equations (ODE) as shown in Chapter 2.

Electromotive Force (EMF)

Fuel cell voltage output is affected by gas partial pressures and is reduced by concentration loss, activation loss and ohmic loss. The dynamic behavior of the voltage is also affected by these factors.

Because reactions take place at *tpbs*, it is partial pressures in the vicinity of *tpbs* that affect the electromotive force (EMF). The appropriate expression of the Nernst equation is (Qi *et al.*, 2005):

$$E = E^0 + \frac{RT}{2F} \ln \left(\frac{P_{\text{H}_2}^{\text{tpb}} P_{\text{O}_2}^{\text{tpb} \frac{1}{2}}}{P_{\text{H}_2\text{O}}^{\text{tpb}}} \right) \quad (3.4)$$

Activation loss can be evaluated from the Butler-Volmer correlation using the partial pressures in the immediate vicinity of *tpb* (Qi *et al.*, 2005).

Impedance

Based on the equivalent circuit approximation of the intrinsic impedance, the dynamic behavior of the voltage output can then be determined by (Qi *et al.*, 2005):

$$\begin{aligned} \dot{V}_{\text{ct}} &= \frac{1}{R_{\text{ct}} C_{\text{ct}}} E - \frac{1}{R_{\text{ct}} C_{\text{ct}}} V_{\text{ct}} - \frac{1}{C_{\text{ct}}} i \\ V_{\text{out}} &= V_{\text{ct}} - i R_{\text{o}} \\ i &= \frac{V_{\text{ct}}}{R_{\text{o}} + R_{\text{load}}} \end{aligned} \quad (3.5)$$

Heat transfer dynamics

Through the electrochemical reaction, Gibbs free energy is converted to electrical energy and the balance of the enthalpy of formation is released as reaction heat. Simultaneously, part of electrical energy is consumed by the SOFC's inherent resistance and converted to heat. Due to temperature differences between CV1 and its surroundings, heat is exchanged through forced convection, radiation and conduction, etc. The electrical energy is exported to the external load.

Therefore, in accord with the 1st law of thermodynamics, the internal energy accumulation rate in CV1 can be written as:

$$m_{\text{cell}} C_{p,\text{cell}} \frac{dT}{dt} = \sum J_i^s H_i - E_e - q_{\text{conv},a} - q_{\text{conv},c} - q_{\text{rad}} - q_{\text{ref}} \quad (3.6)$$

where $\sum J_i^s H_i$ is the summation of enthalpies flowing in and out of the control volume, E_e is electrical power that the control volume supplies to external load, $q_{\text{conv},a}$ and $q_{\text{conv},c}$ are heat flow exchanged through convection with anode and cathode side flow respectively, q_{rad} is heat flow exchanged through radiation, and q_{ref} is heat adsorbed by the reforming reaction, which will be discussed in the next section.

Enthalpy

The effect of pressure on the enthalpy of formation for a ideal gas can be neglected (Smith and Ness, 1987). However temperature has a significant effect, as shown using the model in Appendix II.

If only hydrogen is involved in the anode electrochemical reaction, the enthalpies of formation flow in and out of the control volume are given by:

$$\sum J_i^s H_i = J_{\text{H}_2}^s H_{\text{H}_2}|_{T_{\text{fuel}}} + J_{\text{O}_2}^s H_{\text{O}_2}|_{T_{\text{air}}} + J_{\text{H}_2\text{O}}^s H_{\text{H}_2\text{O}}|_{T_{\text{cell}}} \quad (3.7)$$

where $J_{\text{H}_2}^s$, $J_{\text{O}_2}^s$ and $J_{\text{H}_2\text{O}}^s$ are mass flow rates flowing into CV1.

Electrical power

The electrical power output of the SOFC slice is given by:

$$E_e = V_{\text{out}} i = \frac{V_{\text{out}}^2}{R_{\text{load}}} \quad (3.8)$$

Conduction

Heat flow exchanged through conduction is given by (Welty *et al.*, 1984):

$$q_{\text{cond}} = -k_{\text{cell}} A \frac{dT_{\text{cell}}}{dz} \quad (3.9)$$

where k_{cell} is thermal conductivity of SOFC slice, A is the cross-section area of the slice, and T_{cell} is the temperature.

For a tubular design, the present simulation shows that k_{cell} and A_{cell} are much smaller than the heat transfer efficiency of forced convection and radiation, q_{cond} is less than one tenth of q_{conv} or q_{rad} , and so the net conductive loss for the control volume is relatively minor. The effect of q_{cond} can be neglected in this model, as is consistent with prior models (Rao, 2001).

Convection

Because fuel gas and air flow through the surface of the SOFC slice, forced convection becomes an important heat transfer means, and is expressed as (Welty *et al.*, 1984):

$$q_{\text{conv}} = hA(T_w - T_f) \quad (3.10)$$

where h is the heat transfer coefficient, A is the area of the SOFC slice, T_w is the temperature of the solid wall, and T_f is the temperature of the fluid.

The heat transfer coefficient h depends on a number of properties of the flow bulk. It can be calculated by empirical correlations using the dimensionless Nusselt Number Nu , Reynolds Number Re and Prandtl Number Pr . The Nusselt Number is defined as (Welty *et al.*, 1984):

$$Nu = \frac{hD_f}{k_f} \quad (3.11)$$

where D_f is hydraulic diameter of the flow bulk, k_f is thermal conductivity of the flow bulk, and h is the heat transfer coefficient. These three numbers are interrelated (Welty *et al.*, 1984):

$$\begin{aligned} \text{Laminar flow : } Nu &= 0.332Pr^{\frac{1}{3}}Re^{\frac{1}{2}} \\ \text{Turbulent flow : } Nu &= 0.023Pr^{\frac{1}{3}}Re^{0.8} \end{aligned} \quad (3.12)$$

Thus the heat transfer coefficient can be determined by:

$$h = Nu \frac{k_f}{D_f} \quad (3.13)$$

For the SOFC slice that we have considered, there are two independent convective processes, one at the anode and one at the cathode. For the designed inlet parameters shown in Table.A-1, the Reynolds numbers are 66 and 287 for the respective compartments, so flow is laminar in each volume.

Substituting for the Reynolds number and Prandtl number, the heat transfer coefficients can be calculated as:

$$h = 0.332 \frac{k_f}{D_f} \left(\frac{C_{v,f} \mu_f}{k_f} \right)^{\frac{1}{3}} \left(\frac{D_f M_f}{\mu_f} \right)^{\frac{1}{2}} \left(\frac{u_f P_f}{RT_f} \right)^{\frac{1}{2}} \quad (3.14)$$

Consequently, heat exchange flows through forced convection are:

$$\begin{aligned} q_{\text{conv,a}} &= f_a \left(\frac{u_{\text{fuel}} P_{\text{fuel}}}{RT_{\text{fuel}}} \right)^{\frac{1}{2}} A (T_{\text{cell}} - T_{\text{fuel}}) \\ q_{\text{conv,c}} &= f_c \left(\frac{u_{\text{air}} P_{\text{air}}}{RT_{\text{air}}} \right)^{\frac{1}{2}} A_2 (T_{\text{cell}} - T_{\text{air}}) \end{aligned} \quad (3.15)$$

where:

$$\begin{aligned} f_a &= 0.332 \frac{k_{\text{fuel}}}{D_a} \left(\frac{C_{v,\text{fuel}} \mu_{\text{fuel}}}{k_{\text{fuel}}} \right)^{\frac{1}{3}} \left(\frac{D_a M_{\text{fuel}}}{\mu_{\text{fuel}}} \right)^{\frac{1}{2}} \\ f_c &= 0.332 \frac{k_{\text{air}}}{D_c} \left(\frac{C_{v,\text{air}} \mu_{\text{air}}}{k_{\text{air}}} \right)^{\frac{1}{3}} \left(\frac{D_c M_{\text{air}}}{\mu_{\text{air}}} \right)^{\frac{1}{2}} \end{aligned}$$

Change of fuel mixture composition due to the direct internal reforming and shift reactions (DIR) changes properties such as heat transfer coefficients. The parameters are thus weighted averages of those for each component:

$$k_{\text{fuel}} = \sum \chi_i k_i, C_{v,\text{fuel}} = \sum \chi_i C_{v,i}, \mu_{\text{fuel}} = \sum \chi_i \mu_i, M_{\text{fuel}} = \sum \chi_i M_i \quad (3.16)$$

where χ is the mole fraction and i represents the species H_2 , H_2O , CH_4 , CO , and CO_2 .

Radiation

Radiation is an important heat exchange mechanism in SOFC, because the cell operates at high temperature. The radiation heat flow is proportional to T^4 . The radiation flux emitted by a real body at absolute temperature T is (Welty *et al.*, 1984):

$$q = \varepsilon E_b = \varepsilon \sigma T^4 \quad (3.17)$$

where ε is emissivity of the real body, which lies between zero and unity, and σ is the Stefan-Boltzmann constant.

Neighboring tubes in the tubular SOFC stack have the same dimensions and arrangements of cell tubes in the stack are symmetric. Hence we can assume that their surface temperatures are essentially similar, so the net radiation heat flow transfer between outer surfaces (anode side) of cells is close to zero. Fuel and air are almost transparent; therefore the radiation absorbed by fuel/air flows can be neglected. The main radiation heat flow takes place between the cell tube and the alumina air injection tube. The net radiation heat flow between the cell tube and the injection tube is given by (Welty *et al.*, 1984):

$$q_{\text{rad}} = \frac{\sigma}{R_{\text{rad}}} A_2 (T_{\text{cell}}^4 - T_{\text{tube}}^4) \quad (3.18)$$

R_{rad} is radiation heat transfer resistance and can be calculated as (Welty *et al.*, 1984):

$$R_{\text{rad}} = \frac{1 - \varepsilon_{\text{cell}}}{\varepsilon_{\text{cell}}} + \frac{1}{F_{c-t}} + \frac{1 - \varepsilon_{\text{tube}}}{\varepsilon_{\text{tube}}} \frac{A_2}{A_1} \quad (3.19)$$

where $\varepsilon_{\text{cell}}$ and $\varepsilon_{\text{tube}}$ are emissivity of the cell and the injection tube respectively, F_{c-t} is view factor from the cell to the injection tube, and A_1 , A_2 are outer surface area of the injection tube and inner surface area of the cell respectively.

The view factor from surface A_1 to A_2 is expressed as (Welty *et al.*, 1984)

$$F_{A_1-A_2} = \frac{1}{A_1} \int_{A_1} \int_{A_2} \frac{\cos \theta_1 \cos \theta_2}{\pi r^2} dA_2 dA_1 \quad (3.20)$$

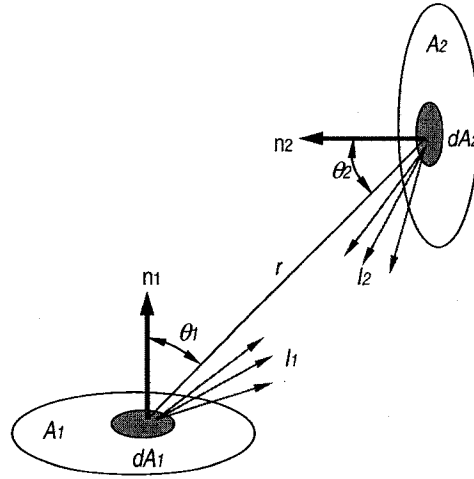


Figure 3.4: Definition of view factor

where A_1, A_2 are area of surface 1 and 2, and other parameters are as shown in Fig.3.4.

For the tubular SOFC design, the view factor from the inner surface of the cell to the outer surface of the injection tube can be determined by (Perry *et al.*, 1997):

$$F_{c-t} = \frac{r_{t,outer}}{r_{c,inner}} \quad \text{when } \frac{\text{length}}{r_{c,inner}} \rightarrow \infty \quad (3.21)$$

Substituting Eqn.3.7,3.8,3.15,3.18 into Eqn.3.6, we get the model which describes the dynamics of SOFC cell temperature:

$$\begin{aligned} m_{\text{cell}} C_{p,\text{cell}} \frac{dT}{dt} = & J_{\text{H}_2}^s H_{\text{H}_2} |_{T_{\text{fuel}}} + J_{\text{O}_2}^s H_{\text{O}_2} |_{T_{\text{air}}} + J_{\text{H}_2\text{O}}^s H_{\text{H}_2\text{O}} |_{T_{\text{cell}}} - \frac{V_{\text{out}}^2}{R_{\text{load}}} \\ & - f_a \left(\frac{u_{\text{fuel}} P_{\text{fuel}}}{RT_{\text{fuel}}} \right)^{\frac{1}{2}} A (T_{\text{cell}} - T_{\text{fuel}}) \\ & - f_c \left(\frac{u_{\text{air}} P_{\text{air}}}{RT_{\text{air}}} \right)^{\frac{1}{2}} A_2 (T_{\text{cell}} - T_{\text{air}}) \\ & - \frac{\sigma}{R_{\text{rad}}} A_2 (T_{\text{cell}}^4 - T_{\text{tube}}^4) - q_{\text{ref}} \end{aligned} \quad (3.22)$$

3.2.4 Modeling for CV2

CV2 encloses fuel gas in the fuel flow channel, as shown in Fig.3.5. Pre-reformed gas mixture flows into CV2 and continues the reforming and shift reactions with the catalytic aid of the Ni component of the anode. Meanwhile H_2 and H_2O diffuse across the control surface.

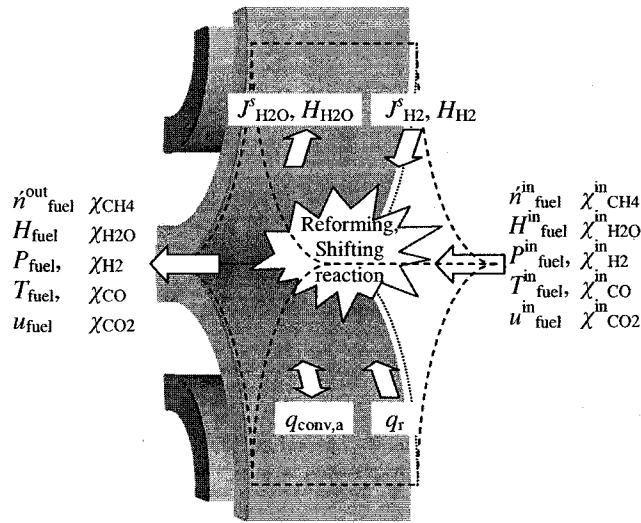
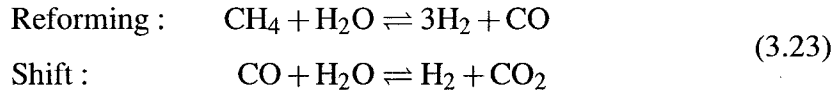


Figure 3.5: Mass and energy balance on CV2

Reforming and shift reaction

Reforming and shift reactions generate H_2 and CO from methane and steam:



Based on the methane consumption rate, the reforming rate is experimentally determined by (Ahmed and Foger, 2000):

$$r_r = -r_{CH_4} = K_r p_{CH_4}^\alpha p_{H_2O}^\beta \exp\left(-\frac{E_r}{RT_{fuel}}\right) \quad (3.24)$$

where K_r is the rate coefficient, E_r is activation energy, and α , β are order coefficients for methane and steam respectively.

The shifting reaction is usually considered to be fast (Campanari and Iora, 2004). The equilibrium constant depends on the temperature (Campanari and Iora, 2004):

$$K_{eq} = \frac{p_{CO_2} p_{H_2}}{p_{CO} p_{H_2O}} = \exp\left(\frac{4276}{T_{fuel}} - 3.961\right) \quad (3.25)$$

In order to establish the mass balance equation, we need to know the shift reaction rate. ^{R1.5} In the absence of reliable electrochemical kinetic data on oxidation of CO on SOFC anode, it is reasonable to make the approximation by neglecting its effect on the

shift reaction rate. ^{R3.6} The approximated rate equation is:

$$r_s = K_s^+ p_{\text{CO}} p_{\text{H}_2\text{O}} - K_s^- p_{\text{CO}_2} p_{\text{H}_2} \quad (3.26)$$

where K_s^+ and K_s^- are the forward and reverse reaction rate coefficients respectively. When it reaches equilibrium, $r_s = 0$, so we have

$$K_{\text{eq}} = \frac{K_s^+}{K_s^-} \quad (3.27)$$

and the reaction rate is:

$$r_s = K_s^- K_{\text{eq}} p_{\text{CO}} p_{\text{H}_2\text{O}} - K_s^- p_{\text{CO}_2} p_{\text{H}_2} \quad (3.28)$$

When the rate coefficient K_s is large, the shift reaction is much faster than the other reactions, with known equilibrium constant K_{eq} , the shift reaction rate can then be written as:

$$r_s = K_s (K_{\text{eq}} p_{\text{CO}} p_{\text{H}_2\text{O}} - p_{\text{CO}_2} p_{\text{H}_2}) \quad (3.29)$$

Taking a value for $K_s = 100$, numerical simulation shows that the shift reaction rate will be almost 10 times the rate of the reforming reaction.

Mass transfer dynamics

Pre-reformed fuel is a mixture of CH_4 , steam, H_2 , CO and CO_2 . Dynamic behaviors of each species in the control volume can be modeled using the law of mass conservation:

$$\frac{dN_i}{dt} = \dot{n}_i^{\text{in}} - \dot{n}_i^{\text{out}} + \dot{n}_i^{\text{gen}} \quad (3.30)$$

where \dot{n}_i^{in} and \dot{n}_i^{out} are the flow rates of species entering and exiting the control volume respectively, and \dot{n}_i^{gen} is the species generation rate inside the control volume.

The rate of mass flowing in the control volume can be expressed by the explicit gas parameters:

$$\dot{n}_i^{\text{in}} = A_a \frac{P_{\text{fuel}}^{\text{in}}}{RT_{\text{fuel}}^{\text{in}}} u_{\text{fuel}}^{\text{in}} \chi_i^{\text{in}} \quad (3.31)$$

where A_a is the cross section area of the anode fuel channel, $P_{\text{fuel}}^{\text{in}}$, $T_{\text{fuel}}^{\text{in}}$ and $u_{\text{fuel}}^{\text{in}}$ are the upstream pressure, temperature, and velocity of the fuel flow body respectively, and χ_i is the mole fraction of each species.

The rate of mass flowing out the control volume is:

$$\dot{n}_i^{\text{out}} = A_a \frac{N_i}{dV_a} u_{\text{fuel}} \quad (3.32)$$

where N_i is mole number of each species inside the control volume, and dV_a is the volume of the anode fuel channel within the control volume.

The rate of mass generation includes not only those materials consumed or produced by internal reforming and shift reactions, but also those due to mass flux diffusion leaving CV2, such as $J_{\text{H}_2}^s$, $J_{\text{O}_2}^s$ and $J_{\text{H}_2\text{O}}^s$, which participate in electrochemical reactions within CV1.

The rate of CH_4 accumulation within the control volume is given by:

$$\frac{dN_{\text{CH}_4}}{dt} = A_a \frac{P_{\text{fuel}}^{\text{in}}}{RT_{\text{fuel}}^{\text{in}}} u_{\text{fuel}}^{\text{in}} \chi_{\text{CH}_4}^{\text{in}} - A_a \frac{N_{\text{CH}_4}}{dV_a} u_{\text{fuel}} - Ar_r \quad (3.33)$$

where Ar_r is the methane consumption rate through the reforming reaction, as shown by Eqn.3.24.

For steam, in addition to the flow in and out of the control volume, consumption due to reforming and shift reactions, the SOFC's electrochemical reaction also produces H_2O flow entering the control volume:

$$\frac{dN_{\text{H}_2\text{O}}}{dt} = A_a \frac{P_{\text{fuel}}^{\text{in}}}{RT_{\text{fuel}}^{\text{in}}} u_{\text{fuel}}^{\text{in}} \chi_{\text{H}_2\text{O}}^{\text{in}} - A_a \frac{N_{\text{H}_2\text{O}}}{dV_a} u_{\text{fuel}} - J_{\text{H}_2\text{O}}^s - Ar_r - r_s \quad (3.34)$$

where $-J_{\text{H}_2\text{O}}^s$ is the steam flow leaving the anode surface and entering the control volume, arising from the electrochemical reaction shown in Eqn.3.1, and r_s is the consumption rate of steam through the shift reaction .

Reforming and shift reactions produce H_2 , at rates of $3r_r$ and r_s respectively. It is consumed by the electrochemical reaction to produce electricity:

$$\frac{dN_{\text{H}_2}}{dt} = A_a \frac{P_{\text{fuel}}^{\text{in}}}{RT_{\text{fuel}}^{\text{in}}} u_{\text{fuel}}^{\text{in}} \chi_{\text{H}_2}^{\text{in}} - A_a \frac{N_{\text{H}_2}}{dV_a} u_{\text{fuel}} - J_{\text{H}_2}^s + 3Ar_r + r_s \quad (3.35)$$

CO is produced by the reforming reaction and consumed by the shift reaction. When CO is not involved in the electrochemical reaction, the mass conservation equation is:

$$\frac{dN_{\text{CO}}}{dt} = A_a \frac{P_{\text{fuel}}^{\text{in}}}{RT_{\text{fuel}}^{\text{in}}} u_{\text{fuel}}^{\text{in}} \chi_{\text{CO}}^{\text{in}} - A_a \frac{N_{\text{CO}}}{dV_a} u_{\text{fuel}} + Ar_r - r_s \quad (3.36)$$

The dynamic model for CO₂ is:

$$\frac{dN_{\text{CO}_2}}{dt} = A_a \frac{P_{\text{fuel}}^{\text{in}}}{RT_{\text{fuel}}^{\text{in}}} u_{\text{fuel}}^{\text{in}} \chi_{\text{CO}_2}^{\text{in}} - A_a \frac{N_{\text{CO}_2}}{dV_a} u_{\text{fuel}} + r_s \quad (3.37)$$

However, CO is involved in the electrochemical reaction. As shown by Eqn.3.3, J_{CO}^s and $p_{\text{CO}}^{\text{tpb}}$ are determined by partial pressure of CO at the flow body p_{CO}^b and the electrochemical consumption rate at tpb J_{CO}^r . How CO and H₂ compete at tpb is not clear when only the total current output is given. As an approximate solution we have assumed that the consumption rates J_{CO}^s and $J_{\text{H}_2}^s$ are given by the following equations:

$$J_{\text{CO}}^s = \frac{\chi_{\text{CO}}}{\chi_{\text{CO}} + \chi_{\text{H}_2}} J^s, \quad J_{\text{H}_2}^s = \frac{\chi_{\text{H}_2}}{\chi_{\text{CO}} + \chi_{\text{H}_2}} J^s \quad (3.38)$$

Eqn.3.35,3.36,3.37 can then be amended according to Eqn.3.38, to include consideration of the electrochemical reaction of CO.

Heat transfer dynamics

The fuel gas temperature is affected by several factors: reforming and shift reactions, internal energy carried by the flow body, and heat transferred from its surroundings, etc.

Because the flow velocity is not high, it is reasonable to assume that insignificant kinetic energy is converted to internal energy. The energy balance for CV2 then becomes:

$$\begin{aligned} \frac{d(\sum(N_i C_{v,i}) T_{\text{fuel}})}{dt} &= \sum(\dot{n}_i^{\text{in}} H_i^{\text{in}}) - \sum(\dot{n}_i^{\text{out}} H_i) \\ &\quad - J_{\text{H}_2}^s H_{\text{H}_2} - J_{\text{H}_2\text{O}}^s H_{\text{H}_2\text{O}} - h_a A (T_{\text{fuel}} - T_{\text{cell}}) + q_{\text{ref}} \end{aligned} \quad (3.39)$$

where:

$$\begin{aligned} \sum(\dot{n}_i^{\text{in}} H_i^{\text{in}}) &= A_a \frac{P_{\text{fuel}}^{\text{in}}}{RT_{\text{fuel}}^{\text{in}}} u_{\text{fuel}}^{\text{in}} \sum(\chi_i^{\text{in}} H_i^{\text{in}}) \\ \sum(\dot{n}_i^{\text{out}} H_i) &= A_a \frac{\sum(N_i H_i)}{dV_a} u_{\text{fuel}} \end{aligned}$$

The first four terms on the right hand side of Eqn.3.39 are the energy carried by mass flows. The fifth term is the heat flow exchanged with the cell tube by convection when fuel flow passes through the cell tube surface. The last term represents the heat flow supplied from the cell tube to satisfy the heating requirement of the reforming reaction.

The reforming reaction is endothermal. Extra heat energy must be supplied to maintain the reaction. The internal reforming reaction takes place on the surface of anode, using Ni as catalyst. Because the heat conduction coefficient of Ni is much larger than that of the gas mixtures, we can assume that the necessary heat flow q_{ref} is supplied by the SOFC cell, and not from decrease of the fuel gas's internal energy. It can be modeled as:

$$q_{\text{ref}} = Ar_r \Delta H|_{T_{\text{fuel}}} \quad (3.40)$$

where r_r is reforming reaction rate, and $\Delta H = (3H_{\text{H}_2} + H_{\text{CO}} - H_{\text{CH}_4} - H_{\text{H}_2\text{O}})$ is the reaction heat.

The shift reaction is exothermal. Compared with the reforming reaction heat, the amount of shift reaction heat is minor and mainly leads to an increase of the internal energy of the fuel mixture. In Eqn.3.39, the shift reaction heat is implied in the inlet and outlet enthalpy difference.

Momentum balance

Fuel flow velocity determines the space time in the fuel channel and thus fuel usage. It affects the heat transfer coefficient as shown in Eqn.3.14 and hence temperatures. On the other hand, it is manipulable, and also affected by reactions, mass transfer, density change etc. Dynamic behaviors of flow velocities can be modeled by the momentum conservation law:

$$\frac{d(\sum(N_i M_i)u_{\text{fuel}})}{dt} = \sum \dot{m}_i^{\text{in}} u_{\text{fuel}}^{\text{in}} - \sum \dot{m}_i^{\text{out}} u_{\text{fuel}}^{\text{out}} - J_{\text{H}_2}^s M_{\text{H}_2} u_{\text{fuel}} + \sum F_a \quad (3.41)$$

where

$$\begin{aligned} \sum \dot{m}_i^{\text{in}} u_{\text{fuel}}^{\text{in}} &= A_a \frac{p_{\text{fuel}}^{\text{in}}}{RT_{\text{fuel}}^{\text{in}}} \sum (\chi_i^{\text{in}} M_i) u_{\text{fuel}}^{\text{in}2} \\ \sum \dot{m}_i^{\text{out}} u_{\text{fuel}}^{\text{out}} &= A_a \frac{\sum (N_i M_i)}{dV_a} u_{\text{fuel}}^2 \end{aligned}$$

The first two terms of the right hand side of Eqn.3.41 are the momentum rate flowing in and out of the control volume. The third term is the momentum out-flow rate resulting from H_2 participation in the electrochemical reaction. We have assumed that the axial velocity of the electrochemical reaction product H_2O , which diffuses into the control volume, is zero; hence the corresponding momentum is zero. The last term represents the summation of forces acting on the flow body.

In the axial direction, there are two kinds of force acting on the flow body: the upstream pressure gradient, which is the force source that keeps the flow moving, and the shear stress along the channel wall that has an effect in the reverse direction. The forces acting on the flow body in CV2 are expressed as:

$$\sum F_a = A_a \Delta P_a - A \tau_{w,a} \quad (3.42)$$

The pressure gradient ΔP_a can be approximately determined using Poiseuille's Law (Young *et al.*, 1996). The wall shear stress τ_w can be calculated from the friction factor f :

$$f = \frac{\tau_w}{\frac{1}{2} \rho u^2} \quad (3.43)$$

In a specific channel, fRe is constant for laminar flow, for which the values are known (Perry *et al.*, 1997). For turbulent flow, surface roughness affects the value of f , which can be calculated from surface roughness and Reynolds number (Perry *et al.*, 1997).

Because no boundary condition is considered in the finite volume model, we have assumed that the forces acting on fuel gas are at equilibrium, $\sum F_a = 0$, when performing the simulation.

3.2.5 Modeling for other control volumes

Modeling for CV3

CV3 encloses the air flow in the cathode side channel as shown in Fig.3.6. In this control volume some O_2 leaves the flow body, diffuses into the cathode reaction site, and participates in the electrochemical reaction. No reaction product enters this control volume.

Mass transfer dynamics

We have approximated that air flow consists only of N_2 and O_2 . N_2 is not involved in the electrochemical reaction, its behavior is affected only by the flow, and it can be modeled as:

$$\frac{dN_{N_2}}{dt} = A_c \frac{P_{air}^{in}}{RT_{air}^{in}} (1 - \chi_{O_2}^{in}) u_{air}^{in} - A_c \frac{N_{N_2}}{dV_c} u_{air} \quad (3.44)$$

where A_c is the cross section area of the cathode flow channel, dV_c the volume and $(1 - \chi_{O_2}^{in})$ the inlet mole fraction of N_2 .

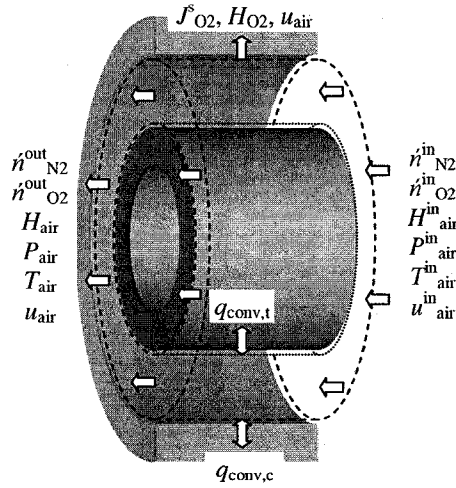


Figure 3.6: Mass and energy balance on CV3

For O_2 the mass balance equation is:

$$\frac{dN_{O_2}}{dt} = A_c \frac{P_{air}^{in}}{RT_{air}^{in}} \chi_{O_2}^{in} u_{air}^{in} - A_c \frac{N_{O_2}}{dV_c} u_{air} - J_{O_2}^s \quad (3.45)$$

where $J_{O_2}^s$ represents O_2 consumed in the electrochemical reaction.

Heat transfer dynamics

The flow body also exchanges heat with the cell tube and injection tube and can be modeled by the following equation:

$$\begin{aligned} \frac{d(\sum(N_j C_{v,j}) T_{air})}{dt} = & A_c \frac{P_{air}^{in}}{RT_{air}^{in}} u_{air}^{in} H_{air}^{in} - A_c \frac{\sum N_j H_{air}}{dV_c} u_{air} - J_{O_2}^s H_{O_2} \\ & - h_c A_2 (T_{air} - T_{cell}) - h_c A_1 (T_{air} - T_{tube}) \end{aligned} \quad (3.46)$$

where h_c is the cathode side heat transfer coefficient, A_2 and A_1 the inner surface area of the cell tube and the outer surface area of the injection tube respectively.

Because enthalpies of air, N_2 , and O_2 are very similar, we do not distinguish between them in this model.

Momentum balance

Similar to the anode side, the dynamics of the cathode side flow velocity is modeled as:

$$\begin{aligned} \frac{d(\sum(N_j M_j) u_{air})}{dt} = & A_c \frac{P_{air}^{in}}{RT_{air}^{in}} \sum(\chi_j^{in} M_j^{in}) u_{air}^{in2} - A_c \frac{\sum(N_j M_j)}{dV_c} u_{air}^2 \\ & - J_{O_2}^s M_{O_2} u_{air} + \sum F_c \end{aligned} \quad (3.47)$$

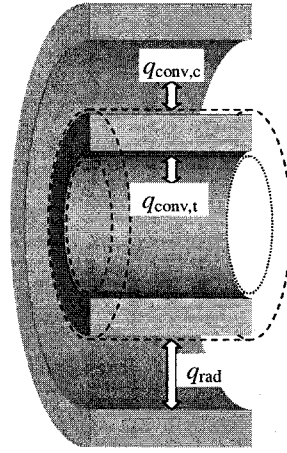


Figure 3.7: Energy balance on CV4

where M_j is the mole mass of N_2 or O_2 and $\sum F_c = A_c \Delta P_c - (A_1 + A_2) \tau_{w,a}$ is the sum of the forces acting on the air flow.

Modeling for CV4

CV4 includes the solid injection tube, as shown in Fig.3.7. It is a heat transfer medium. The tube exchanges heat with the cathode side air flow as well as the air flow inside the injection tube. The tube also exchanges heat energy with the inner surface of the cell tube through radiation. The dynamic behavior of the injection tube temperature is modeled as:

$$m_{\text{tube}} C_{p,\text{tube}} \frac{dT_{\text{tube}}}{dt} = \frac{\sigma}{R_{\text{rad}}} A_1 (T_{\text{cell}}^4 - T_{\text{tube}}^4) - h_c A_1 (T_{\text{tube}} - T_{\text{air}}) - h_t A_0 (T_{\text{tube}} - T_{\text{inj}}) \quad (3.48)$$

where h_t is the convection heat transfer coefficient inside the injection tube, which can be expressed as:

$$h_t = f_t \left(\frac{u_{\text{inj}} P_{\text{inj}}}{RT_{\text{inj}}} \right)^{\frac{1}{2}}$$

where

$$f_t = 0.332 \frac{k_{\text{air}}}{D_t} \left(\frac{C_{v,\text{air}} \mu_{\text{air}}}{k_{\text{air}}} \right)^{\frac{1}{3}} \left(\frac{D_t M_{\text{air}}}{\mu_{\text{air}}} \right)^{\frac{1}{2}}$$

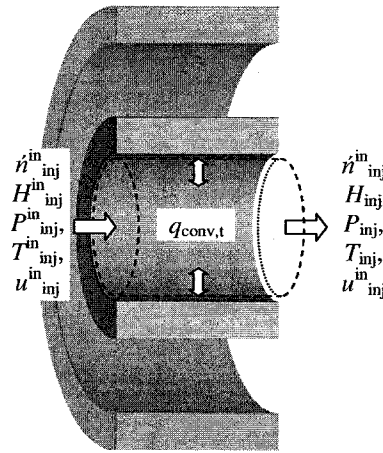


Figure 3.8: Energy balance on CV5

Modeling for CV5

CV5 encloses the air flow in the injection tube, as shown in Fig.3.8. No reaction and no other mass transfer takes place in this control volume. However heat is exchanged with the injection tube. The temperature dynamics can be modeled by:

$$N_{air}C_{v,air} \frac{dT_{inj}}{dt} = A_t \frac{P_{inj}^{in}}{RT_{inj}^{in}} (H_{inj}^{in} - H_{inj}) u_{air}^{in} - h_t A_0 (T_{inj} - T_{tube}) \quad (3.49)$$

where A_t is the cross section area of the inner injection tube flow channel.

3.3 State-space model

A state-space model is an assembly of dynamic equations for the state variables for a process. State variables are a set of variables essential for completely describing the internal state (or condition) of a process. State-space models constitute a well-known class of models describing dynamic systems, especially multi-input and multi-output systems. It is widely used in the area of modeling, control, and simulation. In this section, the dynamic model of SOFC is described in the form of a nonlinear state-space model.

Table 3.1: Input and output variables

Input variables	Output variables
R_{load}	$V_{\text{out}}, I_{\text{out}}$
$P_{\text{fuel}}^{\text{in}}, T_{\text{fuel}}^{\text{in}}, u_{\text{fuel}}^{\text{in}}$ $\chi_{\text{CH}_4}^{\text{in}}, \chi_{\text{H}_2\text{O}}^{\text{in}}, \chi_{\text{H}_2}^{\text{in}}, \chi_{\text{CO}}^{\text{in}}, \chi_{\text{CO}_2}^{\text{in}}$	$P_{\text{fuel}}, T_{\text{fuel}}, u_{\text{air}}$ $\chi_{\text{CH}_4}, \chi_{\text{H}_2\text{O}}, \chi_{\text{H}_2}, \chi_{\text{CO}}, \chi_{\text{CO}_2}$
$P_{\text{air}}^{\text{in}}, T_{\text{air}}^{\text{in}}, u_{\text{air}}^{\text{in}}, \chi_{\text{O}_2}^{\text{in}}$	$P_{\text{air}}, T_{\text{air}}, u_{\text{air}}, \chi_{\text{O}_2}$
$P_{\text{inj}}^{\text{in}}, T_{\text{inj}}^{\text{in}}, u_{\text{inj}}^{\text{in}}$	$P_{\text{inj}}, T_{\text{inj}}, u_{\text{inj}}$

3.3.1 Input/Output variables

For the SOFC slice that we have considered, input variables are related to physical inlet parameters. Any perturbations in the input variables will change the internal states of the process.

The first input variable is the external load impedance. Under normal operating conditions, The external load determines the current output and thus also the electrochemical reactions and mass and heat transfer. To simplify the solution, the external load is assumed to be a pure resistance R_{load} .

The second group of input variables includes the inlet fuel flow parameters: pressure $P_{\text{fuel}}^{\text{in}}$, temperature $T_{\text{fuel}}^{\text{in}}$, and flow velocity $u_{\text{fuel}}^{\text{in}}$. Although the inlet mole fraction of each species in the fuel flow cannot be manipulated, variation in these parameters can affect the performance of SOFC. Thus inlet mole fractions are also defined as input variables.

The third group of input variables are the inlet air flow parameters in the cathode side flow channel: pressure $P_{\text{air}}^{\text{in}}$, temperature $T_{\text{air}}^{\text{in}}$, flow velocity $u_{\text{air}}^{\text{in}}$, and mole fraction of oxygen χ_{O_2} .

The last group of input variables are injection air flow pressure $P_{\text{inj}}^{\text{in}}$, temperature $T_{\text{inj}}^{\text{in}}$, and velocity $u_{\text{inj}}^{\text{in}}$.

Output variables are the voltage V_{out} , current i and other variables related to the physical parameters of the outlet flows, corresponding to those at the inlet, as shown in Table 1.

3.3.2 Non-linear state-space model

We define the input vector \mathbf{u} and output vector \mathbf{y} as follows:

$$\mathbf{u} = \begin{bmatrix} R_{\text{load}} & P_{\text{fuel}}^{\text{in}} & T_{\text{fuel}}^{\text{in}} & u_{\text{fuel}}^{\text{in}} & \chi_{\text{CH}_4}^{\text{in}} & \chi_{\text{H}_2\text{O}}^{\text{in}} & \chi_{\text{H}_2}^{\text{in}} & \chi_{\text{CO}}^{\text{in}} & \chi_{\text{CO}_2}^{\text{in}} \\ & P_{\text{air}}^{\text{in}} & T_{\text{air}}^{\text{in}} & u_{\text{air}}^{\text{in}} & \chi_{\text{O}_2}^{\text{in}} & P_{\text{inj}}^{\text{in}} & T_{\text{inj}}^{\text{in}} & u_{\text{inj}}^{\text{in}} \end{bmatrix}^T \quad (3.50)$$

$$\mathbf{y} = \begin{bmatrix} V_{\text{out}} & i & P_{\text{fuel}} & T_{\text{fuel}} & u_{\text{fuel}} & \chi_{\text{CH}_4} & \chi_{\text{H}_2\text{O}} & \chi_{\text{H}_2} & \chi_{\text{CO}} & \chi_{\text{CO}_2} \\ & P_{\text{air}} & T_{\text{air}} & u_{\text{air}} & \chi_{\text{O}_2} & P_{\text{inj}} & T_{\text{inj}} & u_{\text{inj}} \end{bmatrix}^T \quad (3.51)$$

Eliminating the intermediate variables v_{H_2} , v_{O_2} , $v_{\text{H}_2\text{O}}$ from the model derived in Chapter 2 and define a state vector:

$$\mathbf{x} = \begin{bmatrix} V_{\text{ct}} & J_{\text{H}_2}^s & J_{\text{H}_2}^s & J_{\text{O}_2}^s & J_{\text{O}_2}^s & J_{\text{H}_2\text{O}}^s & J_{\text{H}_2\text{O}}^s & p_{\text{H}_2}^{\text{tpb}} & \dot{p}_{\text{H}_2}^{\text{tpb}} & p_{\text{O}_2}^{\text{tpb}} \\ & \dot{p}_{\text{O}_2}^{\text{tpb}} & \dot{p}_{\text{H}_2\text{O}}^{\text{tpb}} & \dot{p}_{\text{H}_2\text{O}}^{\text{tpb}} & v_{\text{R}} & T_{\text{cell}} & T_{\text{tube}} & T_{\text{fuel}} & T_{\text{air}} & T_{\text{inj}} \\ & N_{\text{CH}_4} & N_{\text{H}_2\text{O}} & N_{\text{H}_2} & N_{\text{CO}} & N_{\text{CO}_2} & N_{\text{N}_2} & N_{\text{O}_2} & u_{\text{fuel}} & u_{\text{air}} \end{bmatrix}^T \quad (3.52)$$

By substituting Eqn.3.24,3.29 into Eqn.3.33-3.37 and substituting Eqn.3.24, 3.40 into Eqn.3.22 and 3.39, combining the dynamics of electricity conversion shown in Chapter 2, and rearranging Eqn.3.22, 3.33-3.37, 3.39, 3.41 and 3.44-3.49, the state space model can be expressed as:

States:

$$\dot{x}_1 = \frac{1}{R_{\text{ct}}C_{\text{ct}}}E - \frac{1}{R_{\text{ct}}C_{\text{ct}}}x_1 - \frac{1}{C_{\text{ct}}} \frac{x_1}{u_1 + R_0}$$

$$\dot{x}_2 = x_3$$

$$\dot{x}_3 = -h_1x_2 - h_2x_3 + h_1 \frac{1}{2F} \frac{x_1}{u_1 + R_0} + h_3 \frac{A}{dV_a} \left(\dot{x}_{22} + \frac{x_{22}}{x_{17}} \dot{x}_{17} \right)$$

$$\dot{x}_4 = x_5$$

$$\dot{x}_5 = -o_1x_4 - o_2x_5 + o_1 \frac{1}{4F} \frac{x_1}{u_1 + R_0} + o_3 \frac{A}{dV_c} \left(\dot{x}_{26} + \frac{x_{26}}{x_{18}} \dot{x}_{18} \right)$$

$$\dot{x}_6 = x_7$$

$$\begin{aligned}
 \dot{x}_7 &= -w_1 x_6 - w_2 x_7 + w_1 \frac{1}{2F} \left(\frac{-x_1}{u_1 + R_0} \right) + w_3 \frac{A}{dV_a} \left(\dot{x}_{21} + \frac{x_{21}}{x_{17}} \dot{x}_{17} \right) \\
 \dot{x}_8 &= x_9 \\
 \dot{x}_9 &= -h_1 x_8 - h_2 x_9 - h_4 \frac{Rx_{15}}{A} \frac{1}{2F} \frac{x_1}{u_1 + R_0} + h_1 \frac{R}{dV_a} x_{22} x_{17} \\
 &\quad - \frac{Rx_{15}}{A} \frac{4}{la} \frac{1}{2F} \left[\frac{\dot{x}_1}{u_1 + R_0} - \frac{x_1}{(u_1 + R_0)^2} (Ku_1 - x_{14}) \right] \\
 \dot{x}_{10} &= x_{11} \\
 \dot{x}_{11} &= -o_1 x_{10} - o_2 x_{11} - o_4 \frac{Rx_{15}}{A} \frac{1}{4F} \frac{x_1}{u_1 + R_0} + o_1 \frac{R}{dV_c} x_{26} x_{18} \\
 &\quad - \frac{Rx_{15}}{A} \frac{4}{lc} \frac{1}{4F} \left[\frac{\dot{x}_1}{u_1 + R_0} - \frac{x_1}{(u_1 + R_0)^2} (Ku_1 - x_{14}) \right] \\
 \dot{x}_{12} &= x_{13} \\
 \dot{x}_{13} &= -w_1 x_{12} - w_2 x_{13} - w_4 \frac{Rx_{15}}{A} \frac{1}{2F} \frac{-x_1}{u_1 + R_0} + w_1 \frac{R}{dV_a} x_{21} x_{17} \\
 &\quad - \frac{Rx_{15}}{A} \frac{4}{la} \frac{1}{2F} \left[-\frac{\dot{x}_1}{u_1 + R_0} + \frac{x_1}{(u_1 + R_0)^2} (Ku_1 - x_{14}) \right] \\
 \dot{x}_{14} &= K^2 u_1 - K x_{14} \\
 \dot{x}_{15} &= \frac{1}{m_{\text{cell}} C_{p,\text{cell}}} \left[x_2 H_{\text{H}_2} + x_4 H_{\text{O}_2} + x_6 H_{\text{H}_2\text{O}} - \frac{u_1}{(u_1 + R_0)^2} x_1^2 \right. \\
 &\quad - f_a \left(x_{27} \frac{\sum_{20}^{24} x_i}{dV_a} \right)^{\frac{1}{2}} A (x_{15} - x_{17}) - f_c \left(x_{28} \frac{x_{25} + x_{26}}{dV_c} \right)^{\frac{1}{2}} A_2 (x_{15} - x_{18}) \\
 &\quad \left. - \frac{\sigma}{R_{\text{rad}}} A_2 (x_{15}^4 - x_{16}^4) - AK_r \left(\frac{x_{20} R x_{17}}{dV_a} \right)^\alpha \left(\frac{x_{21} R x_{17}}{dV_a} \right)^\beta \exp \left(-\frac{E_r}{R x_{17}} \right) \Delta H_r \right] \\
 \dot{x}_{16} &= \frac{1}{m_{\text{tube}} C_{p,\text{tube}}} \left[\frac{\sigma}{R_{\text{rad}}} A_2 (x_{15}^4 - x_{16}^4) - f_c \left(x_{28} \frac{x_{25} + x_{26}}{dV_c} \right)^{\frac{1}{2}} A_1 (x_{16} - x_{18}) \right. \\
 &\quad \left. - f_t \left(u_{16} \frac{u_{14}}{R x_{19}} \right)^{\frac{1}{2}} A_0 (x_{16} - x_{19}) \right] \\
 \dot{x}_{17} &= \frac{1}{\sum_{20}^{24} (x_i C_{v,i})} \left[A_a \frac{u_2}{R u_3} u_4 \sum_5^9 (u_i H_i^{\text{in}}) - A_a x_{27} \frac{\sum_{20}^{24} (x_i H_i)}{dV_a} \right. \\
 &\quad - f_a \left(x_{27} \frac{\sum_{20}^{24} x_i}{dV_a} \right)^{\frac{1}{2}} A (x_{17} - x_{15}) - x_2 H_{\text{H}_2} - x_6 H_{\text{H}_2\text{O}} \\
 &\quad \left. + AK_r \left(\frac{x_{20} R x_{17}}{dV_a} \right)^\alpha \left(\frac{x_{21} R x_{17}}{dV_a} \right)^\beta \exp \left(-\frac{E_r}{R x_{17}} \right) \Delta H_r - x_{17} \sum_{20}^{24} (\dot{x}_i C_{v,i}) \right]
 \end{aligned}$$

$$\begin{aligned}
 \dot{x}_{18} &= \frac{1}{\sum_{25}^{26}(x_j C_{v,j})} \left[A_c \frac{u_{10}}{R u_{11}} u_{12} H_{\text{air}}^{\text{in}} - A_c x_{28} \frac{\sum_{25}^{26} x_j}{dV_c} H_{\text{air}} - x_4 H_{\text{O}_2} \right. \\
 &\quad \left. - f_c \left(x_{28} \frac{\sum_{24}^{26} x_j}{dV_c} \right)^{\frac{1}{2}} (A_2(x_{18} - x_{15}) + A_1(x_{18} - x_{16})) - x_{18} \sum_{25}^{26} (\dot{x}_j C_{v,j}) \right] \\
 \dot{x}_{19} &= \frac{1}{\frac{u_{14} dV_c}{R u_{15}} C_{v,\text{air}}} \left[A_t \frac{u_{14}}{R u_{15}} u_{16} (H_{\text{air}}^{\text{in}} - H_{\text{air}}) - f_t \left(u_{16} \frac{u_{14}}{R x_{19}} \right)^{\frac{1}{2}} A_0(x_{19} - x_{16}) \right] \\
 \dot{x}_{20} &= A_a \frac{u_2}{R u_3} u_4 u_5 - A_a x_{27} \frac{x_{20}}{dV_a} - A K_r \left(\frac{x_{20} R x_{17}}{dV_a} \right)^{\alpha} \left(\frac{x_{21} R x_{17}}{dV_a} \right)^{\beta} \exp \left(-\frac{E_r}{R x_{17}} \right) \\
 \dot{x}_{21} &= A_a \frac{u_2}{R u_3} u_4 u_6 - A_a x_{27} \frac{x_{21}}{dV_a} - A K_r \left(\frac{x_{20} R x_{17}}{dV_a} \right)^{\alpha} \left(\frac{x_{21} R x_{17}}{dV_a} \right)^{\beta} \exp \left(-\frac{E_r}{R x_{17}} \right) \\
 &\quad - A K_s \left[\exp \left(\frac{4276}{x_{17}} - 3.961 \right) \frac{x_{23} R x_{17}}{dV_a} \frac{x_{21} R x_{17}}{dV_a} - \frac{x_{24} R x_{17}}{dV_a} \frac{x_{22} R x_{17}}{dV_a} \right] - x_6 \\
 \dot{x}_{22} &= A_a \frac{u_2}{R u_3} u_4 u_7 - A_a x_{27} \frac{x_{22}}{dV_a} + 3 A K_r \left(\frac{x_{20} R x_{17}}{dV_a} \right)^{\alpha} \left(\frac{x_{21} R x_{17}}{dV_a} \right)^{\beta} \exp \left(-\frac{E_r}{R x_{17}} \right) \\
 &\quad + A K_s \left[\exp \left(\frac{4276}{x_{17}} - 3.961 \right) \frac{x_{23} R x_{17}}{dV_a} \frac{x_{21} R x_{17}}{dV_a} - \frac{x_{24} R x_{17}}{dV_a} \frac{x_{22} R x_{17}}{dV_a} \right] - x_2 \\
 \dot{x}_{23} &= A_a \frac{u_2}{R u_3} u_4 u_8 - A_a x_{27} \frac{x_{23}}{dV_a} + A K_r \left(\frac{x_{20} R x_{17}}{dV_a} \right)^{\alpha} \left(\frac{x_{21} R x_{17}}{dV_a} \right)^{\beta} \exp \left(-\frac{E_r}{R x_{17}} \right) \\
 &\quad - A K_s \left[\exp \left(\frac{4276}{x_{17}} - 3.961 \right) \frac{x_{23} R x_{17}}{dV_a} \frac{x_{21} R x_{17}}{dV_a} - \frac{x_{24} R x_{17}}{dV_a} \frac{x_{22} R x_{17}}{dV_a} \right] \\
 \dot{x}_{24} &= A_a \frac{u_2}{R u_3} u_4 u_9 - A_a x_{27} \frac{x_{24}}{dV_a} \\
 &\quad + A K_s \left[\exp \left(\frac{4276}{x_{17}} - 3.961 \right) \frac{x_{23} R x_{17}}{dV_a} \frac{x_{21} R x_{17}}{dV_a} - \frac{x_{24} R x_{17}}{dV_a} \frac{x_{22} R x_{17}}{dV_a} \right] \\
 \dot{x}_{25} &= A_c \frac{u_{10}}{R u_{11}} u_{12} (1 - u_{13}) - A_c x_{28} \frac{x_{25}}{dV_c} \\
 \dot{x}_{26} &= A_c \frac{u_{10}}{R u_{11}} u_{12} u_{13} - A_c x_{28} \frac{x_{26}}{dV_c} - x_4 \\
 \dot{x}_{27} &= \frac{1}{\sum_{20}^{24}(x_i M_i)} \left[A_a \frac{u_2}{R u_3} \sum_5^9 (u_i M_i) u_4^2 - A_a \frac{\sum_{20}^{24} (x_i M_i)}{dV_a} x_{27}^2 - x_2 M_{\text{H}_2} x_{27} \right. \\
 &\quad \left. + A_a \Delta P_a - A \tau_{w,a} - x_{27} \sum_{20}^{24} (\dot{x}_i M_i) \right] \\
 \dot{x}_{28} &= \frac{1}{\sum_{25}^{26}(x_j M_j)} \left[A_c \frac{u_{10}}{R u_{11}} ((1 - u_{13}) M_{\text{N}_2} + u_{13} M_{\text{O}_2}) u_{12}^2 - A_c \frac{\sum_{25}^{26} (x_j M_j)}{dV_c} x_{28}^2 \right. \\
 &\quad \left. - x_4 M_{\text{O}_2} x_{28} + A_c \Delta P_c - (A_1 + A_2) \tau_{w,c} - x_{28} \sum_{25}^{26} (\dot{x}_j M_j) \right]
 \end{aligned}$$

Outputs:

$$y_1 = \frac{u_1}{u_1 + R_o} x_1$$

$$y_2 = \frac{x_1}{u_1 + R_o}$$

$$y_3 = \frac{\sum_{20}^{24} x_i R x_{17}}{dV_a}$$

$$y_4 = x_{17}$$

$$y_5 = x_{27}$$

$$y_6 = \frac{x_{20}}{\sum_{20}^{24} x_i}$$

$$y_7 = \frac{x_{21}}{\sum_{20}^{24} x_i}$$

$$y_8 = \frac{x_{22}}{\sum_{20}^{24} x_i}$$

$$y_9 = \frac{x_{23}}{\sum_{20}^{24} x_i}$$

$$y_{10} = \frac{x_{24}}{\sum_{20}^{24} x_i}$$

$$y_{11} = \frac{\sum_{26}^{25} x_j R x_{18}}{dV_c}$$

$$y_{12} = x_{18}$$

$$y_{13} = x_{28}$$

$$y_{14} = \frac{x_{26}}{\sum_{26}^{25} x_j}$$

$$y_{15} = u_{14} \frac{x_{19}}{u_{15}}$$

$$y_{16} = x_{19}$$

$$y_{17} = u_{16}$$

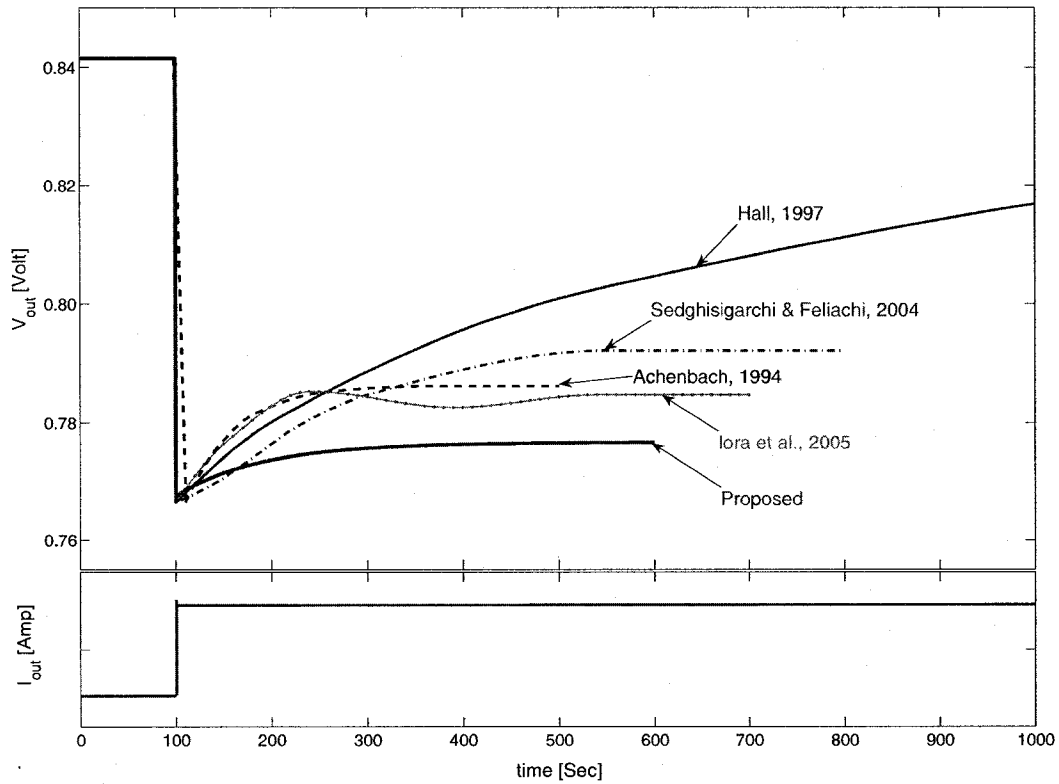


Figure 3.9: Comparison of voltage response trends to load step changes

or, in a compact form:

$$\begin{aligned} \dot{\mathbf{x}} &= f(\mathbf{x}, \mathbf{u}) \\ \mathbf{y} &= g(\mathbf{x}, \mathbf{u}) \end{aligned} \tag{3.53}$$

3.4 Simulations

According to the nonlinear state space model developed in section 3, a Simulink model has been developed using MATLAB. Dynamic behaviors of SOFC in response to different input disturbances were investigated through simulations via their step responses.

Input variables and parameters are shown in Appendix I.

3.4.1 Model validation

Fig. 3.9 is a comparison of the simulated voltage transient response trends due to the same load step using models proposed by different researchers, for similar parameters. Only results derived from those models that considered the cell's temperature dynamics are shown. The dynamic trend from our model is consistent with those from prior models. In our model, however, we have considered not only mass, heat, and momentum transfer and internal reforming and shift reactions, but also the heat source of the reforming reaction. The simulated steady state voltage from our model is lower than that calculated by others, because additional heat is absorbed by the reforming reaction, and consequently the cell temperature is lower.

3.4.2 Step responses due to R_{load} step changes

Step response tests are widely used in investigating process dynamic properties. The method can reveal key process dynamic parameters such as time constant, gain, time delay etc. Step responses of V_{load} , i , T_{cell} , P_{fuel} , T_{fuel} , u_{fuel} and species mole fractions etc. due to R_{load} step changes are shown in Fig.3.10 and Fig.3.11.

When load resistance R_{load} was stepped up the current had an abrupt change followed by a slow change with a time constant of around 0.2 second due to the diffusion and double layer capacitance effect, as described in Chapter 2.

There was a second slow response for all variables, with a time constant around 200s, in addition to the fast response. This was caused mainly by the slow temperature dynamics. When R_{load} was stepped down, the current consumed by the inherent resistant increased and therefore released more heat to the cell. Heat capacity of solid cell materials is large, so the temperature responses were slow, as shown in Fig.3.10c.

Step change in R_{load} also affected properties of fuel flow, shown in Fig.3.10d, e and f. When the current changed, changes of $J_{\text{H}_2}^s$ and $J_{\text{H}_2\text{O}}^s$ in the fuel channel, led to changes in their mole fractions. The shift reaction took place in the reverse direction to maintain the equilibrium. The responses of mole fractions of H_2 , H_2O , CO and CO_2 are shown in Fig.3.11b, c, d and e. The process is endothermic, so the fuel temperature dropped quickly. However, because hot H_2O entered the control volume, the temperature increased again, as shown in Fig.3.10e. Changes of temperature and concentration of H_2O led to the changes in total pressure and concentration of CH_4 as

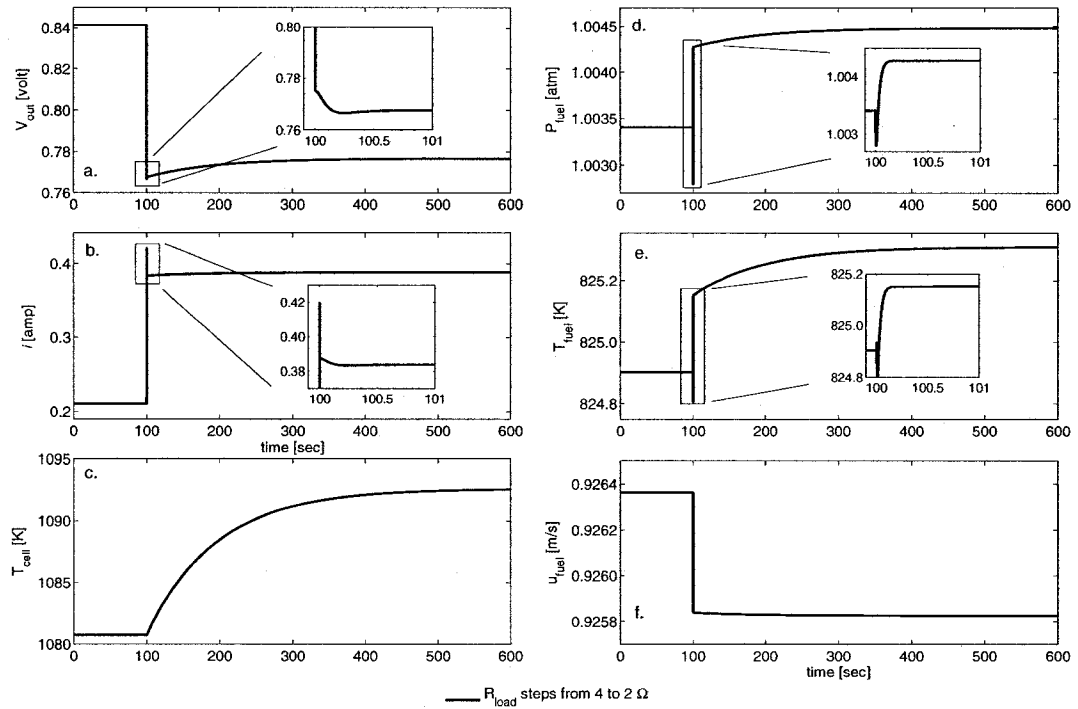


Figure 3.10: Step responses of SOFC slice, when R_{load} changes

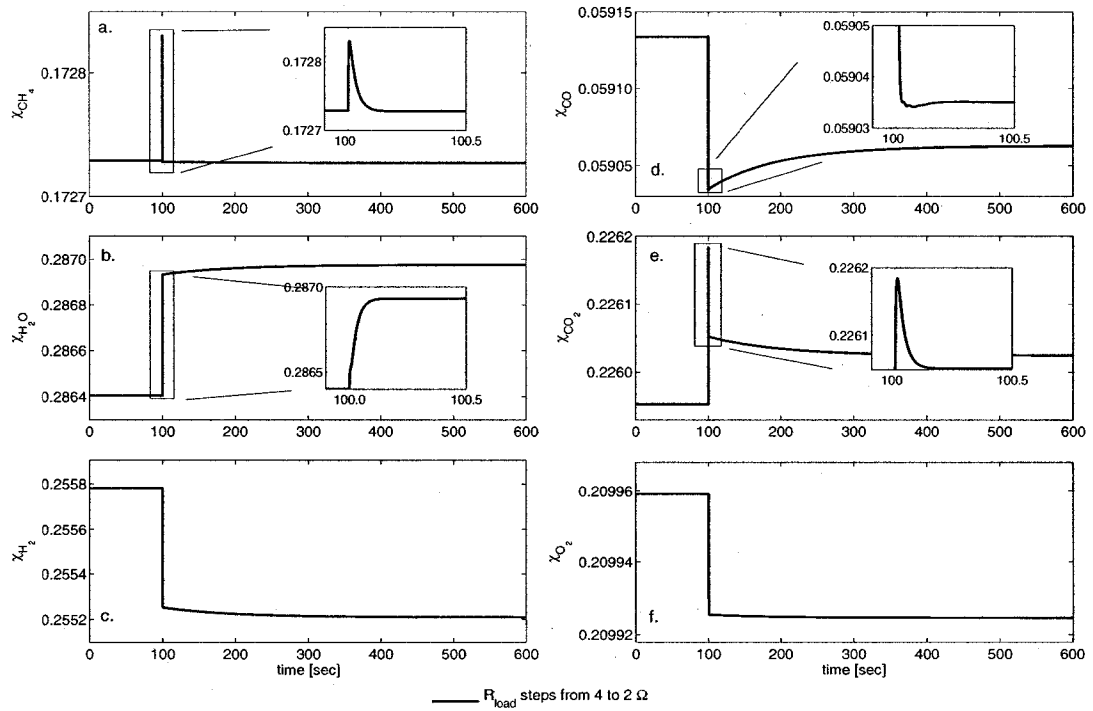


Figure 3.11: Step responses of species mole fractions, when R_{load} changes

shown in Fig.3.10d and Fig.3.11a respectively.

In CV2 more H_2 left the control volume into the anode and more H_2O diffused back to the control volume when R_{load} stepped and more current required. Therefore, more H_2 was replaced by H_2O and this resulted in mass increase from the inlet to the outlet along the fuel flow direction. According to the momentum balance law, the flow velocity decreased as shown in Fig.10f.

The slow increase in cell temperature dominated the whole heat transfer dynamics and had an effect on almost all variables.

Responses of other state variables were similar. All were controlled mainly by the temperature dynamics of the solid phase of the cell. It was also shown that the inherent resistance had a large effect on the dynamic behavior of the fuel cell. Heat capacity of SOFC is an intrinsic property, while the inherent resistance can be changed through proper system design.

3.4.3 Effect of fuel input

Step responses due to step changes in inlet P_{fuel} , T_{fuel} and u_{fuel} were simulated and were compared in Fig.3.12 and Fig.3.13.

When fuel inlet pressure P_{fuel} was stepped up, the concentration of inlet CH_4 and H_2O increased immediately. Then the reforming reaction proceeded faster and absorbed more heat from the cell. The temperature of the cell thus decreased as shown in Fig.3.12c. It also produced H_2 faster, and the concentration of H_2 then increased and led to the changes in voltage V_{out} . Since the external load did not change, the current i changed with V_{out} , as shown in Fig.3.12a and b.

The effects of stepping up inlet fuel pressure P_{fuel} on other properties are shown in Fig.3.12d, e and f and in Fig.3.13. Effects of P_{fuel} step change on other properties were not as significant, except the effect on the total pressure in CV2 and the mole fraction of H_2 , as discussed above.

Step increase of inlet temperature T_{fuel} led to a faster reforming reaction. More heat was absorbed from the cell to support the reforming reaction, so the cell temperature decreased. The step increase of T_{fuel} also changed the equilibrium constant of the shift reaction. The concentration of H_2 decreased and that of H_2O increased. So V_{out} decreased and so did current i . Changing of the equilibrium point of the shift reaction

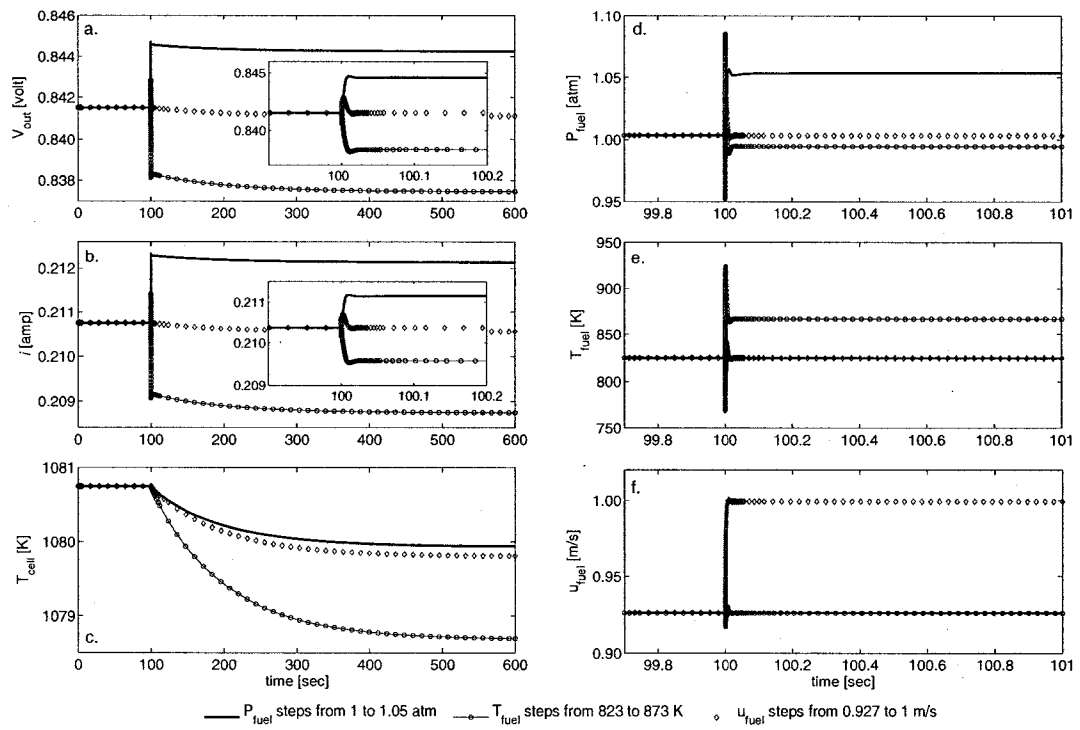


Figure 3.12: SOFC step responses, when fuel input P , T , u stepped respectively

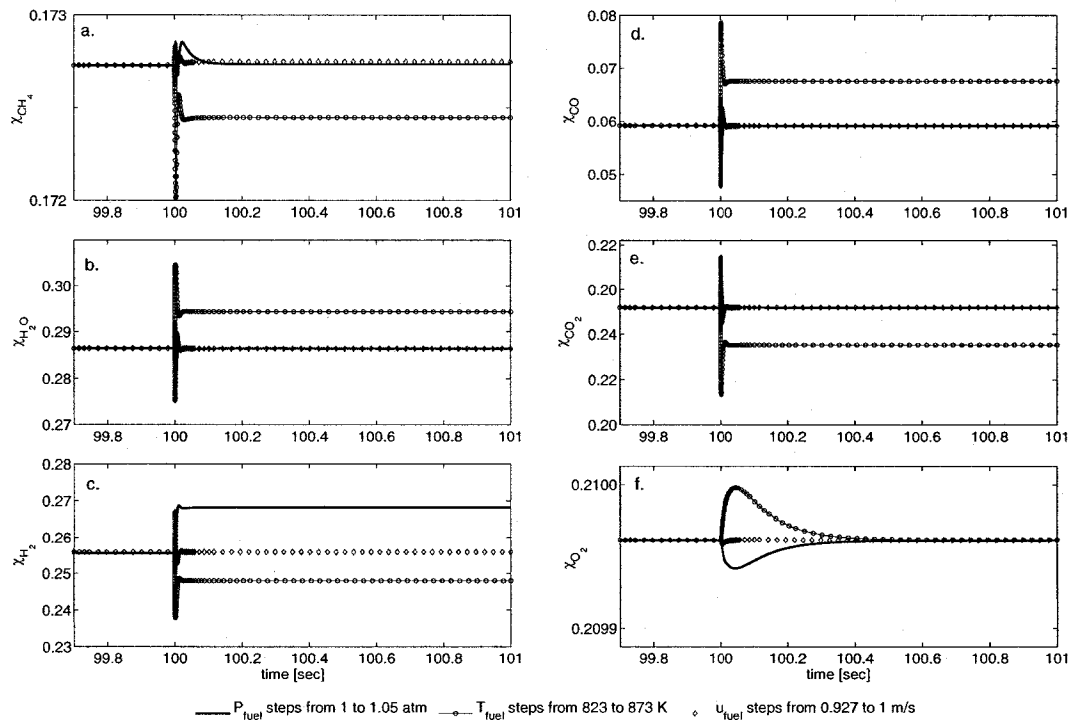


Figure 3.13: Mole fraction responses, when fuel input P , T , u stepped respectively

also led to a slight decrease in the total pressure P_{fuel} . Step response behaviors of the variables are shown in Fig.3.12 and Fig.3.13

Step increase of fuel flow velocity u_{fuel} also affected the performance of SOFC. It increased the heat transfer coefficient h_a , so more heat was transferred to fuel flow from the cell. The cell temperature then decreased, as did V_{out} and i . The effects of u_{fuel} on P_{fuel} and T_{fuel} were minor, as were the impacts on other flow properties, as shown in Fig.3.12 and Fig.3.13.

The effects of fuel inlet flow properties on state variables are compared in Fig.3.12 and Fig.3.13, based on an approximately 5% step up. It was shown that inlet pressure P_{fuel} and temperature T_{fuel} had greater effects on the electrical power output. The effect of the disturbance in flow velocity u_{fuel} was relatively small and slow. It was observed that increase of inlet fuel temperature decreased the voltage output. This was due to the increase of inlet fuel temperature, which led to the reverse shift reaction, which resulted in decrease of hydrogen partial pressure and thus also voltage output. In addition, increase of the inlet fuel temperature also accelerated the reform reaction, which in turn absorbed more heat and led to reduction of the cell temperature and thus the voltage. Therefore it is important that T_{fuel} be optimized to achieve best performance.

3.4.4 Effect of air input

The effects of cathode side air flow parameters on the performance of SOFC were also investigated through step response tests by stepping P_{air} , T_{air} and u_{air} .

When the inlet pressure of cathode side air flow P_{air} was stepped up, the concentration of O_2 in cathode side channel increased. Through diffusion processes as shown in the previous chapter, the result was the increase of fuel cell voltage V_{out} and consequently also current i . Because the mole fraction of O_2 in air was at most 21%, increases of V_{out} and i were not significant, as shown in Fig.3.14a and b. Therefore extra heat released from inherent resistance was minor, and had almost no effect on anode side fuel properties.

The temperature of the air flow had a significant effect on the dynamic performance, as shown in Fig.3.14 and Fig.3.15. Increase of T_{air} affected the cell temperature directly. More heat flowed into the fuel body and increased its temperature T_{fuel} , and thus increased the pressure P_{fuel} and the equilibrium point of the shift reaction. Shifting of equilibrium affected the mole fractions of H_2 , CO_2 , H_2O and CO . V_{out} increased

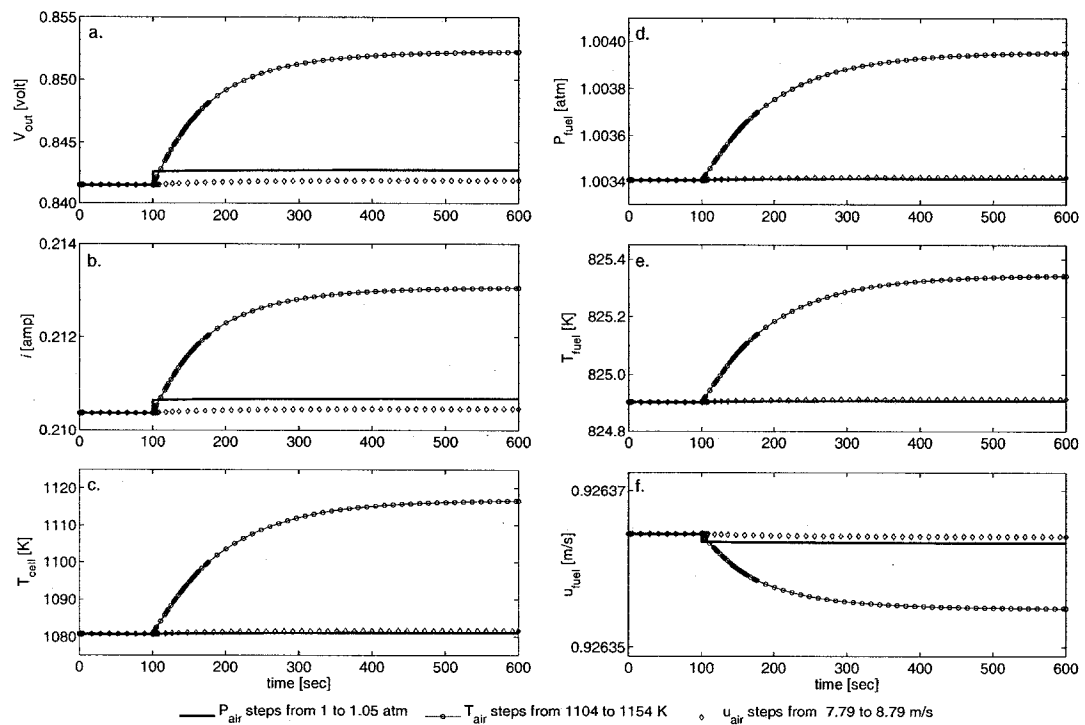


Figure 3.14: SOFC step responses, when air input P , T , u stepped respectively

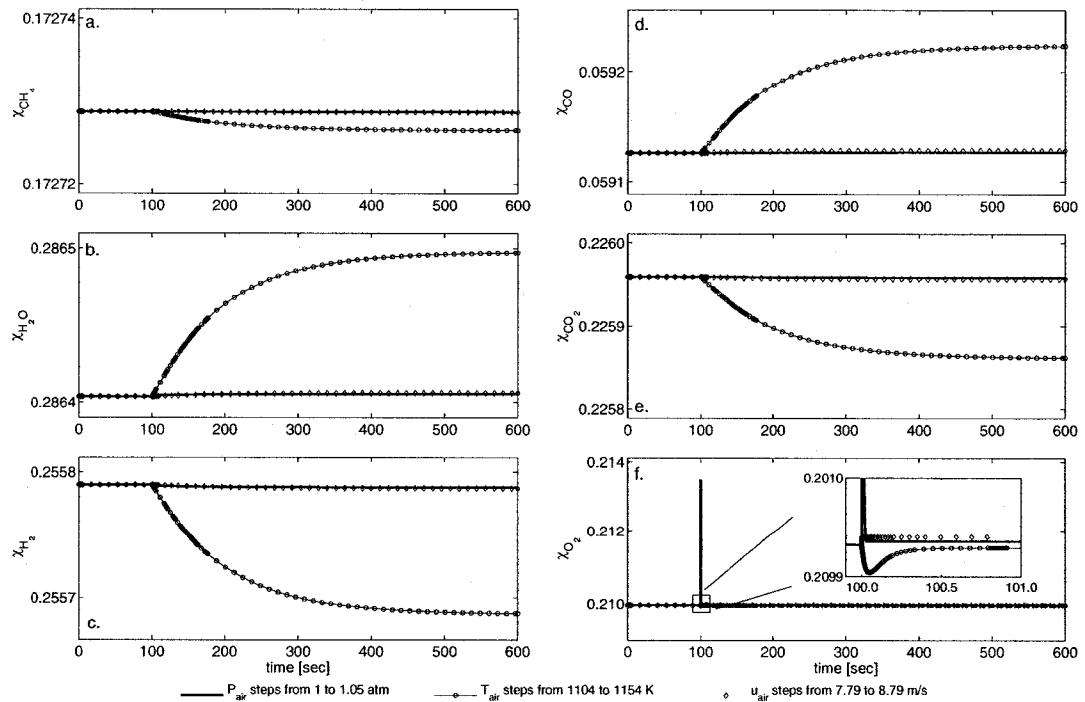


Figure 3.15: Mole fraction responses, when air input P , T , u stepped respectively

because the effect of temperature on voltage was larger than the effect of the shift reaction equilibrium point.

Step change of flow velocity u_{air} mainly affected the heat transfer coefficient h_c , so that heat flowing from air to the cell also increased. The cell temperature increased slightly, but there was almost no effect on other properties.

Effects of P_{air} , T_{air} and u_{air} on the dynamic performance of SOFC are compared in Fig.3.14 and Fig.3.15. The cathode side air inlet temperature had the most significant effect on SOFC solid phase temperature and performance, whether in dynamic or in steady state, when compared to other inlet flow properties.

3.5 Conclusions

A dynamic model for a finite volume of solid oxide fuel cell (SOFC) with a focus on the transport processes has been developed. Dynamics from diffusion processes, inherent impedance, flow processes, heat exchange processes, internal reforming/shifting processes have been considered simultaneously and are modeled in the form of nonlinear state-space equations. Transport phenomena such as diffusion, forced convection, radiation etc. that take place in the operation of SOFC have been investigated and modeled. Cell temperature, ingredient mole fractions etc. are the state variables and their dynamic behaviors were simulated.

The dynamic performance due to step changes in input variables has been investigated through simulations. Dynamic behaviors of each variable when the external load resistance steps were simulated. Fuel flow inlet pressure and temperature have large effects on the dynamic performance of SOFC, especially on its temperature response. It was also shown that cathode side air inlet temperature has the most significant effect on SOFC solid phase temperature and performance when compared to other inlet flow properties. Compared with inlet pressures and temperatures, the effect of flow velocity is not significant. Simulation also indicated that the transient response of SOFC was mainly controlled by the temperature dynamics.

4

1-D Dynamic Model and Approximated Analytical Solution

A first principle 1-D dynamic model for a tubular SOFC stack is developed. As a by-product of this development, an approximated analytical solution to 1-D reacting gas flow problem is presented. The solution is applied to the dynamic 1-D SOFC model and converts the model to the form of nonlinear state-space equations. Compared to numerical solutions, the proposed method can significantly save requirements in computation and thus facilitate dynamic simulations and control applications. Distributed dynamic relations between current density and electromotive force (EMF) are developed. The problem is solved by simultaneously considering diffusion, inherent impedance, primary flow, heat transfer, and internal reforming/shifting reaction. Dynamic responses of the interested variables when external current, fuel and air inlet streams are perturbed by step changes are investigated through simulations.¹

keywords:

SOFC, distributed model, dynamic model, analytical solution, reacting gas flow

¹A version of this chapter was submitted to AICHE Journal, 2007

4.1 Introduction

With recent significant progress of SOFC prototype stacks, dynamic operation and control problems become increasingly important and, as a result, dynamic properties of SOFC stack need to be investigated. Advanced SOFC system configurations also need better understanding of SOFC dynamic characteristics to ensure system stability and operability.

Dynamic modeling of SOFC originated from the lumped parameter assumptions (Achenbach, 1994; Achenbach, 1995; Padullés *et al.*, 2000; Zhu and Tomsovic, 2001; Sedghisigarchi and Feliachi, 2004). Lumped models have limitation to presenting complete SOFC dynamics and are unable to capture dynamic distributions that physically exist in fuel cells.

For more accurate dynamic description, distributed dynamic models need to be considered. Li and Chyu (2003) investigated a distributed model by establishing a steady state 2-D model. Xue *et al.* (2005) and Gemmen and Johnson (2005) considered 1-D mass transfer dynamics induced by flow processes. Iora *et al.* (2005) included internal reforming/shifting reactions in their 1-D dynamic model.

With these efforts, mechanisms that affect dynamic properties of SOFC have been better understood. However, many problems remain open and some important factors have not been considered in the literature, such as processes through which reactants transport from primary flow to reaction sites, the dynamics led by inherent impedance, and the dynamic effect of heat transfer. Although the previously developed 1-D models are also in the form of dynamic models, dynamic properties have not been their focus and solutions are in numerical form.

To build a suitable model that is useful for dynamic simulation and control, our work started by examining the dynamics induced by diffusion and inherent impedance (Qi *et al.*, 2005). Then in a finite volume of SOFC, we modeled dynamic effects from surroundings to the cell through transport dynamics, such as fluid dynamics, reforming/shifting reaction, heat transfer etc. (Qi *et al.*, 2006). Dynamic mechanisms were analyzed and dynamic properties of the finite volume were investigated through simulations.

In this chapter, we will extend our previous dynamic model from the finite volume to a complete tubular SOFC, considering dynamics distributions such as current density,

temperature, and mole fractions etc. along the flow direction. The resultant 1-D dynamic model consists of a set of partial differential equations (PDEs) dependent on both time and axial position.

However, a complex 1-D dynamic model described by a set of PDEs is not suitable for general control applications. In a typical on-line control application, PDEs may need to be solved in every control interval. The distributed dynamic model developed may have heavy computation demands and may not be suitable for on-line applications. In addition, the PDE form of the model creates more complexity in control design. The common practice to convert PDEs to ODEs is through numerical discretization. But this will result in a very large set of ODEs. For example, numerical simulation of 1-D model developed by Iora *et al.* (2005) needs to solve 12,500 nonlinear equations simultaneously.

Instead of relying on numerical solutions, we will consider a novel approach to solving the 1-D problem with considerably less requirements in computations as discussed next.

An 1-D dynamic model of a physical system is usually shown as:

$$\begin{aligned}\frac{\partial v_1}{\partial t} &= -\frac{\partial h_1(v)}{\partial z} + f_1(v) \\ \frac{\partial v_2}{\partial t} &= -\frac{\partial h_2(v)}{\partial z} + f_2(v) \\ &\vdots \\ \frac{\partial v_n}{\partial t} &= -\frac{\partial h_n(v)}{\partial z} + f_n(v)\end{aligned}$$

Obviously the analytical solution of the above PDEs is most desirable for the purpose of control applications or even for dynamic simulations. But it is very difficult, if not impossible, to solve the nonlinear non-homogeneous PDE array explicitly. Instead, we will find an approximated analytical solution and then convert the 1-D model into the ODE form of:

$$\begin{aligned}\frac{dv_1}{dt} &= g_1(v, z) \\ \frac{dv_2}{dt} &= g_2(v, z) \\ &\vdots \\ \frac{dv_n}{dt} &= g_n(v, z)\end{aligned}\tag{4.1}$$

where v_i represents physical variables, $v = [v_1 \ v_2 \ \cdots \ v_n]'$, and z is the location along the flow direction.

This solution is attractive in the sense that simple substitution of position z into the model results in dynamic description at corresponding point. It does not need to integrate all PDEs all way from entry to exit in order to get the dynamics at point z ; thus the proposed strategy can significantly reduce computation efforts. These ordinary differential equations (ODEs) form a nonlinear state space model (SSM) as function of z .

In this chapter, we will derive an approximated analytical solution for general 1-D reacting gas flow problem. The result is then applied to fuel and air flow in the SOFC stack and forms an analytical 1-D dynamic nonlinear state space model.

The remainder of this chapter is organized as follows: 1-D dynamic models of SOFC are discussed in section 2. The approximated analytical solution for a general reacting gas flow problem is derived in section 3. The result is applied to SOFC and the nonlinear state space model is shown in section 4. Distributed dynamics is studied through simulation in section 5, and conclusions are presented in section 6.

4.2 1-D dynamic modeling of SOFC

4.2.1 Brief introduction to tubular SOFC

Mechanical properties of electrode and electrolyte materials limit the strength and durability of SOFC. Significant efforts on SOFC structure have been made to circumvent this problem. Tubular or similar design can significantly increase cell strength. The tubular SOFC developed by Siemens-Westinghouse, shown in Fig.4.1, is one of the most practical and successful designs. The other merit of this design is that it does not need to seal, and consequently avoids the difficult sealing problem.

The SOFC stack consists of hundreds of cell composites. Each composite consists of two tubes, SOFC cell and alumina air injection tube. The cell is an air-electrode-support (AES) tube, onto which the electrolyte is deposited, followed by the anode in the outer surface. Fuel gas is injected from the close end of composites and flows over anode surface through channels formed by composites. Pre-heated air is injected from the injection tube to the bottom of the cell, then turning around and flowing over the

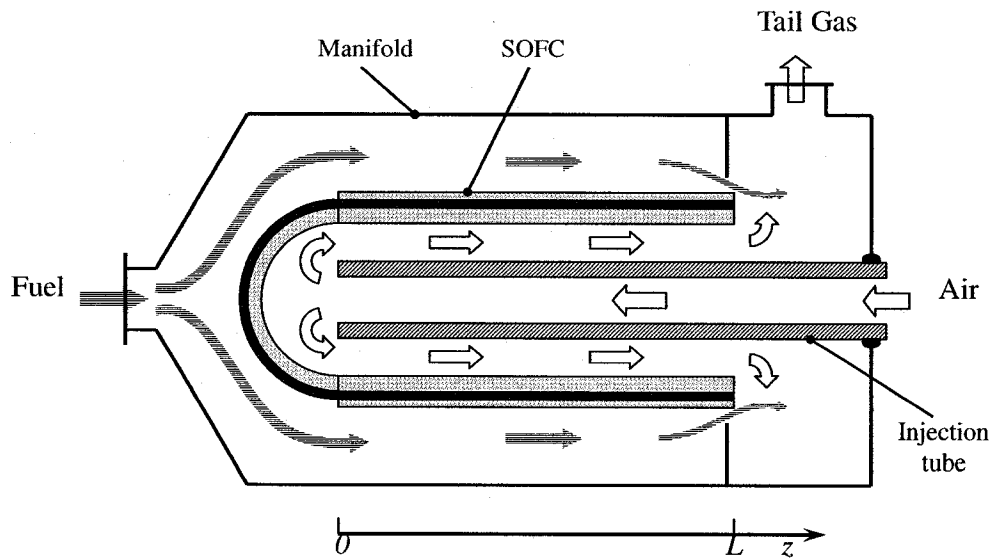


Figure 4.1: Tubular SOFC stack design of Siemens-Westinghouse

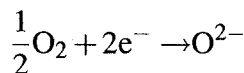
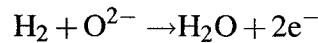
cathode surface through the gap between the cell and the injection tube.

Reactants diffuse away from primary flows, pass through porous electrodes, and reach reaction sites, where they participate in the electrochemical reaction and produce current. The electromotive force (EMF) is established between the anode and the cathode reaction sites, as shown in Fig.4.2.

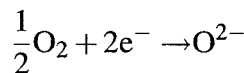
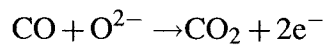
4.2.2 Electricity

Electromotive force (EMF)

The electromotive force (EMF) in the SOFC is established through electrochemical reactions:



or



It is affected by temperature T and reactant partial pressures in the immediate vicinity of triple phase boundary (tpb) p^{tpb} . In addition, the EMF is also reduced by activation

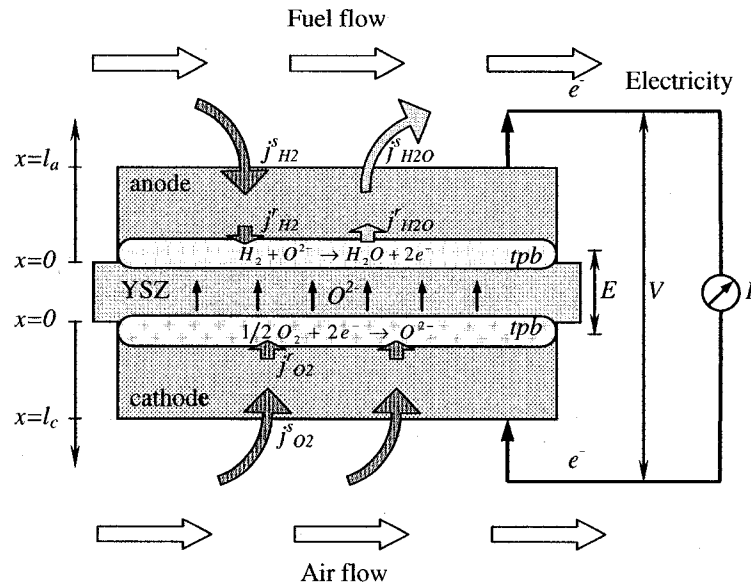


Figure 4.2: Secondary flows of reactant and electrochemical reactions

loss η_{act} :

$$E = E^0 + \frac{RT}{2F} \ln \left(\frac{p_{H_2}^{tpb} p_{O_2}^{tpb \frac{1}{2}}}{p_{H_2O}^{tpb}} \right) - \eta_{act} \quad (4.2)$$

The activation loss η_{act} is determined by current density, exchange current density and partial pressures in the immediate vicinity of *tpb*.

The distribution of the EMF dynamics is thus determined by distributions of factors as discussed above.

Voltage

The intrinsic impedance of the SOFC affects the voltage output when there is an external current demand. For a finite volume of SOFC, the effect has been modeled by an equivalent circuit (Qi *et al.*, 2005), as shown in Fig.4.3. The equivalent circuit can capture the dynamic response of the voltage not only to external current change but also to internal EMF change.

The dynamic behavior of the local voltage can then be modeled through the

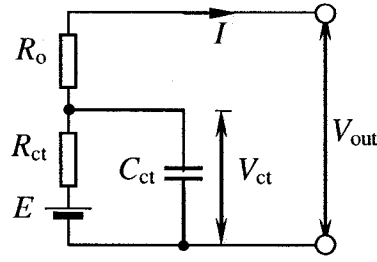


Figure 4.3: Equivalent circuit of local intrinsic impedance

equivalent circuit (Qi *et al.*, 2005):

$$\begin{aligned} V_{ct} &= \frac{1}{\rho_{R_{ct}} l_{R_{ct}} \rho_{C_{ct}}} E - \frac{1}{\rho_{R_{ct}} l_{R_{ct}} \rho_{C_{ct}}} V_{ct} - \frac{1}{\rho_{C_{ct}}} i \\ V_{out} &= V_{ct} - \rho_{R_o} l_{R_o} i \end{aligned} \quad (4.3)$$

where i is the local current density, $\rho_{R_{ct}}$ and ρ_{R_o} are specific resistances of charge transfer and pure Ohmic resistance respectively, $\rho_{C_{ct}}$ is the specific charge transfer capacitance, and $l_{R_{ct}}$ and l_{R_o} are the thicknesses of the charge transfer and pure ohmic resistance layer respectively.

Current density

Current density distribution is determined by the total current demand I and the distribution of EMF. Their relations need to be developed.

A local EMF in a section (a finite volume) has minor effects on the EMF of the neighboring sections; thus they can be assumed to be independent. The tube can be consequently seen as a combination of N independent sections in terms of EMF. Therefore the equivalent circuit for the whole tube is a combination of several equivalent local circuits, as shown in Fig.4.4.

The voltage output V_{out} measured on the inter-connector beam can be assumed uniform due to its large electrical conductivity. So for the equivalent circuits, we have the following relations:

$$\begin{aligned} V_{ct,1} - R_{o,1} I_1 &= V_{ct,2} - R_{o,2} I_2 \\ V_{ct,2} - R_{o,2} I_2 &= V_{ct,3} - R_{o,3} I_3 \\ &\vdots \\ V_{ct,N-1} - R_{o,N-1} I_{N-1} &= V_{ct,N} - R_{o,N} I_N \end{aligned} \quad (4.4)$$

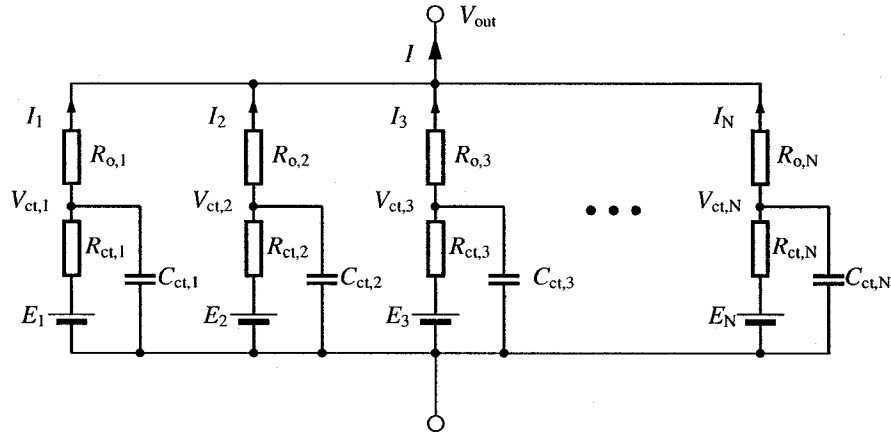


Figure 4.4: Equivalent circuit of SOFC tube

There are totally $N - 1$ equations for the N unknown sub-currents I_i

The total current output I equals to the external load demand, so the current in each sections must satisfy the condition:

$$I = I_1 + I_2 + \dots + I_N \quad (4.5)$$

Solving linear equations expressed in Eqn.4.4 and Eqn.4.5, we can get the solutions of I_i . They are functions of I , $R_{o,i}$ and $V_{ct,i}$. Assuming that $R_{o,i}$ are same and $N \rightarrow \infty$, I_i then converge to the local current and can be expressed as local current density:

$$i = \frac{V_{ct} - \bar{V}_{ct}}{\rho_{R_o} l_{R_o}} + \frac{I}{2\pi r_3 L} \quad (4.6)$$

where \bar{V}_{ct} is the average potential of the whole tube and L the length of the tube.

4.2.3 Diffusion

Reactants must be transported from primary flows to reaction sites to participate in the electrochemical reaction as shown in Fig.4.2. This is done by diffusion. Dynamic behaviors of reactants in the immediate vicinity of the *tpb* and that in the primary flow body are related through the diffusion process.

The dynamic relations among the concentrations in the immediate vicinity of the *tpb*, C^{tpb} , in the primary flow body, C^b , the reactant flux entering the cell surface, j^s , and the reactant flux consumed at the reaction site, j^f , can be modeled in the form of transfer

functions (Qi *et al.*, 2005):

$$\begin{aligned} C^{tpb}(s) &= G_{jc}J^r(s) + G_{cc}C^b(s) \\ j^s(s) &= G_{jj}j^r(s) + G_{cj}C^b(s) \end{aligned} \quad (4.7)$$

where:

$$\begin{aligned} G_{jc} &= \frac{-\frac{l}{D} - \frac{l^3}{6D^2}s}{1 + \frac{l^2}{2D}s + \frac{l^4}{24D^2}s^2}, & G_{cc} &= \frac{1}{1 + \frac{l^2}{2D}s + \frac{l^4}{24D^2}s^2}, \\ G_{jj} &= \frac{1}{1 + \frac{l^2}{2D}s + \frac{l^4}{24D^2}s^2}, & G_{cj} &= \frac{Ls}{1 + \frac{l^2}{2D}s + \frac{l^4}{24D^2}s^2} \end{aligned}$$

and D is the diffusion coefficient, l the thickness of the diffusion layer, and s the Laplace operator.

The reactant consumption rates at reaction sites j^r are directly related to the current density i (Larminie and Dicks, 2003):

$$i = 2F j_{H_2}^r = -2F j_{H_2O}^r = 4F j_{O_2}^r \quad (4.8)$$

where F is the Faraday constant.

Applying the transfer function model to H_2 , H_2O and O_2 respectively, and performing inverse Laplace transform, the species dynamics led by diffusion can be converted to ordinary differential equations (ODE).

So dynamic models for H_2 , H_2O and O_2 fluxes entering cell surfaces are:

$$\ddot{j}_{H_2}^s = -h_1 \dot{j}_{H_2}^s - h_2 j_{H_2}^s + h_1 \frac{1}{2F} \cdot i + h_3 \dot{C}_{H_2}^b \quad (4.9)$$

$$\ddot{j}_{O_2}^s = -o_1 \dot{j}_{O_2}^s - o_2 j_{O_2}^s + o_1 \frac{1}{4F} \cdot i + o_3 \dot{C}_{O_2}^b \quad (4.10)$$

$$\ddot{j}_{H_2O}^s = -w_1 \dot{j}_{H_2O}^s - w_2 j_{H_2O}^s - w_1 \frac{1}{2F} \cdot i + w_3 \dot{C}_{H_2O}^b \quad (4.11)$$

The partial pressures in the immediate vicinity of $tpbs$ are:

$$\ddot{p}_{H_2}^{tpb} = -h_1 \dot{p}_{H_2}^{tpb} - h_2 p_{H_2}^{tpb} - h_4 \frac{RT_{cell}}{2F} \cdot i - \frac{4}{l_a} \frac{RT_{cell}}{2F} \cdot i + h_1 p_{H_2}^b \quad (4.12)$$

$$\ddot{p}_{O_2}^{tpb} = -o_1 \dot{p}_{O_2}^{tpb} - o_2 p_{O_2}^{tpb} - o_4 \frac{RT_{cell}}{4F} \cdot i - \frac{4}{l_c} \frac{RT_{cell}}{4F} \cdot i + o_1 p_{O_2}^b \quad (4.13)$$

$$\ddot{p}_{H_2O}^{tpb} = -w_1 \dot{p}_{H_2O}^{tpb} - w_2 p_{H_2O}^{tpb} + w_4 \frac{RT_{cell}}{2F} \cdot i + \frac{4}{l_a} \frac{RT_{cell}}{2F} \cdot i + w_1 p_{H_2O}^b \quad (4.14)$$

where l_a and l_c are anode and cathode side diffusion layer thickness respectively; coefficients $h_{1\sim 4}$, $o_{1\sim 4}$ and $w_{1\sim 4}$ are functions of diffusion coefficients and diffusion thicknesses. Details can be found in (Qi *et al.*, 2005).

We assume that diffusions only occur in the radial direction, as shown in Fig.4.2, so neighboring diffusion processes along the z direction are independent. The global distribution along the tube depends on the distribution of current density i and distributions of concentrations in the flow C^b , as shown by the diffusion model in Eqn.4.7.

4.2.4 Solid Phase Temperature

Cell Temperature

The electrochemical reaction and the consequent energy conversion occur inside the SOFC cell, which affect the cell temperature. The cell also exchanges heat with the surrounding flow bodies due to their temperature differences, and they affect each other. Our previous investigation has shown that the cell temperature dynamics dominates the dynamics of the SOFC (Qi *et al.*, 2006).

The cell is in solid phase, and it exchanges energy with surroundings along the radial directions, as shown in Fig.4.2. In addition, due to the temperature gradient along the SOFC tube, there is conduction heat transfer. But as analyzed in (Qi *et al.*, 2006), the conductivity of SOFC and the cross section area are small, so the heat flow along axial direction is small compared to that along radius direction. Consequently, dynamic effects due to the conduction along the axial direction can be neglected. We can consequently assume that the neighboring heat transfer processes in the solid phase SOFC cell are non-interacting. The cell temperature can then be modeled locally through the energy conservation law, as we did for the diffusion process.

The energy sources for the electrical power are enthalpies that are carried by reactants. They can be expressed as:

$$\sum j_i^s H_i = j_{H_2}^s H_{H_2}|_{T_{fuel}} + j_{O_2}^s H_{O_2}|_{T_{air}} + j_{H_2O}^s H_{H_2O}|_{T_{cell}} \quad (4.15)$$

where $j_{H_2}^s$, $j_{O_2}^s$ and $j_{H_2O}^s$ are mass fluxes entering the cell, H_{H_2} , H_{O_2} and H_{H_2O} are enthalpy of formations of each reactant. For ideal gases, the enthalpy of formation depends on temperature, and can be approximated by 1st order polynomial of temperature, as shown in table A-7.

Through the electrochemical reaction, the Gibbs free energy is converted to electrical energy. Part of the energy is supplied to the external load, and the leftover is consumed by the intrinsic resistance and converted to heat energy, which heats the cell. The balance of the enthalpy of formation is released as reaction heat. Local electrical energy that leaves the cell is:

$$E_e = V_{\text{out}}i = (V_{\text{ct}} - \rho_{R_o} l_{R_o} \cdot i)i \quad (4.16)$$

where ρ_{R_o} and l_{R_o} are the specific resistance and the thickness of pure ohmic resistance respectively.

Due to temperature differences, heat fluxes transfer between the cell and gases by means of forced convection is:

$$q_{\text{conv}} = h_a(T_{\text{cell}} - T_{\text{fuel}}) + h_c(T_{\text{cell}} - T_{\text{air}}) \quad (4.17)$$

where h_a and h_c are anode and cathode side heat transfer coefficients respectively. They depend on gas property and velocity etc., and can be modeled through the Reynolds number Re , Nusselt Number Nu , and Prandtl Number Pr .

SOFC works at high temperature, and the heat transfer effect through radiation is thus significant. In the SOFC stack, we assume that temperatures of each cell are same, but the injection tube temperature and the cell temperature can be different. So the radiation mainly occurs between the cell and the injection tube in the SOFC cell composite:

$$q_{\text{rad}} = \frac{\sigma}{R_{\text{rad}}}(T_{\text{cell}}^4 - T_{\text{tube}}^4) \quad (4.18)$$

where σ is the Stefan-Boltzman constant, and R_{rad} is the radiation heat transfer resistance. It depends on the view factor and emissivity of the cell and the tube.

In addition, the cell also supplies heat to the fuel channel reforming reaction, and the heat flux is:

$$q_{\text{ref}} = r_{\text{ref}} \cdot \Delta H_{\text{ref}} \quad (4.19)$$

where r_{ref} is the reforming reaction rate and ΔH_{ref} the reaction heat (Qi *et al.*, 2006).

According to the first law of thermodynamics, the energy balance in the cell is:

$$\frac{d\rho_{\text{cell}}C_{p,\text{cell}}T_{\text{cell}}}{dt} = \sum J_i^s H_i - E_e - q_{\text{conv}} - q_{\text{rad}} - q_{\text{ref}} \quad (4.20)$$

With consideration of geometry in Eqn.4.15,4.16,4.17,4.18 and 4.19, and substituting them into the energy conservation equation, Eqn.4.20, the local dynamics

of the cell temperature can be modeled as:

$$\begin{aligned} \frac{dT_{\text{cell}}}{dt} = & \frac{1}{\rho_{\text{cell}} C_{p,\text{cell}}} \cdot \frac{1}{r_3^*} \cdot [\\ & j_{\text{H}_2}^s H_{\text{H}_2} |_{T_{\text{fuel}}} + \frac{r_2}{r_3} \cdot j_{\text{O}_2}^s H_{\text{O}_2} |_{T_{\text{air}}} + j_{\text{H}_2\text{O}}^s H_{\text{H}_2\text{O}} |_{T_{\text{cell}}} - (V_{\text{ct}} - \rho_{\text{R}_o} l_{\text{R}_o} \cdot i) i \\ & - h_a (T_{\text{cell}} - T_{\text{fuel}}) - \frac{r_2}{r_3} \cdot h_c (T_{\text{cell}} - T_{\text{air}}) - \frac{r_2}{r_3} \cdot \frac{\sigma}{R_{\text{rad}}} (T_{\text{cell}}^4 - T_{\text{tube}}^4) \\ & - r_{\text{ref}} \cdot \Delta H_{\text{ref}}] \end{aligned} \quad (4.21)$$

where ρ_{cell} and $C_{p,\text{cell}}$ are the density and the heat capacity of the cell respectively, r_2 and r_3 are inner and outer radius of the cell, and $r_3^* = \frac{r_3^2 - r_2^2}{2r_3}$.

Injection Tube Temperature

Heat transfer in the injection tube is similar to that in the cell, and its temperature can also be modeled locally. The injection tube is a passive component in the heat transfer process. It exchanges heat with air flows through forced convection and is heated by the cell through radiation. The dynamics thus can be modeled following the similar procedure shown above:

$$\begin{aligned} \frac{dT_{\text{tube}}}{dt} = & \frac{1}{\rho_{\text{tube}} C_{p,\text{tube}}} \cdot \frac{1}{r_1^*} \cdot [\\ & - h_c (T_{\text{tube}} - T_{\text{air}}) - \frac{r_0}{r_1} \cdot h_l (T_{\text{tube}} - T_{\text{inj}}) + \frac{r_2}{r_1} \cdot \frac{\sigma}{R_{\text{rad}}} (T_{\text{cell}}^4 - T_{\text{tube}}^4)] \end{aligned} \quad (4.22)$$

where ρ_{tube} and $C_{p,\text{tube}}$ are the density and the heat capacity of the injection tube respectively, r_0 and r_1 are inner and outer radius of the injection tube respectively, and $r_1^* = \frac{r_1^2 - r_0^2}{2r_1}$.

4.2.5 Fuel Flow

In the tubular SOFC stack that we consider, fuel gas is pre-reformed methane, consisting of CH_4 , H_2O , H_2 , CO , and CO_2 . It is injected from the close end side of the composite, flowing through gaps among SOFC tubes, as shown in Fig.4.1. The tail gas passes through the gap on the right side and then leaves the stack.

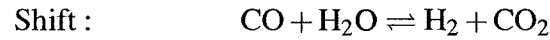
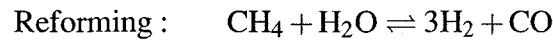
The mixture undergoes reforming/shifting reactions in the fuel channel. Meanwhile, by means of diffusion, H_2 and H_2O transport in and out the cell to participate in the electrochemical reaction.

In the fuel channel, the fuel temperature, velocity and species concentrations etc. are distributed along the flow channel, because of mass, heat and momentum exchange through secondary flow and the reforming/shifting reaction. Gas phase parameter distributions affect solid phase variables. The dynamics of fuel flow can be described by 1-D equation of continuity, the equation of energy and the equation of motion.

At $z = 0$, we assume that physical states such as pressure, temperature, velocity and mole fractions are equal to that of the corresponding properties at the fuel inlet.

Reforming and shifting reactions

Reforming and shifting reactions generate H_2 , CO and CO_2 from methane and steam:



Based on the methane consumption rate, the reforming rate is experimentally determined by (Ahmed and Foger, 2000):

$$r_{\text{ref}} = -r_{CH_4} = K_r p_{CH_4}^{\alpha} p_{H_2O}^{\beta} \exp\left(-\frac{E_r}{RT_{\text{fuel}}}\right) \quad (4.23)$$

where K_r is the rate coefficient, E_r is activation energy, and α , β are order coefficients for methane and steam respectively.

The shifting reaction rate is approximated by (Qi *et al.*, 2006):

$$r_{\text{sft}} = K_s [p_{CO} p_{H_2O} \exp\left(\frac{4276}{T_{\text{fuel}}} - 3.961\right) - p_{CO_2} p_{H_2}] \quad (4.24)$$

where K_s is the rate coefficient.

Concentrations

Accounting mass balances in a finite volume of fuel flow (Qi *et al.*, 2006), and taking the limit as the width of the control volume approaches zero, we can get the species dynamics in the primary flow.

The CH_4 is consumed only by the reforming reaction, and its concentration dynamics is then modeled as:

$$\frac{\partial C_{CH_4}}{\partial t} = -\frac{\partial}{\partial z} u_{\text{fuel}} C_{CH_4} - \frac{1}{r^*} \cdot r_{\text{ref}} \quad (4.25)$$

where $r^* = \frac{4-\pi}{2\pi} r_3$ is geometry fitness parameter and u_{fuel} the fuel velocity.

Reforming and shifting reactions consume H_2O , and the electrochemical reaction produces H_2O flux entering the primary flow. Its concentration dynamics is:

$$\frac{\partial C_{\text{H}_2\text{O}}}{\partial t} = -\frac{\partial}{\partial z} u_{\text{fuel}} C_{\text{H}_2\text{O}} - \frac{1}{r^*} \cdot r_{\text{ref}} - \frac{1}{r^*} \cdot r_{\text{sft}} - \frac{1}{r^*} \cdot j_{\text{H}_2\text{O}}^{\text{s}} \quad (4.26)$$

where $-j_{\text{H}_2\text{O}}^{\text{s}}$ is the steam flux leaving the anode surface and entering the primary flow.

H_2 is produced by reforming and shifting reactions, at the rate of $3r_{\text{ref}}$ and r_{sft} respectively. It is also consumed by the electrochemical reaction. Its dynamic model is:

$$\frac{\partial C_{\text{H}_2}}{\partial t} = -\frac{\partial}{\partial z} u_{\text{fuel}} C_{\text{H}_2} + 3 \cdot \frac{1}{r^*} \cdot r_{\text{ref}} + \frac{1}{r^*} \cdot r_{\text{sft}} - \frac{1}{r^*} \cdot j_{\text{H}_2}^{\text{s}} \quad (4.27)$$

where $j_{\text{H}_2}^{\text{s}}$ is the hydrogen flux leaving the primary flow.

CO is produced by the reforming reaction and consumed by the shifting reaction. It is assumed that CO does not participate in the electrochemical reaction. So its concentration dynamics is:

$$\frac{\partial C_{\text{CO}}}{\partial t} = -\frac{\partial}{\partial z} u_{\text{fuel}} C_{\text{CO}} + \frac{1}{r^*} \cdot r_{\text{ref}} - \frac{1}{r^*} \cdot r_{\text{sft}} \quad (4.28)$$

Qi *et al.* (2006) has discussed the case when CO participates in the electrochemical reaction.

CO_2 is produced by the shifting reaction:

$$\frac{\partial C_{\text{CO}_2}}{\partial t} = -\frac{\partial}{\partial z} u_{\text{fuel}} C_{\text{CO}_2} + \frac{1}{r^*} \cdot r_{\text{sft}} \quad (4.29)$$

Fuel temperature

The fuel gas is a mixture of five different species. Their inherent properties are different. But each specie has same temperature. The temperature is affected by several factors: reforming and shifting reaction heats, enthalpies that are carried by reactant fluxes, and heat transferred from its surroundings, etc. The effect of kinetic energy can be neglected due to low velocity and low density.

Reforming reaction is an endothermal process. The fuel gas must be heated to maintain the reforming reaction. For the internal reforming/shifting design, the fuel flow is heated by the SOFC cell. That is, extra heat flux from the SOFC cell is injected to the fuel flow.

So the temperature dynamics can be modeled through the energy balance:

$$\begin{aligned} \frac{\partial}{\partial t} (\sum (C_i C_{p,i}) \cdot T_{\text{fuel}}) = & - \frac{\partial}{\partial z} (u_{\text{fuel}} \sum (C_i H_i)) \\ & - \frac{1}{r^*} \cdot j_{\text{H}_2}^s H_{\text{H}_2} - \frac{1}{r^*} \cdot j_{\text{H}_2\text{O}}^s H_{\text{H}_2\text{O}} \\ & - \frac{1}{r^*} \cdot h_a (T_{\text{fuel}} - T_{\text{cell}}) + \frac{1}{r^*} \cdot r_{\text{ref}} \cdot \Delta H_{\text{ref}} \end{aligned} \quad (4.30)$$

where C_i are concentrations of each species in the fuel gas, $C_{p,i}$ their specific heats at constant pressure, H_i enthalpy of formations, and $r^* = \frac{4-\pi}{2\pi} r_3$ the geometry fitness parameter.

Fuel velocity

The flow velocity determines space time in the fuel channel and affects the heat transfer coefficient; thus it is the dominant factor that affects concentrations and the temperature.

In the fuel channel, the reforming/shifting reactions and the electrochemical reaction induce pressure gradient. The pressure gradient significantly affects forces acting on the primary flow and consequently the velocity. Due to the electrochemical reaction, some H_2 in the fuel flow is converted to H_2O through secondary flow. The density of the mixture thus changes which leads to the velocity change. In the fuel channel, the effect of friction is minor and may be neglected because the viscosity of fuel is small.

Dynamic behaviors of flow velocities can be modeled through the momentum conservation law:

$$\begin{aligned} \frac{\partial}{\partial t} [\sum (C_i M_i) \cdot u_{\text{fuel}}] = & - \frac{\partial}{\partial z} (\sum (C_i M_i \cdot u_{\text{fuel}}^2)) \\ & - \frac{1}{r^*} \cdot j_{\text{H}_2}^s M_{\text{H}_2} u_{\text{fuel}} - \frac{\partial P_{\text{fuel}}}{\partial z} \end{aligned} \quad (4.31)$$

where M_i are mole masses of each species. Fuel gas can be assumed as ideal gas, and we have:

$$P_{\text{fuel}} = \sum C_i R T_{\text{fuel}}$$

4.2.6 Air Flow

Air is injected from the injection tube as shown in Fig.4.1. It is injected to the bottom of the cell tube, then turns around and goes through the gap formed by the cell and the

injection tube. So air flow is divided into two sections. In the cathode channel, air is co-flow with fuel. O₂ diffuses into the cathode and is reduced to oxygen ion. In the injection channel, air is counter-flow relative to the fuel flow. No reaction or secondary flow occurs.

Boundary conditions for the air flow in the cathode channel at $z = 0$ equal to that of the air flows out of the injection tube. For the air flow in the injection tube at $z = L$, boundary conditions are determined by the inlet air pressure, temperature and velocity.

Cathode channel air flow

We assume that air consists of N₂ and O₂ only. N₂ is not involved in any reactions, and only O₂ diffuses out of the primary flow to participate in the electrochemical reaction. So the species dynamics is:

$$\frac{\partial C_{N_2}}{\partial t} = -\frac{\partial}{\partial z} u_{\text{air}} C_{N_2} \quad (4.32)$$

and

$$\frac{\partial C_{O_2}}{\partial t} = -\frac{\partial}{\partial z} u_{\text{air}} C_{O_2} - \frac{1}{r_2^*} \cdot j_{O_2}^s \quad (4.33)$$

where $r_2^* = \frac{r_2^2 - r_1^2}{2r_2}$ is the geometry adjustment parameter, u_{air} the air velocity in the cathode channel, and $j_{O_2}^s$ the mass flux that enters the cell and is consumed by the electrochemical reaction.

The air flow exchanges heat with the cell tube and the injection tube respectively. Its temperature dynamics can be modeled by the following equation:

$$\begin{aligned} \frac{\partial}{\partial t} ((\sum (C_j C_{p,j}) \cdot T_{\text{air}})) = & -\frac{\partial}{\partial z} (u_{\text{air}} \sum (C_j H_j)) - \frac{1}{r_2^*} \cdot j_{O_2}^s H_{O_2} \\ & - \frac{1}{r_2^*} \cdot h_c (T_{\text{air}} - T_{\text{cell}}) - \frac{1}{r_2^*} \cdot \frac{r_1}{r_2} \cdot h_c (T_{\text{air}} - T_{\text{tube}}) \end{aligned} \quad (4.34)$$

where C_j are concentrations of N₂ and O₂, $C_{p,j}$ their specific heat, H_j their enthalpy of formations, and h_c the cathode side heat transfer coefficient which is affected by the velocity (Qi *et al.*, 2006).

The velocity dynamics of the cathode side air is:

$$\frac{\partial}{\partial t} (\sum (C_j M_j) \cdot u_{\text{air}}) = -\frac{\partial}{\partial z} (\sum (C_j M_j \cdot u_{\text{air}}^2)) - \frac{1}{r_2^*} \cdot j_{O_2}^s M_{O_2} u_{\text{air}} - \frac{\partial P_{\text{air}}}{\partial z} \quad (4.35)$$

where M_j are mole masses of N₂ and O₂ respectively, and the pressure is:

$$P_{\text{air}} = \sum C_j R T_{\text{air}}$$

Injection channel air flow

In the injection tube, except for the primary flow, the air flow only exchanges heat with the tube; no other transport processes occur. The flow direction is opposite to the axial direction, as shown in Fig.4.1. In the 1-D modeling, the location of the air flow in the injection channel is represented by y instead of z . They have the relation $y = L - z$.

So we are only interested in the temperature dynamics for the air flow in the injection tube. Species concentrations and the velocity are assumed to be the same as that at the inlet. The temperature can then be modeled by:

$$C_{\text{air}}^{\text{in}} C_{p,\text{air}} \cdot \frac{\partial T_{\text{inj}}}{\partial t} = -u_{\text{air}}^{\text{in}} C_{\text{air}}^{\text{in}} \cdot \frac{\partial H_{\text{air}}}{\partial y} - \frac{r_0}{2} \cdot h_t (T_{\text{inj}} - T_{\text{tube}}) \quad (4.36)$$

where $C_{\text{air}}^{\text{in}}$ is the air concentration at the inlet, $C_{p,\text{air}}$ the air specific heat at constant pressure, $u_{\text{air}}^{\text{in}}$ the input velocity, H_{air} the enthalpy of formation of air, and h_t the heat transfer coefficient, which is affected by the velocity (Qi *et al.*, 2006).

4.3 Approximate analytical solution

An 1-D dynamic model is usually solved through numerical methods. Numerical integration techniques such as finite element method are often adopted to find the solution. The fundamental approach of numerical methods is discretization of the continuous model. With smaller integration intervals, more accurate solution will be expected. For a complex system such as SOFC, over twenty variables have to be modeled in the form of nonlinear, non-homogeneous PDEs. If employing numerical methods, a large number of equations due to the discretization must be solved simultaneously (Iora *et al.*, 2005). This results in heavy computations. Therefore, numerical methods may not be suitable for certain real time applications, such as control applications.

In control applications, to meet on-line computation requirement, the system model is often simplified. Fast dynamics is approximated by steady state solution (Iora *et al.*, 2005); non-dominant dynamic variables are neglected (Padullés *et al.*, 2000); distributed parameter system is lumped to give a set of ordinary differential equations (Qi *et al.*, 2007b). The objective is to reduce the computation requirement. However, these simplifications unavoidably induce large model errors.

Usually, an analytical solution can satisfy both speed and precision requirements. But it is very difficult, if not impossible, to find exact analytical solutions for those nonlinear, non-homogeneous and coupled PDEs such as the 1-D dynamic model of SOFC. In this section, aiming at solving the 1-D reacting gas flow problem, we attempt to develop an approximated analytical solution that can balance the speed and precision requirements.

4.3.1 Problem description

Analysis in the previous section has shown that model of the SOFC mainly consists of two parts: the non-flowing phase part and the flowing phase part. Parameter distributions of non-flowing phase also depend on that of the flowing phase. In the SOFC stack that we are considering, the flowing phase consists of three primary flow bodies: they are fuel flow, air flow in the cathode channel and, air flow in the injection tube. The fuel flow is the most representative one, and it is used as an example for the 1-D reacting gas flow problem in the following development.

Within the primary flow, the mixed gases are reacting. So concentrations of each species are not constant along the flow channel and the total concentration is affected by the reaction. Simultaneously, the primary flow exchanges heat with the wall of the flow channel. The change of the gas phase temperature thus leads to pressure change. The pressure gradient induced by the reaction and the temperature significantly affects the primary flow velocity. Through the secondary flow, H_2 in the primary flow body gradually changes to H_2O . The density of the mixture is thus changed. This in turn affects the primary flow velocity.

A flow body can be described by three distributed variables: concentrations, energy and velocity. Their dynamic behaviors can be modeled by several PDEs, as shown by Eqn.4.25, 4.26, 4.27, 4.28, 4.29, 4.30, and 4.31. In general, the dynamic 1-D model for a reacting gas flow can be written as:

$$\begin{aligned}
 \frac{\partial C_i}{\partial t} &= -\frac{\partial}{\partial z}(uC_i) + \mathcal{A} \\
 &\vdots \\
 \frac{\partial}{\partial t}CC_pT &= -\frac{\partial}{\partial z}(uCH) + \mathcal{B} \\
 \frac{\partial}{\partial t}CMu &= -\frac{\partial}{\partial z}(CMu^2) - \frac{\partial P}{\partial z} + \mathcal{C}
 \end{aligned} \tag{4.37}$$

where C is the total concentration, u the velocity, $H = a + bT$ enthalpy of formation, T the temperature, and \mathcal{A} , \mathcal{B} , \mathcal{C} combinations of non-homogeneous terms, respectively.

Strict analytical solution for this model is beyond our scope. We shall derive an approximate solution in the form of Eqn.4.1.

4.3.2 Assumptions

As we have analyzed before, the 1-D reacting gas flow has the following characteristics:

- Reaction leading to total mole number change;
- Heat exchange leading to temperature change;
- Momentum change;
- Constant flow area;
- Frictionless;
- Velocity lower than 0.3 Mach.

Gas phase fluid body is compressible, especially considering gas phase dynamics. However, when the flow velocity is lower than 0.3 Mach, compared with the motion of the flow bulk, the effect lead by compressibility can be neglected and gas flow can be assumed incompressible (Zucker and Biblarz, 2002). That is, for the gas phase fluid, its pressure can be assumed uniform along the flow channel if we neglect the friction. Numerical simulations from the detailed model shown by Eqn.4.37 support this assumption (Iora *et al.*, 2005). So, according to the law of mass conservation, the velocity is distributed due to the mole number change led by the reaction. In this case, the velocity is mainly determined by the continuity. The effect of momentum change is minor and may be neglected. Gas dynamics also shows that the dynamic response of velocity to inlet disturbance is very fast. The state changes only occur within a very thin layer named shock wave. The shock wave moves fast, in the sonic speed (Zucker and Biblarz, 2002). So, with the condition that the flow channel is not long, the velocity dynamics can be neglected. Therefore, in order to develop the analytical solution, we make the following assumptions:

- Gas phase flow is incompressible;

- Pressure along the flow channel is uniform;
- Velocity is distributed due to reaction;
- The effect of density change can be neglected;
- Velocity dynamics can be neglected.

4.3.3 Approximated analytical solution

Velocity

Since velocity is the dominant variable of the fluid and it is considered at steady state, the key to obtaining an approximate analytical solution starts from the solution of the velocity.

For the fuel flow, continuity equations are shown in Eqn.4.25, 4.26, 4.27, 4.28 and Eqn.4.29. Dividing them by the total concentration C , concentrations of each species can be converted to their mole fractions:

$$\begin{aligned}\frac{\partial \chi_{\text{CH}_4}}{\partial t} &= -\frac{\partial}{\partial z} u_{\text{fuel}} \chi_{\text{CH}_4} - \frac{1}{r^*} \cdot \frac{1}{C} r_{\text{ref}} \\ \frac{\partial \chi_{\text{H}_2\text{O}}}{\partial t} &= -\frac{\partial}{\partial z} u_{\text{fuel}} \chi_{\text{H}_2\text{O}} - \frac{1}{r^*} \cdot \frac{1}{C} r_{\text{ref}} - \frac{1}{r^*} \cdot \frac{1}{C} r_{\text{sft}} - \frac{1}{r^*} \cdot \frac{1}{C} j_{\text{H}_2\text{O}}^{\text{s}} \\ \frac{\partial \chi_{\text{H}_2}}{\partial t} &= -\frac{\partial}{\partial z} u_{\text{fuel}} \chi_{\text{H}_2} + \frac{1}{r^*} \cdot \frac{3}{C} r_{\text{ref}} + \frac{1}{r^*} \cdot \frac{1}{C} r_{\text{sft}} - \frac{1}{r^*} \cdot \frac{1}{C} j_{\text{H}_2}^{\text{s}} \\ \frac{\partial \chi_{\text{CO}}}{\partial t} &= -\frac{\partial}{\partial z} u_{\text{fuel}} \chi_{\text{CO}} + \frac{1}{r^*} \cdot \frac{1}{C} r_{\text{ref}} - \frac{1}{r^*} \cdot \frac{1}{C} r_{\text{sft}} \\ \frac{\partial \chi_{\text{CO}_2}}{\partial t} &= -\frac{\partial}{\partial z} u_{\text{fuel}} \chi_{\text{CO}_2} + \frac{1}{r^*} \cdot \frac{1}{C} r_{\text{sft}}\end{aligned}$$

Summing them up yields:

$$\frac{\partial}{\partial t} \sum \chi_i = -\frac{\partial}{\partial z} u_{\text{fuel}} \sum \chi_i + \frac{1}{r^*} \cdot \frac{2}{C} r_{\text{ref}} - \frac{1}{r^*} \cdot \frac{1}{C} j_{\text{H}_2\text{O}}^{\text{s}} - \frac{1}{r^*} \cdot \frac{1}{C} j_{\text{H}_2}^{\text{s}} \quad (4.38)$$

Note obvious identities:

$$\sum \chi_i = 1; \quad \frac{d1}{dt} = 0; \quad \text{and} \quad \frac{d1}{dz} = 0$$

For SOFC, we have $j_{\text{H}_2}^{\text{s}} = -j_{\text{H}_2\text{O}}^{\text{s}}$.

Substituting these equations into Eqn.4.38 and rearranging gives:

$$\frac{du_{\text{fuel}}}{dz} = \frac{1}{r^*} \cdot \frac{2}{C} r_{\text{ref}}$$

B.C.

$$\begin{aligned} u_{\text{fuel}} &= u_{\text{fuel}}^{\text{in}}; & \text{at } z = 0 \\ C &= C^{\text{in}}; & \text{at } z = 0 \\ r_{\text{ref}} &= r_{\text{ref}}^{\text{in}}; & \text{at } z = 0 \end{aligned} \quad (4.39)$$

This result shows that the velocity distribution depends on the reaction rate in SOFC anode fuel flow.

Since the distribution of r_{ref} and the total concentration C are affected by other variables and are not constants, direct integration of u_{fuel} is not possible. The velocity at location z can be integrated approximately from Eqn.4.39, using different approximation methods such as the Trapezoidal approximation, according to pre-knowledge of the r_{ref} profile.

With the approximated solution for steady state velocity at location z , we avoid the need of the equation of momentum balance.

Decoupling

Due to the terms of concentrations, the temperature and the velocity affect each other. For a gas flow, the equation of continuity, the equation of energy, and the equation of motion are coupled, as shown by Eqn. 4.37. They should be decoupled in order to find the analytical solution.

Physically, although reactions and the mass transfer within secondary flow affect concentrations of each species, they are dominated by the primary flow itself. That is, the equation of continuity is dominated by the term $\frac{\partial}{\partial z}(uC_i)$. So in solving the continuity equation, we can assume that other factors such as temperature are constant.

For the energy equation, the temperature is dominated by flow velocity and energy exchanges. The change of concentration actually only has minor effects on the dynamic response process. It does not affect the terminal temperature value. So concentration in the energy equation can be seen as constant.

With these two assumptions and the velocity equation developed previously, the equation of continuity and the equation of energy can be resolved independently. This

is the principle behind decoupling in the following derivation.

Approximate Analytical Solution

In general, the 1-D dynamic reacting gas flow model can be simplified to the form of:

$$\frac{\partial v}{\partial t} = -a \cdot u \cdot \frac{\partial v}{\partial z} - b \cdot v - c;$$

B.C.

$$v = v^{\text{in}} \quad \text{at} \quad z = 0; \quad (4.40)$$

We approximate velocity profile by :

$$u = A + B \cdot z$$

where v is the interested physical variable, u the velocity, and a , b , c , A and B coefficients.

Performing Laplace transform to the PDE in terms of time t , it can be converted to an ODE:

$$sv = -a \cdot u \cdot \frac{dv}{dz} - b \cdot v - c;$$

$$u = A + B \cdot z; \quad (4.41)$$

B.C.

$$v = v^{\text{in}} \quad \text{at} \quad z = 0$$

where s is the Laplace operator.

The ODE shown in Eqn.4.41 can be analytically solved:

$$sv = -bv - c + [(b+s)v^{\text{in}} + c] \cdot \left(1 + \frac{B}{A} \cdot z\right)^{-\frac{b+s}{aB}} \quad (4.42)$$

Neglecting the effect of inlet transient process and performing inverse Laplace transform, the result can then be transferred to ODE with respect to time t again:

$$\frac{dv}{dt} = -bv - c + (bv^{\text{in}} + c) \cdot \left(1 + \frac{B}{A}z\right)^{-\frac{b}{aB}} \quad (4.43)$$

This is the approximated analytical solution for 1-D dynamic reacting gas flow problem. Actually, many gas phase reactors in chemical engineering have similar characteristics. This result may be applicable.

4.3.4 Validation

The method and the approximated analytical solution of the reacting gas flow problem is partially tested on a simple example, by comparing the approximated steady state distribution with the exact solution.

Suppose that the process model is:

$$\frac{\partial v}{\partial t} = -1 \cdot u \cdot \frac{\partial v}{\partial z} - 1 \cdot v - 1 \quad u^{\text{in}} = v^{\text{in}} = 1 \text{ at } z = 0$$

Assuming that the reaction rate only depends on the position:

$$r = \frac{1}{(1+z)^2}$$

The profile of r is similar to that of reforming reaction rate in the tubular SOFC.

So the explicit analytical solutions of the velocity and the physical variable distributions are:

$$u = -\frac{1}{z+1} + 2$$

$$v = 2 \cdot \exp\left[-\frac{1}{2}z - \frac{1}{4}\ln(1+2z)\right] - 1$$

Adopting the approximated solution proposed above, the distributions are solved as:

$$u = u^{\text{in}} + \frac{1}{2}(r^{\text{in}} + r) \cdot z$$

$$v = -1 + 2 \cdot \left[\frac{1}{2}(1+r) \cdot z + 1\right]^{\left(\frac{-2}{1+r}\right)}$$

The exact solutions and the approximated solutions are compared in Fig.4.5. It is shown that the approximated distribution matches the actual one reasonably well. The approximated velocity distribution does have some error due to the Trapezoidal approximation. For a specific application, other more appropriate approximations should be developed according to possible velocity distribution. This may need several iterations between approximations and validations.

4.3.5 Application to SOFC

Numerical simulations show that the profile of r_{ref} under the given condition is exponential like, so first order approximation of the velocity u as shown in Eqn.4.40 will lead large error when z increases. A more accurate approximation needs to be developed.

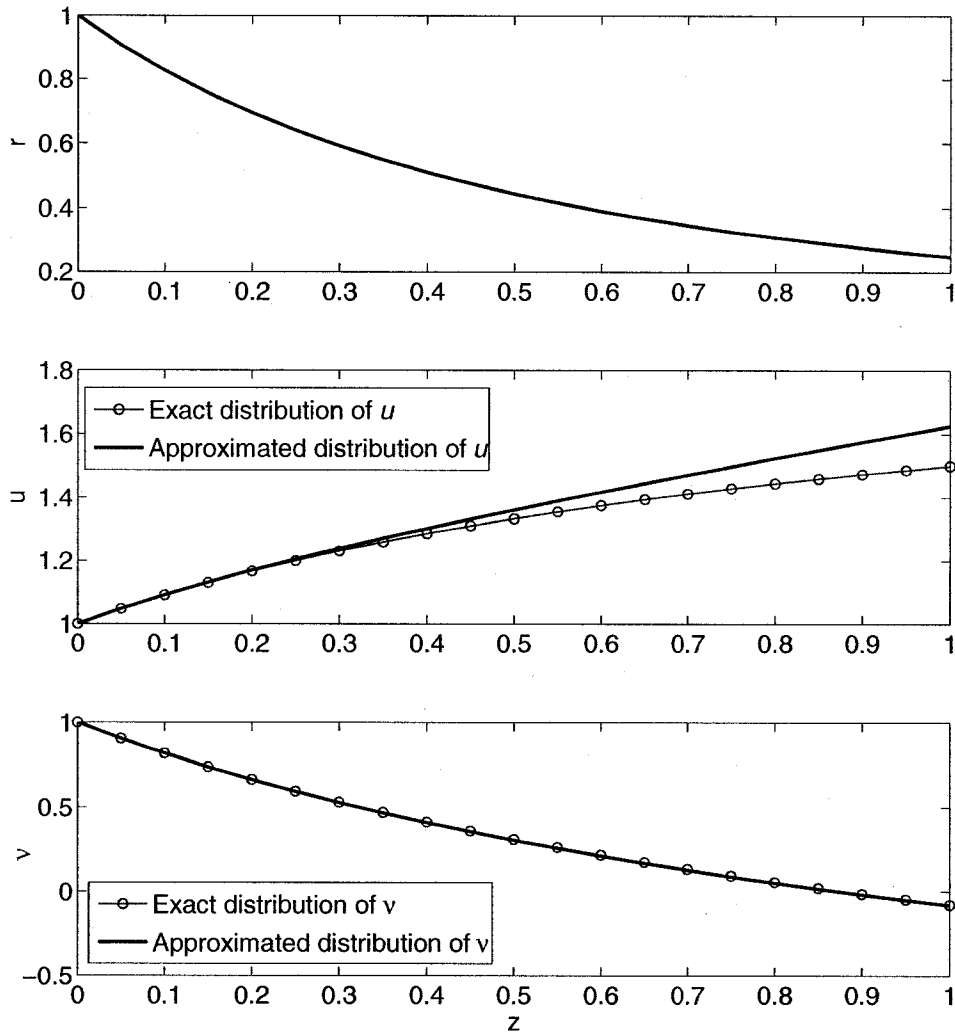


Figure 4.5: Comparison of the approximated analytical solutions of velocity and physical variable distributions and the exact analytical solutions.

Reforming rate and velocity

Assume that the distribution of r_{ref} can be approximated by

$$r_{\text{ref}} = r^{\text{in}} \exp\left(-\frac{z}{\xi}\right) \quad (4.44)$$

we need to find the space constant ξ .

The reforming reaction rate Eqn.4.23 shows that r_{ref} is proportional to $p_{\text{CH}_4}^{0.85}$ and may be approximated by $K p_{\text{CH}_4}$ for the sake of possible analytical solution. Substituting this approximation into the steady state equation of continuity and rearranging it to the form of mole fraction get :

$$\frac{\partial}{\partial z} u \chi_{\text{CH}_4} = -\frac{K}{r^* C} \chi_{\text{CH}_4} \quad (4.45)$$

Obviously, the space constant of χ_{CH_4} is:

$$\xi = \frac{r^* C u^{\text{in}}}{K} \quad (4.46)$$

where $K = \frac{r_{\text{ref}}^{\text{in}}}{\chi_{\text{CH}_4}^{\text{in}}}$. It equals to the space constant of r_{ref} .

So the steady state velocity can be analytically integrated from the r_{ref} approximation Eqn.4.44:

$$u = u^{\text{in}} + \frac{2}{r^* C} r^{\text{in}} \xi \cdot [1 - \exp\left(-\frac{z}{\xi}\right)] \quad (4.47)$$

Analytical solution

Therefore, the reacting gas flow problem in SOFC can be concluded as:

$$\begin{aligned} \frac{\partial v}{\partial t} &= -\frac{\partial}{\partial z} u v + b(z) + c; \\ u &= A + B \cdot [1 - \exp\left(-\frac{z}{\xi}\right)]; \end{aligned} \quad (4.48)$$

B.C.

$$v = v^{\text{in}} \quad \text{at} \quad z = 0;$$

Converting the PDE to a ODE by performing Laplace transform in terms of time t :

$$u \cdot \frac{dv}{dz} + \left(\frac{du}{dz} + s\right) \cdot v = b(z) + c$$

It can be rearranged as:

$$(u + sz) \cdot \frac{dv}{dz} + \left(\frac{du}{dz} + s \right) \cdot v - sz \cdot \frac{dv}{dz} = b(z) + c$$

The position z in the axial coordinate is independent of time t , so sz equals to zero and the term $sz \cdot \frac{dv}{dz}$ can be removed from the equation, and the ODE can then be arranged as:

$$a_1(z) \frac{dv}{dz} + a_0(z)v = b(z) + c \quad (4.49)$$

with $\frac{d}{dz}a_1(z) = a_0(z)$. This linear ODE can be analytically solved. With known $b(z) = \frac{n}{r^*C}r_{\text{ref}}$, the solution is:

$$\frac{dv}{dt} = u^{\text{in}}v^{\text{in}} - uv + \frac{n}{r^*C}r^{\text{in}}\xi \cdot [1 - \exp(-\frac{z}{\xi})] + \frac{c}{r^*C} \cdot z \quad (4.50)$$

Application

Applying the solution shown by Egn.4.50 to the SOFC fuel flow, distributed dynamic models of specie mole fractions are:

$$\frac{d\chi_{\text{CH}_4}}{dt} = \frac{1}{r^*} \cdot \frac{RT_{\text{fuel}}}{P_{\text{fuel}}^{\text{in}}} \cdot \left\{ -u_{\text{fuel}} \cdot \chi_{\text{CH}_4} + u_{\text{fuel}}^{\text{in}} \cdot \chi_{\text{CH}_4}^{\text{in}} - r_{\text{ref}}^{\text{in}} \cdot \xi \cdot [1 - \exp(-\frac{z}{\xi})] \right\} \quad (4.51)$$

$$\begin{aligned} \frac{d\chi_{\text{H}_2\text{O}}}{dt} = \frac{1}{r^*} \cdot \frac{RT_{\text{fuel}}}{P_{\text{fuel}}^{\text{in}}} \cdot \left\{ -u_{\text{fuel}} \chi_{\text{H}_2\text{O}} + u_{\text{fuel}}^{\text{in}} \cdot \chi_{\text{H}_2\text{O}}^{\text{in}} - r_{\text{ref}}^{\text{in}} \cdot \xi \cdot [1 - \exp(-\frac{z}{\xi})] \right. \\ \left. + (-r_{\text{sft}} - j_{\text{H}_2\text{O}}^{\text{s}}) \cdot z \right\} \end{aligned} \quad (4.52)$$

$$\begin{aligned} \frac{d\chi_{\text{H}_2}}{dt} = \frac{1}{r^*} \cdot \frac{RT_{\text{fuel}}}{P_{\text{fuel}}^{\text{in}}} \cdot \left\{ -u_{\text{fuel}} \cdot \chi_{\text{H}_2} + u_{\text{fuel}}^{\text{in}} \cdot \chi_{\text{H}_2}^{\text{in}} + 3r_{\text{ref}}^{\text{in}} \cdot \xi \cdot [1 - \exp(-\frac{z}{\xi})] \right. \\ \left. + (r_{\text{sft}} - j_{\text{H}_2\text{O}}^{\text{s}}) \cdot z \right\} \end{aligned} \quad (4.53)$$

$$\begin{aligned} \frac{d\chi_{\text{CO}}}{dt} = \frac{1}{r^*} \cdot \frac{RT_{\text{fuel}}}{P_{\text{fuel}}^{\text{in}}} \cdot \left\{ -u_{\text{fuel}} \cdot \chi_{\text{CO}} + u_{\text{fuel}}^{\text{in}} \cdot \chi_{\text{CO}}^{\text{in}} + r_{\text{ref}}^{\text{in}} \cdot \xi \cdot [1 - \exp(-\frac{z}{\xi})] \right. \\ \left. - r_{\text{sft}} \cdot z \right\} \end{aligned} \quad (4.54)$$

$$\frac{d\chi_{\text{CO}_2}}{dt} = \frac{1}{r^*} \cdot \frac{RT_{\text{fuel}}}{P_{\text{fuel}}^{\text{in}}} \cdot \left\{ -u_{\text{fuel}} \cdot \chi_{\text{CO}_2} + u_{\text{fuel}}^{\text{in}} \cdot \chi_{\text{CO}_2}^{\text{in}} + r_{\text{sft}} \cdot z \right\} \quad (4.55)$$

where z is the location.

The distributed dynamic model of temperature is:

$$\begin{aligned} \frac{dT_{\text{fuel}}}{dt} = & \frac{1}{r^* C_{p,\text{fuel}}} \cdot \frac{RT_{\text{fuel}}}{P_{\text{fuel}}^{\text{in}}} \cdot \left\{ -j_{\text{H}_2}^{\text{s}} \cdot (a_{\text{H}_2} + b_{\text{H}_2} T_{\text{fuel}}) - h_a \cdot (T_{\text{fuel}} - T_{\text{cell}}) \right. \\ & - j_{\text{H}_2\text{O}}^{\text{s}} \cdot (a_{\text{H}_2\text{O}} + b_{\text{H}_2\text{O}} T_{\text{cell}}) + \left[(j_{\text{H}_2}^{\text{s}} \cdot (a_{\text{H}_2} + b_{\text{H}_2} T_{\text{fuel}}^{\text{in}}) \right. \\ & \left. \left. + h_a \cdot (T_{\text{fuel}}^{\text{in}} - T_{\text{cell}}) + j_{\text{H}_2\text{O}}^{\text{s}} \cdot (a_{\text{H}_2\text{O}} + b_{\text{H}_2\text{O}} T_{\text{cell}}) \right] \right\} \\ & \exp\left(-\frac{1}{r^*} \cdot \frac{RT_{\text{fuel}}}{P_{\text{fuel}}^{\text{in}}} \cdot \frac{j_{\text{H}_2}^{\text{s}} b_{\text{H}_2} + h_a}{u_{\text{fuel}} \chi_i b_i} \cdot z\right) \end{aligned} \quad (4.56)$$

The velocity distribution of fuel flow is given by Eqn.4.47.

Applying the solution to the cathode side air flow, the distributed dynamic model of O_2 mole fraction is:

$$\begin{aligned} \frac{d\chi_{\text{O}_2}}{dt} = & \frac{1}{r_2^*} \cdot \frac{RT_{\text{air}}}{P_{\text{air}}^{\text{b}}} \cdot \left\{ -(1 - \chi_{\text{O}_2}) j_{\text{O}_2}^{\text{s}} + (1 - \chi_{\text{O}_2}^{\text{b}}) j_{\text{O}_2}^{\text{s}} \cdot \right. \\ & \left. \left[1 - \frac{1}{2r_2^*} \cdot \frac{R}{P_{\text{air}}^{\text{b}} u_{\text{air}}^{\text{b}}} \cdot (T_{\text{air}}^{\text{b}} + T_{\text{air}}) j_{\text{O}_2}^{\text{s}} \cdot z \right]^{-2} \frac{T_{\text{air}}}{T_{\text{air}}^{\text{b}} + T_{\text{air}}} \right\} \end{aligned} \quad (4.57)$$

where $P_{\text{air}}^{\text{b}} = P_{\text{air}}^{\text{in}}$, $u_{\text{air}}^{\text{b}} = \frac{r_0}{r_2 - r_1} u_{\text{air}}^{\text{in}}$, and $T_{\text{air}}^{\text{b}} = T_{\text{inj}}|_{z=0}$ are air flow parameters at the close end of the tube.

The distributed dynamic temperature model is:

$$\begin{aligned} \frac{dT_{\text{air}}}{dt} = & \frac{1}{r_2^* C_{p,\text{air}}} \cdot \frac{RT_{\text{air}}}{P_{\text{air}}^{\text{b}}} \cdot \left\{ -(h_c + \frac{r_1}{r_2} h_c) T_{\text{air}} - (-h_c T_{\text{cell}} + \frac{r_1}{r_2} h_c T_{\text{tube}}) \right. \\ & \left. + [(h_c + \frac{r_1}{r_2} h_c) T_{\text{air}}^{\text{b}} + (-h_c T_{\text{cell}} + \frac{r_1}{r_2} h_c T_{\text{tube}})] \cdot \right. \\ & \left. \left[1 - \frac{1}{2r_2^*} \cdot \frac{R}{P_{\text{air}}^{\text{b}} u_{\text{air}}^{\text{b}}} \cdot (T_{\text{air}}^{\text{b}} + T_{\text{air}}) j_{\text{O}_2}^{\text{s}} \cdot z \right]^{-2} \frac{T_{\text{air}}}{T_{\text{air}}^{\text{b}} + T_{\text{air}}} \right\} \end{aligned} \quad (4.58)$$

The velocity distribution is:

$$u_{\text{air}} = u_{\text{air}}^{\text{b}} - \frac{1}{2r_2^*} \cdot \frac{R}{P_{\text{air}}^{\text{b}}} (T_{\text{air}}^{\text{b}} + T_{\text{air}}) \cdot j_{\text{O}_2}^{\text{s}} \cdot z \quad (4.59)$$

We are also interested in the temperature of air flow inside the injection tube:

$$\begin{aligned} \frac{dT_{\text{inj}}}{dt} = & \frac{2}{r_0 C_{p,\text{air}}} \cdot \frac{RT_{\text{inj}}}{P_{\text{air}}^{\text{in}}} \cdot \left\{ -h_t T_{\text{inj}} + h_t T_{\text{tube}} + (h_t T_{\text{air}}^{\text{in}} - h_t T_{\text{tube}}) \cdot \right. \\ & \left. \exp\left[-\frac{2}{r_2} \cdot \frac{R}{P_{\text{air}}^{\text{in}} u_{\text{air}}^{\text{in}}} \cdot \frac{h_t}{b_{\text{air}}} T_{\text{inj}} \cdot (L - z)\right] \right\} \end{aligned} \quad (4.60)$$

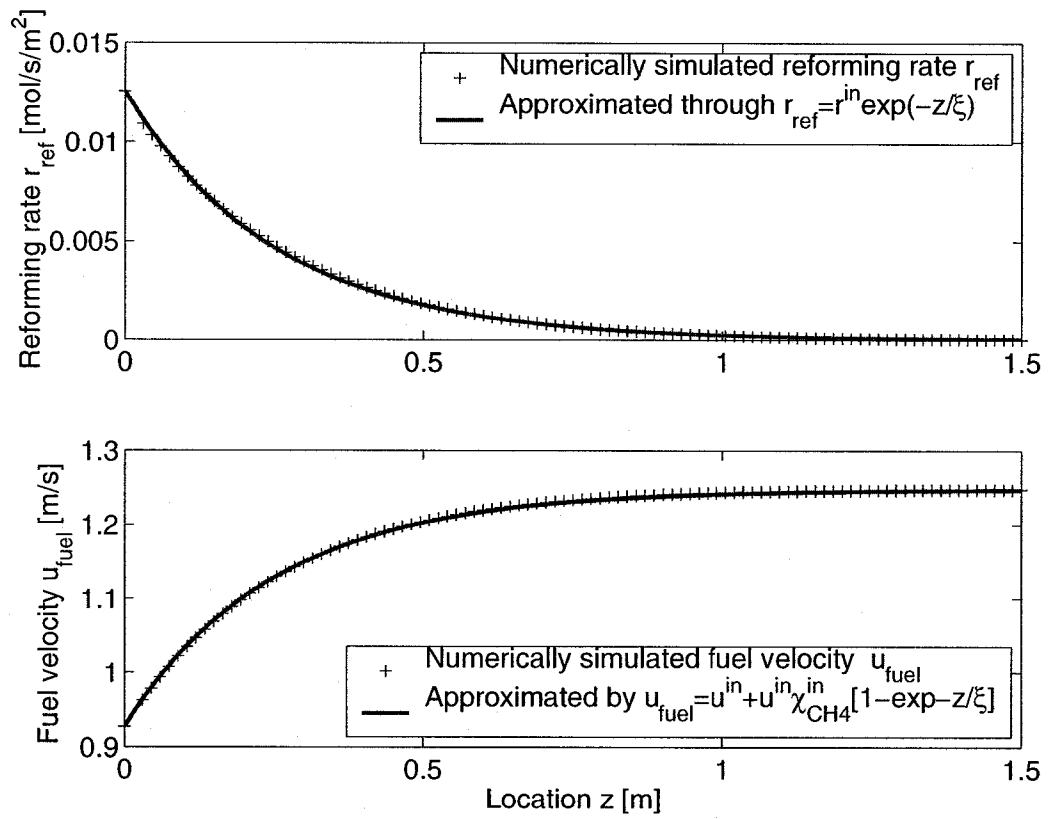


Figure 4.6: Comparison of numerically simulated and the approximate analytical solution of steady state reforming reaction rate and fuel velocity profiles.

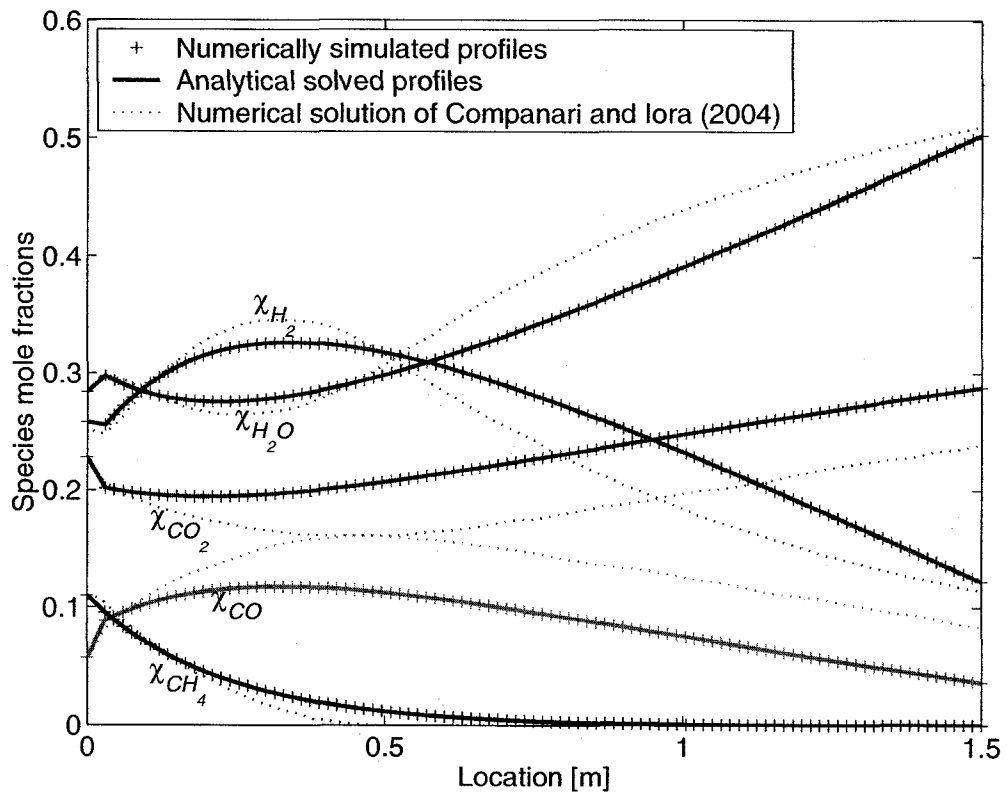


Figure 4.7: Comparison of numerically simulated and the approximate analytical solution of isothermal steady state species mole fraction profiles. Parameters: $I = 200A$, $P_{\text{fuel}} = 1\text{atm}$, $T_{\text{fuel}} = 923\text{K}$, $u_{\text{fuel}}^{\text{in}} = 0.927\text{m/s}$

Steady state simulation

The approximate analytical solution of steady state fuel gas profiles and numerical simulations are compared under the isothermal condition, as shown in Fig.4.6 and Fig.4.7 respectively. Lines with cross mark in Fig.4.6 and Fig.4.7 are numerically simulated profiles, from Eqn. 4.25, 4.26, 4.27, 4.28, and 4.29. Solid lines are analytical solution results, directly from Eqn.4.51, 4.52, 4.53, 4.54, and 4.52. Simulation shows that the approximate solution Eqn.4.50 has good precision for this application.

It also shows in Fig.4.7 that under same input condition, variable profiles of the developed model are consistent with Campanari and Iora's (2004) numerical simulation results. The difference between the proposed simulations and Campanari and Iora's (2004) results is mainly induced by the effect of temperature gradient to the equilibrium of the shifting reaction.

4.4 State-space model

Assembling dynamic models for each physical variables shown above, the dynamic model at any location of the SOFC stack can be described in the form of a nonlinear state-space model.

For the SOFC stack we are considering, physical variables that can be manipulated at the entrance are designated as inputs. Their perturbations affect the dynamic performance of the SOFC stack. Intermediate variables are designated as state variables. The electrical output of the stack is the output variable, and other interested variables that can be measured can also be designed as model output. The location z in the stack and other variables such as mole fractions in the inlet flow are considered as parameters

So the input vector \mathbf{u} is defined as:

$$\mathbf{u} = \left[I \quad P_{\text{fuel}}^{\text{in}} \quad T_{\text{fuel}}^{\text{in}} \quad u_{\text{fuel}}^{\text{in}} \quad P_{\text{air}}^{\text{in}} \quad T_{\text{air}}^{\text{in}} \quad u_{\text{air}}^{\text{in}} \right]^T \quad (4.61)$$

where I is the total external current load demand.

The output vector is:

$$\mathbf{y} = \left[V_{\text{out}} \quad T_{\text{fuel}}^{\text{exit}} \quad u_{\text{fuel}}^{\text{exit}} \quad T_{\text{air}}^{\text{exit}} \quad u_{\text{air}}^{\text{exit}} \quad \chi_{\text{H}_2}^{\text{exit}} \quad \chi_{\text{CO}}^{\text{exit}} \quad \chi_{\text{O}_2}^{\text{exit}} \right]^T \quad (4.62)$$

The state vector is defined as:

$$\mathbf{x} = \left[V_{ct} \quad j_{H_2}^s \quad j_{H_2}^{is} \quad j_{O_2}^s \quad j_{O_2}^{is} \quad j_{H_2O}^s \quad j_{H_2O}^{is} \quad p_{H_2}^{tpb} \quad \dot{p}_{H_2}^{tpb} \quad p_{O_2}^{tpb} \quad \dot{p}_{O_2}^{tpb} \quad p_{H_2O}^{tpb} \quad \dot{p}_{H_2O}^{tpb} \quad v_I \quad T_{cell} \quad T_{tube} \quad T_{fuel} \quad T_{air} \quad T_{inj} \quad \chi_{CH_4} \quad \chi_{H_2O} \quad \chi_{H_2} \quad \chi_{CO} \quad \chi_{CO_2} \quad \chi_{O_2} \right]^T \quad (4.63)$$

where v_I is the intermediate variable to approximate the derivative of the current input (Qi *et al.*, 2005).

A second order process:

$$\frac{d^2 v}{dt^2} = f(v)$$

can be expressed by two first order processes:

$$\begin{aligned} \frac{dv}{dt} &= \dot{v} \\ \frac{d\dot{v}}{dt} &= f(v) \end{aligned}$$

Applying this method to models shown by Eqn.4.9, 4.10, 4.11, 4.12, 4.13 and 4.14, and combining electrical model Eqn.4.3, physical models shown by Eqn.4.21, 4.22, 4.56, 4.58, 4.60, 4.51, 4.52, 4.53, 4.54, 4.55 and 4.57, the state space model can be expressed as:

States:	
\dot{x}_1	$= \frac{1}{\rho_R \rho_C} E - \frac{1}{\rho_R \rho_C} x_1 - \frac{1}{\rho_C} \frac{u_1}{2\pi r_3 L}$
\dot{x}_2	$= x_3$
\dot{x}_3	$= -h_1 x_2 - h_2 x_3 + h_1 \frac{1}{2F} \frac{u_1}{2\pi r_3 L} + h_3 \frac{1}{R x_{17}} (\dot{u}_2 x_{22} + u_2 \dot{x}_{22})$
\dot{x}_4	$= x_5$
\dot{x}_5	$= -o_1 x_4 - o_2 x_5 + o_1 \frac{1}{4F} \frac{u_1}{2\pi r_3 L} + o_3 \frac{1}{R x_{18}} (\dot{u}_5 x_{25} + u_5 \dot{x}_{25})$
\dot{x}_6	$= x_7$
\dot{x}_7	$= -w_1 x_6 - w_2 x_7 + w_1 \frac{1}{2F} \frac{-u_1}{2\pi r_3 L} + w_3 \frac{1}{R x_{17}} (\dot{u}_2 x_{21} + u_2 \dot{x}_{21})$
\dot{x}_8	$= x_9$
\dot{x}_9	$= -h_1 x_8 - h_2 x_9 - h_4 \frac{R x_{15}}{2F} \frac{u_1}{2\pi r_3 L} + h_1 u_2 x_{22} - \frac{4 R x_{15}}{l_a} \frac{1}{2F} \left(\frac{K u_1}{2\pi r_3 L} - x_{14} \right)$
\dot{x}_{10}	$= x_{11}$
\dot{x}_{11}	$= -o_1 x_{10} - o_2 x_{11} - o_4 \frac{R x_{15}}{4F} \frac{u_1}{2\pi r_3 L} + o_1 u_5 x_{25} - \frac{4 R x_{15}}{l_c} \frac{1}{4F} \left(\frac{K u_1}{2\pi r_3 L} - x_{14} \right)$

$$\begin{aligned}
 \dot{x}_{12} &= x_{13} \\
 \dot{x}_{13} &= -w_1 x_{12} - w_2 x_{13} - w_4 \frac{R x_{15} - u_1}{2F} + w_1 u_2 x_{21} - \frac{4 R x_{15}}{l_a} \left(\frac{-K u_1}{2\pi r_3 L} + x_{14} \right) \\
 \dot{x}_{14} &= K^2 \frac{u_1}{2\pi r_3 L} - K x_{14} \\
 \dot{x}_{15} &= \frac{1}{r_3^*} \frac{1}{\rho_{\text{cell}} C_{p,\text{cell}}} \left[x_2 (a_{\text{H}_2} + b_{\text{H}_2} x_{17}) + \frac{r_2}{r_3} x_4 (a_{\text{O}_2} + b_{\text{O}_2} x_{18}) \right. \\
 &\quad + x_6 (a_{\text{H}_2\text{O}} + b_{\text{H}_2\text{O}} x_{17}) - x_1 \frac{u_1}{2\pi r_3 L} - h_a (x_{15} - x_{17}) - \frac{r_2}{r_3} h_c (x_{15} - x_{18}) \\
 &\quad \left. - \frac{r_2}{r_3} \frac{\sigma}{R_{\text{rad}}} (x_{15}^4 - x_{16}^4) - r_{\text{ref}} \Delta H_f \right] \\
 \dot{x}_{16} &= \frac{1}{r_1^*} \frac{1}{\rho_{\text{tube}} C_{p,\text{tube}}} \left[-h_c (x_{16} - x_{18}) - \frac{r_0}{r_1} h_t (x_{16} - x_{19}) + \frac{r_2}{r_1} \frac{\sigma}{R_{\text{rad}}} (x_{15}^4 - x_{16}^4) \right] \\
 \dot{x}_{17} &= \frac{1}{r^*} \frac{1}{C_{p,\text{fuel}}} \frac{R x_{17}}{u_2} \left\{ -x_2 (a_{\text{H}_2} + b_{\text{H}_2} x_{17}) - x_6 (a_{\text{H}_2\text{O}} + b_{\text{H}_2\text{O}} x_{17}) \right. \\
 &\quad - h_a (x_{17} - x_{15}) + [x_2 (a_{\text{H}_2} + b_{\text{H}_2} u_3) + h_a (u_3 - x_{15}) + x_6 (a_{\text{H}_2\text{O}} + b_{\text{H}_2\text{O}} x_{15})] \cdot \\
 &\quad \left. \exp \left(-\frac{1}{r^*} \frac{R x_{17}}{u_2} \frac{x_2 b_{\text{H}_2} + h_a}{u_{\text{fuel}} \sum_{20}^{24} x_i b_i} \cdot z \right) \right\} \\
 \dot{x}_{18} &= \frac{1}{r_2^*} \frac{1}{C_{p,\text{air}}} \frac{R x_{18}}{u_5} \left\{ -\left(h_c + \frac{r_1}{r_2} h_c \right) x_{18} - \left(-h_c x_{15} + \frac{r_1}{r_2} h_c x_{16} \right) \right. \\
 &\quad + \left[\left(h_c + \frac{r_1}{r_2} h_c \right) x_{19} \Big|_{x=0} + \left(-h_c x_{15} + \frac{r_1}{r_2} h_c x_{16} \right) \right] \cdot \\
 &\quad \left. \left[1 - \frac{1}{2r_2^*} \frac{R}{u_5} \frac{r_0}{r_2 - r_1} \frac{u_7}{u_7} x_4 (x_{19} \Big|_{x=0} + x_{18}) \cdot z \right]^{-2} \frac{x_{18}}{x_{19} \Big|_{x=0} + x_{18}} \right\} \\
 \dot{x}_{19} &= \frac{2}{r_0} \frac{1}{C_{p,\text{air}}} \frac{R x_{19}}{u_5} \left\{ -h_t x_{19} + h_t x_{16} + (h_t u_6 - h_t x_{16}) \right. \\
 &\quad \left. \exp \left[-\frac{2}{r_2} \frac{R}{u_5 u_7} \frac{h_t}{b_{\text{air}}} x_{19} \cdot (L - z) \right] \right\} \\
 \dot{x}_{20} &= \frac{1}{r^*} \frac{R x_{17}}{u_2} \left\{ -u_{\text{fuel}} x_{20} + u_4 \chi_{\text{CH}_4}^{\text{in}} - r_{\text{ref}}^{\text{in}} \xi \left[1 - \exp \left(-\frac{z}{\xi} \right) \right] \right\} \\
 \dot{x}_{21} &= \frac{1}{r^*} \frac{R x_{17}}{u_2} \left\{ -u_{\text{fuel}} x_{21} + u_4 \chi_{\text{H}_2\text{O}}^{\text{in}} - r_{\text{ref}}^{\text{in}} \xi \left[1 - \exp \left(-\frac{z}{\xi} \right) \right] - (r_{\text{sft}} + x_6) \cdot z \right\}
 \end{aligned}$$

$$\dot{x}_{22} = \frac{1}{r^*} \frac{Rx_{17}}{u_2} \left\{ -u_{\text{fuel}}x_{22} + u_4\chi_{\text{H}_2}^{\text{in}} + 3r_{\text{ref}}^{\text{in}}\xi \left[1 - \exp\left(-\frac{z}{\xi}\right) \right] + (r_{\text{sft}} - x_2) \cdot z \right\}$$

$$\dot{x}_{23} = \frac{1}{r^*} \frac{Rx_{17}}{u_2} \left\{ -u_{\text{fuel}}x_{23} + u_4\chi_{\text{CO}}^{\text{in}} + r_{\text{ref}}^{\text{in}}\xi \left[1 - \exp\left(-\frac{z}{\xi}\right) \right] - r_{\text{sft}} \cdot z \right\}$$

$$\dot{x}_{24} = \frac{1}{r^*} \frac{Rx_{17}}{u_2} \left\{ -u_{\text{fuel}}x_{24} + u_4\chi_{\text{CO}_2}^{\text{in}} + r_{\text{sft}} \cdot z \right\}$$

$$\dot{x}_{25} = \frac{1}{r_2^*} \frac{Rx_{18}}{u_5} \left\{ -(1 - x_{25})x_4 + (1 - \chi_{\text{O}_2}^{\text{in}})x_4 \cdot \left[1 - \frac{1}{2r_2^*} \frac{R}{u_5} \frac{r_0}{r_2 - r_1} u_7 (x_{19}|_{z=0} + x_{18})x_4 \cdot z \right]^{-2 \frac{x_{18}}{x_{19}|_{z=0} + x_{18}}} \right\}$$

Outputs:

$$y_1 = \frac{1}{2} (x_1|_{z=0} + x_1|_{z=L}) - \rho_{\text{R}_0} l_{\text{R}_0} \frac{u_1}{2\pi r_3 L}$$

$$y_2 = x_{17}|_{z=L}$$

$$y_3 = u_4 + 2\chi_{\text{CH}_4}^{\text{in}} u_4 \left[1 - \exp\left(-\frac{Rx_{17}|_{z=L}}{r^* u_2} \frac{r_{\text{ref}}^{\text{in}}}{u_4 \chi_{\text{CH}_4}^{\text{in}}} \cdot L\right) \right]$$

$$y_4 = x_{18}|_{z=L}$$

$$y_5 = \frac{r_0}{r_2 - r_1} u_7 - \frac{1}{2r_2^*} \frac{R}{u_5} (x_{19}|_{z=0} + x_{18}|_{z=L})x_4|_{z=L} \cdot L$$

$$y_6 = x_{22}|_{z=L}$$

$$y_7 = x_{23}|_{z=L}$$

$$y_8 = x_{25}|_{z=L}$$

Where:

$$\begin{aligned}
E &= 1.273 - 2.7645 \times 10^{-4} x_{15} + \frac{Rx_{15}}{2F} \ln \left(\frac{x_8 x_{10}^{1/2}}{x_{12}} \right) \\
&\quad - \frac{Rx_{15}}{F} \sinh^{-1} \left(\frac{\frac{u_1}{2\pi r_3 L}}{7 \times 10^9 (x_8 x_{12}) \exp \left(-\frac{E_{\text{act},a}}{Rx_{15}} \right)} \right) \\
&\quad - \frac{Rx_{15}}{F} \sinh^{-1} \left(\frac{\frac{u_1}{2\pi r_3 L}}{7 \times 10^9 (x_{10})^{0.25} \exp \left(-\frac{E_{\text{act},c}}{Rx_{15}} \right)} \right) \\
u_{\text{fuel}} &= u_4 + 2\chi_{\text{CH}_4}^{\text{in}} u_4 \left[1 - \exp \left(-\frac{Rx_{17}}{r^* u_2 u_4 \chi_{\text{CH}_4}^{\text{in}}} \cdot L \right) \right] \\
\xi &= \frac{r^* u_2}{Rx_{17}} u_4 \chi_{\text{CH}_4}^{\text{in}} \\
r_{\text{ref}} &= K_r (u_2 x_{20})^\alpha (u_2 x_{21})^\beta \exp \left(-\frac{E_r}{Rx_{17}} \right) \\
r_{\text{ref}}^{\text{in}} &= K_r (u_2 \chi_{\text{CH}_4}^{\text{in}})^\alpha (u_2 \chi_{\text{H}_2\text{O}}^{\text{in}})^\beta \exp \left(-\frac{E_r}{Ru_3} \right) \\
r_{\text{sft}} &= K_s u_2^2 \left[x_{23} x_{21} \exp \left(\frac{4276}{x_{17}} - 3961 \right) - x_{22} x_{24} \right]
\end{aligned}$$

or, in a compact form:

$$\begin{aligned}
\dot{\mathbf{x}} &= f(\mathbf{x}, \mathbf{u}, z) \\
\mathbf{y} &= g(\mathbf{x}, \mathbf{u}, z)
\end{aligned} \tag{4.64}$$

4.5 Simulations

A Simulink model of the tubular SOFC with analytical solution for the 1-D dynamic reacting gas flow problem has been developed according to the state space equations. Dynamic behaviors and parameter distributions of SOFC were simulated through the model. The SOFC model parameters are listed in Table A-2. Gas phase parameters can be found in (Qi *et al.*, 2006). Default input conditions for simulation are shown in Table A-1. Perturbations of input variables are relative to these default settings.

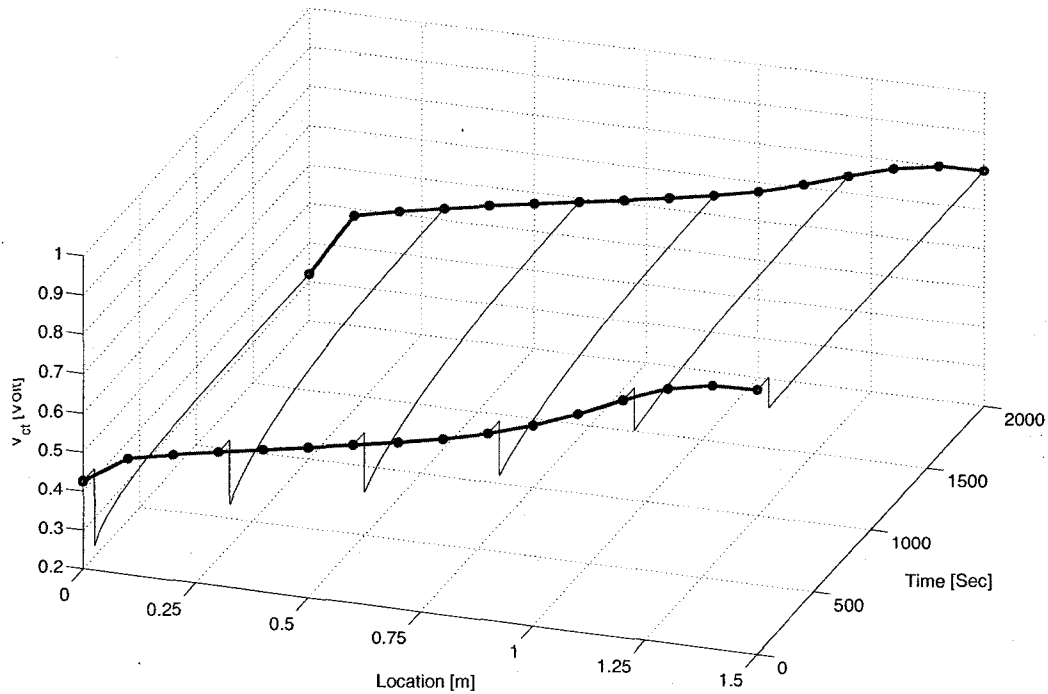


Figure 4.8: V_{ct} profile and step response, when I step changes from 100 to 150 Amp at 100 second.

4.5.1 Step responses due to current demand changes

Step response tests can effectively reveal process dynamic parameters such as time constant, gain, time delay etc. In fact, the industrial model predictive control often uses step response as the model. Step responses and distributed profiles of voltage, temperatures, and species mole fractions etc. due to the step change in current demand I are shown in Fig.4.8, Fig.4.9, and Fig.4.10 respectively.

When external load current demand I was stepped up, diffusion processes and the intrinsic impedance prevented the immediate jump of voltage, and the time constant of the consequent dynamic response is around 0.2 seconds.

Because more current was consumed by the inherent resistance, the cell is therefore heated and its temperature is increased gradually as shown by Fig.4.9. The response time constant is around 1000 seconds due to its large heat capacity. The behavior of cell temperature consequently dominates behavior of other temperatures.

Step change of current I changes the secondary reactant fluxes $j_{H_2}^s$, $j_{H_2O}^s$, and $j_{O_2}^s$. They consequently affect composition distributions, as shown by Fig.4.10. Step

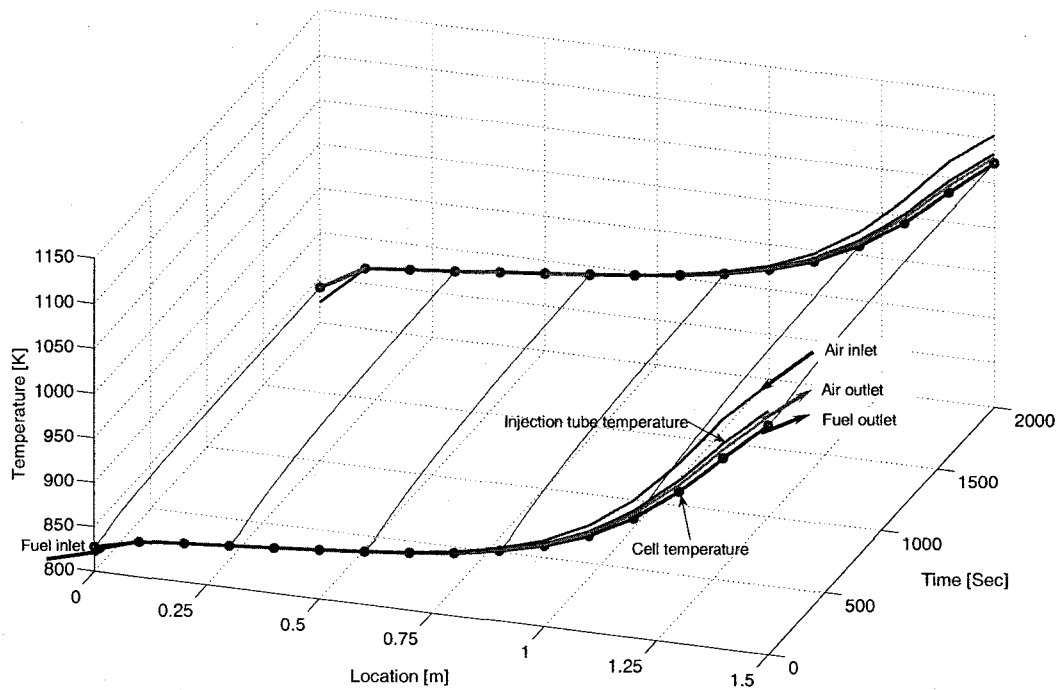


Figure 4.9: Profiles and step responses of temperatures, when I step changes from 100 to 150 Amp at 100 second.

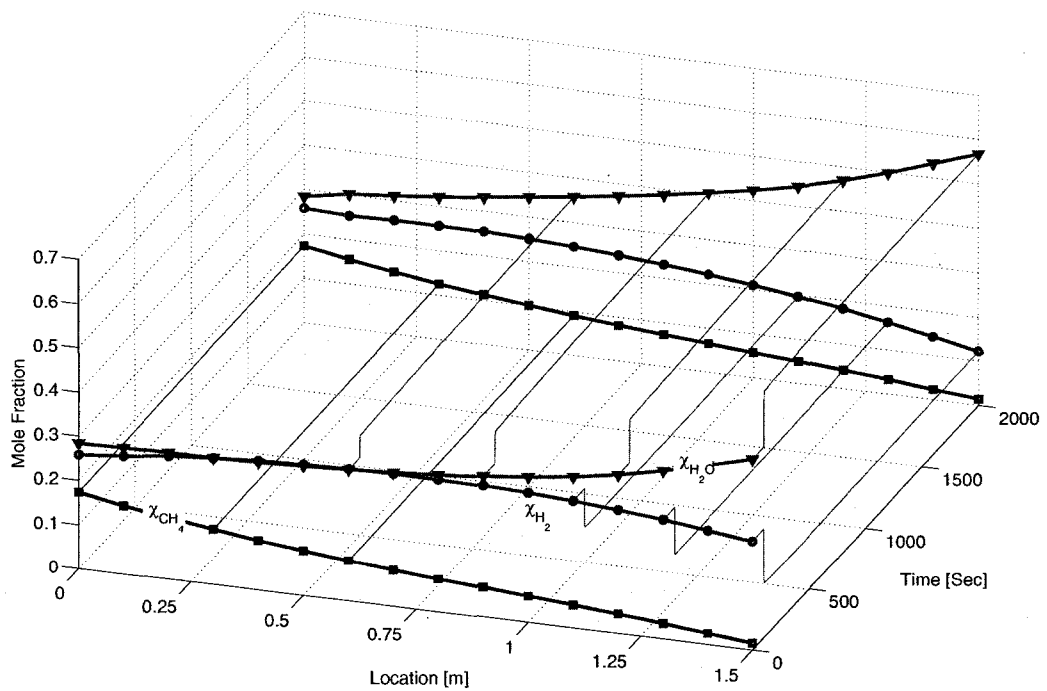


Figure 4.10: Profiles and step responses of species fractions, when I step changes from 100 to 150 Amp at 100 second.

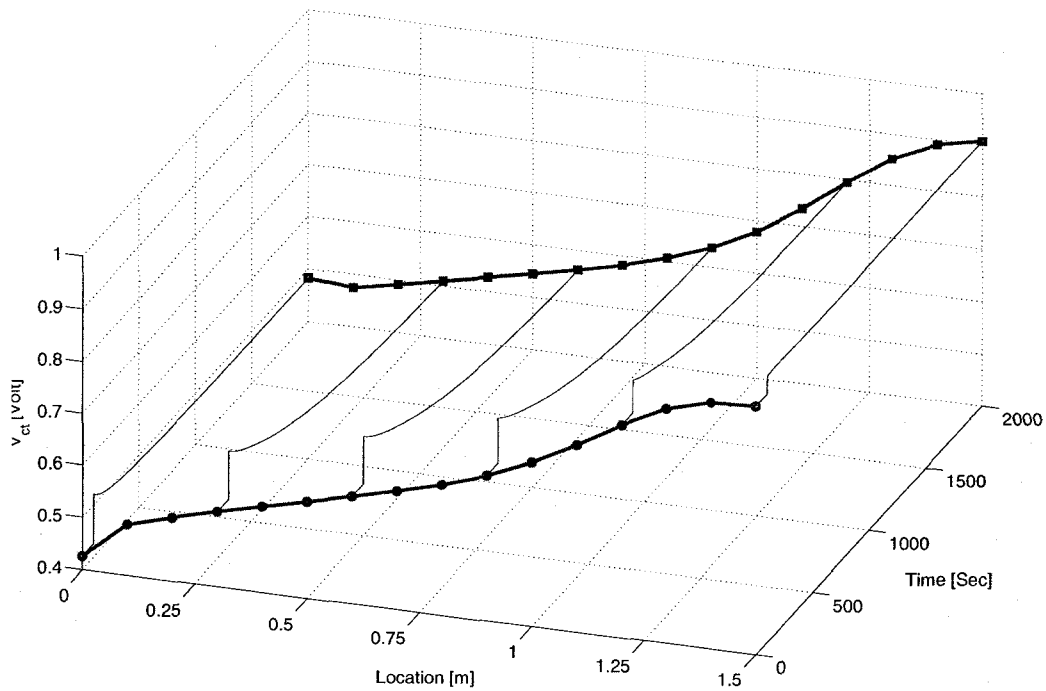


Figure 4.11: V_{ct} profile and step response, when P_{fuel}^{in} step changes from 1 to 2 atm at 100 second.

responses are shown in this figure. Obviously, their responses are dominated by the response of cell temperature.

Because air input rate is very high, the decrease of oxygen mole fraction due to the electrochemical reaction is minor. The profile is almost a flat line. So the cathode side oxygen step response and profile are not shown in the figures.

4.5.2 Effect of fuel inlet

Pressure

Step responses of the SOFC stack due to the step in fuel inlet pressure P_{fuel}^{in} are shown in Fig.4.11, Fig.4.12, and Fig.4.13.

When fuel inlet pressure P_{fuel}^{in} was stepped up, concentration of CH_4 increased immediately. So the reforming reaction rate increased and more H_2 was produced. The voltage V_{ct} then increased as shown in Fig.4.11. Consequently, more heat was absorbed from the cell tube and its temperature decreased. Profiles and step responses of other temperatures are shown in Fig.4.12. Profile and step responses of fuel species

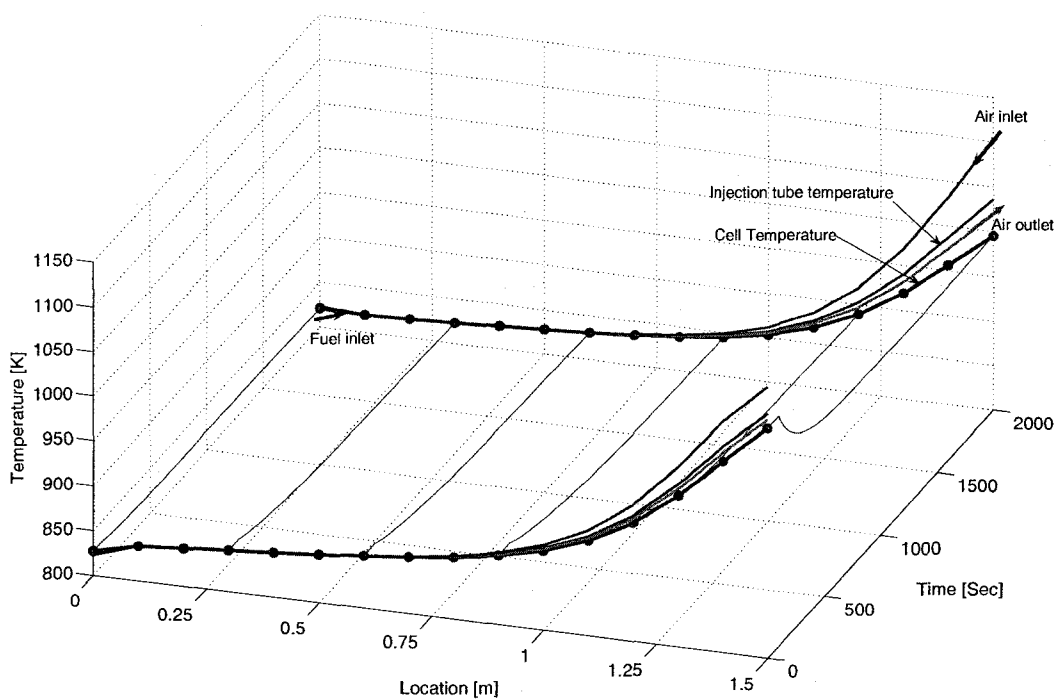


Figure 4.12: Profiles and step responses of temperatures, when P_{fuel}^{in} step changes from 1 to 2 atm at 100 second.

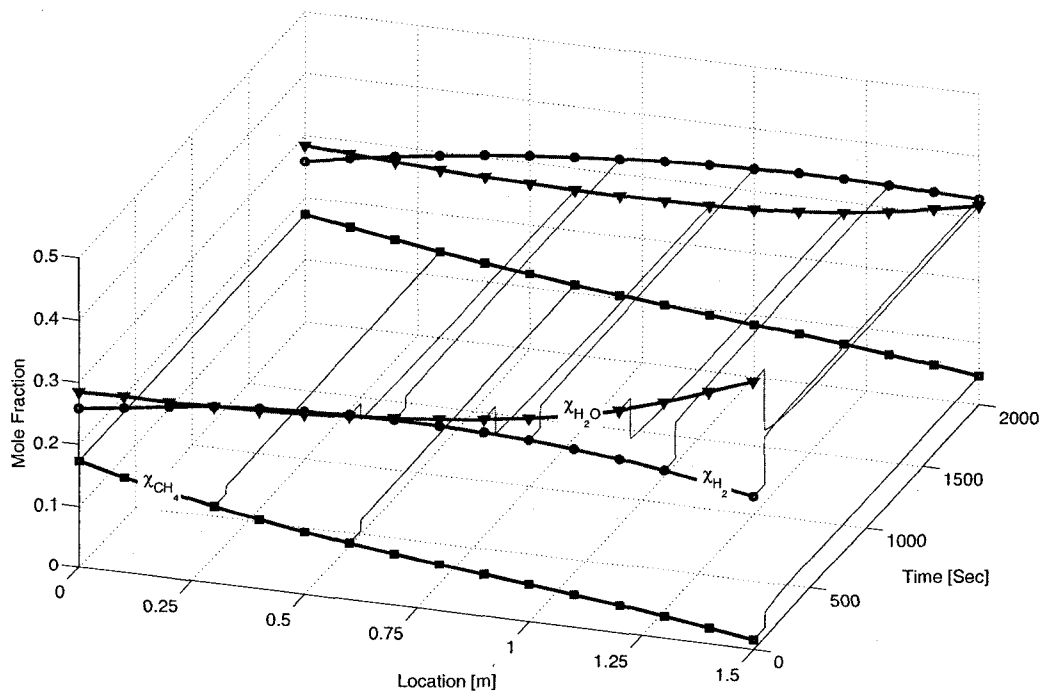


Figure 4.13: Profiles and step responses of species fractions, when P_{fuel}^{in} step changes from 1 to 2 atm at 100 second.

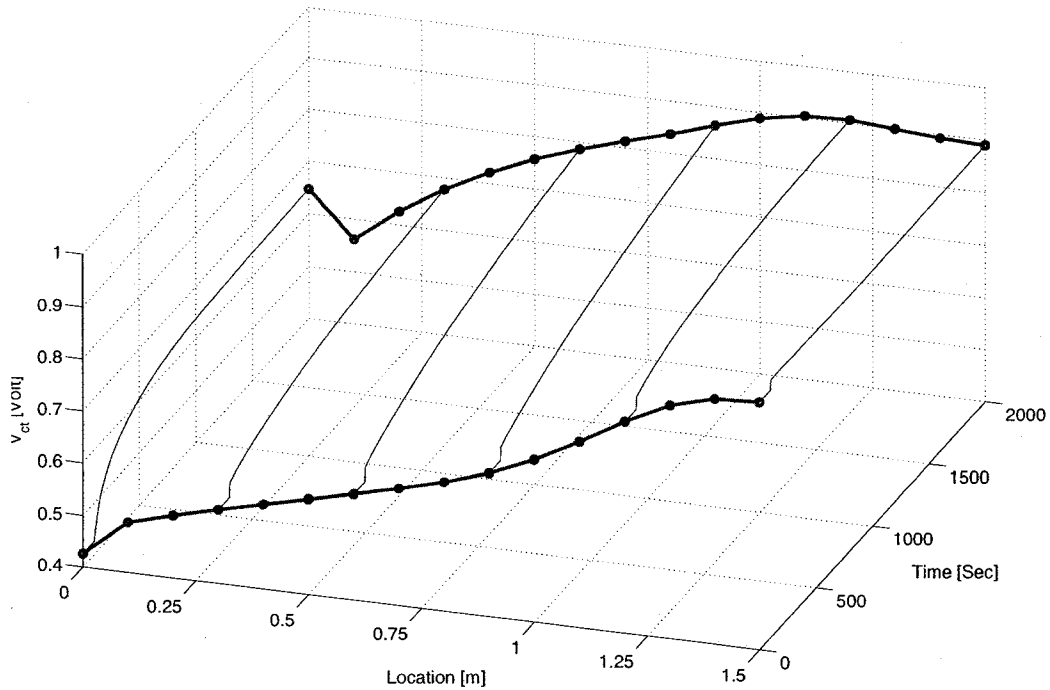


Figure 4.14: V_{ct} profile and step response, when T_{fuel}^{in} step changes from 823 to 923 K at 100 second.

are shown in Fig.4.13.

Temperature

Effects of step change in fuel inlet temperature T_{fuel}^{in} are shown in Fig.4.14, Fig.4.15, and Fig.4.16.

When fuel inlet temperature T_{fuel}^{in} was stepped up, concentration of CH_4 increased immediately. So the reforming reaction rate increased and more H_2 was produced. The voltage V_{ct} then increased as shown in Fig.4.11. Consequently, more heat was absorbed from the cell tube and its temperature decreased.

Velocity

Effects of step change in fuel inlet velocity u_{fuel}^{in} are shown in Fig.4.17, Fig.4.18, and Fig.4.19.

Step change of fuel inlet velocity u_{fuel}^{in} changes the heat transfer coefficient h_a . So heat is transferred from cell to fuel. Therefore it affects temperatures as shown in

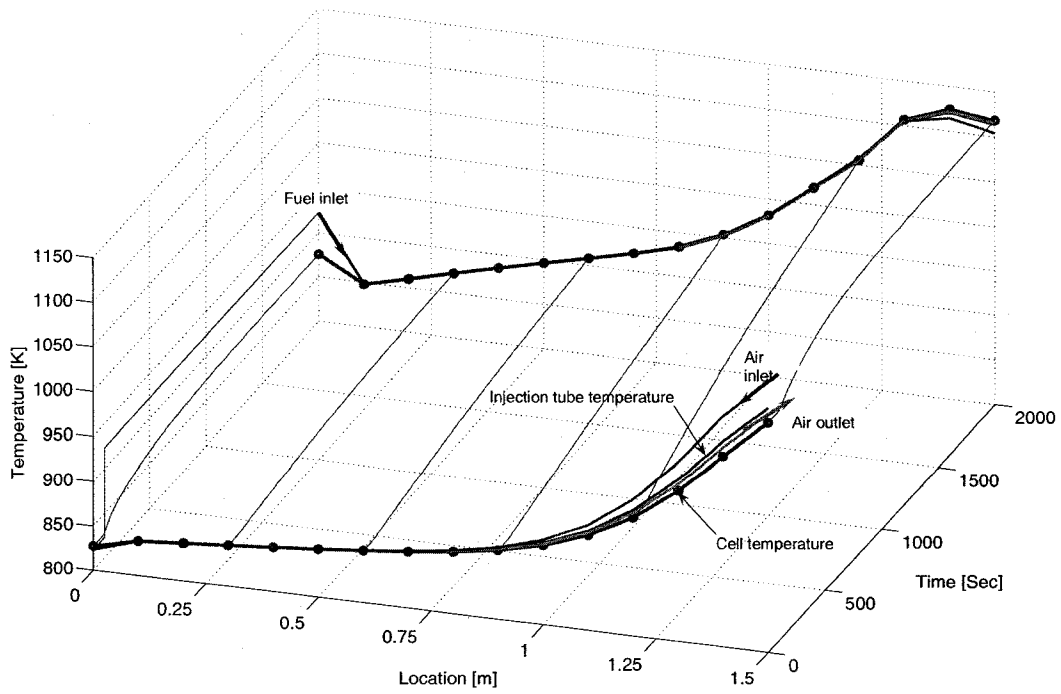


Figure 4.15: Profiles and step responses of temperatures, when $T_{\text{fuel}}^{\text{in}}$ step changes from 823 to 923 K at 100 second.

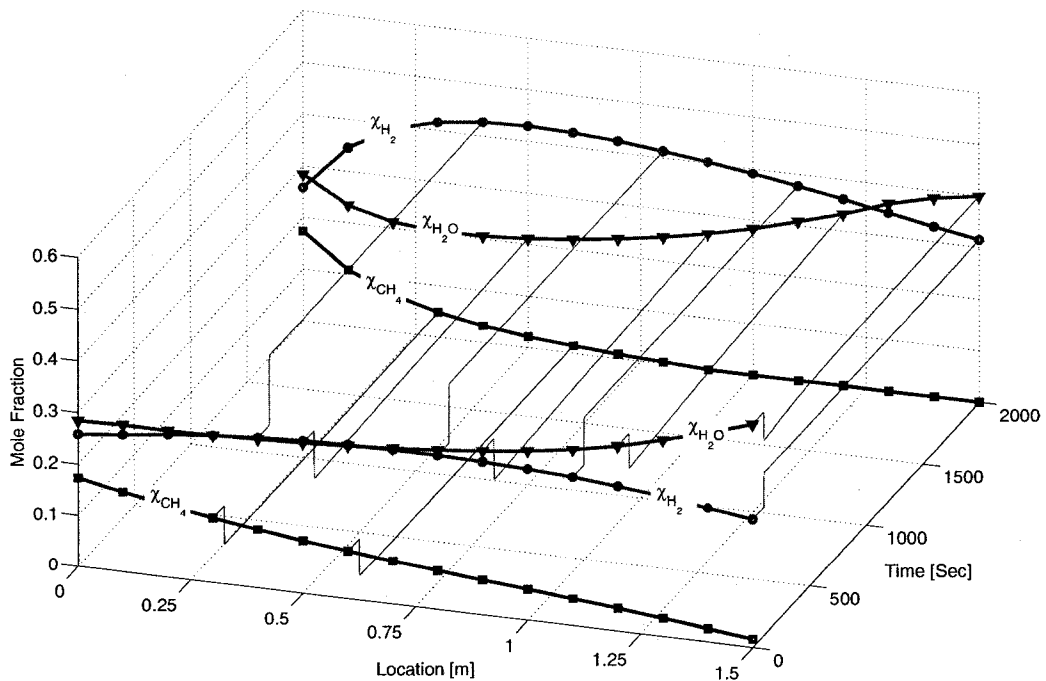


Figure 4.16: Profiles and step responses of species fractions, when $T_{\text{fuel}}^{\text{in}}$ step changes from 823 to 923 K at 100 second.

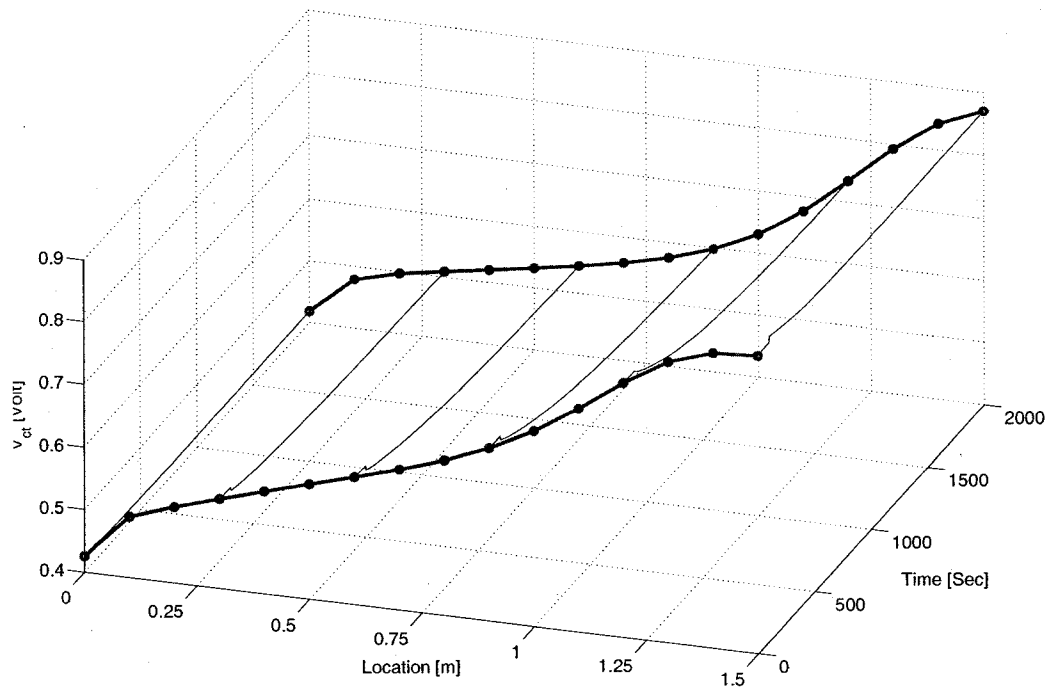


Figure 4.17: V_{ct} profile and step response, when u_{fuel}^{in} step changes from 0.927 to 1.927 m/s at 100 second.

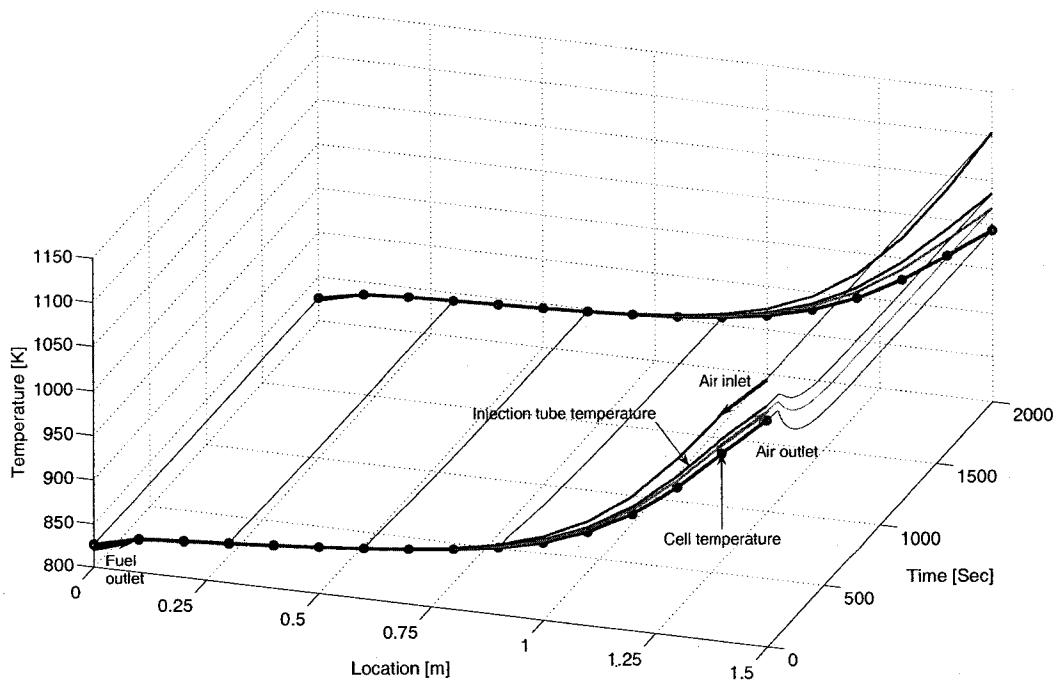


Figure 4.18: Profiles and step responses of temperatures, when u_{fuel}^{in} step changes from 0.927 to 1.927 m/s at 100 second.

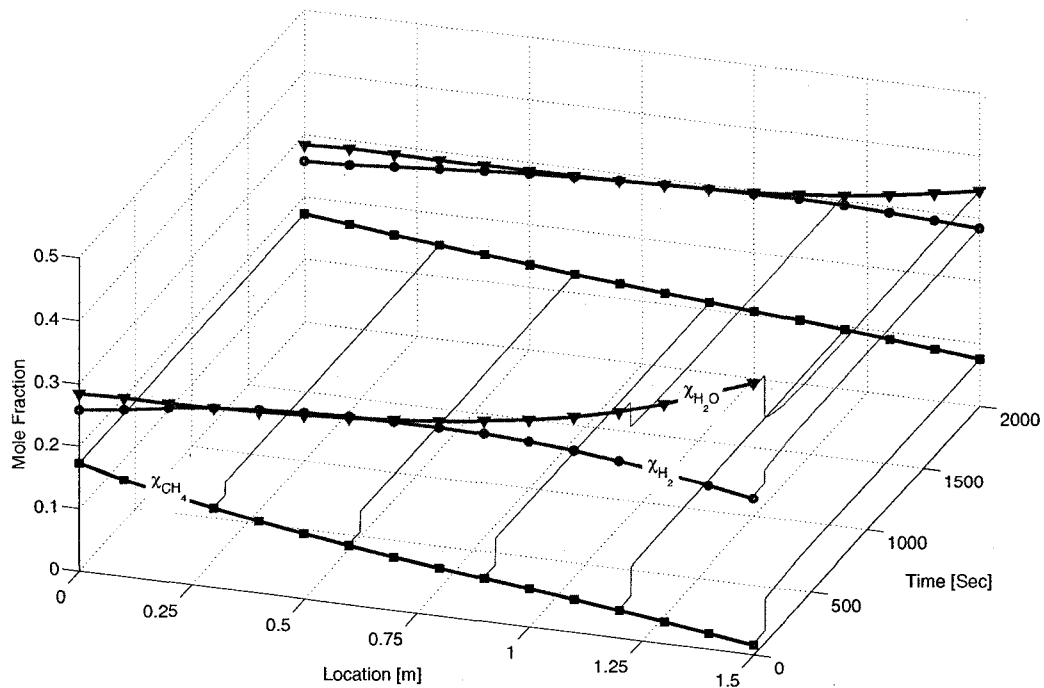


Figure 4.19: Profiles and step responses of species fractions, when u_{fuel}^{in} step changes from 0.927 to 1.927 m/s at 100 second.

Fig.4.18. The change of velocity directly affects species profiles as shown in Fig.4.19.

4.5.3 Effect of air inlet

Pressure

The step change of the air pressure affects the oxygen concentration, and as a result affects the voltage, cell temperature, and consequently other variable distributions, as shown in Fig.4.20, Fig.4.21, and Fig.4.22.

Temperature

The air inlet temperature step change affects the heating conditions of the the SOFC stack. Therefore, all other variables are affected. These effects are shown in Fig.4.23, Fig.4.24, and Fig.4.25 respectively.

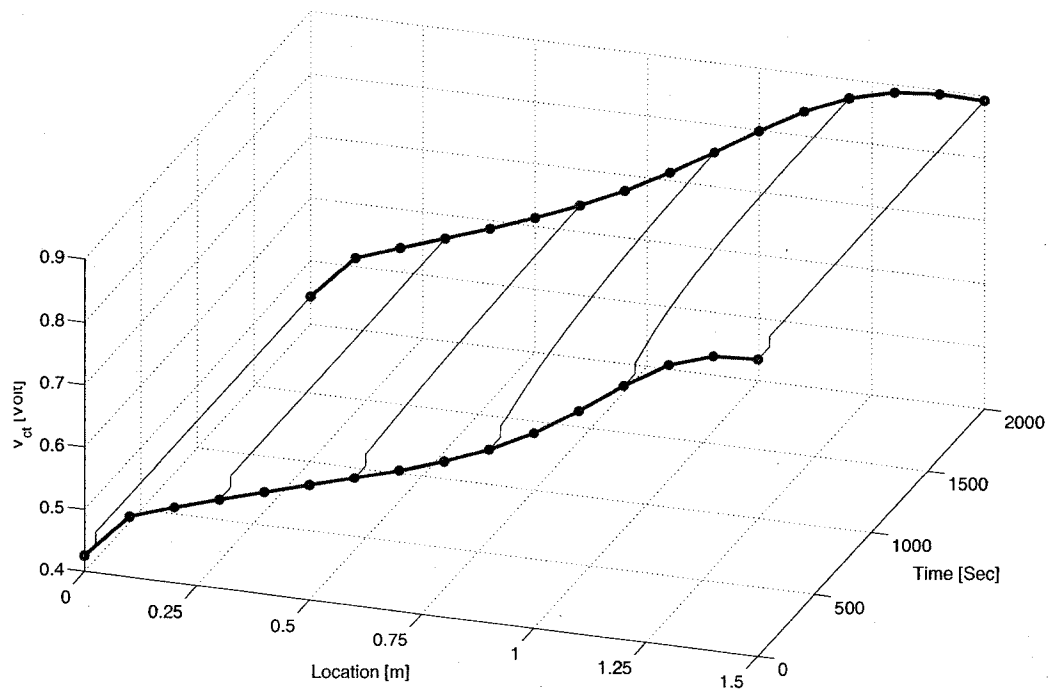


Figure 4.20: V_{ct} profile and step response, when P_{air}^{in} step changes from 1 to 2 atm at 100 second.

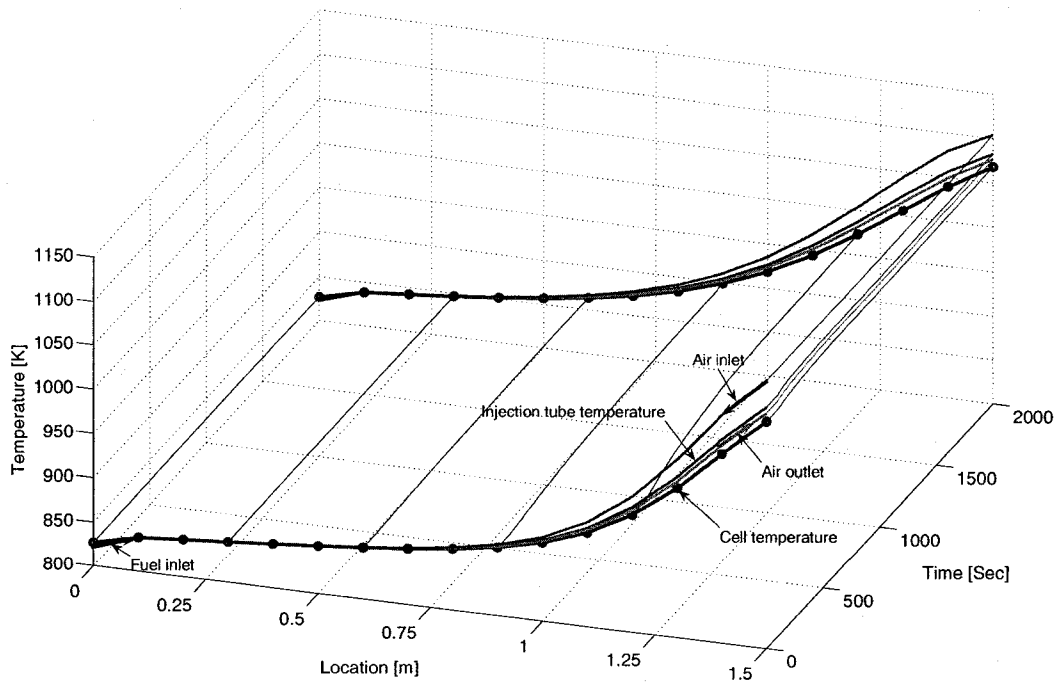


Figure 4.21: Profiles and step responses of temperatures, when P_{air}^{in} step changes from 1 to 2 atm at 100 second.

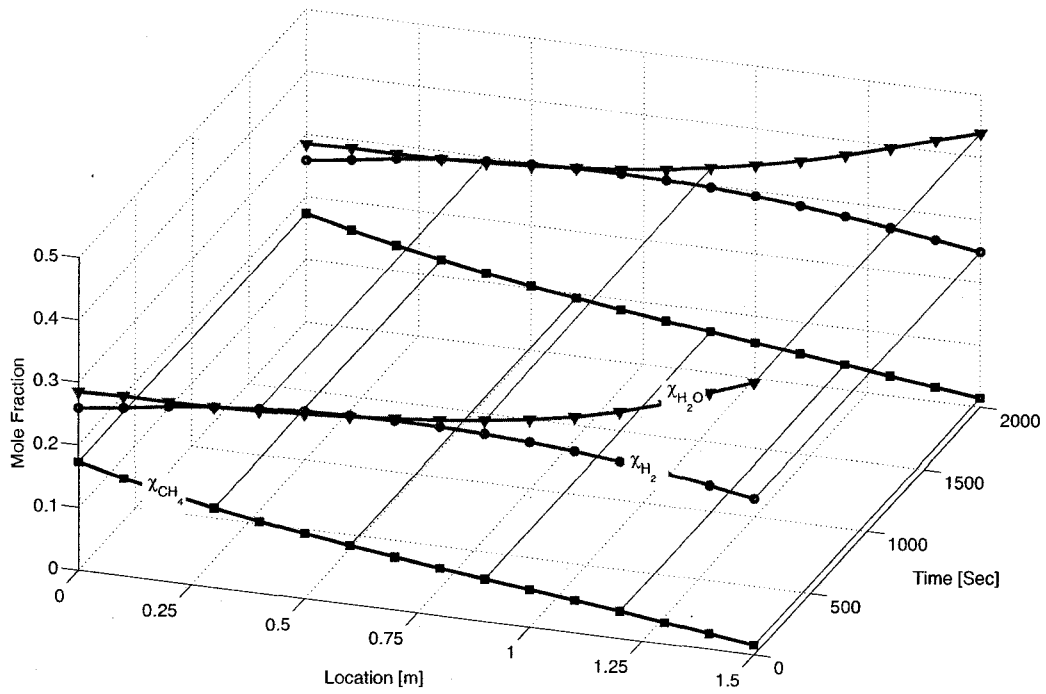


Figure 4.22: Profiles and step responses of species fractions, when P_{air}^{in} step changes from 1 to 2 atm at 100 second.

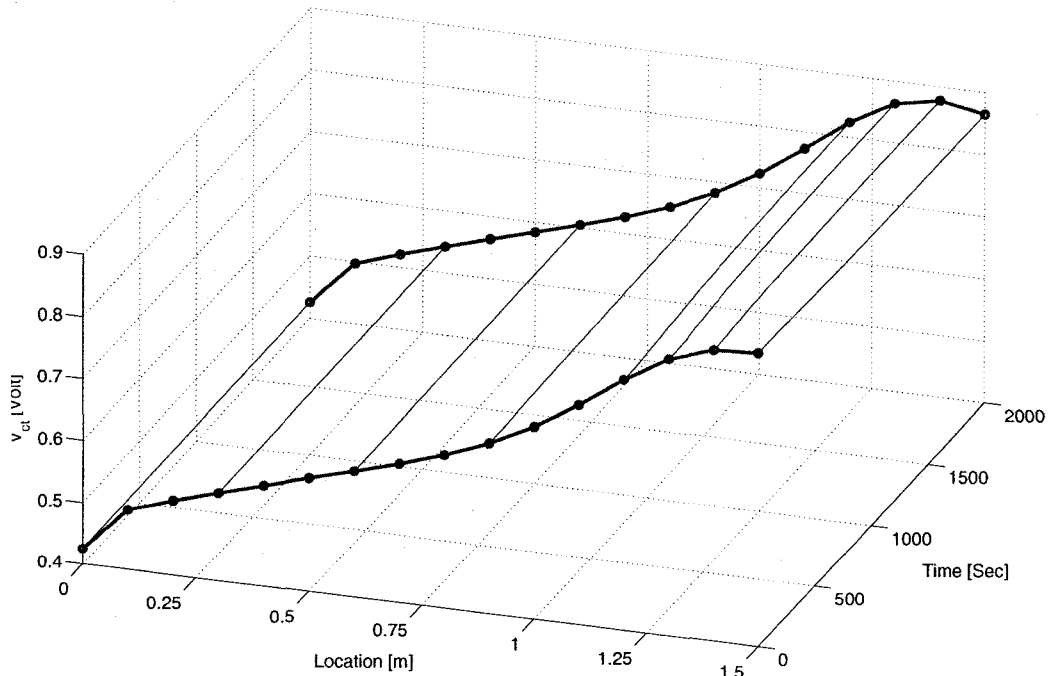


Figure 4.23: V_{ct} profile and step response, when T_{air}^{in} step changes from 1104 to 1184 K at 100 second.

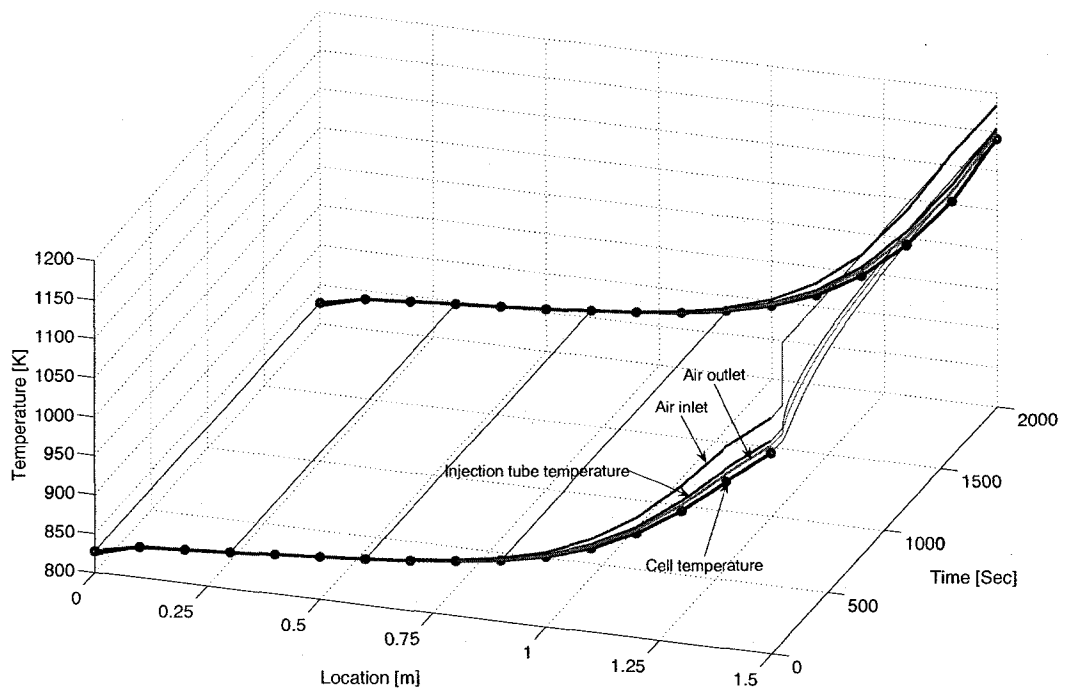


Figure 4.24: Profiles and step responses of temperatures, when T_{air}^{in} step changes from 1104 to 1184 K at 100 second.

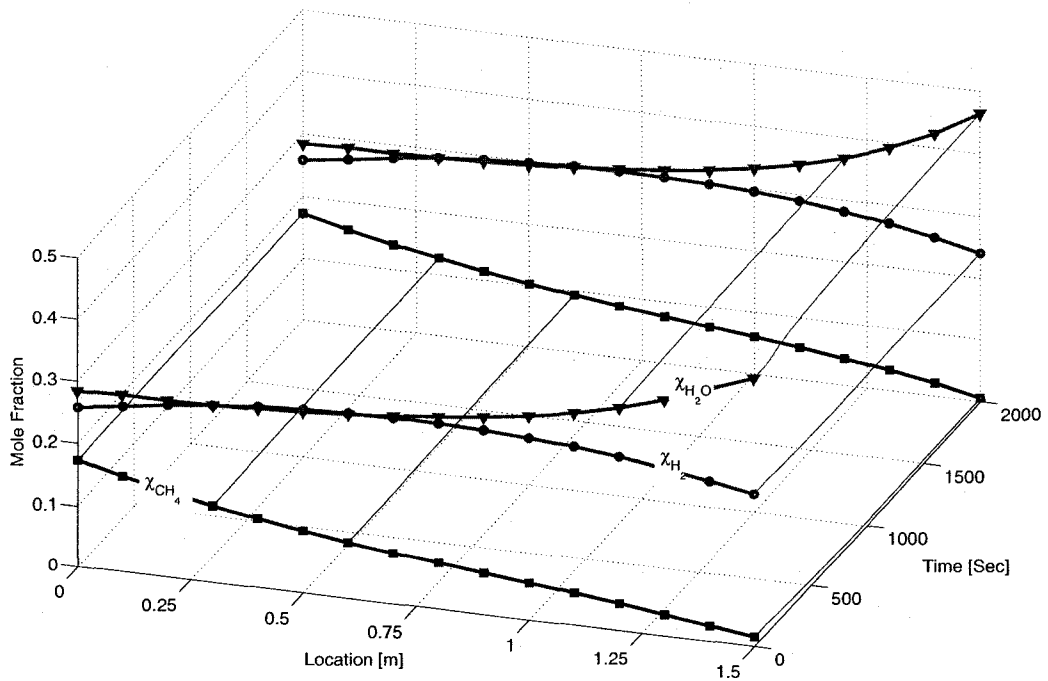


Figure 4.25: Profiles and step responses of species fractions, when T_{air}^{in} step changes from 1104 to 1184 K at 100 second.

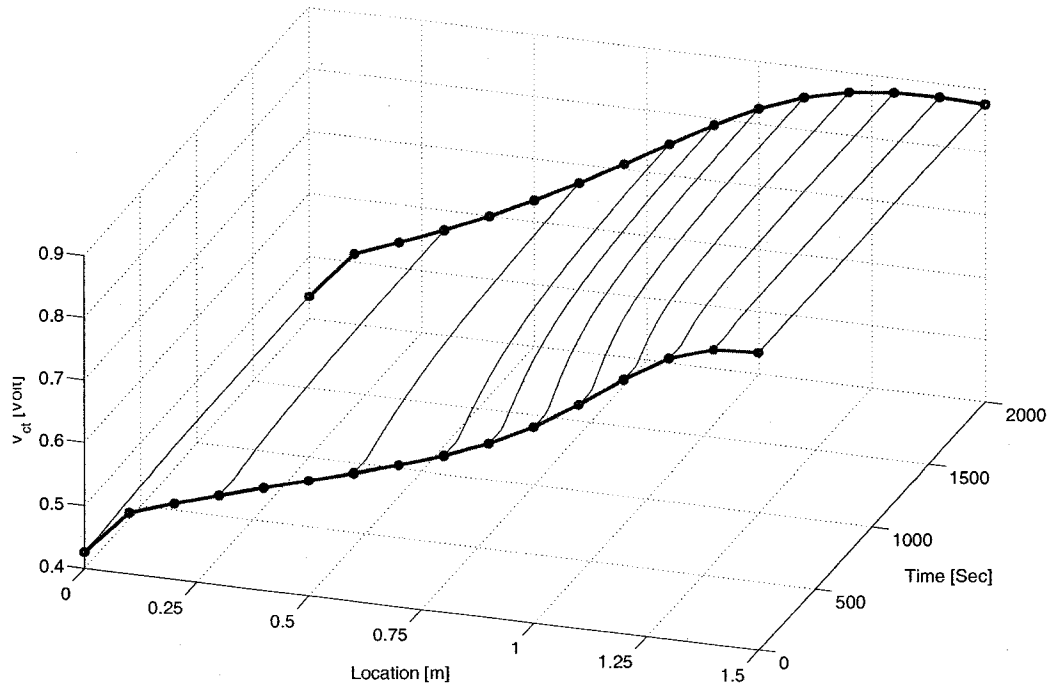


Figure 4.26: V_{ct} profile and step response, when u_{air}^{in} step changes from 7.79 to 23.37 m/s at 100 second.

Velocity

The air inlet velocity step change affects the heat transfer coefficient and therefore affects temperature profiles of the injection tube, cell and gas phase temperatures. Air flow rate can be designed changing in a large range of scope, due to its low cost, to recondition the temperature distributions along the cell tube. The effects due to air inlet flow rate step change are shown in Fig.4.26, Fig.4.27, and Fig.4.28.

4.6 Conclusions

An 1-D dynamic model for a tubular solid oxide fuel cell (SOFC) stack has been developed. Distributed dynamic relations of current density and electromotive force (EMF) have been developed. Solid phases non-flowing parameters dynamics have been investigated. Distributed dynamics of flowing phases such as fuel and air flow has been addressed by simultaneously considering diffusion, inherent impedance, primary flow, heat transfer, and internal reforming/shifting reactions. They are modeled in the form

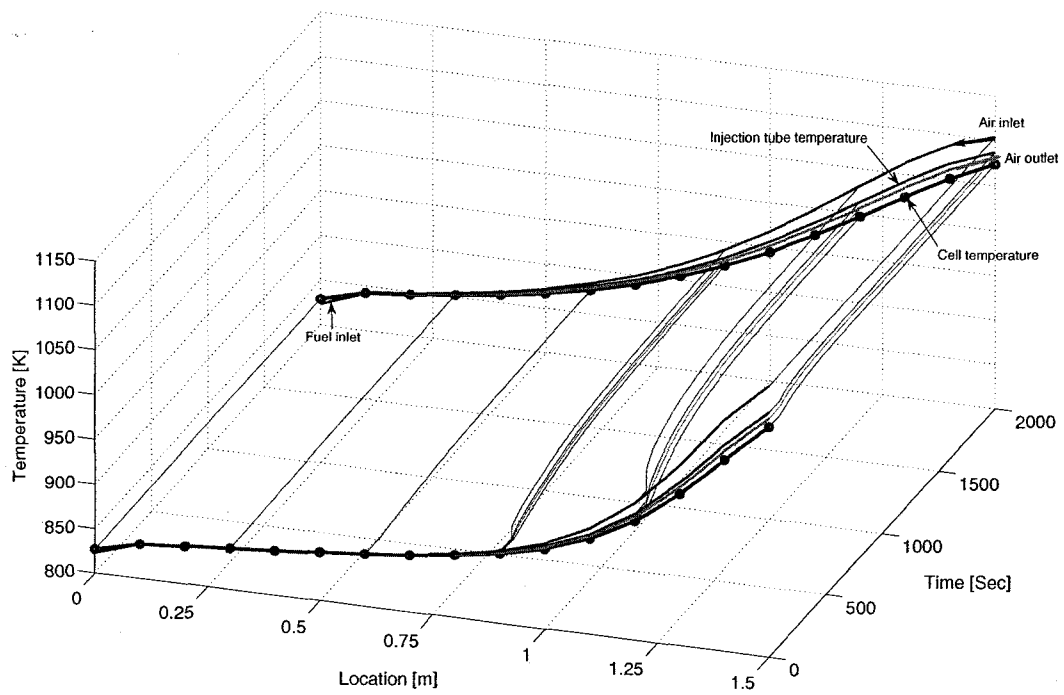


Figure 4.27: Profiles and step responses of temperatures, when u_{air}^{in} step changes from 7.79 to 23.37 m/s at 100 second.

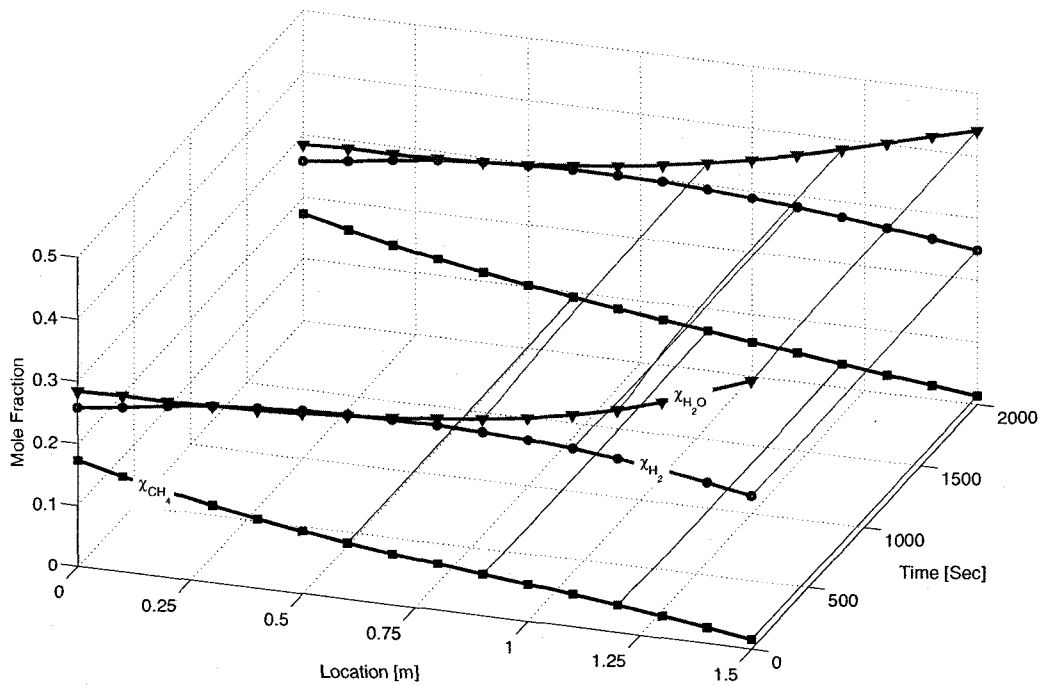


Figure 4.28: Profiles and step responses of species fractions, when u_{air}^{in} step changes from 7.79 to 23.37 m/s at 100 second.

of partial differential equations (PDEs).

An approximated analytical solution for 1-D dynamic reacting gas flow problem has been proposed. It has been applied to the 1-D SOFC model and analytically solved velocity, mole fraction and temperature distributions for primary flows. PDEs in the 1-D dynamic model is then converted to ordinary differential equations (ODEs). Combined with the dynamic models for non-flowing parameters, the 1-D dynamic model for the tubular SOFC has been presented in the form of nonlinear state-space equations.

Dynamic performances and parameter distributions have been investigated through simulated step responses of the SOFC stack to changes of external current demand, and fuel and air input parameters respectively. They are investigated along the whole length of the tube and the results are presented in this chapter.

5

Low-Order State Space Model

To facilitate control study of fuel cells, a low-order nonlinear state space model of the tubular SOFC stack is built in this chapter based on the first-principles. Input-output parameters of the SOFC stack are analyzed. Input variables are fuel and air upstream pressures. The voltage output of the SOFC stack and the cell temperature are model outputs. Other variables such as current demand and the fuel and air inlet temperatures are considered as disturbances. Faster processes such as reforming reaction, shifting reaction, and mass transfers are considered but modeled at steady state. Temperature response is modeled by dynamic equations owing to its slow response and dominant role played in SOFC dynamic performance. Dynamics of the SOFC stack is investigated through simulations and compared with more detailed models available in the literature.¹

keywords:

SOFC, dynamic modeling, simulation, diffusion, impedance

¹A version of this chapter was submitted to the Journal of Process control, 2007

5.1 Introduction

Considerable amount of research and development work has been devoted to investigating SOFC system, making the SOFC system closer to the commercial application. The most likely market of SOFC is for the distributed power generation. However, before SOFC system can be marketed as a distributed power source, the dynamic operation problem, namely control problem under distributed power generation environment must be resolved. Dynamic modeling of SOFC is a necessary first step towards this direction.

Dynamic modeling of SOFC has been relatively sparse in the literature. Some researchers proposed lumped parameter models which are suitable for control implementation (Achenbach, 1994; Achenbach, 1995; Padullés *et al.*, 2000; Zhu and Tomsovic, 2001; Sedghisigarchi and Feliachi, 2004; Murshed *et al.*, 2007). However, without the detailed analysis of mass/energy transport, these lumped models may not be sufficient to describe the SOFC dynamics.

Fuel cell process is a complex chemical and electrochemical process. Mass /energy /momentum transports are all involved in this process. These dynamic processes affect each other as well as the macroscopic performance of the fuel cell. The static mechanism model of Li and Chyu (2003), and analysis of Campanari and Iora (2004) showed more details of fuel cell process. Our previous work in Chapter 2 and 3 modeled the detailed dynamic relations with reforming/shifting reactions, mass transfer, heat transfer and fluid dynamics that occur in a finite volume of SOFC cell.

Unlike models that are used for simulation and analysis, a model that used for control requires that the model can describe not only the dynamic response of the system, but also the explicit input/output relations. It also requires that the system order is relatively low to be suitable for control design. Thus, the target model should be relatively simple but can capture dominant dynamics of the cell stack. Built upon our previous detailed modeling work, a second order lumped model for a tubular SOFC stack is presented in this chapter. This low-order dynamic model is not a model simply reduced from our previously established high-order models by a model reduction technique, but is a lumped model directly derived from first principles by considering all mechanisms.

The remainder of this chapter is organized as follows: a brief introduction to SOFC technology is discussed in section 2. Fast responses of transport phenomena are considered at steady state and slow temperature responses are considered dynamically

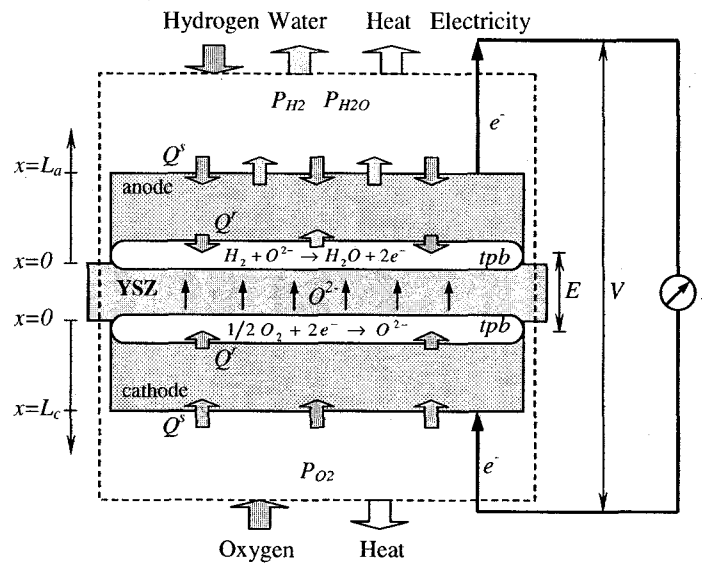


Figure 5.1: Principle of Solid Oxide Fuel Cell

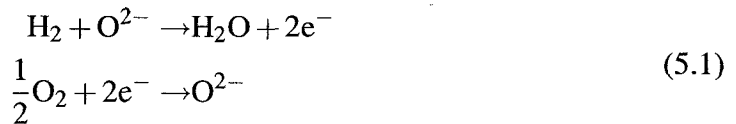
in Section 3 in detail. The nonlinear state space model is derived in Section 4. Model validation and simulations are given in Section 5, followed by conclusions in Section 6.

5.2 Introduction to SOFC

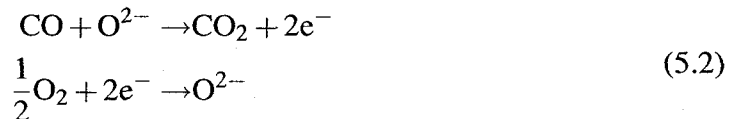
5.2.1 Fuel cell principles revisit

Solid oxide fuel cell (SOFC) converts chemical energy to electrical energy through electrochemical reactions. They include:

Conversion of H_2 :



Conversion of CO:



As shown in Fig. 5.1, the electrons flow through the external circuit forms current. The current and the reactant consumption rates have the simple relations as (Larminie and

Dicks, 2003):

$$I = 2FJ_{\text{H}_2}^r = 2FJ_{\text{H}_2\text{O}}^r = 4FJ_{\text{O}_2}^r \quad (5.3)$$

where superscript *r* represents the reaction sites, *F* is the Faraday constant which is the charges carried by one mole of electrons, $J_{\text{H}_2}^r$, $J_{\text{H}_2\text{O}}^r$ and $J_{\text{O}_2}^r$ are the consumption rate of H_2 , production rate of H_2O , and the consumption rate of O_2 respectively.

The potential difference between anode and cathode reaction sites due to the release of Gibbs free energy (Larminie and Dicks, 2003) produces the electromotive force (EMF). It drives the flow of electrons. The EMF is affected by temperature and reactant activities and is usually modeled by the Nernst equation (Larminie and Dicks, 2003):

$$E = E^0 + \frac{RT}{2F} \ln \left(\frac{a_{\text{H}_2} \cdot a_{\text{O}_2}^{0.5}}{a_{\text{H}_2\text{O}}} \right) \quad (5.4)$$

where a_{H_2} , a_{O_2} and $a_{\text{H}_2\text{O}}$ are activities.

Fuel cell voltage output comes from the EMF. By computing the reactant partial pressures in the immediate vicinity of the reaction sites, the detailed dynamic model of fuel cell voltage output was derived in Chapter 2.

When the external load is connected, due to the existence of current, the voltage output of the SOFC stack is reduced by activation loss, Ohmic loss and concentration losses, (Larminie and Dicks, 2003). The static voltage output is usually modeled by (Larminie and Dicks, 2003):

$$V_{\text{out}} = E - iR_{\text{in}} - A \ln \left(\frac{i}{i_0} \right) - B \ln \left(1 - \frac{i}{i_l} \right) \quad (5.5)$$

where i is the current produced by the cell, R_{in} the intrinsic resistance of the fuel cell, i_0 the exchange current, and i_l the limiting current, at which the fuel is used up at a rate equal to its maximum supply rate. A and B are coefficients. The first term in the RHS of the equation is the EMF. The second term represents the voltage drop on the intrinsic resistance. The third term is the voltage drop that drives the electrochemical reactions. The last term represents the voltage drop due to the concentration drop at the reaction sites.

5.2.2 Logic correlations of physical effects

From the fuel and air inlets to the electrical output, the fuel cell energy conversion process is complex. Mass/energy/momentum transfer processes and conversions occur

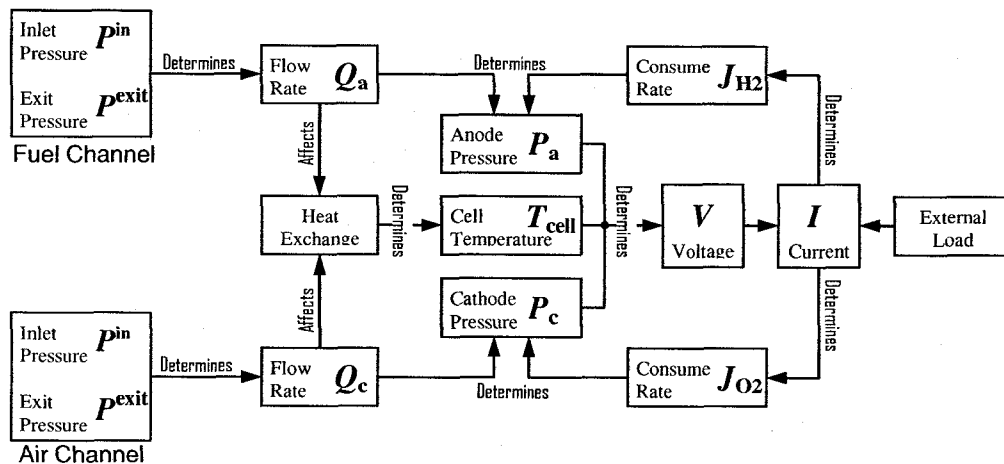


Figure 5.2: Schematic logic correlations of fuel cell process

simultaneously in the SOFC stack. These processes and physical factors such as pressure, temperature etc. affect each other. Their logic relations are schematically shown in Fig. 5.2.

In fuel and air flow channels, inlet pressures and exit pressures determine their flow rates. These flows are called primary flow, and they affect the heat exchange process inside the stack and thus the cell temperature, as shown in Fig. 5.2. On the other hand, the external load determines the current that the SOFC produces, and consequently consumption rates of reactants due to the electrochemical reaction. Pressures and partial pressures of each species are then determined by primary flow rates and consumption rates together, as shown in Fig. 5.2. Voltage output that the SOFC stack can produce is affected by reactant partial pressures and the temperature. It will then affect the current output as shown in Fig. 5.2.

5.2.3 Limitations to power output

The first factor that restricts the electrical power output is reactant supply rates. Limitations due to the primary flow can be neglected. Reactants in the flow channel must pass through porous electrodes to reach reaction sites. The processes are controlled by concentration gradients between *tpbs* and the primary gas flow bulks. This process limits the reactant supply rates. When the current output increases, hydrogen and oxygen concentrations at *tpbs* decrease to create larger concentration gradients. Once one of them decreases to zero, the supply rate reaches its maximum.

At this point current can not be increased further, and it is the maximum current that the fuel cell can provide. Under this condition, the voltage drops to zero as described by Nernst equation.

Second, when reactant supply rates are sufficient, reaction rates and the available reaction sites where reactions occur will limit the current production. In most cases, reactions are fast in anode. However, because cathode reaction is slow (Mitterdorfer and Gauckler, 1999c), current output is also limited by the maximum ion production rate.

Third, in most common situation, that is, fuel cell works at the point at which both reactants supply rates and reaction rate are sufficient, current output is controlled by voltage and external load impedance. In this case, current is the common factor that determines electrochemical reactions and diffusions, as shown in Fig.5.5, in the cell section.

Fourth, current is limited by the ionic conductivity of electrolyte and the internal resistance. They obey Ohm's law, and are usually considered together as the inherent resistance. When the voltage drop over the inherent resistance is equal to the potential that the fuel cell produces, the voltage output decreases to zero. In normal operating ranges, the reactions do not reach the limits mentioned before. Thus the current is determined mainly by the Ohm's law.

5.2.4 Planar and tubular design

A SOFC stack is composed of a number of SOFC cells to produce a high voltage output. In designing SOFC stack and cells, there are many factors that need to be considered, such as gas delivering, thermal stresses, mechanical strength, inherent resistance, seal materials etc. There are two types of SOFC structure design, namely planar design and tubular design, as shown in Fig.5.3 and in Fig.5.4 respectively.

One of the most important advantages of the tubular design is that it does not need the seal to separate fuel and air flow. Another advantage is that the tubular shape can improve the strength of the cell. The tubular shape can also improve the gas delivering property. This kind of design is suitable for stationary and large scale power generation applications.

The most significant advantage of planar SOFC design is its lower inherent

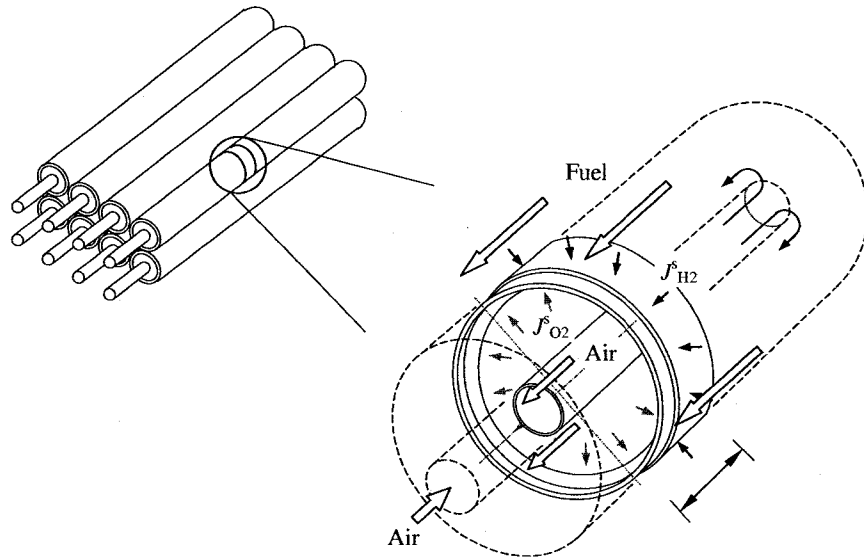


Figure 5.3: Tubular design of SOFC stack and cell

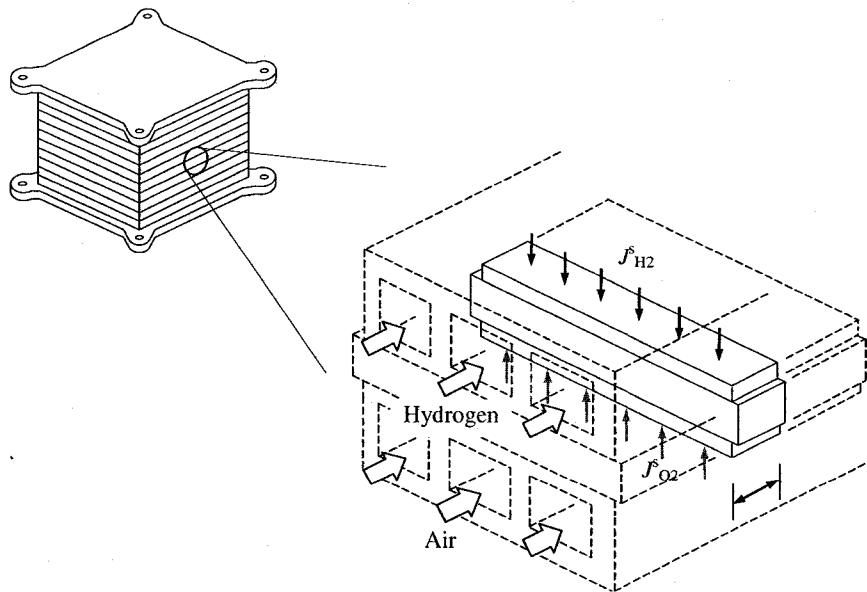


Figure 5.4: Planar design of SOFC stack and cell

resistance. It is more suitable for mobile and low power applications.

5.3 Lumped model of SOFC stack

Being a distributed power generator, SOFC stack can only run under proper control with the consideration of several factors. The first factor to be considered for the control is the safety in the dynamic operation. Working at high temperature, the pressure difference between anode and cathode as well as the cell temperature must be maintained within some limits. The second factor to be considered is that the DC voltage output of the stack must be stabilized to reduce its disturbance to the power conditioner. The third factor that should be considered is the efficiency. Inlet flow should be operated appropriately according to the load demand to optimize the fuel utilization.

5.3.1 Physical processes

The detailed fuel cell processes are expressed by a block diagram, as shown in Fig. 5.5.

Inlet fuel and air flows are described by states such as pressure, temperature, velocity, enthalpies and compositions. With known boundary conditions at the exit, the primary mass flow rates are determined by the inlet properties and the geometry of the stack. The secondary flow occurs along the flow channel due to the consumption of reactants that flow from main flow body to the reaction sites. If the fuel is syngas, in the anode flow channel there are also reforming/shifting reactions. Those reactions change the compositions of the fuel gas. All these factors together determine the total fuel pressure as well as partial pressures of each ingredients in the flow channel. The processes are shown by the stack/channel section in Fig.5.5

Partial pressures in the primary flow body and the current output determine diffusion processes as well as the partial pressures in the immediate vicinity of the reaction sites. The correlations are shown in the cell section in Fig.5.5 . Diffusion processes form the secondary flows. Partial pressures in the immediate vicinity of the reaction sites determine the EMF and the electrochemical reaction rates.

Accompanied with the mass flow and reactions, there are also energy transports. The

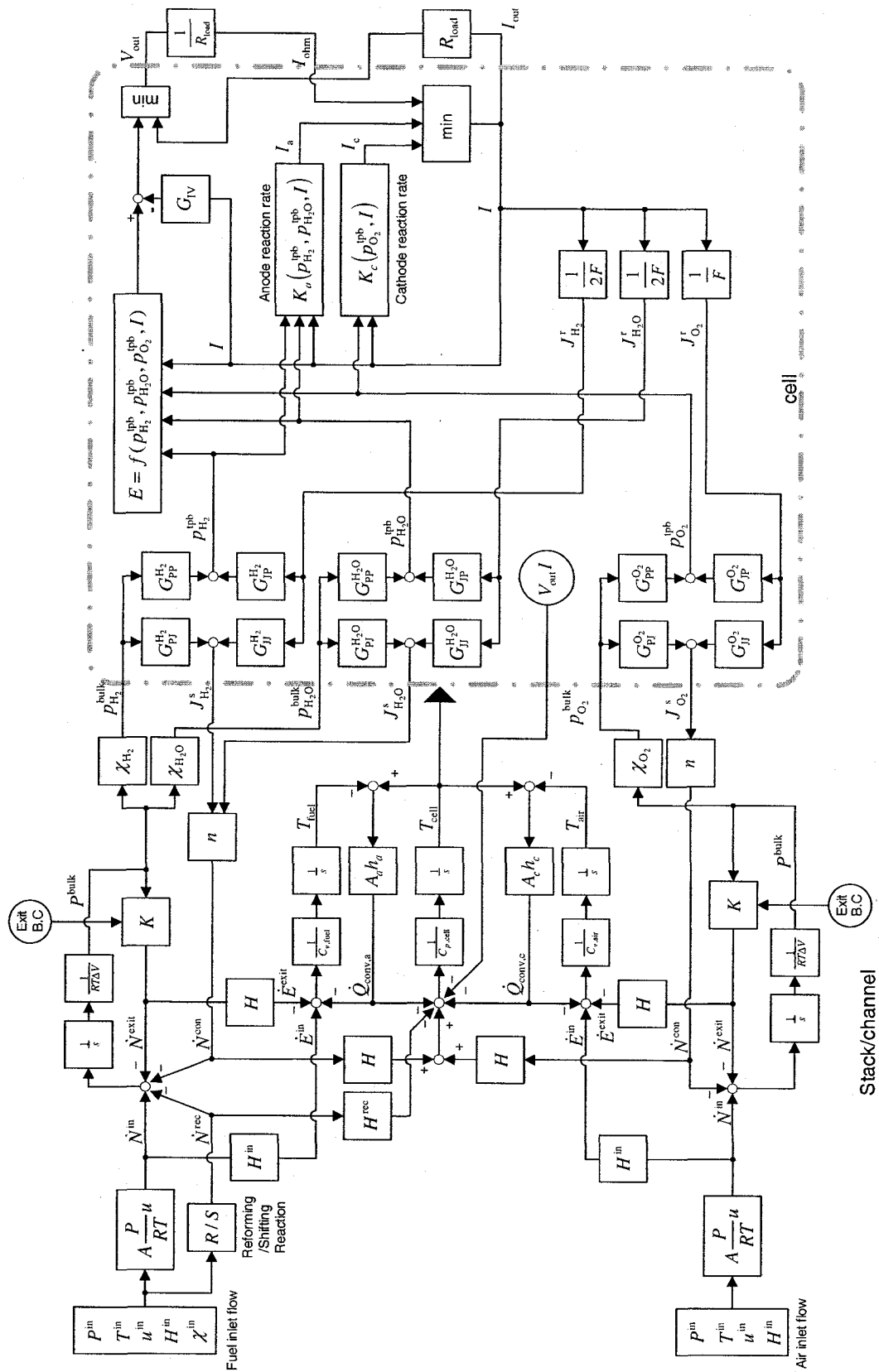


Figure 5.5: Block diagram of fuel cell process

main energy form that is carried by mass flows is enthalpy. Reactants diffuse into cell to participate in the electrochemical reaction and then release energy. The Gibbs free energy is converted to electrical energy and the balance of the enthalpy of formation is released as reaction heat. Part of electrical energy supplies to the external load, and part of energy is consumed by the intrinsic resistance and converted to heat.

Due to the temperature differences, the cell exchanges heat with surrounding fuel and air, and consequently transports heat from the cell to the surrounding flows. Temperatures of surrounding flows in turn affect heat transfer processes and the temperature of the cell. The cell also supplies heat to the reforming reaction. The energy flow and conversion processes are shown in Fig.5.5, in the stack/channel section.

5.3.2 Model assumptions

The lumped SOFC stack model has the following assumptions:

- Fuel supplied to the SOFC stack is pre-reformed methane and air;
- exit of the SOFC stack is open; consequently pressure at the exit is 1 atm;
- fuel temperatures, pressures, flow velocities are uniform in the flow channel;
- all cells of the stack have the same temperatures;
- voltages of each cell are same;
- cells in the stack are connected in series electronically;
- CO does not involve in the electrochemical reaction;
- no disturbances in terms of heat transfer from the surrounding to the stack.

5.3.3 I/O variables

The objective of the dynamic SOFC stack model is mainly for control applications. Only those external, explicit, measurable and operable physical parameters are designated as I/O variables.

Input variables

Inputs of the SOFC stack are fuel/air flows. The properties of inlet flows are determined by their pressures, temperatures, flow rates, and compositions.

Output of the SOFC stack is electrical power. It is determined by the voltage and current. Voltage is related to the fuel pressures and current is related to the fuel flow rates. In order to operate the stack to satisfy the load demand, one needs to regulate the fuel/air pressures in the stack and their flow rates.

Because of the assumption that the exit of the stack is open, the exit pressure is fixed, and pressures in stack and flow rates are all determined by the inlet pressures $P_{\text{fuel}}^{\text{in}}$, $P_{\text{air}}^{\text{in}}$ and the flow resistances. So $P_{\text{fuel}}^{\text{in}}$ and $P_{\text{air}}^{\text{in}}$ are selected as the input variables of the model.

Operation of the exit orifice of SOFC stack as proposed in (Padullés *et al.*, 2000) can also regulate the in-stack pressures and flow rates. This strategy however has two main weaknesses: First, the tail gas pressure will fluctuate and it is not suitable to send the tail gas to the turbine engine. Second, it requires relatively higher inlet pressures to warrant the sufficient operation range.

Output variables

As mentioned above, the output of the SOFC stack is electrical power. It can be defined by voltage V and current I . V is an important variable that should be controlled and kept stable. It is one of the output variables of the model.

In the general operating range, current I is determined by V and load of the stack. External load is often not manipulated.

Due to internal resistance, the cell temperature T_{cell} is higher than that of its surroundings. It affects the performance of SOFC stack significantly. Too high T_{cell} will lead to malfunction of the stack. Therefore, T_{cell} must also be controlled and monitored. It is the second output variable of the model.

Disturbances

Current output I is determined by voltage and load impedance. However, load impedance of the power distribution network may not be measured or manipulated.

Table 5.1: I/O variables of the model

Inputs	Outputs	Disturbance
$P_{\text{fuel}}^{\text{in}}$ [atm]	V [volt]	I [amp]
$P_{\text{air}}^{\text{in}}$ [atm]	T_{cell} [K]	$T_{\text{fuel}}^{\text{in}}$ [K]
		$T_{\text{air}}^{\text{in}}$ [K]

It means that the current output of the stack I can not be manipulated through the operation of the stack. On the other hand, current I determines the electrochemical reaction rates, and in turn the performance of the stack. So I is defined as a disturbance variable of the model.

Fluctuations of inlet flow temperatures $T_{\text{fuel}}^{\text{in}}$, $T_{\text{air}}^{\text{in}}$ all affect the performance of the stack. But they can not be manipulated and therefore also designated as disturbances for the model. Fuel compositions χ_i^{in} are system parameters.

The I/O variables of the lumped SOFC stack model are listed in Table 5.1.

5.3.4 Voltage

Through the electrochemical reaction shown by Eqn.5.1, EMF of the fuel cell is established between anode and cathode reaction sites. It is the source of fuel cell voltage output. To simplify the problem as well as consider the actual operating range of SOFC during dynamic operations, we can neglect the effect of activation loss and concentration loss in the model, focusing on the effect of pressure, temperature and internal resistance. The voltage output of the SOFC stack can then be modelled as:

$$V_{\text{out}} = N \left[E^0 + \frac{RT_{\text{cell}}}{2F} \ln \left(\frac{p_{\text{H}_2} p_{\text{O}_2}^{\frac{1}{2}}}{p_{\text{H}_2\text{O}}} \right) - R_{\text{in}} I \right] \quad (5.6)$$

where N is the number of cells and can be assigned as $N = 1$ without loss of generality, $E^0 = 1.273 - 2.7645 \times 10^{-4} T_{\text{cell}}$ is the EMF at standard condition, p_{H_2} , p_{O_2} and $p_{\text{H}_2\text{O}}$ are partial pressures of reactants, and R_{in} is the intrinsic resistance of the fuel cell.

Dynamic responses of V_{out} is thus affected by current I , temperature T_{cell} and partial pressures p_{H_2} , $p_{\text{H}_2\text{O}}$ and p_{O_2} .

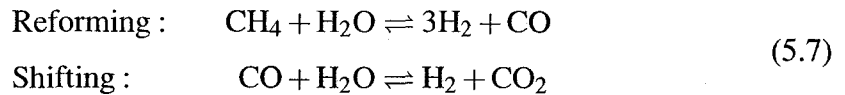
V_{out} is also dynamically affected by diffusion processes and double layer capacitance (Qi *et al.*, 2005). Their effects are shown by the Ohmic loss and the concentration loss respectively. The responses due to the diffusion process and the double layer

capacitance are fast, in the time scale of 10^{-2} and 10^{-1} seconds. Thus dynamics of these two sources can be neglected and we can focus on their steady state processes.

5.3.5 Partial pressures

In flow channels of the SOFC stack, partial pressures of reactants are affected by temperatures, the fluid dynamics, reforming/shifting reactions and electrochemical reactions, etc. Simulation shows that the dynamic responses of partial pressures induced by fluid dynamics, reforming/shifting reactions and the electrochemical reactions are fast, at the time scale of $10^{-2} - 10^0$ seconds (Qi *et al.*, 2006). So the dynamics can also be neglected and we can focus on the steady state process of the reactant partial pressures.

Reforming/shifting reactions play an important role in determination of the composition of fuel gas. They generate H_2 and CO from methane and steam:



When fuel flows into the anode channel, with the catalytic aid of Ni in anode and heat from the cell, the reforming and the shifting reactions start. Along the flow direction, methane is consumed gradually and produces hydrogen H_2 . The steady state composition profile can be found in (Campanari and Iora, 2004).

The reforming reaction rate depends on fuel temperature (Ahmed and Foger, 2000) and is usually faster than the flow velocity. This means CH_4 is completely reacted inside the stack. In the stack, steam H_2O is consumed by the reforming and shifting reactions. Simultaneously, the electrochemical reaction produces steam. The reforming and shifting reactions produce hydrogen H_2 . It is then consumed by the electrochemical reaction. The consumption rate is determined by current demand I as shown by Eqn.5.3.

In the stack, the partial pressure of each component can be calculated from mass conservation law following the procedures shown in (Qi *et al.*, 2006). At steady state, the moles of each components left in the flow channel can be calculated by subtracting the moles that are consumed from the initial moles. The partial pressures of each species are then determined by the moles that are left in the flow channels, as listed in Table 5.2.

In Table 5.2, Δ is the moles consumed due to shifting reaction, and \dot{Q}_{fuel} and \dot{Q}_{air} are

Table 5.2: Variation of species in the SOFC stack from the inlet to the outlet

	Initial	Reformed	Shifted	Reacted	Residue
CH ₄	$P_{\text{fuel}}^{\text{in}} \chi_{\text{CH}_4}^{\text{in}}$	$-P_{\text{fuel}}^{\text{in}} \chi_{\text{CH}_4}^{\text{in}}$	-0	-0	0
H ₂ O	$P_{\text{fuel}}^{\text{in}} \chi_{\text{H}_2\text{O}}^{\text{in}}$	$-P_{\text{fuel}}^{\text{in}} \chi_{\text{CH}_4}^{\text{in}}$	$-\Delta$	$+\frac{I}{2F} RT_{\text{fuel}} \frac{1}{\dot{Q}_{\text{fuel}}}$	$p_{\text{H}_2\text{O}}$
H ₂	$P_{\text{fuel}}^{\text{in}} \chi_{\text{H}_2}^{\text{in}}$	$+3P_{\text{fuel}}^{\text{in}} \chi_{\text{CH}_4}^{\text{in}}$	$+\Delta$	$-\frac{I}{2F} RT_{\text{fuel}} \frac{1}{\dot{Q}_{\text{fuel}}}$	p_{H_2}
CO	$P_{\text{fuel}}^{\text{in}} \chi_{\text{CO}}^{\text{in}}$	$+P_{\text{fuel}}^{\text{in}} \chi_{\text{CH}_4}^{\text{in}}$	$-\Delta$	-0	p_{CO}
CO ₂	$P_{\text{fuel}}^{\text{in}} \chi_{\text{CO}_2}^{\text{in}}$	-0	$+\Delta$	-0	p_{CO_2}
O ₂	$P_{\text{air}}^{\text{bot}} \chi_{\text{O}_2}^{\text{in}}$	-0	-0	$-\frac{I}{4F} RT_{\text{air}} \frac{1}{\dot{Q}_{\text{air}}}$	p_{O_2}

the volumetric flow rate of fuel and air respectively.

The final composition is determined by the shifting reaction, which is considered to reach the equilibrium at a very fast rate. The equilibrium constant depends on fuel temperature and is defined as (Ahmed and Foger, 2000):

$$K_{\text{eq}} = \frac{p_{\text{CO}_2} p_{\text{H}_2}}{p_{\text{CO}} p_{\text{H}_2\text{O}}} = \exp\left(\frac{4276}{T_{\text{fuel}}} - 3.961\right) \quad (5.8)$$

The consumed mole due to shifting reaction Δ can then be resolved from Eqn.5.8:

$$\Delta = \frac{K_{\text{eq}}(a_1 + a_3) + a_2 + a_4}{2(K_{\text{eq}} - 1)} - \frac{\sqrt{[K_{\text{eq}}(a_1 + a_3) + a_2 + a_4]^2 - 4(K_{\text{eq}} - 1)(K_{\text{eq}}a_1a_3 - a_2a_4)}}{2(K_{\text{eq}} - 1)} \quad (5.9)$$

where:

$$\begin{aligned} a_1 &= P_{\text{fuel}}^{\text{in}} \chi_{\text{H}_2\text{O}}^{\text{in}} - P_{\text{fuel}}^{\text{in}} \chi_{\text{CH}_4}^{\text{in}} + \frac{I}{2F} \frac{RT_{\text{fuel}}}{\dot{Q}_{\text{fuel}}} \\ a_2 &= P_{\text{fuel}}^{\text{in}} \chi_{\text{H}_2}^{\text{in}} + 3P_{\text{fuel}}^{\text{in}} \chi_{\text{CH}_4}^{\text{in}} - \frac{I}{2F} \frac{RT_{\text{fuel}}}{\dot{Q}_{\text{fuel}}} \\ a_3 &= P_{\text{fuel}}^{\text{in}} \chi_{\text{CO}}^{\text{in}} + P_{\text{fuel}}^{\text{in}} \chi_{\text{CH}_4}^{\text{in}} \\ a_4 &= P_{\text{fuel}}^{\text{in}} \chi_{\text{CO}_2}^{\text{in}} \end{aligned}$$

So the in-stack partial pressures $p_{\text{H}_2\text{O}}$, p_{H_2} , p_{CO} and p_{CO_2} can be calculated from the input variable $P_{\text{fuel}}^{\text{in}}$, disturbances I , $T_{\text{fuel}}^{\text{in}}$ and initial compositions $\chi_{\text{CH}_4}^{\text{in}}$, $\chi_{\text{H}_2\text{O}}^{\text{in}}$, $\chi_{\text{H}_2}^{\text{in}}$, $\chi_{\text{CO}}^{\text{in}}$ and $\chi_{\text{CO}_2}^{\text{in}}$.

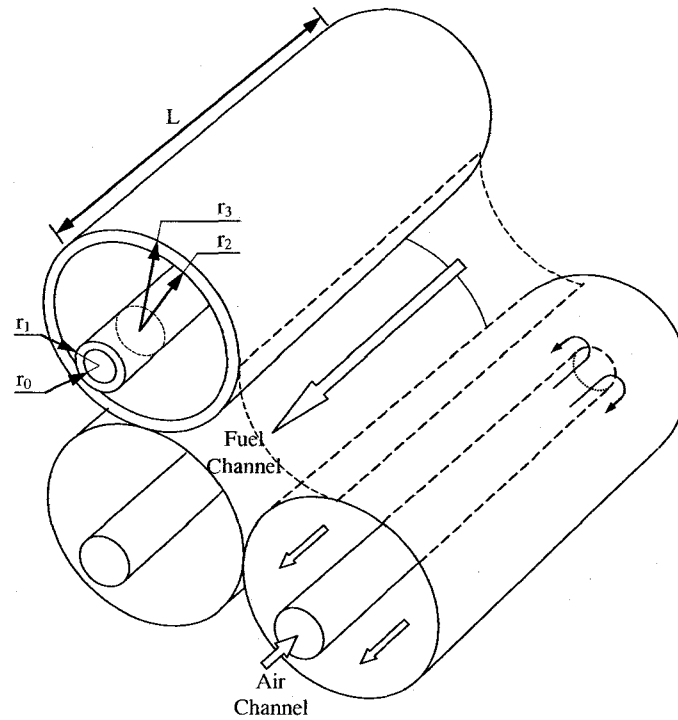


Figure 5.6: Fuel and air flow channels in the tubular SOFC stack

5.3.6 Flow rates

Fuel and air flow rates are determined by three main factors: the upstream pressure, the down stream pressure and the flow resistance. Assuming that the exit pressure is fixed to 1 atm, flow rates are then determined by inlet pressures and the flow resistances.

Fuel flow rate

Usually, fuel velocities are in the range of 1 m/s to 10 m/s. So the residence time for the SOFC stack is in the time scale of 0.1 to 1 second (Gemmen and Johnson, 2005). Compared with the slow solid phase temperature response, the response of flow process is fast. In addition, because fuel and air flows are compressible fluid, disturbances on the fluid lead to a short wave moving at the sonic speed. So we need only to consider the steady state flow process, and the transit process can be neglected.

In the fuel flow channel as shown in Fig.5.6, at steady state, force balance on the fuel fluid is given as:

$$\tau_{w,\text{fuel}} 2\pi r_3 L = (P_{\text{fuel}}^{\text{in}} - P_{\text{fuel}}^{\text{exit}}) (4 - \pi) r_3^2 \quad (5.10)$$

where $\tau_{w,\text{fuel}}$ is the wall shear stress, r_3 the radius of the outer cell tube, and L the length of the flow channel.

Therefore,

$$\tau_{w,\text{fuel}} = \frac{(4 - \pi)r_3}{2\pi} \frac{101325(P_{\text{fuel}}^{\text{in}} - P_{\text{fuel}}^{\text{exit}})}{L} \quad (5.11)$$

For laminar flow in a specific channel, the product of friction factor f and Reynolds number Re is fixed. The fuel channel, which has a shape shown in Fig.5.6, may be approximated by that of square duct: $f\text{Re} = 56.91$ (John and Haberman, 1988).

According to the definition of f and Re , we have:

$$f\text{Re} = \frac{\tau_{w,\text{fuel}}}{\frac{1}{8}\rho\bar{u}^2} \cdot \frac{\rho\bar{u}D_h}{\mu} = 56.91 \quad (5.12)$$

where $D_h = \frac{4(4 - \pi)r_3^2}{2\pi r_3}$ is the hydraulic diameter of the fuel channel.

Solving the fuel velocity \bar{u}_{fuel} from Eqn.5.12 and substituting the result into Eqn.5.11, the volumetric flow rate is given as:

$$\begin{aligned} \dot{Q}_{\text{fuel}} = A_a \bar{u}_{\text{fuel}} &= (4 - \pi)r_3^2 \cdot \frac{8}{56.91} \cdot \frac{\tau_{w,\text{fuel}}D_h}{\mu\bar{u}_{\text{fuel}}} \\ &= 101325 \cdot \frac{8(4 - \pi)^3 r_3^4}{56.91\pi^2 L} \cdot \frac{1}{\mu_{\text{fuel}}} \cdot (P_{\text{fuel}}^{\text{in}} - P_{\text{fuel}}^{\text{exit}}) \end{aligned} \quad (5.13)$$

Air flow rate

Unlike fuel flow, air is injected into the bottom of a SOFC cell tube through an alumina injection tube first. Then flow passes through the cathode flow channel – the gap between the injection tube and the cell tube, as shown in Fig.5.6.

The air flow velocity can be as high as 10 m/s. So we only need to consider the steady state flow.

Simulation from detailed models has shown that the flow is laminar (Qi *et al.*, 2006) whether inside the injection tube or inside the cathode flow channel. So in the injection tube we have $f\text{Re} = 64$. Following the similar procedure the air flow rate in the injection tube can be derived as:

$$\dot{Q}_{\text{air}}^{\text{inj}} = 101325 \cdot \frac{\pi r_0^4}{8L} \cdot \frac{1}{\mu_{\text{air}}} \cdot (P_{\text{air}}^{\text{in}} - P_{\text{air}}^{\text{bot}}) \quad (5.14)$$

where $P_{\text{air}}^{\text{bot}}$ is the air pressure at the bottom of the cell tube. It is also the inlet pressure of the cathode flow channel. r_0 is the inner radius of the injection tube.

Cathode flow channel is an annulus channel. The air flow rate is:

$$\dot{Q}_{\text{air}} = 101325 \cdot \frac{\pi r^*}{8L} \cdot \frac{1}{\mu_{\text{air}}} \cdot (P_{\text{air}}^{\text{bot}} - P_{\text{air}}^{\text{exit}}) \quad (5.15)$$

where

$$r^* = r_2^4 - r_1^4 - \frac{(r_2^2 - r_1^2)^2}{\ln(r_2/r_1)} \quad (5.16)$$

r_2 and r_1 are the inner radius of the cell tube and outer radius of the injection tube respectively.

Air flow in the injection tube and in the cathode channel is continuous so the flow rates are same:

$$\dot{Q}_{\text{air}} = \dot{Q}_{\text{air}}^{\text{inj}} \quad (5.17)$$

Substituting Eqn.5.14 and Eqn.5.15 into Eqn.5.17 and solving the resultant equation, the air pressure at the bottom of the cell tube is:

$$P_{\text{air}}^{\text{bot}} = \frac{r_0^4 \cdot P_{\text{air}}^{\text{in}} + r^* \cdot P_{\text{air}}^{\text{exit}}}{r_0^4 + r^*} \quad (5.18)$$

5.3.7 Temperatures

In the SOFC stack, there are five different temperatures affecting each other. They are gas phase fuel temperature T_{fuel} , air temperature in the injection tube $T_{\text{air}}^{\text{inj}}$, air temperature in the cathode channel T_{air} , solid phase cell tube temperature T_{cell} , and the temperature of the injection tube T_{tube} .

Gas phase temperatures

Because fuel and air flow at speeds ranging from 1 m/s to 10 m/s, their temperature responses to load change, velocity fluctuation and solid phase temperature changes are all minor. Specific heats of fuel and air are relatively small, and the response time is small, in the time scale of 10^{-1} seconds. So we assume that temperatures of gases inside the stack are the same as their inlet temperatures:

$$\begin{aligned} T_{\text{fuel}} &= T_{\text{fuel}}^{\text{in}} \\ T_{\text{air}} &= T_{\text{air}}^{\text{inj}} = T_{\text{air}}^{\text{in}} \end{aligned} \quad (5.19)$$

Detailed simulations in Chapter 3 support these approximations.

Solid phase temperatures

Due to large specific heats, time scales of temperature responses of the solid cell tube and the injection tube are in the order of 10^2 seconds (Qi *et al.*, 2006). Analysis shows that it is solid phase temperature especially the cell temperature T_{cell} that dominates the transit response of the SOFC (Qi *et al.*, 2006). Therefore temperatures of the cell and the injection tube need to be modelled dynamically.

Consider the cell tube as a control volume. Energy flow in and out the control volume can be summarized the following terms::

1. chemical energy carried by reactants JH , where J is mass flow that enters the cell, and H is the enthalpy of formation ;
2. electrical energy supplied to external load $V_{\text{out}}I$;
3. heat flow that the cell tube exchanging with its surroundings through convection $hA(T_w - T_f)$, where h is the heat transfer coefficient;
4. net heat exchange flow through radiation between the cell and the injection tube $\frac{\sigma}{R_{\text{rad}}}A(T_{\text{cell}}^4 - T_{\text{tube}}^4)$, where R_{rad} is the radiation heat transfer resistance;
5. heat flow absorbed by the reforming reaction $r_{\text{ref}}\Delta H$, where r_{ref} is the reforming reaction rate, ΔH the reaction heat.

According to the energy conservation law, the internal energy change of the control volume is given by:

$$\begin{aligned}
 m_{\text{cell}}C_{p,\text{cell}}\frac{dT_{\text{cell}}}{dt} &= \frac{I}{2F} \cdot H_{\text{H}_2}|_{T_{\text{fuel}}} + \frac{I}{4F} \cdot H_{\text{O}_2}|_{T_{\text{air}}} - \frac{I}{2F} \cdot H_{\text{H}_2\text{O}}|_{T_{\text{cell}}} \\
 &\quad - V_{\text{out}} \cdot I \\
 &\quad - h_a \cdot 2\pi r_3 L \cdot (T_{\text{cell}} - T_{\text{fuel}}) - h_c \cdot 2\pi r_2 L \cdot (T_{\text{cell}} - T_{\text{air}}) \\
 &\quad - \frac{\sigma}{R_{\text{rad}}} \cdot 2\pi r_2 L \cdot (T_{\text{cell}}^4 - T_{\text{inj}}^4) \\
 &\quad - A_r K_r p_{\text{CH}_4}^\alpha p_{\text{H}_2\text{O}}^\beta \cdot \exp\left(-\frac{E_r}{RT_{\text{fuel}}}\right) \cdot \Delta H|_{T_{\text{fuel}}}
 \end{aligned} \tag{5.20}$$

The injection tube is only an internal media in the heat transfer process. But due to its high specific heat, it affects the temperature of the cell. The injection tube

accepts heat energy from the cell tube through radiation and exchanges heat flow with its surroundings through forced convection:

$$m_{\text{inj}} C_{p,\text{inj}} \frac{dT_{\text{inj}}}{dt} = \frac{\sigma}{R_{\text{rad}}} \cdot 2\pi r_2 L \cdot (T_{\text{cell}}^4 - T_{\text{inj}}^4) - h_c \cdot 2\pi r_1 L \cdot (T_{\text{inj}} - T_{\text{air}}) - h_t \cdot 2\pi r_0 L \cdot (T_{\text{inj}} - T_{\text{air}}) \quad (5.21)$$

5.4 Nonlinear state-space model

Define the input vector \mathbf{u} :

$$\mathbf{u} = [u_1 \quad u_2]^T = [P_{\text{fuel}}^{\text{in}} \quad P_{\text{air}}^{\text{in}}]^T \quad (5.22)$$

the disturbance vector \mathbf{d} :

$$\mathbf{d} = [d_1 \quad d_2 \quad d_3]^T = [I \quad T_{\text{fuel}}^{\text{in}} \quad T_{\text{air}}^{\text{in}}]^T \quad (5.23)$$

the output vector \mathbf{y} :

$$\mathbf{y} = [y_1 \quad y_2]^T = [V_{\text{out}} \quad T_{\text{cell}}]^T \quad (5.24)$$

and the state vector \mathbf{x} :

$$\mathbf{x} = [x_1 \quad x_2]^T = [T_{\text{cell}} \quad T_{\text{inj}}]^T \quad (5.25)$$

Substituting Eqn.5.13, 5.15 and 5.18 into the expression in Table.5.2, then substituting the partial pressures from Table.5.2 into the voltage expression in Eqn.5.6, the nonlinear state-space model of the SOFC stack is:

States:

$$\begin{aligned} \dot{x}_1 &= \frac{1}{m_{\text{cell}} C_{p,\text{cell}}} \left\{ \frac{1}{2F} (H_{\text{H}_2} + \frac{1}{2} H_{\text{O}_2} - H_{\text{H}_2\text{O}}) d_1 \right. \\ &\quad - \left[E^0 + \frac{R}{2F} x_1 \ln \left(\frac{p_{\text{H}_2} p_{\text{O}_2}^{0.5}}{p_{\text{H}_2\text{O}}} \right) - R_{\text{in}} d_1 \right] d_1 \\ &\quad - h_a \cdot 2\pi r_3 L \cdot (x_1 - d_2) - h_c \cdot 2\pi r_2 L \cdot (x_1 - d_3) \\ &\quad \left. - A_r K_r x_1^{(\alpha+\beta)} \cdot \chi_{\text{CH}_4}^{\text{in} \alpha} \chi_{\text{H}_2\text{O}}^{\text{in} \beta} \cdot \exp \left(-\frac{E_r}{R \cdot d_2} \right) \cdot \Delta H \right\} \end{aligned}$$

$$\dot{x}_2 = \frac{1}{m_{\text{inj}} C_{p,\text{inj}}} \left\{ \frac{\sigma}{R_{\text{rad}}} \cdot 2\pi r_2 L \cdot (x_1^4 - x_2^4) - 2\pi L \cdot (h_c r_1 + h_t r_0) \cdot (x_2 - d_3) \right\}$$

Outputs:

$$y_1 = E^0 + \frac{R}{2F} x_1 \ln \left(\frac{p_{\text{H}_2} p_{\text{O}_2}^{0.5}}{p_{\text{H}_2\text{O}}} \right) - R_{\text{in}} d_1$$

$$y_2 = x_1$$

where:

$$H_{\text{H}_2} = -0.9959 \times 10^4 + 30.73 d_2$$

$$H_{\text{O}_2} = -1.2290 \times 10^4 + 35.12 d_3$$

$$H_{\text{H}_2\text{O}} = -25.790 \times 10^4 + 42.47 d_2$$

$$E^0 = 1.273 - 2.7645^{-4} x_1$$

$$p_{\text{H}_2} = u_1 (\chi_{\text{H}_2}^{\text{in}} + 3\chi_{\text{CH}_4}^{\text{in}}) + \Delta - 1.0955 \times 10^{-3} \frac{R}{2F} \cdot \frac{\mu_{\text{fuel}} L}{r_3^4} \cdot \frac{d_1 d_2}{u_1 - p_{\text{fuel}}^{\text{exit}}}$$

$$p_{\text{H}_2\text{O}} = u_1 (\chi_{\text{H}_2\text{O}}^{\text{in}} - \chi_{\text{CH}_4}^{\text{in}}) - \Delta + 1.0955 \times 10^{-3} \frac{R}{2F} \cdot \frac{\mu_{\text{fuel}} L}{r_3^4} \cdot \frac{d_1 d_2}{u_1 - p_{\text{fuel}}^{\text{exit}}}$$

$$p_{\text{O}_2} = \frac{0.21 r_0^4}{r_0^4 + r^*} u_2 + \frac{0.21 r^* p_{\text{air}}^{\text{exit}}}{r_0^4 + r^*} - 2.5132 \times 10^{-5} \frac{R}{4F} \cdot \frac{\mu_{\text{air}} L}{r_0^4} \cdot \frac{r_0^4 + r^*}{r^*} \cdot \frac{d_1 d_3}{u_1 - p_{\text{air}}^{\text{exit}}}$$

$$\Delta H = -20.73 \times 10^4 - 19.41 d_2$$

$$R_{\text{in}} = 2.94 \times 10^{-5} \exp \left(\frac{10350}{x_1} \right) \cdot \frac{0.12 \times 10^{-3}}{2\pi r_3}$$

or, in a compact form:

$$\begin{aligned} \dot{\mathbf{x}} &= f(\mathbf{x}, \mathbf{u}, \mathbf{d}) \\ \mathbf{y} &= g(\mathbf{x}, \mathbf{u}, \mathbf{d}) \end{aligned} \tag{5.26}$$

This model, in SIMULINK format, is available at:

www.ualberta.ca/~bhuang/research/research.htm

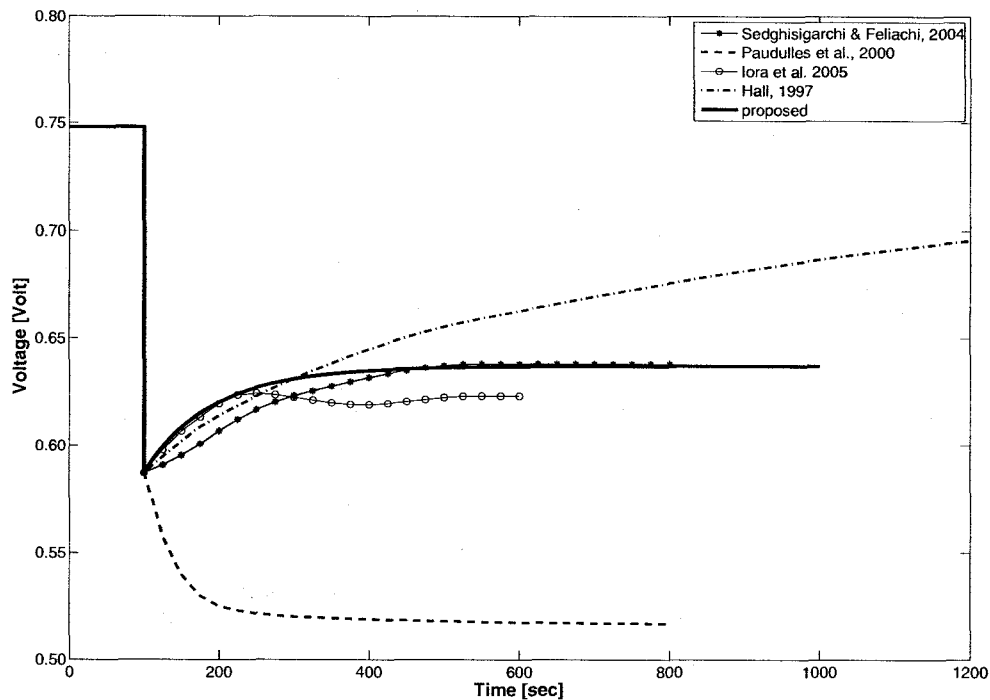


Figure 5.7: Compare of stack voltage response trends to current demand step change

5.5 Simulation

5.5.1 Validation

The SOFC stack parameters are given in Table A-2. Cells are simply electrically connected in series to form the stack. We shall just investigate the performance of a single cell without loss of generality.

The simulated trend of voltage dynamic response for current step change from 300 to 500A is compared with other simulation results available in the literature, as shown in Fig.5.7. Hall and Colclaser's (1999) model only considered the dynamics led by temperature. Padullés *et al.* (2000) assumed that the SOFC stack is a choked system and no temperature dynamics was considered. Sedghisigarchi and Feliachi (2004) assumed that the stack is a choked system and considered the temperature dynamics. Their voltage trend is similar to ours. Iora *et al.* (2005) gave more detailed 1-D numerical model. They also considered the effects of fluid dynamics, reforming/shifting reactions, heat transfer etc.

For the reason of lacking experimental and simulated results of dynamic response to fuel/air inlet fluctuations, the trend of the simulated voltage response is compared with the simulation results from the detailed model shown in Chapter 3. It is shown that the dynamics responses due to inlet and disturbance fluctuations are consistent with that of detailed model.

5.5.2 Step response to inputs

The dynamic operation properties of the SOFC stack have been investigated through simulation.

As shown in Fig.5.8, when fuel upstream pressure $P_{\text{fuel}}^{\text{in}}$ is stepped from 1.0008 to 1.0016atm, the flow rate of syngas fuel is increased about twice at once. This means that more CH_4 is converted into H_2 in the stack. The partial pressure of hydrogen p_{H_2} is increased. Thus the voltage output V_{out} increases quickly. But more heat is extracted from the cell to support the reforming reaction; thus the cell temperature T_{cell} slightly decreases gradually due to its large heat capacity. This results in a slight decrease of V_{out} , synchronized with the response of T_{cell} .

Similar to the effect of fuel inlet pressure increase, when air upstream pressure $P_{\text{air}}^{\text{in}}$ is stepped from 1.01 to 1.02atm, oxygen partial pressure p_{O_2} in the stack and the air flow rate in the channel increase, so does the voltage output V_{out} . The step responses are shown in Fig.5.9.

Simulations show that the step of u_1 has immediate and significant effect to y_1 . Its effect on y_2 is however minor and slow, similar to a first order response, with the time constant of around 150 seconds. The effects of u_2 are similar to that of u_1 .

5.5.3 Step responses to disturbance

The response of the stack due to the disturbances coming from power demand and the inlet fuel and air temperatures have also been investigated through simulations.

When the external current demand I is stepped from 300 to 500 Amp, the response of the stack is shown in Fig.5.10. It is seen that the response of y_1 to the step change of d_1 is immediate and significant. d_1 has also a great effect on y_2 . The step response of y_2 is similar to a first order response with the time constant of around 150 seconds due to the large heat capacity of the cell tube.

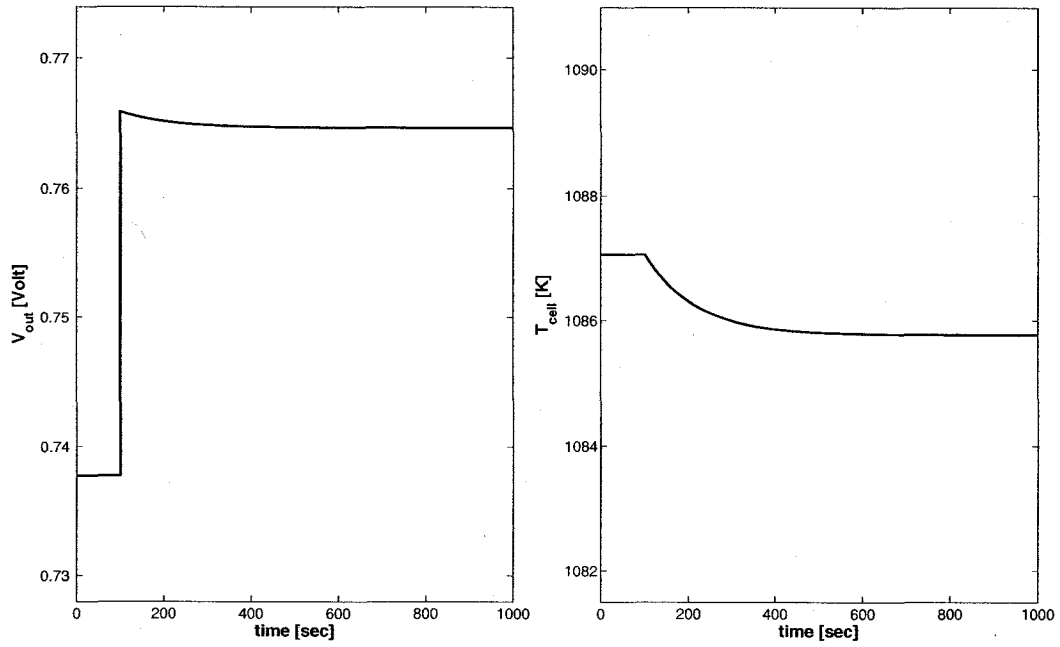


Figure 5.8: Step response of outputs due to u_1 , the fuel inlet pressure P_{fuel}^{in} , stepped from 1.0008 to 1.0016 atm

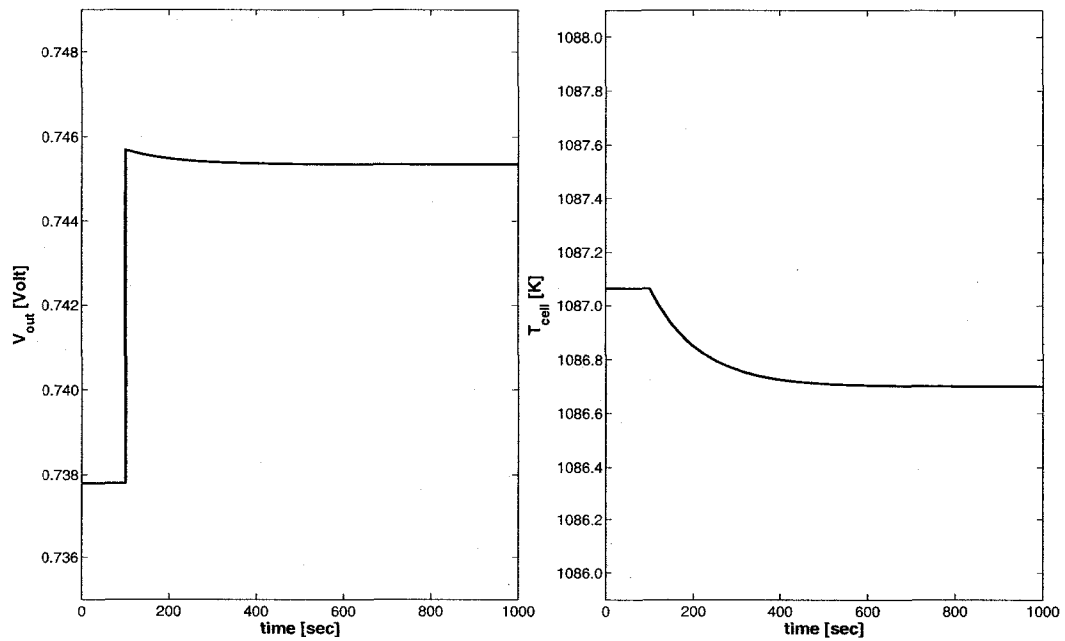


Figure 5.9: Step response of outputs due to u_2 , the air inlet pressure P_{air}^{in} , stepped from 1.01 to 1.02 atm

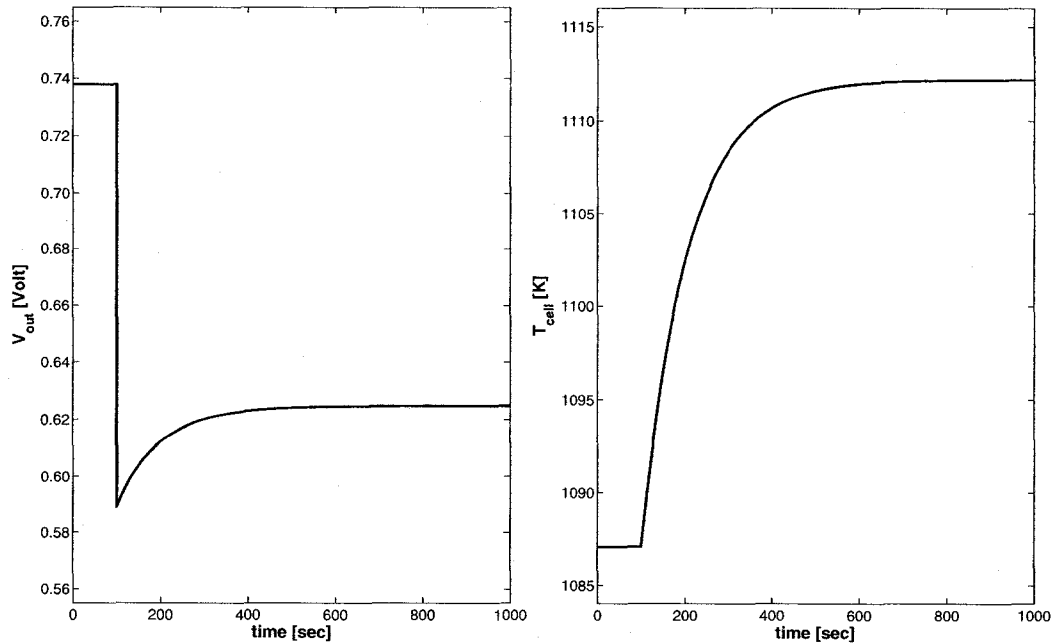


Figure 5.10: Step response of outputs due to d_1 , the external current demand I , stepped from 300 to 500 amp

Due to the increase of I , the voltage drop on the intrinsic resistance of the cell increases immediately and more hydrogen H_2 and oxygen O_2 are consumed. So p_{H_2} and p_{O_2} decrease and p_{H_2O} increases. The result is a decrease of V_{out} in a short period. The energy consumed by the intrinsic resistance increases with the increase of I . That part of energy heats the cell and consequently T_{cell} increases. So V_{out} is recovered slightly with the increase of T_{cell} after the initial sudden drop.

When the fuel inlet temperature T_{fuel}^{in} is stepped from 823 to 873K, the direct result is the reverse of the shift reaction equilibrium, and the partial pressure of hydrogen p_{H_2} decreases. So the voltage output V_{out} decreases immediately. Meanwhile, increasing of T_{fuel}^{in} decreases the temperature difference between the fuel and the cell. T_{cell} then increases with the time constant of around 150 seconds. Step responses of y_1 and y_2 due to the step change of d_2 are shown in Fig.5.11.

The effect of air inlet temperature disturbance T_{air}^{in} is more direct and significant. When T_{fuel}^{in} steps from 1104 to 1154K, it heats the cell. So T_{cell} increases gradually, and the voltage output V_{out} increases with T_{cell} , as shown in Fig.5.12.

Simulation shows that both y_1 and y_2 respond to the step change of d_3 significantly

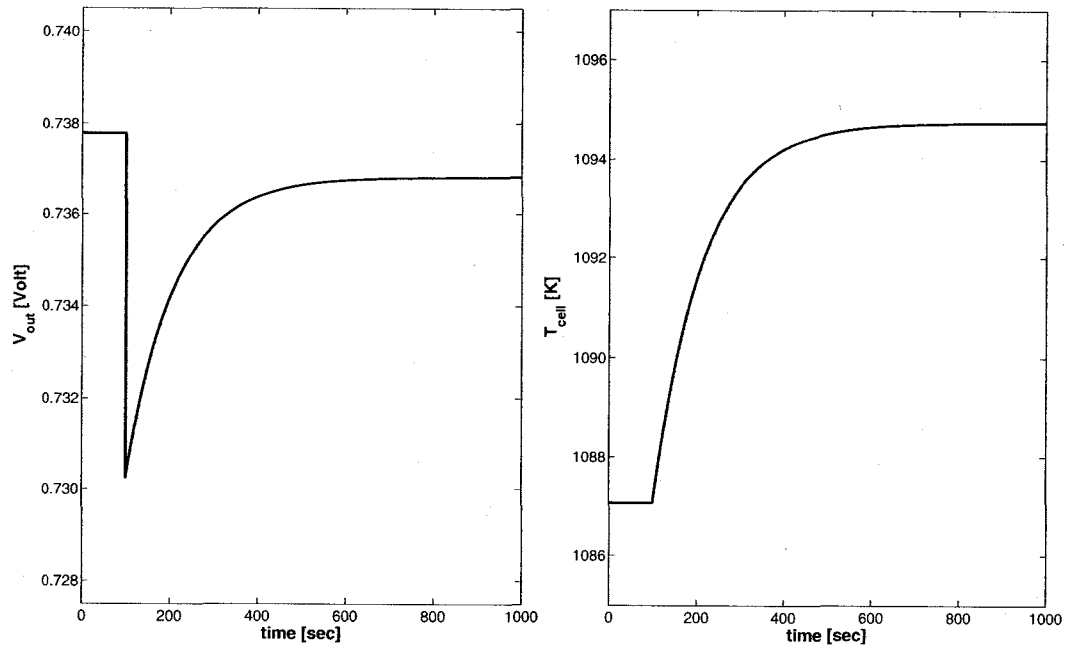


Figure 5.11: Step response of outputs due to d_2 , the fuel inlet temperature T_{fuel}^{in} , stepped from 823 to 873 K

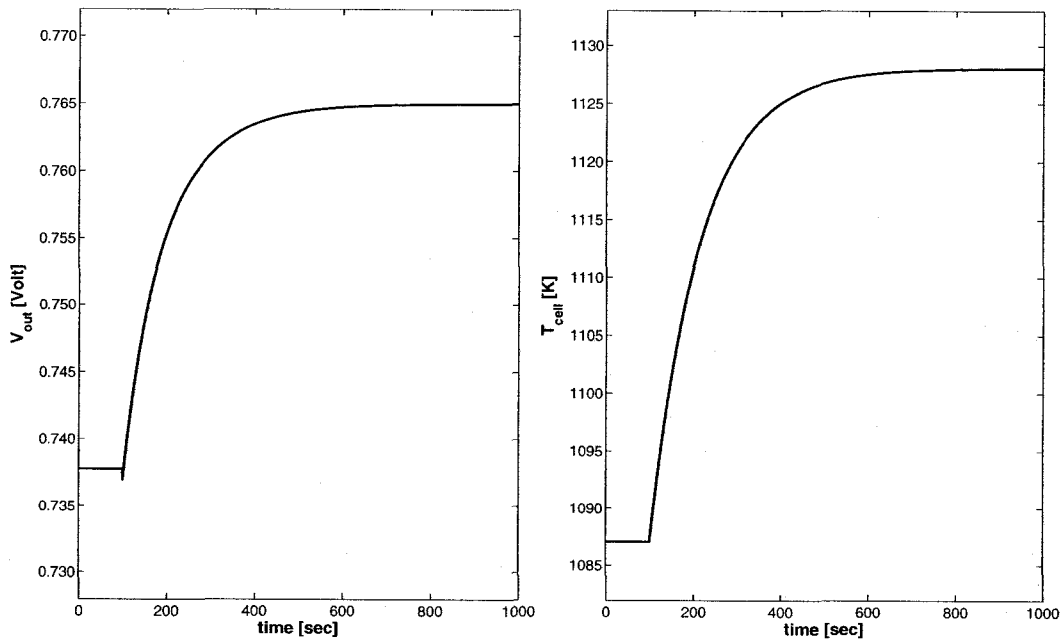


Figure 5.12: Step response of outputs due to d_3 , the air inlet temperature T_{air}^{in} , stepped from 1104 to 1154 K

and is similar to first order responses with time constant of around 150 seconds.

All the simulated dynamic responses to the inlet parameters shown above, including input variables and disturbances, are consistent with those simulated results from the detailed 28th order SOFC model shown in Chapter 3. It means that the second order lumped model can indeed capture the main dynamic characteristics of the SOFC stack.

5.6 Conclusion

A control relevant lumped 2nd order dynamic model for a tubular solid oxide fuel cell (SOFC) stack has been built. Input-output variables and control objectives of the SOFC stack were analyzed. Fuel and air upstream pressures were designated as the control variables. The SOFC stack can be operated by manipulating the fuel and air upstream pressure. The voltage output of the SOFC stack and the cell temperature were designated as outputs of the model. Variables that can not be directly manipulated such as current demand, the fuel and air inlet temperatures were considered as disturbance. Fast processes such as reforming and shift reactions, flow processes, mass transfer processes etc. have been considered at steady states. Owing to that the response of cell temperature is slow and plays a dominate role in the performance of the SOFC stack, its dynamic modeling was studied in details.

The dynamic operational properties of the SOFC stack have been investigated through simulations. It is shown that operation of fuel or air inlet pressure has immediate effects on the stack voltage output but leads to minor change of the cell temperature. Disturbance coming from the external power demand has great effects on the cell temperature and then the voltage. Disturbances of fuel or air inlet temperature also have significant effects on the performance of the SOFC stack.

The dynamic performance simulated from the 2nd order state space model is consistent with that from the more detailed model. It is shown that the second order lumped model proposed in this chapter can capture the main dynamic characteristics of the SOFC stack and thus can be used to represent the SOFC stack for controller design.

6

Conclusions and recommendations

This chapter lists the contributions of this thesis and the directions identified for future research.

6.1 Concluding remarks

The main contributions of this thesis are the development of the first principle dynamic model of the solid oxide fuel cell (SOFC), the simulation of the dynamic response characteristics of SOFC, and the development of the approximate analytical solution for 1-D reacting gas flow problem. Specific contributions include:

1. A brief overview of SOFC modeling approaches. Through literature review it is found that dynamic processes that occur inside a SOFC have not been well understood, dynamic characteristics of SOFC have not been well described, and existing models have been insufficient to capture the essential dynamic properties of SOFC. A project consisting of four phases is planned to fill these gaps.
2. A presentation of a block diagram with a conceptual interpretation for

the complicated dynamic physical processes that occur in SOFC, including electrochemical reactions, transport processes, limitations to power production, and their interactions.

3. Development of dynamic relations of concentrations and mass fluxes between primary flow and triple phase boundary (*tpb*), in the form of transfer function. Dynamics led by diffusion is investigated through simulation.
4. Development of a new equivalent circuit for the inherent impedance of SOFC. The circuit can capture the performance of SOFC led not only by external current demand but also by the internal electromotive force (EMF) fluctuation.
5. The adjustment to the Nernst equation and the Butler-Volmer correlation, by using the concentrations at *tpb* directly. With this modification, in the calculation of EMF, the concentration loss therefore does not need to be considered.
6. A new physical explanation for the result of Current Interrupt Experiment, by comparing the dynamic effects led by diffusion and inherent impedance. It is found that the slower response of the voltage, with the time constant being in the order of 0.1 seconds, is led by diffusion. The reasonable quantity of the double layer capacitance is several hundreds of μF , not several F. The dynamic effect that led by the double layer capacitance is therefore in the order of 0.001 seconds.
7. A relative comprehensive dynamic model SOFC dynamics, in the form of state-space model. Dynamics led by internal reforming/shifting reaction, heat transfer, mass transfer, momentum balance, diffusion, impedance, convection, and radiation are considered. The model can be applied in control applications and it can also be used in detailed investigating of dynamic properties, parameter sensitivities, and operation properties of SOFC. It is programmed as a Simulink model, and can simulate the performance of SOFC under different input conditions.
8. Investigation of dynamic characteristics of SOFC through simulation, by step changing input parameters such as external load, fuel/air pressure, temperature and velocity etc, and comparing the responses. Simulation shows that the fuel pressure and temperature have large effects on the dynamic performance of SOFC, owing to the internal Reforming/Shifting reaction. It is also shown that

the air temperature has the most significant effect on SOFC temperature and thus the overall performance of SOFC.

9. Development of a relation between current density distribution, total current demand and local EMF, by solving a developed equivalent circuit for the SOFC tube. The current density distribution along the cell tube therefore can be predicted from the measurable total current demand.
10. Development of a 1-D dynamic model for a tubular SOFC. The dynamics of the overall SOFC tube including the distributions of each physical variable and distributed dynamics can then be simulated through the 1-D dynamics model.
11. An analytical solution and a method to solve the 1-D reacting gas flow problem. The solution converts the 1-D dynamic model from the form of coupled partial differential equations to the form of ordinary differential equations. The method has a reasonable precision and can significantly reduce the computation requirements. It can be applied to a wide range of control and simulation studies.
12. An 1-D dynamic of SOFC in the form of state-space model. Using the analytical solution of the 1-D reacting gas flow problem developed, the 1-D SOFC dynamic model is converted from partial differential equations to a state-space model and coded in Simulink. The established Simulink model can simulate distributed dynamic performance of the overall SOFC tube in a high speed.
13. Investigation of parameter distributions and dynamic performances of a tubular SOFC, through simulating step responses to inlet variable changes. The distributed dynamic response of SOFC including electromotive, temperatures, and species mole fractions are shown in 3-D figures. It is found that dynamics and distributions of SOFC are dominated by the cell temperature. It is also found that the existence of the injection tube and thus the air flow turning around process actually dim the effect of air temperature and if air flow rate can change in an relatively large range, 2 to 3 times, the air flow rate can significantly affect the cell temperature distribution.
14. A low order lumped parameter model suitable for control application, by simplifying fast processes with steady state. Control variables, manipulable variables, and disturbances are also analyzed. The model can capture the key dynamics that is shown by the detailed model.

6.2 Recommendations for future work

First principle dynamic modeling of SOFC is a relatively new and active research area. It is an essential part of the development of SOFC technology, particularly for solving the control problem. The ultimate objective is to develop a feasible and reliable SOFC technology as an alternative new energy. It is a long-term and challenging interdisciplinary research. The results presented in this thesis address some of the problems. Many problems remain that need to be investigated and solved in the future:

1. According to a specific SOFC geometry design, the effect of radiation heat that is absorbed by fuel and air flow needs to be considered in the model. The effect due to the tail gas combustion and the consequent heat transfer from the combustion chamber to the stack need to be included and investigated. For a SOFC stack, the effect of heat lost from the stack to the surroundings and the consequent temperature gradient inside the stack need to be modeled and investigated.
2. The dynamic model needs to be experimentally calibrated, directly or indirectly. Because properties of SOFC are in the development and direct experimental calibration is difficult, some indirect methods can be developed and adopted to verify the model.
3. Dynamic properties of SOFC need to be investigated in more detail. In this thesis, the dynamic characteristics of SOFC investigated through simulating step responses to a single input variable change. Only part of the dynamic characteristics can be found through this method. In order to grasp the comprehensive dynamic property of SOFC, other methods such as frequency domain analysis can be introduced in the investigation.
4. Sensitivity of performance to the parameters and mechanism should be analyzed and investigated for the purpose of system design.
5. In order to fit current control techniques, under the condition of maintaining the main dynamic characteristics of SOFC, the model can be further simplified.
6. Controllability of SOFC should be analyzed and combined in the system configuration. Control strategies for the operation of SOFC stack and system can be developed in advance.

7. Specific control problems such as control of temperature gradient inside the stack and fuel utilization need to be balanced and solved.
8. Other subsystems of a SOFC hybrid system should be investigated and modeled.

Other than these control related problems, in the development of SOFC technology there are still bottleneck challenges that a researcher with process control and chemical engineering background could contribute to:

- Modeling and optimization of composite electrode. A composite electrode can significantly increase the length of *tpb* and decrease the contact resistance, therefore greatly improve the performance of SOFC.
- Innovative stack design can also significantly improve the performance of SOFC. A proper stack design can decrease the cost, improve the durability, and increase the current density. It may also avoid some bottleneck challenges such as sealing problem, temperature gradient problem and the consequent thermal stress and durability problem.
- Advanced system configuration. Considering the balance of plant (BoP), an advanced system configuration can improve the stability and controllability of the system and thus can greatly increase the efficiency and decrease the operation cost.

Bibliography

- Achenbach, Elmar (1994). Three-dimensional and time dependent simulation of a planar solid oxide fuel cell stack. *Journal of Power Sources* **49**, 333–348. 6, 7, 13, 41, 74, 122
- Achenbach, Elmar (1995). Response of a solid oxide fuel cell to load change. *Journal of Power Sources* **57**, 105–109. 6, 7, 13, 41, 74, 122
- Ahmed, Khaliq and Karl Foger (2000). Kinetics of internal steam reforming of methane on Ni/YSZ-based anodes for solid oxide fuel cells. *Catalysis Today* **63**, 479–487. 51, 85, 133, 134, 160
- Ahmed, S., C. McPheeters and R. Kumar (1991). Thermal-hydraulic model of monolithic solid oxide fuel cells. *Journal of the Electrochemical Society*. 5
- Barbucci, A., R. Bozzo, G. Cerisola and P. Costamagna (2002). Characterization of composite SOFC cathodes using electrochemical impedance spectroscopy. Analysis of Pt/YSZ and LSM/YSZ electrodes. *Electrochimica Acta* **47**, 2183–2188. 16
- Berthier, F., J. P. Diard, B. Le Gorrec and C. Montella (1995). Method for determining the Faradaic impedance of an electrode reaction: Application to metal corrosion rate measurements. *Corrosion Science* **51(2)**, 105–115. 6
- Bessette, Norman Frederic (1994). Modeling and Simulation for Solid Oxide fuel Cell Power Systems. PhD thesis. Georgia Institute of Technology. 160
- Bieberle, A. and L. J. Gauckler (2000). Reaction mechanism of Ni pattern anodes for solid oxide fuel cells. *Solid State Ionics* **135**, 337–345. 20
- Campanari, S. (2001). Thermodynamic model and parametric analysis of a tubular SOFC module. *Journal of Power Sources* **92(1-2)**, 26–34. 5

- Campanari, S. and P. Iora (2004). Definition and sensitivity analysis of a finite volume SOFC model for a tubular cell geometry. *Journal of Power Sources* **132**, 113–126. 5, 19, 23, 29, 51, 102, 122, 133, 158, 159, 160
- Cengel, Yunus A. and Michael A. Boles (1994). *Thermodynamics: An Engineering Approach*. 2nd ed.. McGraw-Hill, Inc.. New York, London, Mexico City, Milan, Montreal, New Delhi, Singapore, Sydney, Tokyo, Toronto. 161
- Chan, S. H. and Z. T. Xia (2001). Anode micro model of solid oxide fuel cell. *Journal of The Electrochemical Society* **148**(4), A388–A394. 20
- Chan, S. H., K. A. Khor and Z. T. Xia (2001). A complete polarization model of a solid oxide fuel cell and its sensitivity to the change of cell component thickness. *Journal of Power Sources* **93**, 130–140. 20, 23
- Chan, S. H., X. J. Chen and K. A. Khor (2004). Cathode micromodel of solid oxide fuel cell. *Journal of the Electrochemical Society* **151**(1), A164–A172. 20
- Debendetti, P. G. and C. G. Vayenas (1983). Steady-state analysis of high temperature fuel cells. *Chemical Engineering Science* **38**(11), 1817–1829. 5
- Domergue, J., A. Rufer and N. Buchheit (1998). Dynamic model of a solid oxide fuel cell stack and power converter. In: *Proceedings of The 3rd European SOFC Forum*. 7
- Dunbar, W. R. (1983). Computer simulation of solid electrolyte fuel cells. Master's thesis. Marquette University. 5
- Gemmen, R. (2000). Development of dynamic modeling tools for solid oxide and molten carbonate hybrid fuel cell gas turbine systems. In: *Proceedings of The International Gas Turbine Institute Meeting*. 7
- Gemmen, Randall S. and Christopher D. Johnson (2005). Effect of load transients on SOFC operation - current reversal on loss of load. *Journal of Power Sources* **144**, 152–164. 7, 41, 74, 135
- Hall, D. J. and R. G. Colclaser (1999). Transient modeling and simulation of a tubular solid oxide fuel cell. *IEEE TRANSACTIONS ON ENERGY CONVERSION* **14**(3), 749–753. 141

- Hall, David Jonathan (1997). Transient Modeling and Simulation of a Solid Oxide Fuel Cell. PhD thesis. University of Pittsburgh. 159, 160
- Holtappels, P., J. Bradley, J. T. S. Irvine, A. Kaiser and M. Mogensen (2001). Electrochemical characterization of ceramic SOFC anodes. *Journal of The Electrochemical Society* **148**(8), A923–A929. 6, 16
- Iora, P., P. Aguiar, C. S. Adjiman and N. P. Brandon (2005). Comparison of two IT DIR-SOFC models: Impact of variable thermodynamic, physical and flow properties. Steady-state and dynamic analysis. *Chemical Engineering Science* **60**, 2963–2975. 7, 41, 74, 75, 89, 91, 141
- John, James E. A. and William L. Haberman (1988). *Introduction to Fluid Mechanics*. 3th ed.. Prentice Hall. London, Sydney, Toronto, Mexico City, Tokyo, Rio de Janeiro. 136
- Jørgensen, M. J. and M. Mogensen (2001). Impedance of solid oxide fuel cell LSM/YSZ composite cathodes. *Journal of The Electrochemical Society* **148**(5), A433–A442. 6, 16
- Jørgensen, M. J., S. Primdahl and M. Mogensen (1999). Characterization of composite SOFC cathodes using electrochemical impedance spectroscopy. *Electrochimica Acta* **44**, 4195–4201. 16
- Kandepu, Rambabu, Lars Imsland, Bjarne A. Foss, Christoph Stiller, Bjorn Thorud and Olav Bolland (2007). Modeling and control of a SOFC-GT-based autonomous power system. *Energy* **32**(4), 406–417. 8
- Larminie, James and Andrew Dicks (2003). *Fuel Cell Systems Explained*. 3rd ed.. John Wiley & Sons, Inc.. Chichester, West Sussex. 5, 15, 24, 31, 81, 123, 124, 163
- Li, Pei-Wen and Minking K. Chyu (2003). Simulation of the chemical / electrochemical reactions and heat / mass transfer for a tubular SOFC in a stack. *Journal of Power Sources* **124**, 487–498. 5, 43, 74, 122
- Liese, E. A. (1999). Technical development issues and dynamic modeling of gas turbine and fuel cell hybrid systems. In: *Proceedings of The International Gas Turbine Institute Meeting*. 7

- Lukas, M. D., K. Y. Lee and H. Ghezal-Ayagh (1999). Development of a stack simulation model for control study on direct reforming molten carbonate fuel cell power plant. *IEEE Transaction on Energy Conversion* **14**(4), 1651–1657. 7
- Macdonald, J. Ross (1987). *Impedance spectroscopy: Emphasizing solid materials and systems*. John Wiley & Sons, Inc.. New York and Chichester and Brisbane and Toronto and Singapore. 6, 16, 24
- Mitterdorfer, A. and L. J. Gauckler (1999a). Identification of the reaction mechanism of the Pt, O₂(g)|yttria-stabilized zirconia system Part I: General framework, modelling, and structural investigation. *Solid State Ionics* **117**, 187–202. 6, 20
- Mitterdorfer, A. and L. J. Gauckler (1999b). Identification of the reaction mechanism of the Pt, O₂(g)|yttria-stabilized zirconia system Part II: Model implementation, parameter estimation, and validation. *Solid State Ionics* **117**, 203–217. 6
- Mitterdorfer, A. and L. J. Gauckler (1999c). Reaction kinetics of the Pt, O₂(g)|c – ZrO₂ system: precursor mediated adsorption. *Solid State Ionics* **117**, 203–217. 6, 16, 126
- Mogensen, Mogens and Steen Skaarup (1996). Kinetic and geometric aspects of solid oxide fuel cell electrodes. *Solid State Ionics* **86-88**, 1151–1160. 16
- Murshed, AKM M., Biao Huang and K. Nandakumar (2007). Control relevant modeling of planar solid oxide fuel cell system. *Journal of Power Sources* **163**, 830–845. 8, 122
- Padullés, J., G. W. Ault and J. R. McDonald (2000). An integrated SOFC plant dynamic model for power systems simulation. *Journal of Power Sources* **86**, 495–500. 7, 13, 41, 74, 89, 122, 131, 141
- Perry, Robert H., Green, Don W. and Maloney, James O., Eds.) (1997). *Perry's Chemical Engineers' Handbook*. 7th ed.. McGraw-Hill, Inc.. New York, London, Mexico City, Milan, Montreal, New Delhi, Singapore, Sydney, Tokyo, Toronto. 50, 56, 159, 161, 162, 163, 164
- Perumal, T. Pramananda, V. Sridhar and K. P. N. Murthy (2002). Molecular dynamics simulations of oxygen ion diffusion in yttria-stabilized zirconia. *Physica A* **309**, 35–44. 6

- Qi, Yutong, Biao Huang and Jingli Luo (2006). Dynamic modeling of a finite volume of solid oxide fuel cell: The effect of transport dynamics. *Chemical Engineering Science* **61**(18), 6057–6076. 8, 74, 82, 83, 85, 86, 88, 89, 106, 133, 136, 138, 160
- Qi, Yutong, Biao Huang and Jingli Luo (2007a). 1-D dynamic modeling of SOFC with analytical solution for reacting gas flow problem. *AIChE Journal*, Submitted. 8
- Qi, Yutong, Biao Huang and Jingli Luo (2007b). Low-order state space model of solid oxide fuel cell. *Journal of Process Control*, Submitted. 8, 89
- Qi, Yutong, Biao Huang and Karl T. Chuang (2005). Dynamic modeling of solid oxide fuel cell: The effect of diffusion and inherent impedance. *Journal of Power Sources* **150**, 32–47. 7, 46, 74, 78, 79, 81, 82, 103, 132
- Rao, Askok Domalpalli (2001). A Thermodynamic Analysis of Tubular SOFC based Hybrid Systems. PhD thesis. University of California, Irvine. 47
- Seborg, Dale E., Thomas F. Edgar and Duncan A. Mellichamp (1989). *Process Dynamics and Control*. 1 ed.. John Wiley Brisbane, Toronto, Singapore. 26
- Sedghisigarchi, Kouros and Ali Feliachi (2004). Dynamic and transient analysis of power distribution systems with fuel cells - part I. *IEEE Transactions on Energy Conversion* **19**(2), 423–428. 7, 13, 41, 74, 122, 141
- Smith, J. M. and H. C. Van Ness (1987). *Introduction to Chemical Engineering Thermodynamics*. 4th ed.. McGraw-Hill Book Company. New York, London, Milan, Montreal, New Delhi, Panama, Paris, Singapore, Sydney, Tokyo, Toronto. 47, 163
- Solheim, A. (1992). In sofc micromodelling, an international energy agency sofc task report. p. 9. Swiss Federal Office of Energy. Brene, Switzerland. 22
- Stiller, Christoph, Bjorn Thorud, Olav Bolland, Rambabu Kandepu and Lars Imsland (2006). Control strategy for a solid oxide fuel cell and gas turbine hybrid system. *Journal of Power Sources* **158**(1), 303–315. 8
- Tsai, Tsepin and Scott A. Barnett (1997). Effect of LSM-YSZ cathode on thin-electrolyte solid oxide fuel cell performance. *Solid State Ionics* **93**, 207–217. 28, 29, 30

- Wächter, Christian, Reinhart Lunderstadt and Franz Joos (2006). Dynamic model of a pressurized SOFC/gas turbine hybrid power plant for the development of control concepts. *Journal of Fuel Cell Science and Technology* 3(3), 271–279. 8
- Wagner, N., W. Schnurnberger, B. Müller and M. Lang (1998). Electrochemical impedance spectra of solid-oxide fuel cells and polymer membrane fuel cells. *Electrochimica Acta* 43, 3785–3793. 6, 16, 18, 24, 28, 29, 30, 31
- Wayland, Harold (1957). *Differential Equations Applied in Science and Engineering*. D. Van Nostrand Company, Ltd.. Princeton, New Jersey and Toronto and London and New York. 20
- Welty, James R., Charles E. Wicks and Robert E. Wilson (1984). *Fundamentals of momentum, heat, and mass transfer*. John Wiley & Sons, Inc.. New York. 21, 22, 29, 47, 48, 49
- Wepfer, W. J. and M. H. Woolsey (1985). High temperature fuel cells for power generation. *Energy Conversion Management* 25(4), 477–486. 5
- Xue, X., J. Tang, N. Sammes and Y. Du (2005). Dynamic modeling of single tubular SOFC combining heat/mass transfer and electrochemical reaction effects. *Journal of Power Sources* 142, 211–222. 7, 41, 74
- Yamamura, Yoshihiko, Shinji Kawasaki and Hiroaki Sakai (1999). Molecular dynamics analysis of ionic conduction mechanism in yttria-stabilized zirconia. *Solid State Ionics* 126, 181–189. 6
- Young, Donald F., Bruce R. Munson and Theodore H. Okiishi (1996). *A brief introduction to fluid mechanics*. John Wiley & Sons, Inc.. New York, Chichester, Brisbane, Toronto, Singapore, Weinheim. 56
- Zhu, Y. and K. Tomsovic (2001). Development of models for analyzing the load-following performance of microturbines and fuel cells. *Electric Power Systems Research* 62, 1–11. 7, 13, 41, 74, 122
- Zucker, Robert D. and Oscar Biblarz (2002). *Fundamentals of Gas Dynamics*. 2th ed.. John Wiley and Sons, Inc. 91

Appendix

A-I. Parameters

Input conditions of simulation are shown in Table.A-1.

Table A-1: Simulation input conditions

Symbol	Description	Data source
$R_{\text{load}} = 4 [\Omega]$	External load resistance	
$I_{\text{load}} = 200 [\text{A}]$	External load current demand	
$P_{\text{fuel}}^{\text{in}} = 1 [\text{atm}]$	Fuel flow inlet pressure	(Campanari and Iora, 2004)
$T_{\text{fuel}}^{\text{in}} = 823 [\text{K}]$	Fuel flow inlet temperature	(Campanari and Iora, 2004)
$u_{\text{fuel}}^{\text{in}} = 0.927 [\text{m/s}]$	Fuel flow inlet velocity	(Campanari and Iora, 2004)
$\chi_{\text{CH}_4}^{\text{in}} = 0.173$	Inlet mole fraction of CH_4	(Campanari and Iora, 2004)
$\chi_{\text{H}_2\text{O}}^{\text{in}} = 0.284$	Inlet mole fraction of H_2O	(Campanari and Iora, 2004)
$\chi_{\text{H}_2}^{\text{in}} = 0.258$	Inlet mole fraction of H_2	(Campanari and Iora, 2004)
$\chi_{\text{CO}}^{\text{in}} = 0.057$	Inlet mole fraction of CO	(Campanari and Iora, 2004)
$\chi_{\text{CO}_2}^{\text{in}} = 0.228$	Inlet mole fraction of CO_2	(Campanari and Iora, 2004)
$P_{\text{air}}^{\text{in}} = 1 [\text{atm}]$	Cathode side air flow inlet pressure	(Campanari and Iora, 2004)
$T_{\text{air}}^{\text{in}} = 1104 [\text{K}]$	Cathode side air flow inlet temperature	(Campanari and Iora, 2004)

$u_{\text{air}}^{\text{in}}$	= 7.79 [m/s]	Cathode side air flow inlet velocity	(Campanari and Iora, 2004)
$\chi_{\text{O}_2}^{\text{in}}$	= 0.21	Inlet mole fraction of O ₂	
$P_{\text{inj}}^{\text{in}}$	= 1 [atm]	Injection air flow inlet pressure	(Campanari and Iora, 2004)
$T_{\text{inj}}^{\text{in}}$	= 1104 [K]	Injection air flow inlet temperature	(Campanari and Iora, 2004)
$u_{\text{inj}}^{\text{in}}$	= 12.08 [m/s]	Injection air flow inlet velocity	(Campanari and Iora, 2004)

Parameters of SOFC are shown in Table.A-2.

Table A-2: Model parameters

Symbol	Description	Source	
<i>Geometry parameters</i>			
A	= 1[cm ²]	Area of an finite piece of cell	
L	= 1.5[m]	Cell length	(Campanari and Iora, 2004)
r_3	= 11×10^{-3} [m]	Radius of outer cell tube	(Campanari and Iora, 2004)
r_2	= 8.66×10^{-3} [m]	Radius of inner cell tube	(Campanari and Iora, 2004)
r_1	= 6×10^{-3} [m]	Radius of outer Injection tube	(Campanari and Iora, 2004)
r_0	= 5×10^{-3} [m]	Radius of inner injection tube	(Campanari and Iora, 2004)
l_a	= 0.1×10^{-3} [m]	Thickness of anode	(Campanari and Iora, 2004)
l_c	= 2.21×10^{-3} [m]	Thickness of cathode	(Campanari and Iora, 2004)
l_e	= 0.04×10^{-3} [m]	Thickness of electrolyte	(Campanari and Iora, 2004)
F_{c-t}	= 0.69	View factor: cell to injection tube	(Perry <i>et al.</i> , 1997)
<i>Properties of solid materials</i>			
ρ_{cell}	= 4592 [kg/m ³]	Entire density of SOFC cell	(Hall, 1997)

$C_{p,cell}$	$= 740 \text{ [J/(kgK)]}$	Entire specific heat of SOFC cell	(Hall, 1997)
k_{cell}	$= 2.0 \text{ [W/(mK)]}$	Entire conductivity of anode	(Campanari and Iora, 2004)
ϵ_{cell}	$= 0.9$	Emissivity of cell inner surface	(Hall, 1997)
ρ_a	$= 2.98 \times 10^{-5} \exp(-\frac{1392}{T_{cell}}) \text{ [\Omega m]}$	Specific resistivity of anode	(Besette, 1994)
ρ_e	$= 2.94 \times 10^{-5} \exp(\frac{10350}{T_{cell}}) \text{ [\Omega m]}$	Specific resistivity of electrolyte	(Besette, 1994)
ρ_c	$= 8.11 \times 10^{-5} \exp(\frac{600}{T_{cell}}) \text{ [\Omega m]}$	Specific resistivity of cathode	(Besette, 1994)
ρ_{tube}	$= 3900 \text{ [kg/m}^3\text{]}$	Density of injection tube	(Hall, 1997)
$C_{p,tube}$	$= 976.8 + 0.2409T \text{ [J/(kgK)]}$	Specific heat of injection tube	(Hall, 1997)
k_{tube}	$= 31.86 - 0.03706T + 1.317 \times 10^{-5} T^2 \text{ [W/(mK)]}$	Conductivity of injection tube	(Hall, 1997)
ϵ_{cell}	$= 0.4$	Emissivity of cell inner surface	(Hall, 1997)

Reforming and shifting

K_r	$= 8542$	Reforming reaction rate coefficient	(Ahmed and Foger, 2000)
K_s	$= 100$	Shift reaction rate coefficient	
E_r	$= 95 \text{ [KJ/mol]}$	Activation of reforming reaction	(Ahmed and Foger, 2000)
α	$= 0.85$	order coefficient of reforming	(Ahmed and Foger, 2000)
β	$= -0.35$	order coefficient of reforming	(Ahmed and Foger, 2000)

Lumped Heat transfer

h_a	$= 8.744 \text{ [W/(m}^2\text{K)]}$	Anode side convection heat transfer coefficient	(Qi <i>et al.</i> , 2006)
h_c	$= 63.83 \text{ [W/(m}^2\text{K)]}$	Cathode side convection heat transfer coefficient	(Qi <i>et al.</i> , 2006)
h_t	$= 79.57 \text{ [W/(m}^2\text{K)]}$	Convection heat transfer coefficient in injection tube	(Qi <i>et al.</i> , 2006)
R_{rad}	$= 4.69$	Radiation heat transfer resistance	(Qi <i>et al.</i> , 2006)

Table A-3: Inherent property parameters of gas ingredients

Gas	Mole Mass M [kg/kmol]	Critical temperature T_C [K]	Critical pressure P_C [Pa]	Data source
CH ₄	16	191	4.59×10^6	(Perry <i>et al.</i> , 1997)
H ₂ O	18	647	21.94×10^6	(Perry <i>et al.</i> , 1997)
H ₂	2	33	1.32×10^6	(Perry <i>et al.</i> , 1997)
CO	28	133	3.49×10^6	(Perry <i>et al.</i> , 1997)
CO ₂	44	304	7.39×10^6	(Perry <i>et al.</i> , 1997)
N ₂	28	126.7	3.39×10^6	(Perry <i>et al.</i> , 1997)
O ₂	32	155	5.02×10^6	(Perry <i>et al.</i> , 1997)
Air	29	132	3.79×10^6	(Perry <i>et al.</i> , 1997)

A-II. Gas properties

Fuel gas consists of different components, each having their own properties. Different fractions lead to different composite properties of fuel gas. Because mole fractions are changed by the reforming and shift reaction and fuel cell reaction, the components fractions are time dependent. Thus we need to know those properties for each ingredient and calculate the properties of fuel gas using weighted averages.

Specific heat data C_p of each ingredient are taken from (Perry *et al.*, 1997) (Chapter 2, Table.2-198). Because in the SOFC application, we have assumed that fuel gas and air flow within fixed volumes, and what we need is the specific heat at constant volume C_v , calculated according to (Cengel and Boles, 1994):

$$C_v = C_p - R \quad (\text{A.1})$$

where R is the universal gas constant.

In the SOFC working temperature range 700-1500K, the specific heats of each gas component is approximated by first or second order polynomials of temperature, as listed in Table.A-4. The maximum relative errors of the approximation are also listed.

Gas viscosity at low pressure can be estimated by the method of Reichenberg (Perry *et al.*, 1997) (Chapter 2, Eqn.2-103):

$$\mu = \frac{AT_r}{[1 + 0.36T_r(T_r - 1)]^{1/6}} \quad (\text{A.2})$$

Table A-4: Approximation of specific heat of gas ingredients between 700-1500K

Gas	Approximation	Unit	Max. Error	Original data source
CH ₄	$C_{v,CH_4} = 1515 + 83.47T - 0.02053T^2$	[J/(kmolK)]	0.08%	(Perry <i>et al.</i> , 1997)
H ₂ O	$C_{v,H_2O} = 2.075 \times 10^4 + 12.15T$	[J/(kmolK)]	0.48%	(Perry <i>et al.</i> , 1997)
H ₂	$C_{v,H_2} = 1.829 \times 10^4 + 3.719T$	[J/(kmolK)]	0.9%	(Perry <i>et al.</i> , 1997)
CO	$C_{v,CO} = 1.966 \times 10^4 + 5.019T$	[J/(kmolK)]	1.35%	(Perry <i>et al.</i> , 1997)
CO ₂	$C_{v,CO_2} = 23690 + 31.01T - 8.875 \times 10^{-3}T^2$	[J/(kmolK)]	0.16%	(Perry <i>et al.</i> , 1997)
N ₂	$C_{v,N_2} = 1.910 \times 10^4 + 5.126T$	[J/(kmolK)]	1.11%	(Perry <i>et al.</i> , 1997)
O ₂	$C_{v,H_2} = 2.201 \times 10^4 + 4.936T$	[J/(kmolK)]	1.49%	(Perry <i>et al.</i> , 1997)
Air	$C_{v,air} = 1.948 \times 10^4 + 4.936T$	[J/(kmolK)]	1.12%	(Perry <i>et al.</i> , 1997)

For inorganic gases:

$$A = 1.6104 \times 10^{-10} \left[\frac{M^{1/2} P_c^{2/3}}{T_c^{1/6}} \right] \quad (A.3)$$

where $T_r = \frac{T}{T_c}$, $P_r = \frac{P}{P_c}$ are the reduced temperature and pressure, T_c and P_c are the critical temperature and pressure, and M is the molar mass, listed in Table.A-3.

Within the temperature range of 700-1500K, calculated gas viscosities and temperature distributions are approximated by first order polynomials of temperature, as listed in Table.A-5

Thermal conductivity can be estimated as in (Perry *et al.*, 1997) (Chapter 2, Eqn.2-128):

$$k = \frac{\mu}{M} \left(1.30C_v + 14644.0 - \frac{2928.8}{T_r} \right) \quad (A.4)$$

Thermal conductivity of methane can be estimated by (Perry *et al.*, 1997) (Chapter 2, Eqn.2-125):

$$k = 10^{-7} (14.52T_r - 5.14)^{2/3} \left(\frac{C_p}{\lambda} \right) \quad (A.5)$$

Table A-5: Approximation of viscosity of gas ingredients between 700-1500K

Gas	Approximation	Unit	Max. Error	Original data source
CH ₄	$\mu_{\text{CH}_4} = 9.177 \times 10^{-6} + 1.755 \times 10^{-8}T$	[Pa · s]	1.56%	(Perry <i>et al.</i> , 1997)
H ₂ O	$\mu_{\text{H}_2\text{O}} = 4.567 \times 10^{-6} + 2.209 \times 10^{-8}T$	[Pa · s]	2.22%	(Perry <i>et al.</i> , 1997)
H ₂	$\mu_{\text{H}_2} = 6.162 \times 10^{-6} + 1.145 \times 10^{-8}T$	[Pa · s]	1.26%	(Perry <i>et al.</i> , 1997)
CO	$\mu_{\text{CO}} = 1.399 \times 10^{-5} + 2.582 \times 10^{-8}T$	[Pa · s]	1.39%	(Perry <i>et al.</i> , 1997)
CO ₂	$\mu_{\text{CO}_2} = 1.273 \times 10^{-5} + 2.822 \times 10^{-8}T$	[Pa · s]	1.98%	(Perry <i>et al.</i> , 1997)
N ₂	$\mu_{\text{N}_2} = 1.435 \times 10^{-5} + 2.642 \times 10^{-8}T$	[Pa · s]	1.36%	(Perry <i>et al.</i> , 1997)
O ₂	$\mu_{\text{H}_2} = 1.668 \times 10^{-5} + 3.108 \times 10^{-8}T$	[Pa · s]	1.45%	(Perry <i>et al.</i> , 1997)
Air	$\mu_{\text{air}} = 1.514 \times 10^{-5} + 2.793 \times 10^{-8}T$	[Pa · s]	1.39%	(Perry <i>et al.</i> , 1997)

where

$$\lambda = T_c^{1/6} M^{1/2} \left(\frac{101325}{P_c} \right)^{2/3} \quad (\text{A.6})$$

Between 700K and 1500K, thermal conductivities are approximated using first order polynomials of temperature, as listed in Table.A-6:

The enthalpies of formation at different temperatures can be calculated using (Smith and Ness, 1987) (Chapter 4, Eqn.4.1):

$$H|_T = H|_{298.15} + \int_{298.15}^T C_p dT \quad (\text{A.7})$$

$H_{\text{H}_2}|_{298.15} = 0[\text{J/mol}]$, $H_{\text{O}_2}|_{298.15} = 0[\text{J/mol}]$ and $H_{\text{H}_2\text{O}}|_{298.15} = -241827[\text{J/mol}]$ (Larminie and Dicks, 2003).

The first order polynomials of temperature approximations are listed in Table.A-7

Table A-6: Approximation of Thermal conductivity of gases between 700-1500K

Gas	Approximation	Unit	Max. Error	Orig. Data Source
CH ₄	$k_{\text{CH}_4} = -0.04446 + 2.093 \times 10^{-4}T$	[W/(mK)]	0.41%	(Perry <i>et al.</i> , 1997)
H ₂ O	$k_{\text{H}_2\text{O}} = -0.01450 + 9.782 \times 10^{-5}T$	[W/(mK)]	0.61%	(Perry <i>et al.</i> , 1997)
H ₂	$k_{\text{H}_2} = 0.08525 + 2.964 \times 10^{-4}T$	[W/(mK)]	0.22%	(Perry <i>et al.</i> , 1997)
CO	$k_{\text{CO}} = 0.01275 + 5.384 \times 10^{-5}T$	[W/(mK)]	1.42%	(Perry <i>et al.</i> , 1997)
CO ₂	$k_{\text{CO}_2} = 0.005485 + 6.272 \times 10^{-5}T$	[W/(mK)]	2.36%	(Perry <i>et al.</i> , 1997)
N ₂	$k_{\text{N}_2} = 0.01258 + 5.444 \times 10^{-5}T$	[W/(mK)]	1.18%	(Perry <i>et al.</i> , 1997)
O ₂	$k_{\text{H}_2} = 0.01569 + 5.690 \times 10^{-4}T$	[W/(mK)]	0.79%	(Perry <i>et al.</i> , 1997)
Air	$k_{\text{air}} = 0.01329 + 5.539 \times 10^{-5}T$	[W/(mK)]	1.25%	(Perry <i>et al.</i> , 1997)

Table A-7: Approximation of enthalpy of formation between 700-1500K

Gas	Approximation	Unit	Max. Error	Orig. Data Source
CH ₄	$H_{\text{CH}_4} = -10.081 \times 10^4 + 62.12T$	[J/mol]	17.3%	(Perry <i>et al.</i> , 1997)
H ₂ O	$H_{\text{H}_2\text{O}} = -25.790 \times 10^4 + 42.47T$	[J/mol]	0.26%	(Perry <i>et al.</i> , 1997)
H ₂	$H_{\text{H}_2} = -0.9959 \times 10^4 + 30.73T$	[J/mol]	1.48%	(Perry <i>et al.</i> , 1997)
CO	$H_{\text{CO}} = -12.150 \times 10^4 + 31.81T$	[J/mol]	0.37%	(Perry <i>et al.</i> , 1997)
CO ₂	$H_{\text{CO}_2} = -41.700 \times 10^4 + 50.89T$	[J/mol]	0.25%	(Perry <i>et al.</i> , 1997)
N ₂	$H_{\text{N}_2} = -1.059 \times 10^4 + 31.40T$	[J/mol]	1.73%	(Perry <i>et al.</i> , 1997)
O ₂	$H_{\text{O}_2} = -1.2290 \times 10^4 + 35.12T$	[J/mol]	2.17%	(Perry <i>et al.</i> , 1997)
Air	$H_{\text{air}} = -1.0947 \times 10^4 + 32.50T$	[J/mol]	2.43%	(Perry <i>et al.</i> , 1997)